Universidade Estadual de Campinas

Instituto de Química

Cesar Brinatti Antonio

Calorimetric study on the interactions between ionic surfactants and pristine and modified cellulose nanocrystals (CNC)

Estudo calorimétrico da interação entre surfactantes iônicos e nanocristais de celulose (CNC) puros e modificados

CAMPINAS

2016

Cesar Brinatti Antonio

Calorimetric study on the interactions between ionic surfactants and pristine and modified cellulose nanocrystals (CNC)

Estudo calorimétrico da interação entre surfactantes iônicos e nanocristais de celulose (CNC) puros e modificados

Tese de Doutorado apresentada ao Instituto de Química da Universidade Estadual de Campinas como parte dos requisitos exigidos para a obtenção do título de Doutor em Ciências.

Doctor's dissertation presented to the Institute of Chemistry of the University of Campinas as part of the requirements to obtain the title of Doctor in Sciences.

Supervisor: Prof. Dr. Watson Loh
Co-supervisor: Prof. Dr. Michael Kam Chiu Tam

ESTE EXAMPLAR CORRESPONDE À VERSÃO FINAL DA TESE DEFENDIDA PELO ALUNO CESAR BRINATTI ANTONIO E ORIENTADA PELO PROF. DR. WATSON LOH.

CAMPINAS
2016

Informações para Biblioteca Digital

Título em outro idioma: Estudo calorimétrico da interação entre surfactantes iônicos e nanocristais de celulose (CNC) puros e modificados
Palavras-chave em inglês:
Cellulose nanocrystals
Calorimetry
Surfactants
Área de concentração: Físico-Química
Titulação: Doutor em Ciências
Banca examinadora:
Watson Loh [Orientador]
Denise Freitas Siqueira Petri
Rilton Alves de Freitas
Pedro Luiz Onófrio Volpe
José de Alencar Simoni
Data de defesa: 28-07-2016
Programa de Pós-Graduação: Química

BANCA EXAMINADORA

Prof. Dr. Watson Loh (Orientador)

Profa. Dra. Denise Freitas Siqueira Petri (USP-SP)

Prof. Dr. Rilton Alves de Freitas (UFPR)

Prof. Dr. Pedro Luiz Onófrio Volpe (IQ-UNICAMP)

Prof. Dr. José de Alencar Simoni (IQ-UNICAMP)

A Ata da defesa com as respectivas assinaturas dos membros encontra-se no processo de vida acadêmica do(a) aluno(a).

Este exemplar corresponde à redação final da Tese de Doutorado defendida pelo aluno **CESAR BRINATTI ANTONIO,** aprovada pela Comissão Julgadora em 28 de julho de 2016.

Dedication

To my mom Rosana Brinatti and to my aunt Marina Brinatti. They loved me to the very end and they believed that I would and I could make a difference. I will not disappoint them.

"I like the stars. It's the illusion of permanence, I think I mean, they`re always flaring up and caving in and going out. But from here, I can pretend. I can pretend that things last. I can pretend that lives last more than moments..."

Destruction – Brief Lives

Acknowledgements

The amazing Inés Joekes who had taught me a lot in a short period of time and for showing me how to put passion in my writings.

The Professor Luis Santos, whose company was a most pleasant one in walking around Atlantic City and eventually having some breaks to drink a cold beer.

Virgilio and Victor Vettorazzo, whose friendship started more than 20 years ago. Also, Juliana Pereira who became a good and valuable friend.

My best man Fabio Fico who I shared music, beer, life, laughs, and tears. I am blessed to have met him and his whole family.

Rodrigo and Lisandra who are always willing to share moments of their lives with me and my wife. They are good friends indeed.

Paulo, Daniel (Mamute), and Miyata, for their companionship in all kinds of situations.

My cousin Marco Novello for simply everything he had done in the past for me, my mom and my grandmother. None of his efforts were in vain, and he and his family will always have a special place inside my heart.

My cousin Patricia Storel for being there until I had time to arrive, before the end. Thank you for not letting her alone.

My dear friend and always a "savior" Ilda Bafa, who showed me what family was supposed to be.

My cousins in Piracicaba Sueli, Zezo, Cláudio, Eliana and Guilherme. They always have their house open for us, no matter what.

Claudia Martelli, for all the conversations we had and for always being an upbeat person.

Mário, from "micromechanics". He saved my life twice by performing magic in fixing some ITC parts.

David Remeta and Conceição Minetti for all their support during my time in Atlantic City and New York.

The entire lab in Canada, where I spent one incredible year (in every possible way). Nishil, Juntao, Debbie, Li, Yibo, Hanna, Shi, Hairong, Luya, Patrick, Nate, Ambrose, Eric and Pritpal. Especially to John Huang, my co-op student who became a good friend, and Micky Lee, who became my very first friend in Canada. We will always have the memories together.

Resumo

Nanocristais de celulose (CNC) são comumente obtidos por hidrólise ácida da celulose, o polímero mais abundante na natureza. Eles são biodegradáveis, não tóxicos e anfifílicos. A substituição de alguns grupos hidroxila em sua superfície por grupos éster de sulfato (OSO_3^-) proveniente da hidrólise com ácido sulfúrico confere uma estabilidade eletrostática e coloidal em dispersões aquosas. É esperada então uma forte interação eletrostática com surfatantes catiônicos, por exemplo, da mesma maneira que polímeros iônicos o fariam, podendo ocasionar sua precipitação/floculação. Este fenômeno é observado ao estudarem-se misturas aquosas contendo uma concentração fixa de CNC em presença de uma série homóloga de surfatantes brometos de alquiltrimetilamônio (C_nTAB). Diferentes técnicas experimentais foram utilizadas como: titulação calorimétrica, medidas de espalhamento de luz e potencial zeta, fluorescência de sondas etc. Os resultados indicaram que a força motriz inicial é a interação eletrostática entre ambos em baixa concentração de surfatante, e a precipitação ocorre para toda a série homóloga quando a concentração de surfatante atinge o valor de cerca de metade de sua concentração micelar crítica (*cmc*), o que denota uma importante contribuição hidrofóbica por parte do surfatante. Adicionando-se surfatantes não iônicos à mistura, a precipitação pôde ser modificada (mas não impedida) por uma faixa de concentração maior de surfatante catiônico. Uma maneira de tentar conferir uma estabilidade estérica adicional à CNC foi com as modificações de alguns grupos hidroxilas restantes com um polímero hidrofílico derivado do poli (oxido de etileno), o poli (dietileno óxido metil éter metacrilato), P(MEO_2MA). Este polímero passa por uma transição de fase reversível com o aumento da temperatura, reversibilidade esta que pode ser alterada na presença de surfatantes iônicos: enquanto o surfatante aniônico dodecilsulfato de sódio (SDS) pode-se ligar apenas à cadeia polimérica por interações hidrofóbicas (independente da temperatura), o surfatante catiônico brometo de dodeciltrimetilamônio ($C_{12}TAB$) pode-se ligar tanto ao polímero (interações hidrofóbicas) quanto aos grupos éster de sulfato (interações eletrostáticas), alterando a carga da CNC-*g*-P(MEO_2MA). Outra maneira de estudar a influência de surfatantes iônicos foi modificar a superfície da CNC com grupos amino (NH_2) que respondem a alterações de pH, alterando a carga elétrica total da superfície. Em baixos valores de pH, SDS interage fortemente com CNC-NH_2, enquanto $C_{12}TAB$ interage apenas em altos valores de pH. De modo geral, os presentes resultados adicionaram informações

importantes sobre o comportamento coloidal de CNC e suas misturas com surfatantes, e entender como a estabilidade da CNC e seus derivados em água varia em presença de surfatantes iônicos é de grande valia no preparo de novos nanocompósitos, o que leva a ampliação de seu campo de aplicações.

Abstract

Cellulose nanocrystals (CNC) are commonly obtained by acid hydrolysis of cellulose, the most abundant homopolymer in nature. They are biodegradable, nontoxic, and amphiphilic. The substitution of some of the hydroxyl groups on its surface by sulfate-ester groups (OSO_3^-) when hydrolysis is performed using sulfuric acid, renders an electrostatic and colloidal stability in aqueous dispersions. A strong electrostatic interaction between CNC and cationic surfactants is expected in a similar fashion to ionic polymers, which might lead to precipitation/flocculation. This phenomenon was observed when studying aqueous mixtures with a fixed CNC concentration in the presence of a homologous series of alkyltrimethylammonium bromide surfactants (C_nTAB). Different experimental techniques were used such as: calorimetric titration, light scattering and zeta potential, probe fluorescence, etc. The results indicated that the initial driving force is the electrostatic interactions between CNC and surfactants at low surfactant concentration and, precipitation occurs for the entire homologous series when the surfactant concentration reaches half the critical micellar concentration (*cmc*), denoting an important hydrophobic contribution from the surfactant. Precipitation could be modified for a larger cationic surfactant concentration range and not avoided though, by adding nonionic surfactants to the CNC-C_nTAB mixture. One attempt of bestowing an additional sterical stability to CNC was by modifying some of its remaining hydroxyl groups with a hydrophilic poly (ethylene oxide) derivative, poly (diethylene oxide methyl ether methacrylate), P(MEO$_2$MA). This polymer can undergo a reversible phase-transition with a temperature increase and this reversibility can be changed in the presence of ionic surfactants: while an anionic surfactant, sodium dodecylsulfate (SDS) can only bind to the polymer chains via hydrophobic interactions (temperature independent), a cationic surfactant, dodecyltrimethylammonium bromide ($C_{12}TAB$) can bind to both the polymer chains (hydrophobic interactions) and the sulfate-ester groups (electrostatic interactions), changing the CNC-*g*-P(MEO$_2$MA) charge. Another way of studying the influence of ionic surfactants was to modify the surface of CNC with amine groups (NH$_2$) that are pH-responsive and therefore can change the overall surface charge. At low pH values, SDS strongly interacts with CNC-NH$_2$, while $C_{12}TAB$ interacts only at high pH values. Overall the present results added important information regarding the colloidal behavior of CNC and its mixtures with surfactants and understanding how the stability of CNC and its derivatives in aqueous dispersions may

vary in the presence of ionic surfactants is of great value in preparing new nanocomposites, which in turn broadens its field of applications.

List of Figures

List of Schemes

List of Tables

Abbreviations

Acronym	Full name
CNC	Cellulose Nanocrystals
ITC	Isothermal Titration Calorimetry
C_nTAB	Alkyltrimethylammonium bromide surfactants
$P(MEO_2MA)$	Poly(diethylene glycol methyl ether methacrylate)
$CNC-NH_2$	Amine surface-modified CNC
SDS	Sodium dodecylsulfate
$C_{12}TAB$	Dodecyltrimethylammonium bromide
DP	Degree of polymerization
M_{AGL}	Molecular weight of the anhydroglucose unit
M_{CELL}	Molecular weight of the cellulose polymer chains
η	Intrinsic viscosity
XRD	X-ray diffraction
DS	Degree of substitution
MC	Methyl cellulose
HPC	Hydroxypropyl cellulose
LCST	Lower Critical Solution Temperature
UCST	Upper Critical Solution Temperature
HCl	Hydrochloric acid
ESI-MS	Electrospray ionization-mass spectroscopy
GPC	Gel permeation chromatography
cmc	Critical micellar concentration
ΔH_{dil}^0	Normalized enthalpy of dilution
DSC	Differential Scanning Calorimetry
HSDSC	High Sensitivity Differential Scanning Calorimetry
SAXS	Small Angle X-ray Scattering
C_nPyCl	Hexadecylpyridinium chloride

C_nTAC	Hexadecyltrimethylammonium chloride
$C_{14}TAB$	Tetradecyltrimethylammonium bromide
cac	Critical aggregation concentration
PEO	Poly (ethylene oxide)
PPG	Poly (propylene glycol)
PP	Poly (propylene)
P4VP	Poly (4-vinylpyridine)
PPy	Poly (pyrole)
PNIPAM	Poly (N-isopropylacrylamide)
$C_{16}TAB$	Hexadecyltrimethylammonium bromide
PSS	Poly (sodium 4-styrenesulfonate)
C_2	Saturation concentration
PDADMAC	Poly (diallyldimethylammonium chloride)
ISE	Ion-specific Electrode
DLS	Dynamic Light Scattering
EHEC	Ethyl (hydroxyethyl) cellulose
HLB	Hydrophilic-lipophilic balance
ANS	5-dimethylamino-1-naphthalenesulfonic acid hydrate
d_H	Hydrodynamic diameter
EPH	Epichlorohydrin
HCPA	2-hydroxy-3-chloro propylamine
EPH	Epichlorohydrin
DMSO	Dimethylsulfoxide
TBAH	Tetrabutylammonium hydroxide
TEM	Transmission electron microscopic
SEM	Scanning Electron Microscopy
AFM	Atomic Force Microscopy
POM	Polarized Optical Microscopy

ATRP   Atom-Transfer Radical Polymerization

Summary

Chapter 1: Introduction

1.1 Overview

Cellulose nanocrystals (CNC) are a class of biomaterials obtained by acid hydrolysis of cellulose.[1–6] All the amazing and fantastic intrinsic properties of cellulose remained such as, high mechanical strength (100-130 GPa), low density (1.566 g cm^{-3}), optical properties, biodegradability, biocompatibility,[2,3,5,7–13] remain once its amorphous regions are removed and CNC is formed.

CNC is a negatively charged rod-like nanoparticle and presents a high aspect ratio of 10-20, with dimensions of 200-500 nm (length) and 5-20 nm (diameter) and a high surface area (hundreds of m^2 g^{-1}),[12,14,15] that are dependent on the source that it is obtained. On one hand the negative charges (most commonly sulfate ester groups) present on the surface are responsible for its dispersion and colloidal stability in water and polar solvents.[11,16,17] On the other hand its high surface area and high aspect ratio, together with the possibility of forming hydrogen bonds between the rods is an opposite force to create a dispersion.[3,18,19] The balance between these two opposite phenomena and furthermore controlling and understanding it is a key factor in enhancing the use of CNC in different applications.

CNC and its derivatives obtained by the chemical modification of its surface hydroxyl groups have found their way into the most varied range of applications: reinforcement,[20,21] Pickering emulsions,[22–26] drug carrier systems,[27,28] nanocomposites,[29–33] supercapacitors.[34]

Although we see many studies published every year, there is still some information lacking when it comes to understanding the energetic of interactions of both pristine and surface-modified CNC with oppositely charged molecules such as surfactants.[20,25,35–38] Most publications are studies of the interactions between all types of surfactants (ionics, nonionics, and zwitterionics) and polymers, both natural and manmade.[39–44] and nanoparticles.[45–47]

Our attempt in this thesis was to contribute with some knowledge regarding pristine CNC and two other surface-modified CNC derivatives in the presence of surfactants. To achieve this purpose we chose mainly isothermal titration calorimetry (ITC) technique as a guide for all further experiments. Throughout the entire experiments the concentrations of the two species involved, i.e. titrant and analyte are

known.[40,48] Besides, ITC is the only technique that can provide thermodynamic data within a single experiment,[43,49,50] and it is the only one to measure enthalpy of reactions directly. In our research, ITC results provided us valuable information on the three following subjects: **1)** The interactions between CNC and cationic surfactants, both electrostatic and hydrophobic are so strong that it leads to flocculation/precipitation of the mixtures at a concentration of half the critical micellar concentration (*cmc*) value, regardless the surfactant alkyl chain length; **2)** When adding a nonionic surfactant to this mixture the binding of cationic surfactants is enhanced and the concentration at which precipitation occurs is only delayed and it is not avoided, though. The surface modification of CNC with a thermoresponsive polymer that undergoes phase separation when the temperature of the system is increased, showed that ionic surfactants (both anionic and cationic) are able to change this phenomenon; **3)** And finally, when modifying the CNC surface with an amine group that acts as a pH-responsive group, the overall electrical charge can be tuned from positive at low pH, to negative at high pH. Accordingly, the interactions with ionic surfactants can be suppressed or enhanced depending on the pH of the mixture.

1.2 Research Objectives

Our aim was to understand how surfactants with different features such as polar headgroup, electrical charge and, alkyl chain length would interact and bind to both pristine and surface-modified CNC rods. The experiments were performed in different conditions as well: in the presence of electrolytes or other surfactants and at different temperatures in order to assess the contributions of both hydrophilic and hydrophobic moieties of the surfactants to the interactions with CNC.

We pursued the aforementioned ideas by:

- Studying the interactions of pristine CNC and a homologous series of alkyltrimethylammonium bromide surfactants (C_nTAB) at different temperatures and in the presence of electrolytes;

- Surface modifying CNC with a thermoresponsive polymer poly(diethylene oxide methyl ether methacrylate) P(MEO_2MA) via free radical polymerization and its interactions at temperatures below and above the lower critical solution temperature

(LCST) with the ionic surfactants sodium dodecylsulfate (SDS) and dodecyltrimethylammonium bromide ($C_{12}TAB$);

- Studying a pH-responsive system comprised by an amine surface-modified CNC ($CNC-NH_2$) with the ionic surfactants sodium dodecylsulfate (SDS) and dodecyltrimethylammonium bromide ($C_{12}TAB$) at different pH and temperature values.

In this thesis we anticipated to contribute with valuable information regarding the energetic of the surfactant/CNC mixtures that in turn could help with new formulations and prospect applications in the most varied of fields.

1.3 Thesis Outline

This thesis consists of 6 chapters. Chapter 1 is comprised of the introduction, where we briefly describe CNC and its derivatives in the presence of surfactants. Chapter 2 presents a literature review on cellulose, pristine and modified CNC and their applications. Chapter 3 deals with the interactions between pristine CNC and a homologous series of cationic surfactants (C_nTAB). In Chapter 4 we discuss about surface modification of CNC with a thermoresponsive polymer and its interactions with ionic surfactants. Chapter 5 we present the study of interactions between ionic surfactants with an amine-modified CNC. In Chapter 6 we present a general discussion and conclusions, along with our final considerations. Supporting information related to Chapters 3, 4 and 5 can be found in Appendixes A, B, and C, respectively. In Appendix D we present a review paper focused on ITC, the main technique throughout this thesis. Appendix E includes a paper on CNC surface modification with pH-responsive amine groups.

Chapter 2: Literature Review

2.1 Cellulose

Cellulose is one of the most abundant renewable sources in nature. It would be unwise not to start this text with the aforementioned phrase, which has been stated in a similar way by many authors.[51–65] According to Ullmann's Encyclopedia[64] if all the cellulose chains that are produced by a tree in a year (on average) were to be aligned in a single chain, it would have 2.62×10^{10} km in length, which is equivalent of 175 times the distance between the Earth and the Sun.

Cellulose is one of the most studied natural polymers ever since its discovery in 1838 by Anselme Payen.[55,56,60] Its structure was the very first one to be investigated by X-ray diffraction (XRD) technique in 1913,[62] by Nishikawa and Ono.[65] It was only in 1920 that its configuration was determined by Hermann Staudinger.[60,62] In Zugenmaier's wonderful review[62] "Conformation and packing of various crystalline cellulose fibers" there is a list of all the most important and relevant authors including their meaningful discoveries related to the structure of cellulose.

Cellulose is present in all types of plants and trees, being part of the cell walls, stems and trunks, and its percentage varies among different species: it is constituent of 50% (dry mass) of wood and 90% of cotton's mass;[60,65,66] it is also present in algae cell walls, bacteria,[55,56,60,63,67] fungi, and even in some marine animals such as tunicate.[56] In vegetables the rest of their dry mass is comprised by both lignin (20-30%, possessing one of the most complex and yet most studied structures)[55,56,68] that has a role of protection and reinforcement acting as a physical barrier to protect cellulose from enzymatic and hydrolytic attacks,[53,69,70] and hemicellulose (10-20%, possessing a non-crystalline structure)[64,71] which is considered to be a compatibilizer between cellulose (hydrophilic nature) and lignin (hydrophobic nature)[55] **Figure 2.1** shows a tridimensional molecular dynamic simulation of cellulose chains surrounded by lignin and enzymes.[72]
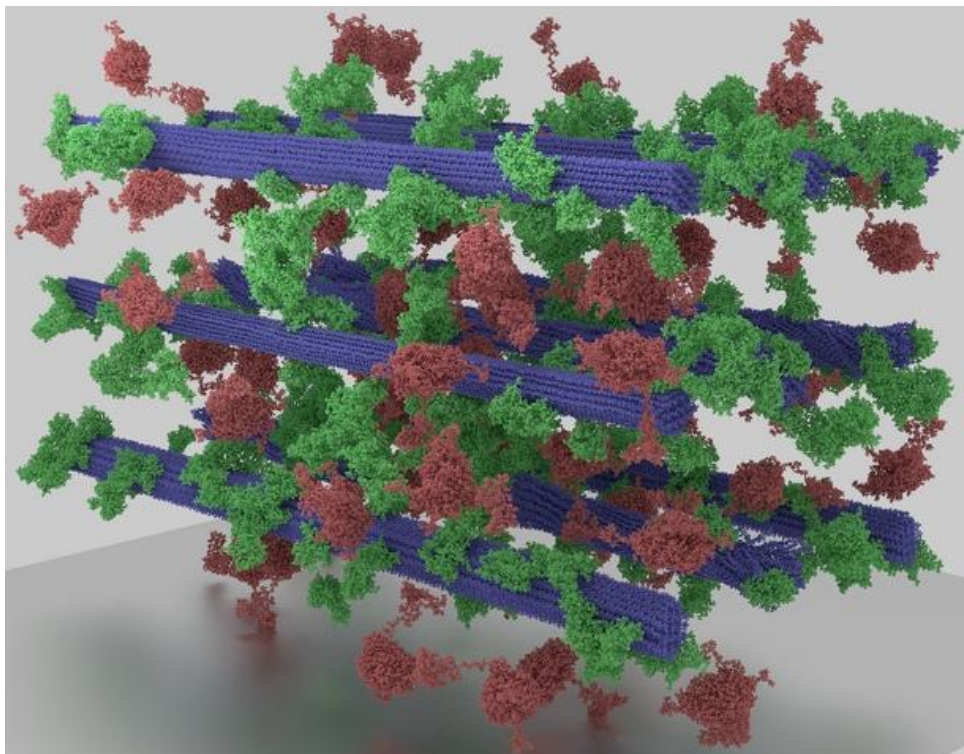
Figure 2.1 Computer simulation of biomass model portraying cellulose (blue), lignin (red) and enzymes (green). It can be seen crystalline domains (flat regions) and amorphous regions (twisted regions) at the right end of the picture (taken from reference 72).

There are many different applications for cellulose ranging from textile, paper, food, bio-composites, electronics, pharmaceutical, and medicine.[55] To be of use for any of the aforementioned processes is pivotal that its "impurities – lignin and hemicellulose" are removed by either chemical or physical processes. These processes might alter its primary structure that leads to modifications in its behavior and, consequently, its field of application. This broad range of its use in so many distinct fields by itself is the responsible for a large part of time and research devoted to cellulose around the world. On top of that, the available hydroxyl groups on its surface allow it to undergo chemical functionalization by inorganic or organic groups, with the latter by conversion into ether or ester groups,[56,59,61,64,66,67,73–81] are responsible for a change on its field of application and use. The review by Kalia et al.[55] encompass many of its uses.

From a macroscopic point of view, cellulose possesses a fibril structure, white color and is odorless.[56,60] From a microscopic point of view, its polymeric chain lengths vary with different sources accordingly:[56,63,64] in wood, for instance, the cross-sectional dimension of the polymer chains that make up the elemental fibrils or nanofibrils vary

between 3 to 5 nm. These nanofibrils bundle up forming microfibrils with a larger dimension of 15-20 nm, that further aggregate into larger bundles which form wood fibers.[58,64,68,73,82] These large bundles present a Young Modulus' that, depending on the way they are obtained,[55,56,68] could reach up to 130-250 GPa due to its crystalline domains. However, cellulose presents amorphous regions as well in its structure (in a variable amount depending on its source) that weaken the fibers and make them susceptible to hydrolysis and solubilisation in different solvents.[51,53,56,57,60,68,83,84]

In order for us to understand the use of cellulose and its derivatives and more importantly the use of cellulose nanocrystals in several different applications, we must first know and understand its chemical and physical structure; that is to say which ones are the basic units, what are the chemical bonds that hold together its internal structure and consequently, shape its spatial structure, granting many desired properties such as, reinforcement and compatibilization with different materials,[79,85] viscosity modifier,[64,75] solubilisation in distinct solvents,[57,66] application as pharmaceutical hydrogels and drug-carriers,[58,61,73,80,81] and the manufacture of thin films.[59,77]

2.2 Molecular Structure – What is cellulose made of?

Before we begin, a basic question must be asked and this question will lead to a chain reaction of more questions: *what is cellulose*? Cellulose is a *homopolymer*, a macromolecule which basic units are identical and repeat itself all along its polymer chain. *And what are these basic repeating units made of*? Well, when the alcohol group from a D-glucose (a *monosaccharide*) molecule reacts with the *hemiacetal* group from another D-glucose molecule an *acetal* is formed (molecules bound together by an oxygen atom),[55,63] with the elimination of a water molecule. Therefore the glucose bound units are now called *anhydroglucose*. A *disaccharide* is formed named cellobiose, which is the basic repeating unit of cellulose (Figure 2.2).
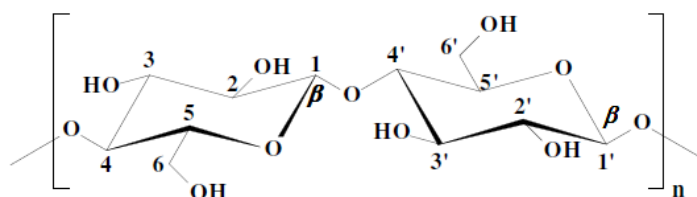
Figure 2.2 Structure of cellobiose (chair conformation). It is the basic repeating unit of cellulose that repeats itself throughout the whole polymer chain.

The consecutive addition of D-glucose molecules to cellobiose leads to the formation of larger structures named cellotriose, cellotetrose, cellopentose, etc., rendering cellulose as a *polysaccharide* that belongs to the carbohydrate class. On average the cellulose chains have a degree of polymerization (DP) ranging from 10,000 to 15,000 anhydroglucose units. Given that the cellulose production relies on different enzymes (cellulose synthases) present on the specific vegetable, different sources will produce cellulose with different polymer chain lengths (Table 2.1).[56,63,64]

Knowing that the molecular weight of the anhydroglucose unit (MAGL) is approximately 162 g mol^{-1}, it is possible to estimate the average molecular weight of the cellulose polymer chains (M_{CELL}) using the following equation: $M_{CELL} = DP \times M_{AGL}$.[64] The actual molecular weight is determined by obtaining the intrinsic viscosity (η) using copper (II)-ehtylenediamine as a solvent.[64,66]

Table 2.1 Degree of polymerization (DP) for different sources of cellulose (adapted from references 56,63,64)

Cellulose Source	DP
Cotton, pure	7.000
Line	8.000
Ramie	6.500
Beech wood	3.050
Spruce	3.300
Gluconobacter	600

An appropriate explanation must be made here: in Figure 2.2 all the carbon atoms are numbered and the acetal linkage is denoted by using the Greek letter β. This is an important indication that the linkage between the two D-glucose molecules is a β–linkage or a β–configuration, in which the hydroxyl group bound to C1 is on the same plane of the –CH$_2$OH group bound to C5 in a Haworth's projection. When these groups are in distinct planes, the linkage is designated as α (Figure 2.3). There is a spontaneous conversion between α and β configurations on glucose molecules, named *mutarotation*. These type of isomers are called anomers because the change occurs on the hemiacetal or anomeric carbon atom.[55,63] The 6 carbons atoms ring such as it is with glucose are also called pyranose for they are similar to the pyrane ring.

CH₂OH represented in the figure...

Figure shows two Haworth projections labeled *α*-D-glucose and *β*-D-glucose.
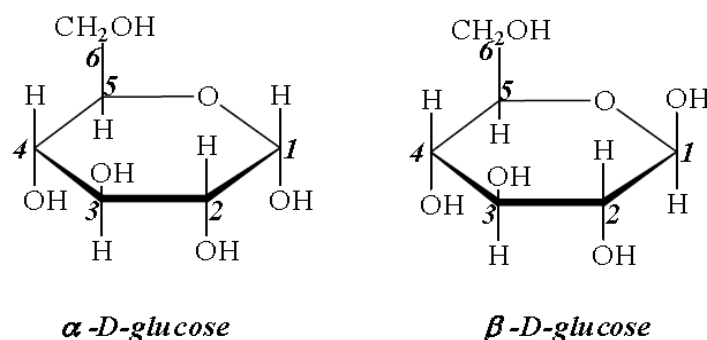
Figure 2.3 Haworth's projection for *α* and *β* D-glucose anomers.

We now are able to come up with a more accurate definition and nomenclature for cellulose – it is a *poly (βl→4'-ᴅ-anhydroglucopyranose)*. *So what is the importance* of defining and pointing that cellulose has an acetal linkage between its anhydroglucose units? It is pivotal to distinguish it from other polysaccharides like starch and glycogen when it comes to their spatial structures formed by their polymer chains, which in turn will affect their physical-chemical properties and their roles. With that being said, let us take a closer look at the secondary structure of cellulose.

2.2.1 Secondary Structure – What is the structure of cellulose?

While the main role of cellulose is to work as a mechanical reinforcement and to be part of a cell wall structure,[55,60,63,85] starch and glycogen are homopolymers as well and yet they possess an entirely different role: both of them act as energy storage in plants and animals respectively.[63] Both of them present branched structures: starch is made of a main *amylose* chain ((*α*l→4')-ᴅ-glucose), with highly branched *amylopectin* chains that are connected to amylose by a *α*l→6' linkage. Glycogen has a similar structure to starch except for a much higher number of branches.[63,66] It is noteworthy to say that the difference among these three polysaccharides lies solely on the type of the acetal bond (besides the branching, of course). The *α* – linkage is readily hydrolysed and only a few organisms are capable of hydrolyzing the *β* – linkage. Termites are able to digest cellulose due to the fact that they possess a symbiotic microorganism inside their intestinal tract, of the *Thriconympha* genre, that is able to secrete cellulases. Some other organisms such as bacteria and the saprobe fungus *Pycnoporus sanguineus* are able to do it as well.[56,63,68] The type of acetal linkage and the structure adopted by the

polymer chains render cellulose its mechanical strength that is not observed in the other aforementioned polysaccharides, though.

Cellulose presents a well-known polymorphism,[52,58,60,62,64–66,86] and its structures are classified as it follows:

Cellulose I: its native form, it has two allomorphs I_α (metastable) found in algae and bacteria, and I_β (stable) found in plants and marine animals.[6,56,62,87]

Cellulose II: when cellulose I undergoes regeneration or mercerization process, its polymer chains can be crystallized as bundles in an antiparallel fashion and it has a more stable lattice than cellulose I, thus it presents an irreversible process.[65]

Cellulose III: it possesses two polymorphs that are source-dependent, cellulose III_I and cellulose III_{II}. They both present a nearly identical X-ray diffraction pattern and their difference lies in their infrared spectra.

Cellulose IV: it possesses two polymorphs that are source-dependent, cellulose IV_I and cellulose IV_{II}, and their difference lies on their polarity.

Figure 2.4[56] shows how each structure is obtained from one another. Horii[65] and Zugenmmaier[62] present the cellulose polymorphs tridimensional structures and how they can be shifted to one another.
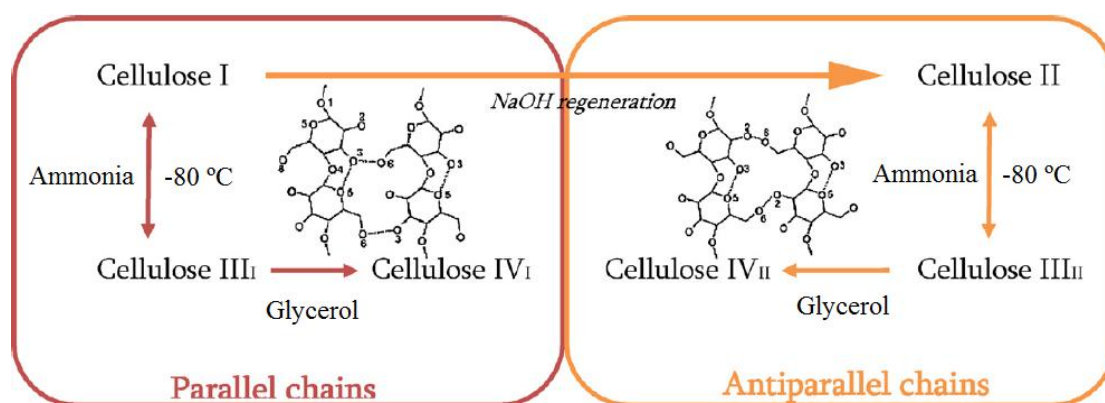
Figure 2.4 Cellulose polymorphs and how they are obtained (adapted from ref.56).

Considering cellulose I polymorph, *which conformation will be adopted by its polymer chains?* Figure 2.2 shows us that there is the possibility of both intra and intermolecular hydrogen bonds to be made by the three hydroxyl groups on the carbon atoms 2, 3 and 6 present on the anhydroglucose molecules. Intramolecular hydrogen

bonds can be formed between the groups OH(3) – O(5) and OH(2) – OH(6), while intermolecular hydrogen bonds can be established between the groups OH(6) – OH(3). The possibility of so many hydrogen bonds allows the polymer chains to adopt *parallel* and *linear conformation*, in a *twisted-ribbon* shape[56–58,62,65,87] as seen in Figure 2.5.
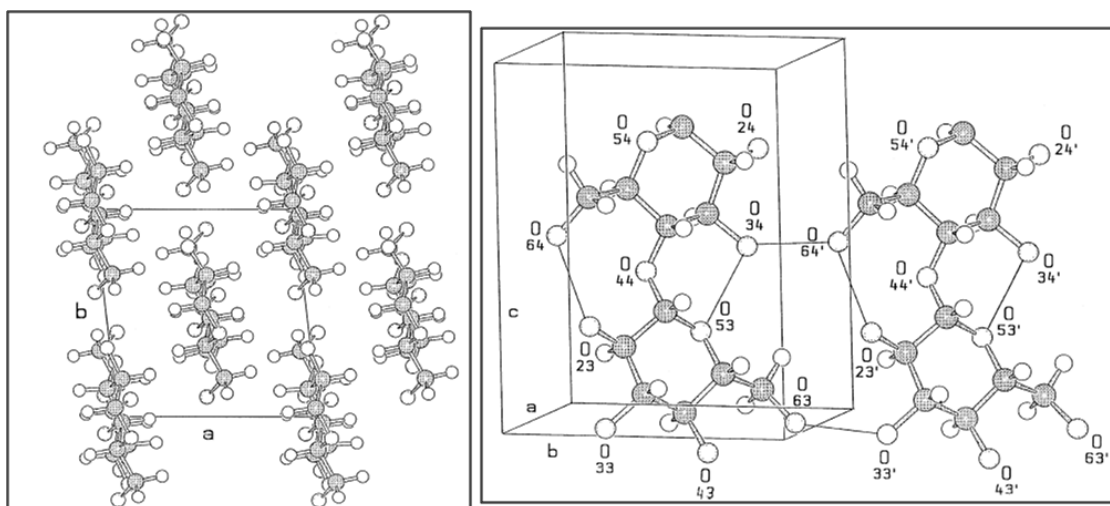
Figure 2.5 Spatial representation of the structure of cellulose I$_\beta$. To the left is the a-b plane showing the polymer chains in a parallel stacking. To the right the intra and intermolecular hydrogen bonds are represented by thin continuous lines (adapted from ref.62).

The presence of these hydroxyl groups provides to the cellulose surface a high degree of hydrophilicity.[59,64,66,73] The reactivity of different hydroxyl groups towards chemical modifications is not the same, though. Horii[65] placed the order of reactivity as OH(2) > OH(6) > OH(3). The degree of substitution (DS) of the hydroxyl groups vary from zero (no substitution of any hydroxyl groups) to three (all the hydroxyl groups are substituted).

It is this "microcrystalline" lattice adopted by cellulose polymer chains (and its derivatives) that allows us to study their structures by X-ray diffraction technique.[52,55,56,59,60,62,65,66,78,79,86–89] The "twisted-ribbon" structure adopted by cellulose is due to the presence of intramolecular hydrogen bonds and its crystallinity is responsible for the observed and so desired strength and rigidity for the production of new materials.[52,73] Additional data on cellulose is presented on Table 2.2.[64]

Table 2.2 Physical-chemical data on cellulose (adapted from ref.64)

Density / g cm^{-3}	Refractive Index	Dielectric Constant (at 50 Hz) *	Insulation Resistance / Ω*	Specific Internal Surface / m^2 g^{-1}
1.52 –1.59	1.62 parallel to the fiber axis 1.54 perpendicular to the fiber axis	2.2 – 7.2	1014 – 1017	10 – 200
Heat of Combustion / kJ g^{-1}	**Heat of Crystallization / kJ mol^{-1} of glucose**	**Specific Heat / J g^{-1} K^{-1}**	**Coefficient of Thermal Conductivity / kJ m^{-1} h^{-1} K^{-1}**	**Electric Strength / kV cm^{-1}**
17.46	18.7 – 21.8	1.00 – 1.21	0.255 (loosely packed) 0.920 (compressed)	500
Heat of Wetting / J g^{-1}				
44.8-51.9				

*Highly dependent on humidity conditions

**Taken from references [90,91]

One might assume that cellulose is highly soluble in polar solvents, especially in water given the number of hydroxyl groups on its surface (pointing "out" of the chair structure, on the equatorial position) and the many hydrogen bonds that could be formed with water molecules. The opposite would be held true for nonpolar solvents given the lack of favorable interactions.[57,64,66] Nonetheless this is not the case – cellulose is not soluble in water and it merely goes under swelling. And why is that? It is precisely because the packed crystalline structure adopted by the polymer chains, that is its ability to form intra and intermolecular hydrogen bonds is highly favorable on one hand when it comes to its strength,[55,60,68,84] and also highly unfavorable on the other hand when it is

regarding the solubility matter.[77,79] The degree of substitution of the available surface hydroxyl groups of cellulose is directly related to its solubility and its derivatives'.

2.2.2 (In)Solubility of cellulose in water – physical-chemical aspects and the importance of hydrophobic interactions

Considering cellulose as a nonionic polymer, on one hand the kinetic factor presents a high impact on the solubility of the polymer chains because water diffusion to the interstices is hindered by the high crystallinity level of cellulose. On the other hand the thermodynamic parameters do not contribute favorably: the enthalpic term is positive ($\Delta H > 0$) and the entropic term is negative ($\Delta S < 0$). The β linkage stabilizes its structure by stiffening it, causing a decrease in the translational entropy of the polymer chains, which contributes to insolubility. When analysing both kinetic and thermodynamic approaches, we observe that they have one thing in common: hydrogen bonds.[57,92]

That being said there would be two ways of increasing the solubility of cellulose: **a)** use of a solvent that could break or hinder intermolecular hydrogen bonds and/or **b)** derivatization of the hydroxyl groups in order to modify/reduce the crystalline packing structure. Two different examples of derivatization would be the modification with methyl groups ($-CH_3$) to obtain *methyl cellulose* (MC), that possesses a reduced polarity due to lowering the number of hydrogen bonds in comparison with cellulose and yet is soluble. Another modification would be with *hydroxypropyl* groups ($-CH_2$-$CH(OH)$-CH_3) resulting in *hydroxypropyl cellulose* (HPC) where the number of hydrogen bonds remains the same as cellulose and is also soluble. Cellulose derivatives present a **LCST** (**L**ower **C**ritical **S**olution **T**emperature) behavior:[76,80,81] which means that their solubility increases when the temperature decreases (LCST for MC lies in the range of 60-80 ºC and for HPC it is in the range of 41-46 ºC)[93–96]

Another important feature is the amphiphilic nature portrayed by cellulose – it has a high hydrophilic surface and also the glucopyranose rings in the chair conformation that renders some degree of hydrophobicity. Some authors[52,54,55,64,92] not only mention this important feature but they also present a fair amount of discussion pointing that cellulose can form organized structures in a self-assembled way, similar to what is observed for surfactants and the formation of micelles. This self-assembly

phenomena would come from the segregation of the hydrophobic regions from the aqueous environment, thus maximizing the interactions among the polymer chains, exposing the hydroxyl groups towards the water. The combination of hydrophobic interactions and the crystalline domains due to hydrogen bonds are responsible for a decrease in the total free energy of the system. A good visual example that highlights the aforementioned statement is showed in Figure 2.6, a computer simulation model of cellulose I$_\beta$ crystal.
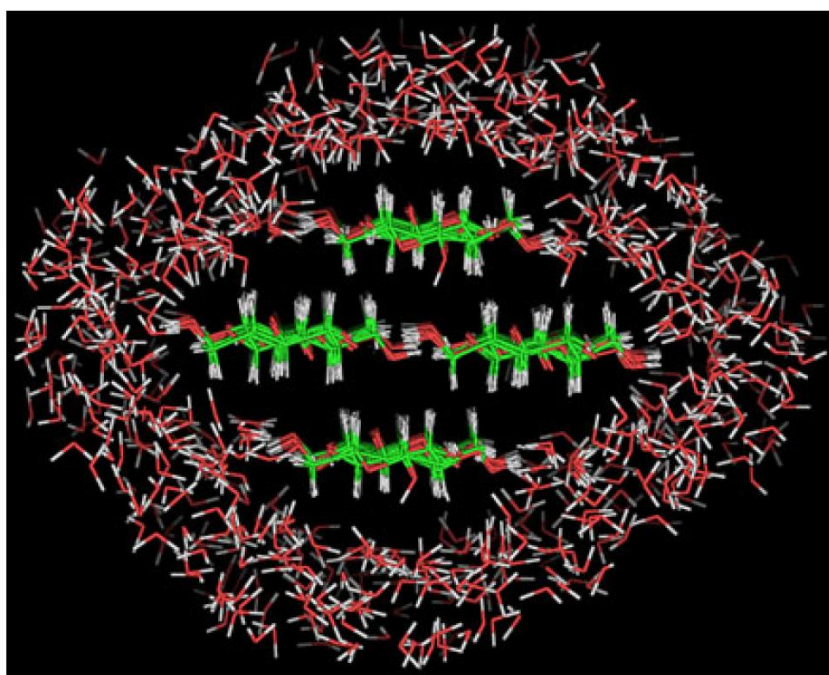
Figure 2.6 Computer simulation model of a 4 chain cellulose I$_\beta$ crystal with hydration layers (taken from reference 92).

It is extremely important to point out the presence of amorphous regions that are found in between the crystalline domains and on the surface of the microfibrils[55,57,66] regarding enzymatic attacks, chain strength/stiffness and, solubility.[51,53,57,60,68,84] The chemical reactivity of cellulose when going through processes such as, hydrolysis, oxidation, derivatization and swelling has a direct correlation. All the aforementioned processes start on the surface due to the possibility of cellulases, water, acids and bases to attack and later penetrate the inner polymer chains and then alter the general structure. Studies performed by Hidayat and coworkers,[53] and Henriksson and coworkers,[68] showed that the enzymatic attack of cellulose fibrils takes place and is more favorable at the amorphous regions, which in turn is responsible for weakening

and obtaining cellulose microfibrils, without the use of any special solvents. Stephens and collaborators[84] came up with a different approach by using hydrochloric acid (HCl) to hydrolyze the amorphous regions. The reaction was followed by using electrospray ionization-mass spectroscopy (ESI-MS) and gel permeation chromatography (GPC) techniques where they could analyze that the velocity of reaction is fast while the amorphous region is broken down, and it then decreases when the attack moves towards the crystalline domains.

The removal of the amorphous regions leads to a final product of high interest that has been extensively researched in the past decades. This product is known as cellulose nanocrystals (CNC) and we are going to discuss and focus about it in the next pages.

2.3 Cellulose Nanocrystals (CNC)

The removal of the amorphous regions of cellulose leads to a final product of growing interest that has been extensively researched in the past decade known as cellulose nanocrystals (CNC). The acid hydrolysis conditions (temperature, reaction time, cellulose source) are key factors in the obtained CNC. Whether it is obtained by using sulfuric, hydrochloric or phosphoric acid.[1] will also have an impact on the final colloidal stability of CNC. Not only will the acid attack and remove the amorphous regions of cellulose, it will also render some negatively charged groups on the CNC surface, most commonly being sulfate-ester groups (OSO_3^-), that are randomly distributed on the CNC surface. On average, there would be one sulfate-ester group per each cellobiose unit.[25] This can be seen in Scheme 2.1. adapted from Habibi and coworkers.[2] The crystalline structure of CNC remains intact as seen by the presence of intramolecular hydrogen bonds (in blue).
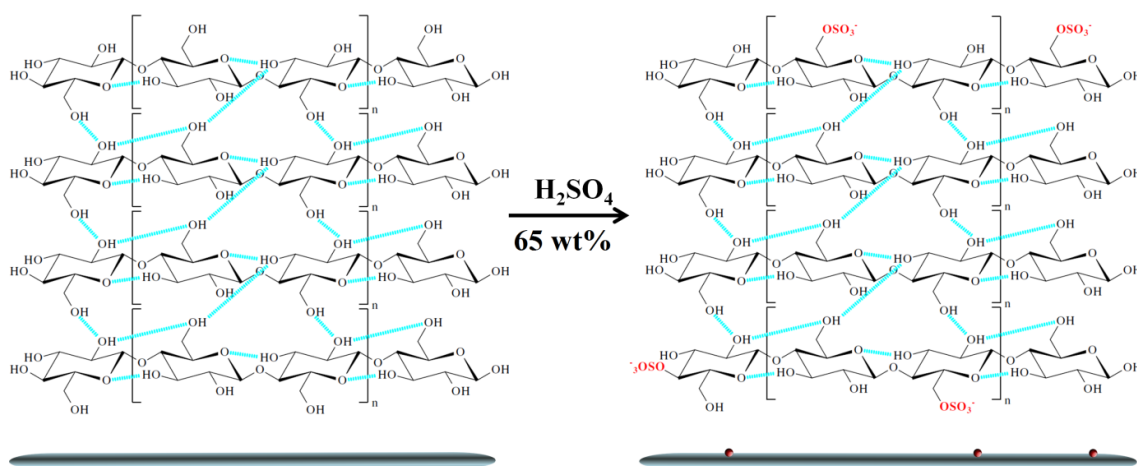
Scheme 2.1 Representation of sulfuric acid hydrolysis of cellulose (left) to obtain cellulose nanocrystals (right). Only the crystalline domains are charged with ester-sulfate groups and they are represented as rods (bottom) in this Scheme.

2.3.1 CNC properties

CNC is a renewable and nontoxic biopolymer, that presents a rod-like structure (that is sometimes named as needle-like or whisker)[12] and its aqueous solutions display colloidal stability.[3] This stability arises from the presence of sulfate-ester groups, which in turn render it an average zeta potential of -47 mV in water.[97] It is important to keep in mind that the zeta potential values will vary with depending on the source and the way the CNC are obtained.

One of the many features of the high crystallinity of CNC is reflected on its specific Young's Modulus (ratio of Young modulus/density): 85 J g^{-1} against 25 J g^{-1} for steel.[7] This crystallinity is also reflected on the occasional swelling behavior when in aqueous solutions.[9,98]

CNC has a high surface area (100-1000 of m^2 g^{-1})[12,14,15] and a high aspect ratio (length/diameter ratio) ranging from 3 to 150,[99] that is closely related to the source that it is obtained from (cotton = 20, bacterial = 10 – 20, tunicate = 50 , ramie = 10, sisal = 43)[2,21] (**Figure 2.7**).This physical aspect counteracts its colloidal stability for the rods would have a tendency to agglomerate in order to reduce such feature.[3,18,19] The main techniques that are used to directly determine the CNC particle size parameters are microscopy ones: transmission electron microscopy (TEM),[17,100] scanning electron microscopy (SEM),[33] and atomic force microscopy (AFM).[14,101] Light scattering

techniques such as dynamic and static light scattering (DLS and SLS)[12,102] can also be used to indirectly measure the CNC dimensions.
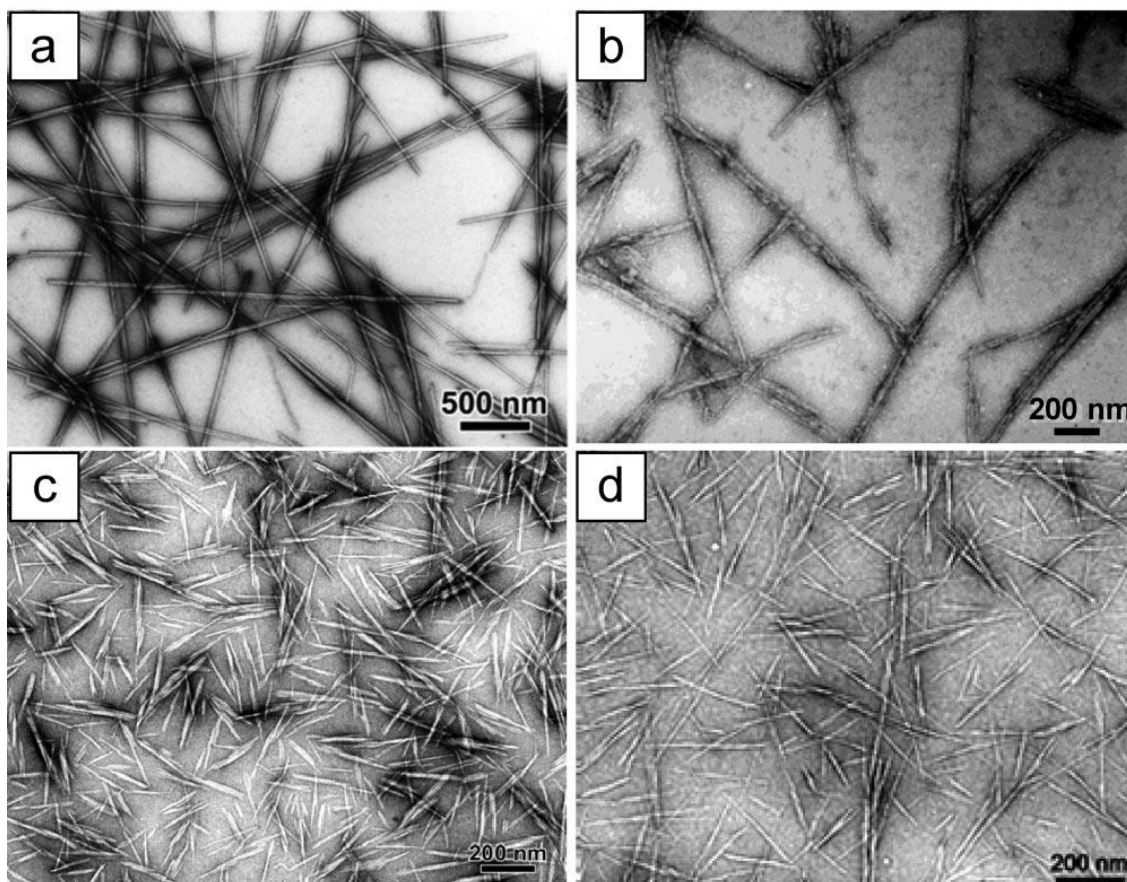
Figure 2.7 TEM images of CNC derived from different sources: a) tunicate; b) bacterial; c) ramie; d) sisal (Taken from reference 2 - reproduced with permission from ACS)

2.3.2 Surface modification

The presence of hydroxyl groups on the CNC surface renders it a hydrophilicity that is disadvantageous in nonaqueous solutions, such as THF (tetrahydrofuran) for instance. However, the same hydroxyl groups can be functionalized via different routes and chemistries[7,103,104] that will enhance the use of CNC in many applications. These modifications can be either physical or chemical.[103]

A few chemical derivatization are showed in **Figure 2.8**.[7] Not only CNC can be modified with different chemical functions, it can also be modified with different types of polymers, with different lengths and architectures. From this perspective, CNC derivatives can respond to different stimuli such as pH,[105–107] and temperature.[38,108,109]

Silylation is one of the examples of a derivatization that allows CNC to be dispersed in THF, as demonstrated by Goussé et al.[110] Nagalakshmaiah and co-workers[111] were able to modify the CNC with a quaternary hexadecyltrimethylammonium surfactant ($C_{16}TA^+$) and use it as a filler into a hydrophobic polymer matrix of poly (propylene), PP. In an earlier study performed by Araki et al.[112] it was reported that even the modification with PEO chains, a hydrophilic polymer, can render CNC to be dispersed into nonpolar solvents.
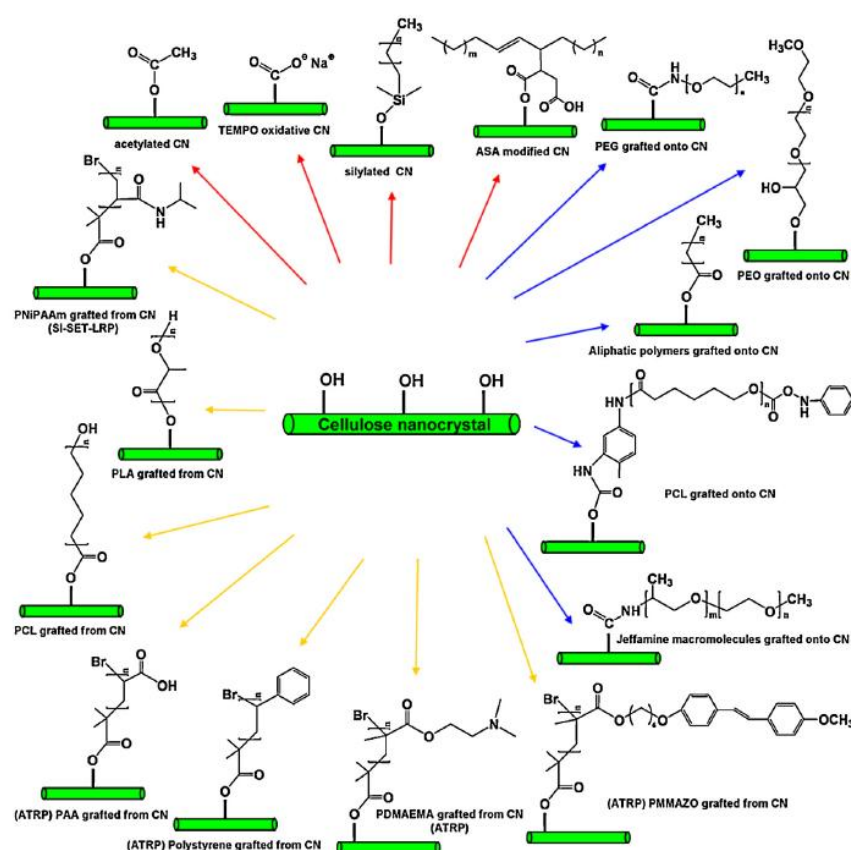
Figure 2.8 Surface derivatization of CNC via different chemistries (taken from reference 4).

2.3.2.1 Surface modification with thermoresponsive polymers

Polymer chains that undergo a change in their conformation (from a coil to globule structure)[95,113] when triggered by temperature, are known as thermoresponsive. This process is related to the dehydration of the polymer chains and release of water molecules to the bulk solution and is characteristic of an endothermic process.[114,115] This phase transition could be achieved most commonly by an increase in the

temperature, where we have LCST behavior, or by a decrease in the temperature, a **UCST** (**U**pper **C**ritical **S**olution **T**emperature)[116,117] behavior.

Grafting of thermoresponsive polymers onto the CNC surface has been performed by a few groups. Peng et al.[35] grafted a polypropylene glycol (PPG) derivative on the CNC surface (CNC-*g*-M600) that presented a LCST of 55 ℃ and studied it in the presence of surfactants. Grishkewich and co-workers[108] grafted poly (oligoethylene glycol) methyl ether acrylate (POEGMA) with varying length chains on the CNC surface. They observed that the LCST of the grafted chains were lower than the ones observed for the free polymers, and this phenomena could be tuned by varying the grafted polymer chain lengths,(Figure 2.9) in the same way as it was observed by Lutz et al.[118] Yi and co-workers[109] modified the CNC surface via atom-transfer radical polymerization (ATRP) with poly(N,N-dimethylaminoethyl methacrylate) (PDMAEMA), which is both a pH and thermoresponsive polymer. They observed a thermal-dependent fingerprint behavior with polarized optical microscopy (POM) on the CNC-*g*-PDMAEMA. Tang et al.[26] examined the potentials of the CNC-*g*-PDMAEMA system for applications in Pickering emulsions.
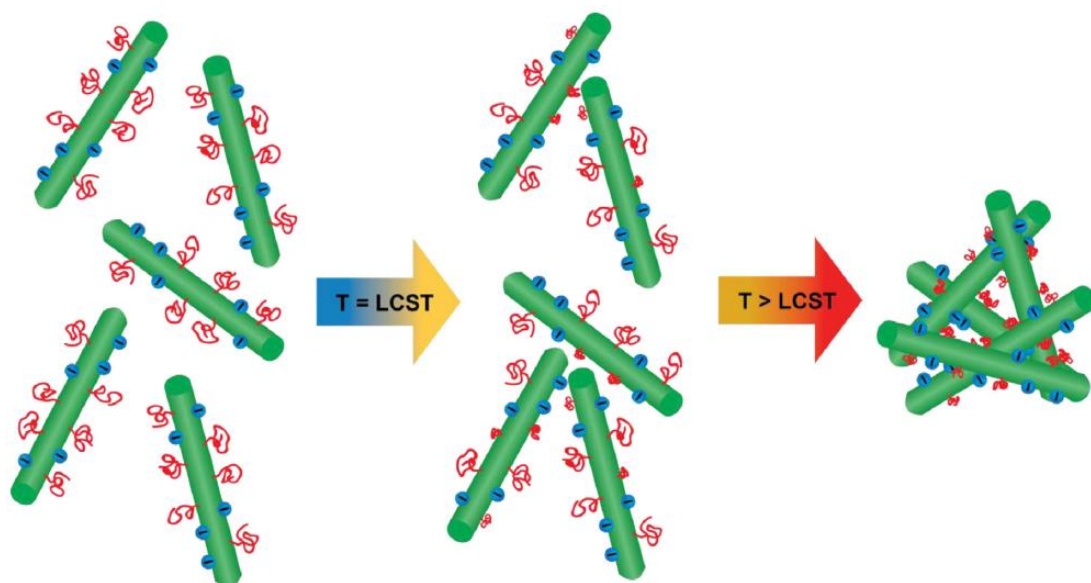
Figure 2.9 CNC grafted with a thermoresponsive polymer POEGMA and its proposed phase separation mechanism (taken from reference 108).

2.3.2.2 Surface modification with pH responsive groups

Among the many types of stimuli that could trigger different phenomena such as phase transitions, swelling behavior, precipitation, and molecular recognition, pH is one of the most important stimuli. Systems that are pH-responsive have been used in many applications such as Pickering emulsions,[119,120] hydrogels,[96,121] and biorecognition.[122] The most common group to respond to pH is comprised of amine-derivative groups, due to their protonation in acidic medium and deprotonation in basic medium.

The surface modification of CNC with amine groups has gained an increased interest in the past few years (Figure 2.10). Kan and co-workers[105] used free radical polymerization with ceric (IV) ammonium nitrate (CAN) to graft poly (4-vinylpyridine), P4VP onto CNC and observed a reversible flocculation behavior in their system. Akhlaghi et al.[107] grafted amine groups onto CNC (CNC-NH$_2$) via a two step process: ring opening with epichlorohydrin (EPH) to produce 2-hydroxy-3-chloro propylamine (HCPA), followed by etherification of HCPA onto CNC. Zhou and co-workers[122] functionalized CNC with two different groups for selective recognition of cognate lectins: carbohydrate ligands and quinolone fluorophores.
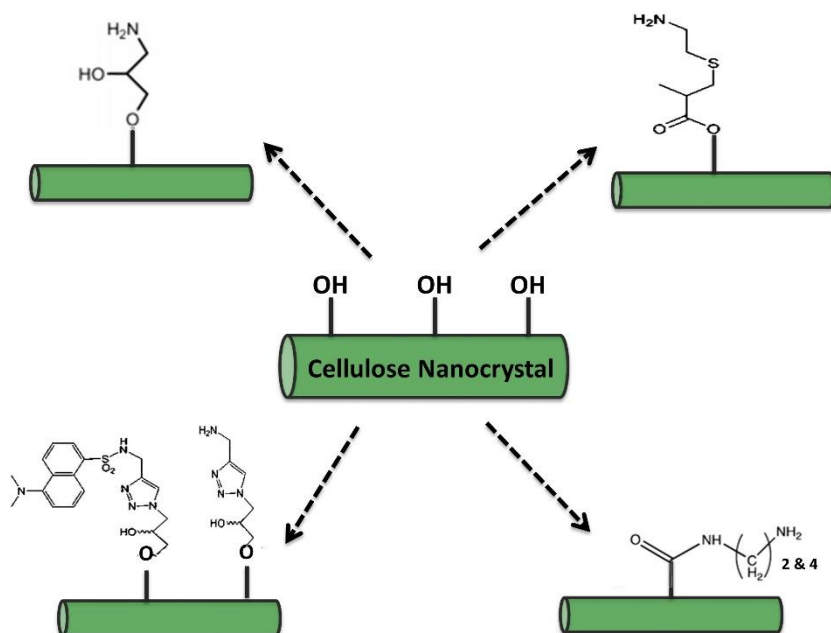
Figure 2.10 CNC surface modification with pH-responsive amine groups (taken from reference 123).

2.3.3 Applications

As it happens with cellulose, the uses of CNC can be limited unless it undergoes surface modification.[104] As mentioned in the previous section the hydroxyl groups on the surface of CNC can be modified into different groups in order to achieve different applications such as, compatibility with nonpolar matrices,[29,32,100,111,124,125] biorecognition,[28,122] drug delivery,[126] nanocomposites,[29–31,127] Pickering emulsion,[22,24–26] hydrogels,[128] supercapacitors,[34] present optical properties,[33,129] and microfiltration systems,[130,131] to name a few (Figure 2.11).
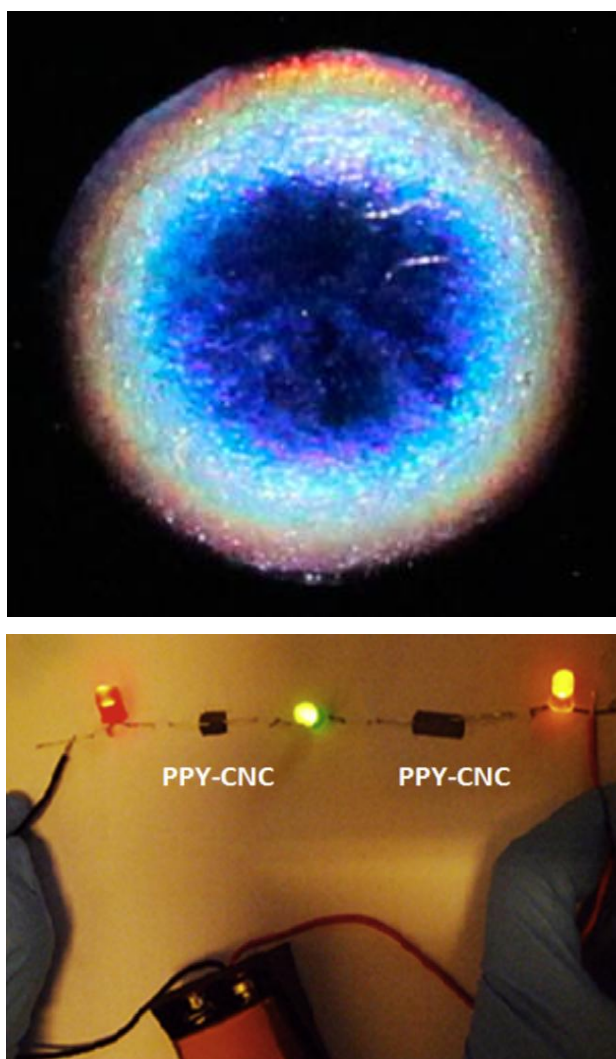
Figure 2.11 Different applications of pristine CNC and its derivatives. Top: pristine CNC with added D-(+)-glucose forming a chiral nematic film (taken from reference 13). Bottom: modified CNC with poly (pyrole) (PPY-CNC) working as supercapacitor (taken from reference 34).

Chapter 3: Structural and Energetic Studies on the Interaction of Cationic Surfactants and Cellulose Nanocrystals†

My contributions to this paper

Performed all the experiments except for surface tension and settling behavior and wrote the paper.

Abstract

We report a comprehensive study on the interactions between cationic surfactants homologues C_nTAB (n = 12, 14 and 16) with negatively charged cellulose nanocrystals (CNCs). By combining different techniques, such as isothermal titration calorimetry (ITC), surface tension, light scattering, electrophoretic mobility, and fluorescence anisotropy measurements, we identified two different driving forces for the formation of surface induced micellar aggregates. For the $C_{12}TAB$ surfactant, a surfactant monolayer with the alkyl chains exposed to the water is formed via electrostatic interactions at low concentration. At a higher surfactant concentration, micellar aggregates are formed at the CNC surface. For the $C_{14}TAB$ and $C_{16}TAB$ systems, micellar aggregates are formed at the CNC surface at a much lower surfactant concentration via electrostatic interactions, followed by hydrophobic interactions between the alkyl chains. At higher surfactant concentration, charge neutralization and association of the surfactant decorated CNC aggregates led to flocculation.

3.1 Introduction

Cellulose nanocrystal (CNC) is a renewable, biodegradable, practically non-toxic, and rod-shaped nanomaterial commonly obtained by sulfuric acid hydrolysis from the world's most abundant natural polymer, cellulose. While the amorphous regions are removed during the hydrolysis process on native cellulose, the original crystalline domains are retained showing reinforcing capabilities, high mechanical strength

---

(Young's modulus of 100-130 GPa), low density (1.566 g cm^{-3}), high aspect ratio and high surface area of hundreds of m^{2}g^{-1}.[2,7,12,14,25,55,97] The substitution of some of the hydroxyl groups by sulfur-ester groups derived from acid hydrolysis imparts electrostatic stabilization in aqueous solutions.[3,37] Surface modification can be performed on the available primary hydroxyl groups to not only provide steric stabilization, but to broaden its applications in areas such, as drug delivery,[28,106] thermo and pH-responsive polymers,[26,109] nanocomposites,[21,30,31,33] and supercapacitors.[34]

Because CNC is a negatively charged particle, it is expected to strongly interact with cationic surfactants via electrostatic interactions in a similar fashion as observed with polyelectrolytes.[132–134] The difference is that CNC is a rigid rod-shaped particle, and it does not present the same flexibility as a polymer chain. Nonetheless, some important thermodynamic parameters such as critical concentration aggregation (*cac*), associated with the particle-induced micellization process,[135] and a second critical aggregation concentration (C_2) where the particle becomes saturated, after which only the formation of unbound micelles in solution are observed.[39]

Isothermal titration calorimetry (ITC) can be used to elucidate the behavior and stability of CNC in aqueous solutions in the presence of oppositely charged molecules, such as cationic surfactants. The use of ITC has proven to be a straightforward way of measuring the energy of interactions between mixtures containing surfactants and polymers.[35,36,39,135–137] Calorimetric data can also provide valuable information on the thermodynamics of the association process.[39,135] Once the concentration of the species is known during the titration experiment, different experimental conditions such as changes in temperature and ionic strength along with ancillary techniques such as surface tension, light scattering, and electrophoretic mobility provide further information on the system.

The interactions between ionic surfactants and cellulose fibers and their derivatives have been reported.[138–140] In a study performed by Alila et al.[138] the interactions between carboxylic acid modified cellulose and a homologous series of alkyltrimethylammonium bromides (C$_n$TAB) showed the influence of the alkyl chain length of the surfactants on the aggregation process. By using a surfactant-selective electrode, they observed that an increase in the alkyl chain length from 12 to 18 carbon atoms led to a transition from surfactant monolayers adsorbed onto the cellulosic fibers, named hemimicelles, to bilayers named admicelles. Ghoreishi et al.[139] studied the interactions between ethyl (hydroxyethyl) cellulose (EHEC) and two cationic

surfactants with an alkyl chain of 14 carbon atoms but different headgroups using surfactant-selective electrode and ITC. Wang et al.[140] also studied the interactions between EHEC and $C_{14}TAB$ using ITC and viscosity.

Recently, the focus has shifted to studying mixtures containing surfactants and CNC and its derivatives.[25,37,125] A recent report by Dhar et al.[36] showed that the colloidal stability of CNC in water decreased in the presence of $C_{14}TAB$. As well, the CNC-surfactant mixture displayed interfacial activity at a surfactant concentration below the surface induced micellization concentration, a process similar to a polymer-induced aggregation. Peng et al.[35] studied the interactions of a polymer-grafted CNC with ionic and nonionic surfactants. They observed electrostatic interactions between $C_{12}TAB$ and the sulfate-ester groups on the CNC surface; hydrophobic interactions were observed between sodium dodecylsulfate (SDS) and the polymer while no interactions were recorded with the nonionic Brij 30. In a recent publication, Cranston and coworkers[25] studied the binding of two cationic surfactants (with one and two alkyl chains) to CNC, showing that they could change the particle surface properties and affect their tendency to stabilize Pickering emulsions. This study revealed that the hydrophobicity of CNC aggregates can be varied depending on the type and amount of bound surfactant molecules, which has shown to determine whether oil-in-water (o/w) or water-in-oil (w/o) emulsions are favored, similar to the HLB (hydrophilic-lipophilic balance) principle.

In this paper, we present a comprehensive study on the interaction of a homologous series of alkyltrimethylammonium bromides and CNC at three different temperatures, in water and in the presence of electrolytes, and at a wide surfactant concentration range. We combined data from ITC, surface tension, light scattering, electrophoretic mobility and fluorescence anisotropy measurements to elucidate the nature of these interactions, and the results revealed that the mode of surfactant binding to negatively charged CNC varies with their hydrophobicity.

3.2 Experimental Section

3.2.1 Chemicals

The alkyltrimethylammonium surfactants C_nTAB (n = 12, 14, 16), hexadecylpyridinium bromide, $C_{16}PyB$, and hexadecyltrimethylammonium chloride,

$C_{16}TAC$, were purchased from Sigma-Aldrich® (≥ 98% purity). Cellulose nanocrystal (CNC) hydrolyzed from wood pulp was provided by CelluForce Inc. NaBr was purchased from Synth® (98% purity). All the chemicals were used without further purification. ANS (5-dimethylamino-1-naphtalenesulfonic acid hydrate) (> 99% purity, Sigma-Aldrich®) was a kind gift from Prof. Frank Quina (USP – São Paulo). The water used to prepare all solutions was of Milli-Q grade (18.2 $M\Omega cm^{-1}$).

3.2.2 CNC samples preparation

A 2.0 wt% CNC stock dispersion was prepared by ultrasonication with Hielscher UP100H equipment (Germany), using a MS3 sonication probe, and later kept in the refrigerator. All the other dispersions of 0.1 wt% were prepared from the stock dispersion by simple dilution. Desulfation of CNC was performed according to a method described by Lokanathan et al.[17] using NaOH solutions of 0.25 and 0.50 mol L^{-1}. The CNC dispersions were kept under magnetic stir and were heated up to 65 ºC for 30 minutes. After this, 0.25 and 0.50 mol L^{-1} HCl was added to the dispersions in order to neutralize the NaOH in solution. The dispersions were then dialyzed against deionised water for three days. These desulfated CNC samples are denoted, respectively, as $d_{0.25}$ and $d_{0.50}$-CNC in the text. For the experiments in the presence of electrolytes, NaBr was chosen in order to avoid the presence of a different third counterion.

3.2.3 Isothermal Titration Calorimetry

The calorimeter used was the MicroCal VP-ITC (Northampton, MA, USA). Aliquots ranging from 3 to 15 μL were added stepwise by an automatic injection syringe containing 270 μL of a concentrated surfactant solution (typically at least ten times above their *cmc* values) into the reaction cell of 1.43 mL containing either water or CNC dispersion with a 5 min interval between each injection. The dilution effects for the titration of water into CNC dispersion were negligible. Three different temperatures were used in the experiments: 25, 45 and 55 ºC. In the case of C16TAB the lower temperature used was 28 ºC to ensure being above its Krafft point, which is near 25 °C. Experiments at a lower CNC concentration (0.01 wt%) and in the presence of NaBr

25.0 mmol L^{-1} solution were performed only at room temperature. All the experiments were performed at least in duplicate. Data obtained were treated with the Origin® 7.0 software.

3.2.4 Surface Tension Measurements

The experiments were conducted using a Data Physics DCAT 21 at 25 ℃ for $C_{12}TAB$ and 28 ℃ for $C_{16}TAB$. Small aliquots of surfactant were added to water for the control samples and to 0.1 wt% CNC dispersions under stirring. The method used was the Wilhelmy plate to measure the dynamic surface tension. All the experiments were performed in duplicate.

3.2.5 Electrophoretic Mobility and Particle Size Determination

Electrophoretic measurements were carried out using a NanoZS Zetasizer (Malvern Instruments). It uses a M3-PALS technique – a combination of phase analysis light scattering and laser Doppler velocimetry. The CNC concentration was fixed at 0.1 wt% while varying the surfactant concentration. When measuring high concentrated surfactant solutions only the $\mu\zeta$ sign is relevant, for there is a contribution from both the C_nTAB-CNC complex and the bulk micelles.[141] For particle size determination (detection angle of 173º), the apparent hydrodynamic diameter (d_H) was measured in the presence of NaBr 1.0 mmol L^{-1}. The experiments were performed at 25.0 ± 0.1 ℃ for $C_{12}TAB$ and $C_{14}TAB$, and 28 ± 0.1 ℃ for $C_{16}TAB$. All the experiments were performed in triplicate.

3.2.6 Turbidity Measurements

Transmittance measurements were carried out on an 8453 Spectrophotometer (Hewlett-Packard), equipped with a Peltier system, at a wavelength of 600 nm. CNC 0.1 wt% dispersions were titrated with a surfactant solution under stirring (700 rpm).

3.2.7 Fluorescence Anisotropy Experiments

The equipment used was a Fluorolog-3 spectrofluorometer (Horiba FL3-22-iHR320), with a quartz cuvette of 1 cm length used in all experiments. All measurements were performed at 25 ℃. ANS (5-dimethylamino-1-naphthalenesulfonic acid hydrate) was used as a fluorescent probe, with a constant concentration of 5.0 µmol L^{-1}. Previous experiments indicated that ANS fluorescence intensity was affected by its interaction with the cationic surfactants (results not shown). Therefore, we decided to focus on its fluorescence anisotropy instead to verify the presence of surfactant aggregates. The excitation wavelength was 320 nm, and the emission wavelength was obtained from 380 to 700 nm. All the experiments were performed with polarizers in the vertical (I_{vv}) and horizontal (I_{vh}) positions, in order to measure the fluorescence depolarization of ANS. The fluorescence anisotropy can be described as:[142,143]

$$r(t) = \frac{I_{vv}(t) - I_{vh}(t)}{I_{vv}(t) + 2I_{vh}(t)} \qquad \text{Equation 3.1}$$

Where I_{vv} and I_{vh} are the polarized components parallel and perpendicular to the incident light direction respectively.

3.3 Results

3.3.1 Isothermal Titration Calorimetry Measurements

Figure 3.1 shows the calorimetric curves for the addition of C_nTAB to CNC dispersions, along with the surfactant titration in water, for comparison. The C_nTAB *cmc* values were obtained by the first derivative method[39,135] from the dilution curves (open symbols) providing the following results: $C_{12}TAB$ (16.0 mmol kg^{-1}), $C_{14}TAB$ (4.0 mmol kg^{-1}) and $C_{16}TAB$ (1.0 mmol kg^{-1}), in accordance with previous reports.[144–147] To analyze the effect of both the alkyl chains and the temperature in the interaction and due to the fact that the *cmc* differs drastically for the homologous series, the concentration axis was normalized as a function of the *cmc* for each surfactant (C_T/cmc). We focused our attention on the more hydrophilic $C_{12}TAB$ and the more hydrophobic $C_{16}TAB$ surfactants due to the fact that some results with a mixture of $C_{14}TAB$-CNC were previously reported.[36]

All the curves in the presence of CNC display a similar trend that is much clearer for $C_{16}TAB$ than for the other surfactants: there is an endothermic reaction above the dilution curve at a low surfactant concentration up to approximately 0.15 *cmc*. After this point, there is a pronounced plateau for $C_{12}TAB$ (0.15-0.5 *cmc*), indicating no interaction between the CNC and surfactant (both curves are superimposed). This is followed by a cooperative process corresponding to a surface induced aggregation, with the curves not merging within the studied concentration range. For $C_{16}TAB$, the initial endothermic interaction occurs for a wider surfactant concentration range. At the concentration of 0.30 *cmc* there is a "bump" probably related to a surfactant rearrangement at the CNC followed by a process that seems more cooperative than the one with $C_{12}TAB$.

This type of profile was also reported for other electrostatic complexation studies by ITC involving surfactants or polymers and other colloids.[148] Vitorazi et al.[149] recently reported similar results when studying the interaction between oppositely charged polymers, emphasizing that this bump occurs close to charge neutralization. The observation of this feature in the present ITC curves confirms our hypothesis when assuming a sulfate ester (negative charges) concentration of 0.23 mmol $kg^{-1}CNC^{-1}$, as estimated from earlier reports.[3] The two curves merge at a high surfactant concentration denoting the saturation of the CNC rods and the formation of free unbound micelles in solution. Results for $C_{14}TAB$ are in between those for the other homologues and agree with those previously reported.[36]

Lowering the CNC concentration to 0.01 wt% result in a decreased interaction between the surfactants and CNC (ITC curves shown in Figure A.2 in Appendix A), keeping the same overall features described above.

In order to identify specific contributions from the hydrophobic interaction, we performed ITC experiments at different temperatures because enthalpy values associated with this interaction should vary significantly with temperature. These results are shown in Figure 3.2. To confirm the electrostatic contributions, we added an electrolyte (results shown in Figure 3.3) to partially screen the charges on both CNC and surfactants, and also removed some of the negatively charged sulfate ester groups from the CNC surface by desulfation, therefore reducing electrostatic interactions (results shown in Figure 3.4).
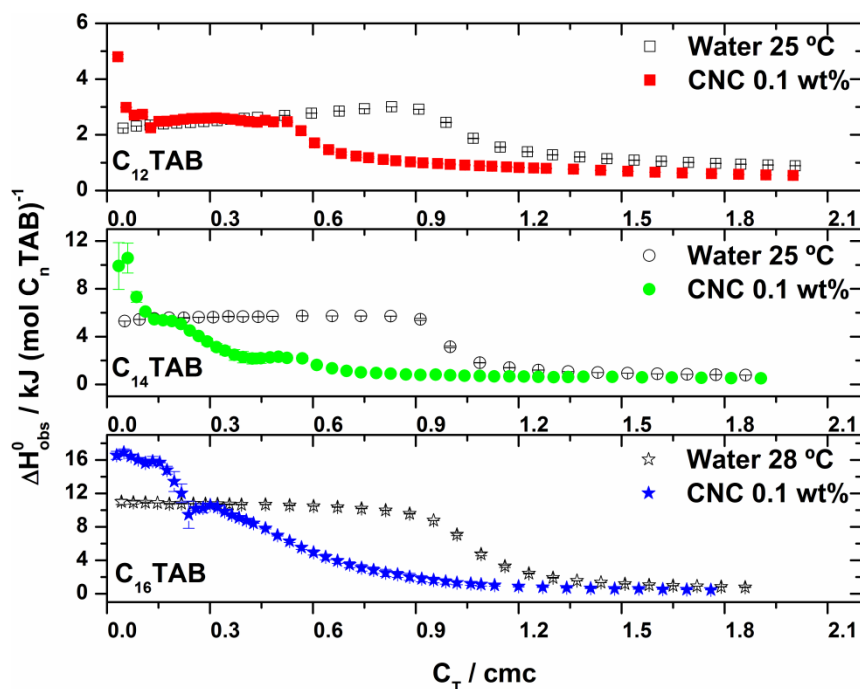
Figure 3.1 Calorimetric titration curves obtained for the titration of C_nTAB into water (empty symbols) and into 0.1 wt% CNC dispersion (filled symbols) at 25 °C for C_{12}TAB and C_{14}TAB, and 28 °C for C_{16}TAB, as a function of normalized surfactant concentration (C_T/cmc).
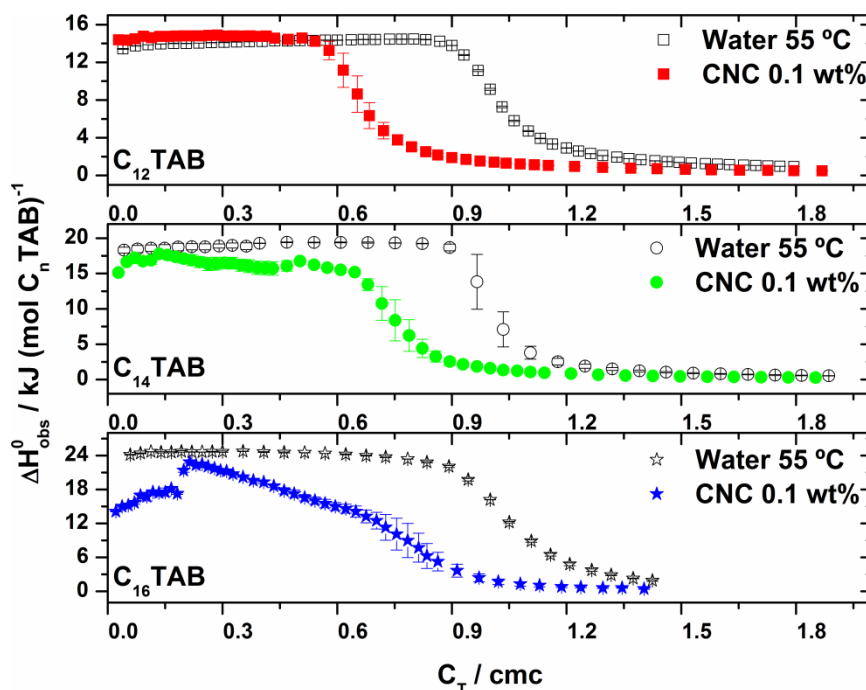
Figure 3.2 Calorimetric titration curves obtained at 55 °C for the titration of C_nTAB into water (empty symbols) and into 0.1 wt% CNC dispersion (filled symbols), as a function of normalized surfactant concentration (C_T/cmc).
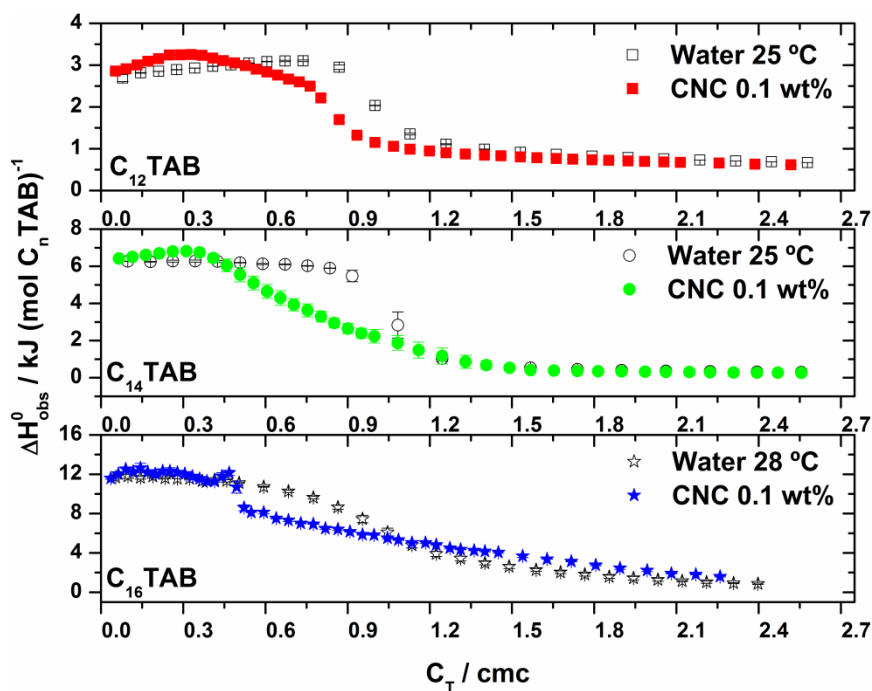
Figure 3.3 Calorimetric titration curves obtained for the titration of C_nTAB into 25 mmol L^{-1} NaBr (empty symbols) and into 0.1 wt% CNC dispersion (filled symbols) in 25 mmol L^{-1} NaBr at 25 °C for C_{12}TAB and C_{14}TAB, and 28 °C for C_{16}TAB, as a function of normalized surfactant concentration (C_T/cmc).
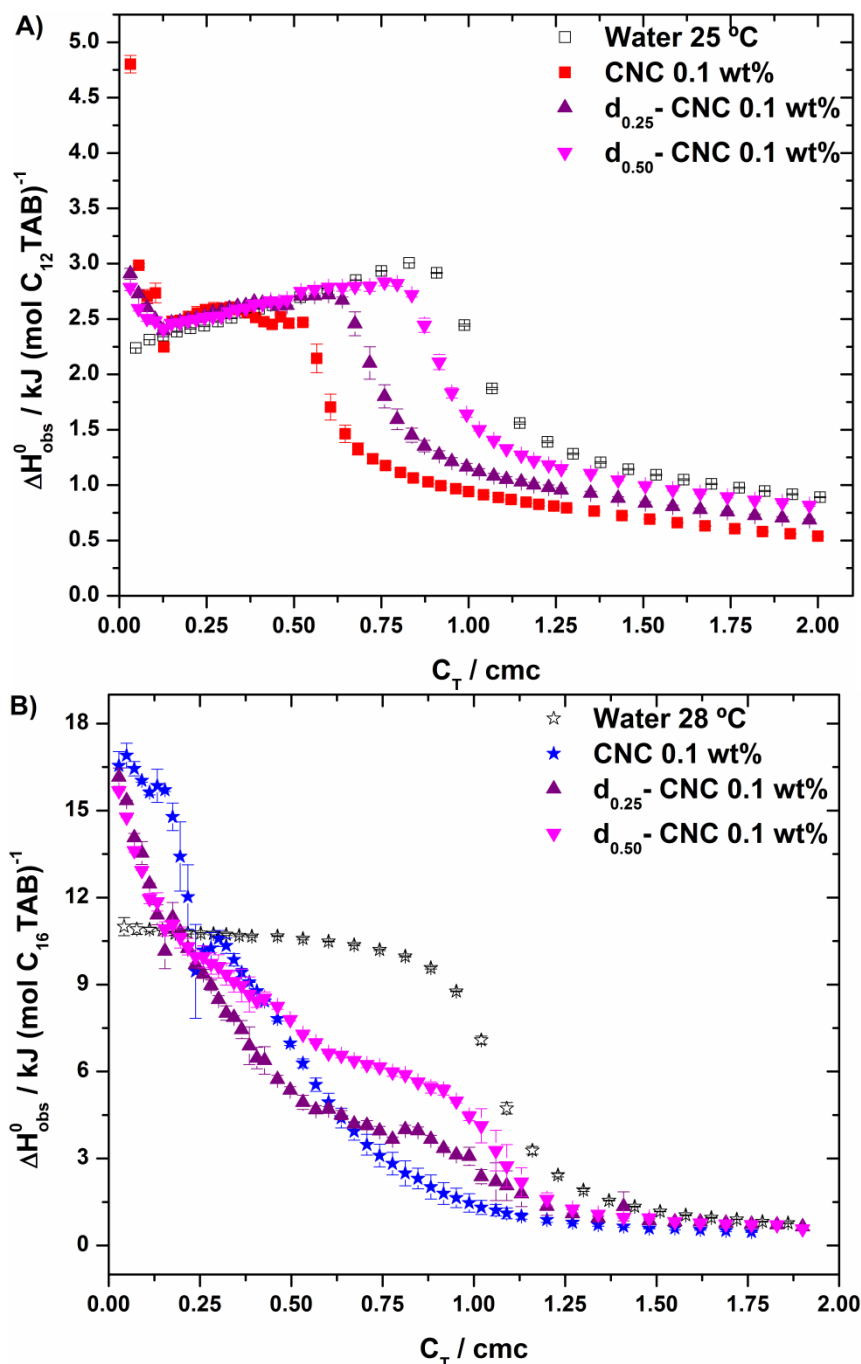
Figure 3.4 Calorimetric titration curves obtained for the titration of C_nTAB into water (empty symbols) and into 0.1 wt% desulfated CNC (d-CNC) dispersions (filled symbols) at 25 °C for $C_{12}TAB$ (A) and 28 °C for $C_{16}TAB$ (B), as a function of normalized surfactant concentration (C_T/cmc).

The temperature increase had a similar effect at low surfactant concentration on all mixtures, with different features (see Figure A.1 for results at 45 °C in Appendix A). It has a more prominent impact on the system containing the more hydrophobic surfactant $C_{16}TAB$, where the initial interaction became dramatically less positive

resulting in a fall below the surfactant dilution curve. Additionally, at a concentration range from 0.3 to 0.9 *cmc*, the interaction became less cooperative, having two different slopes. These results show that hydrophobic interactions are playing a more significant role for the $C_{16}TAB$-CNC mixture. For the system with $C_{12}TAB$, the initial endothermic interaction had almost disappeared with the titration curve in the presence of CNC being slightly more endothermic and shifted to a lower surfactant concentration than the dilution curve.

As for the addition of an electrolyte (NaBr), there is also a decrease in the initial interaction for all surfactants, but it is still endothermic and more positive than the dilution curve. It had more impact on the $C_{12}TAB$-CNC mixture, in which the two curves are almost superimposed. For the $C_{16}TAB$-CNC mixture the "bump" is still present at a concentration of 0.5 *cmc* but with a lower intensity, followed by a continuous decrease of the titration curve in the presence of CNC compared to the dilution curve.

The desulfation of the CNC surface (d-CNC) has a higher impact on the interaction with $C_{12}TAB$ than with $C_{16}TAB$. A higher desulfation degree ($d_{0.50}$-CNC) leads to a lower interaction between $C_{12}TAB$ and CNC, with a shift to higher surfactant concentration of titration curve in the presence of CNC. In the mixture with $C_{16}TAB$ the curve is similar to the one with pristine CNC (Figure 3.1) but instead of a "bump" there is a continuous decrease (lower cooperative process). Experiments performed with $C_{16}PyB$, a cationic surfactant with a pyridinium group instead of a trimethylammonium headgroup, and $C_{16}TAC$ (chloride instead of bromide as the counterion) show the same trend as $C_{16}TAB$ at 28 ℃, corroborating the hypothesis of an ongoing sequential binding process for the more hydrophobic surfactants (see Figures A.3 and A.4 in Appendix A).

3.3.2 Surface Tension Measurements

We performed surface tension measurements in the same concentration range as for the ITC experiments with $C_{12}TAB$ at 25 ℃ and $C_{16}TAB$ at 28 ℃. The dilution curves (empty symbols) present the same behavior with increasing surfactant concentration while the titrations in the presence of CNC (filled symbols) display distinct features. The dotted lines in Figure 3.5 are related to the ITC results at a surfactant concentration where the initial endothermic interaction ends (see Figure 3.1).

The C_{12}TAB-CNC mixture has a lower surface tension than the dilution curve at a low surfactant concentration denoting a more surface active mixture as earlier reported by Dhar et al. for C_{14}TAB.[36] A constant value of 39 mN m^{-1} is reached at a surfactant concentration of 0.40 *cmc*. As for C_{16}TAB there is no difference between the dilution curve and the mixture up to a relative surfactant concentration of 0.22 *cmc* (dotted line in Figure 3.5). After this point the two curves diverge with the C_{16}TAB-CNC mixture showing a higher surface tension than the dilution one. Once a plateau of 39 mN m^{-1} is reached, the same value is obtained for the mixture containing C_{12}TAB. These higher surface tension values agree with the removal of the more hydrophobic surfactant from the air-solution interface and with the formation on non-surface active complexes.
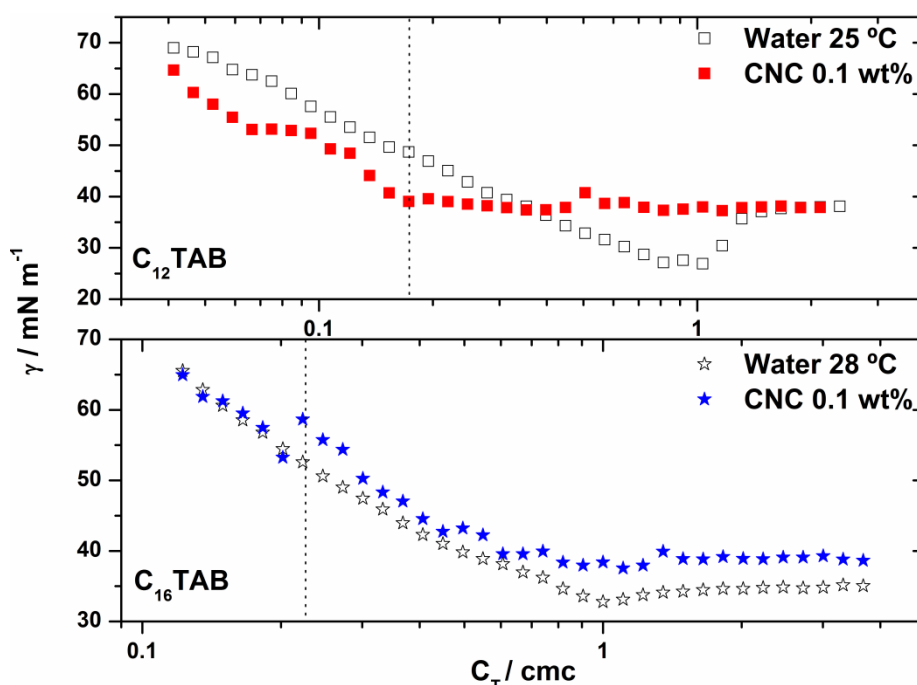
Figure 3.5 Surface tension measurements obtained for the titration of C_nTAB into water (empty symbols) and into 0.1 wt% CNC dispersion (filled symbols) as a function of normalized surfactant concentration (C_T/cmc).

3.3.3 Light Scattering and Particle Size Measurements

For a better understanding on the interactions between C_nTAB and CNC, we fixed the CNC concentration at 0.1 wt% while varying the surfactant concentration within a broader range, in the presence and as well as the absence of NaBr (see Figure A.5 in Appendix A for the images). Interestingly, the same behavior was observed for

all the three surfactants: the mixtures are translucent at very low concentration range (bluish color), followed by sedimentation starting at half the *cmc* value. Also, samples with $C_{12}TAB$ display a higher light scattering intensity than those with $C_{16}TAB$, as can be seen from the brightness of the images (see Figure A.5 in Appendix A for the images). It is expected that an increase in the surfactant concentration in the mixtures above the charge neutralization region would cause particle redispersion due to electrostatic repulsion arising from the surfactant micelles covering the CNC rods. This was not the case here despite the high surfactant concentration (30 times the *cmc* value for $C_{16}TAB$, for instance). We also monitored the settling behavior (see Figures A.7 and A.8 in Appendix A) for the mixtures for 2 months. After 75 hours settling would cease, showing a much clearer phase separation for $C_{12}TAB$ compared to $C_{16}TAB$ (see Figures A.9 and A.10 in Appendix A). For $C_{16}TAB$ samples there appears to be a concentration range around 5 to 10 times its *cmc* where the mixtures might be flocculating but with no visible sedimentation.

The settling experiments were based on visual observation only; therefore the use of a more accurate technique to ascertain the turbidity of the samples was required. We have monitored the transmittance of the samples (Figure 3.6) as an indirect way of measuring particle growth. As mentioned above, there was no sedimentation at low surfactant concentration (not shown in the Figure). The first point corresponds to half of the *cmc* value and the transmittance has decreased considerably following the order C_{12} $< C_{16}$. At the *cmc* region (dotted line on the graphic) there is an increase in the transmittance values, followed by a continuous decrease up to a value of 40%, indicating a particle growth responsible for the settling behavior. Viscosity measurements in this region show no significant difference for the two surfactants with a slight increase in its value due to an increase in the surfactant concentration (Figure A.11 in Appendix A).

Even though at low surfactant concentration there is neither visible change nor observation of sedimentation or flocculation it does not mean the particles are not growing. By using dynamic light scattering measurements, we can estimate the apparent hydrodynamic diameter (d_H) of the scattering particles. These data, shown in Figure 3.7, revealed a significant growth of the particles, from 80.8 ± 0.1 nm (pure CNC) up to 235.0 ± 0.3 nm for $C_{12}TAB$, 97.7 ± 0.4 nm for $C_{14}TAB$ and 139.7 ± 0.2 nm for $C_{16}TAB$, in the region prior to their visual sedimentation.

Considering that these particles assume an anisometric shape, one can relate their diffusion coefficients to their dimensions L and d, respectively to the long and short axes by using Equation 3.2 and Equation 3.3 (valid within $5 < L/d < 30$):[150]

$$D_0 = \frac{k_B T}{3\pi L \eta_0} \left(\ln(L/d) + v\right) \qquad \text{Equation 3.2}$$

$$v = 0.312 + 0.565/(L/d) - 0.1/(L/d)^2 \qquad \text{Equation 3.3}$$

Where k_B = Boltzmann constant; T = temperature; L = length of the rod; d = diameter of the rod; η_0 = viscosity of the solvent.

By substitution of D_0 on the Stokes-Einstein (Equation 3.4) we can obtain the hydrodynamic diameter of the CNC particles to ascertain if they are freely dispersed or aggregated as bundles at the concentration of 0.1 wt% in the absence of surfactant.

$$D_0 = \frac{k_B T}{3\pi \eta_0 d_H} \qquad \text{Equation 3.4}$$

Assuming L = 200 nm and d = 20 nm (L/d = 10) as typical average dimensions for CNC[1225] we obtain a value of d_H = 75 nm for pure CNC, which is close to the one obtained experimentally, confirming there should be no significant aggregation of particles at the 0.1 wt% concentration. The observed increase in CNC particle size must be due to aggregation induced by the presence of oppositely charged surfactants.
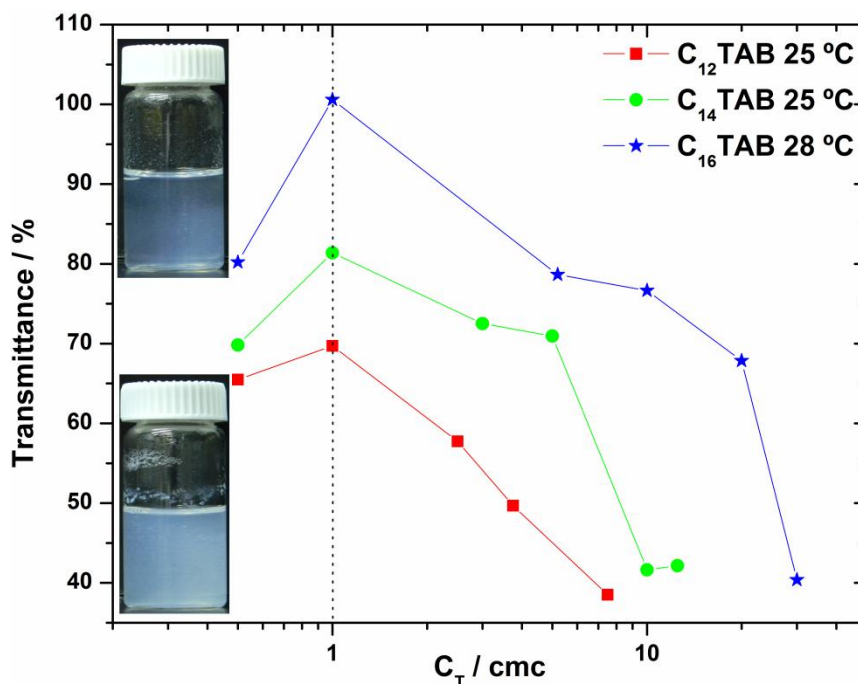
Figure 3.6 Transmittance of CNC-C$_n$TAB mixtures. Visual particle sedimentation starts to occur at half the cmc value (first point), with inset showing the samples with C$_{12}$TAB (bottom) and C$_{16}$TAB (top). Cmc value is denoted by a dotted line.
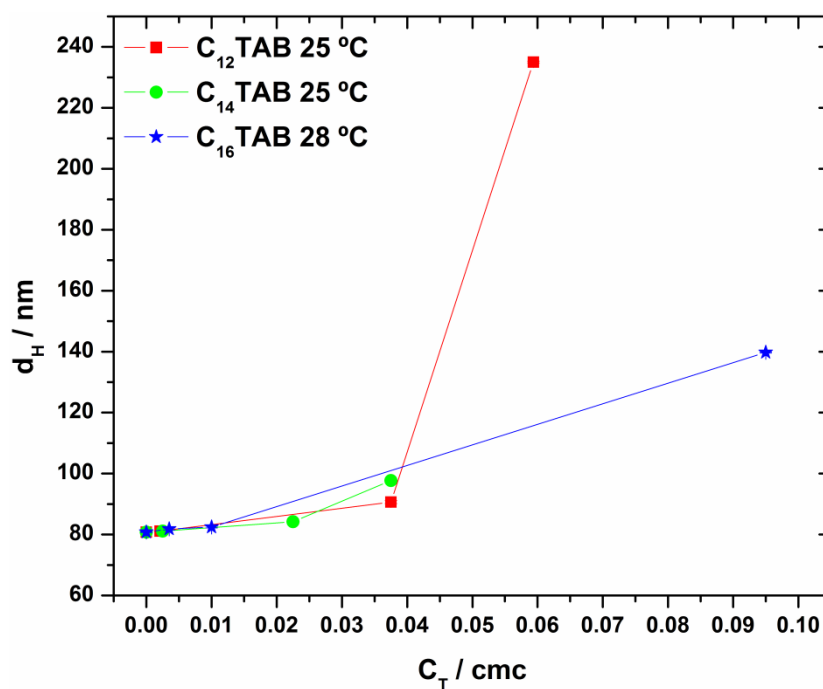
Figure 3.7 Apparent hydrodynamic diameter (d$_H$) for mixtures containing 0.1 wt% CNC dispersions and surfactants at concentrations low enough to avoid sedimentation.

3.3.4 Anisotropy Fluorescence Measurements

Molecular probes can be used to provide information on mobility, flexibility and binding of molecular complexes by measuring the increase or decrease of fluorescence anisotropy.[142,143,151] Small aggregates tumble faster than large aggregates and therefore, should possess higher anisotropy values. If this probe interacts with surfactants bound to the CNC surface, an even greater reduction in the anisotropy values is expected due to a lower mobility of the complex. The fluorescence anisotropy of ANS in the presence of pure surfactant and with C_nTAB-CNC mixtures was measured to gather more information on the structure of the complexes formed (Figure 3.8). The results are shown together with the respective ITC data for the sake of comparison.

In the curves without CNC, there is a sharp decrease in the absolute anisotropy values, with an inflection point close to the *cmc* region that denotes the incorporation of the probe at the micellar surface. In the presence of CNC, the curves are at first superimposed with the dilution curves for all mixtures (the first points are not shown in the Figure 3.8). The absolute anisotropy values in the presence of CNC start to change at lower surfactant concentration with the inflection now close to where the ITC curves indicate the beginning of an endothermic interaction. These results confirm that the interaction of surfactant monomers with CNC starts at low concentration, but it is only at the point where the ITC data indicates an endothermic process that surfactant aggregation at the CNC surface initiates. At a higher surfactant concentration the curves in the presence and in the absence of CNC merge, with both curves displaying anisotropy values close to zero due to the full coverage of the CNC rods by the surfactants as a result of the probe fully incorporated into the aggregates.
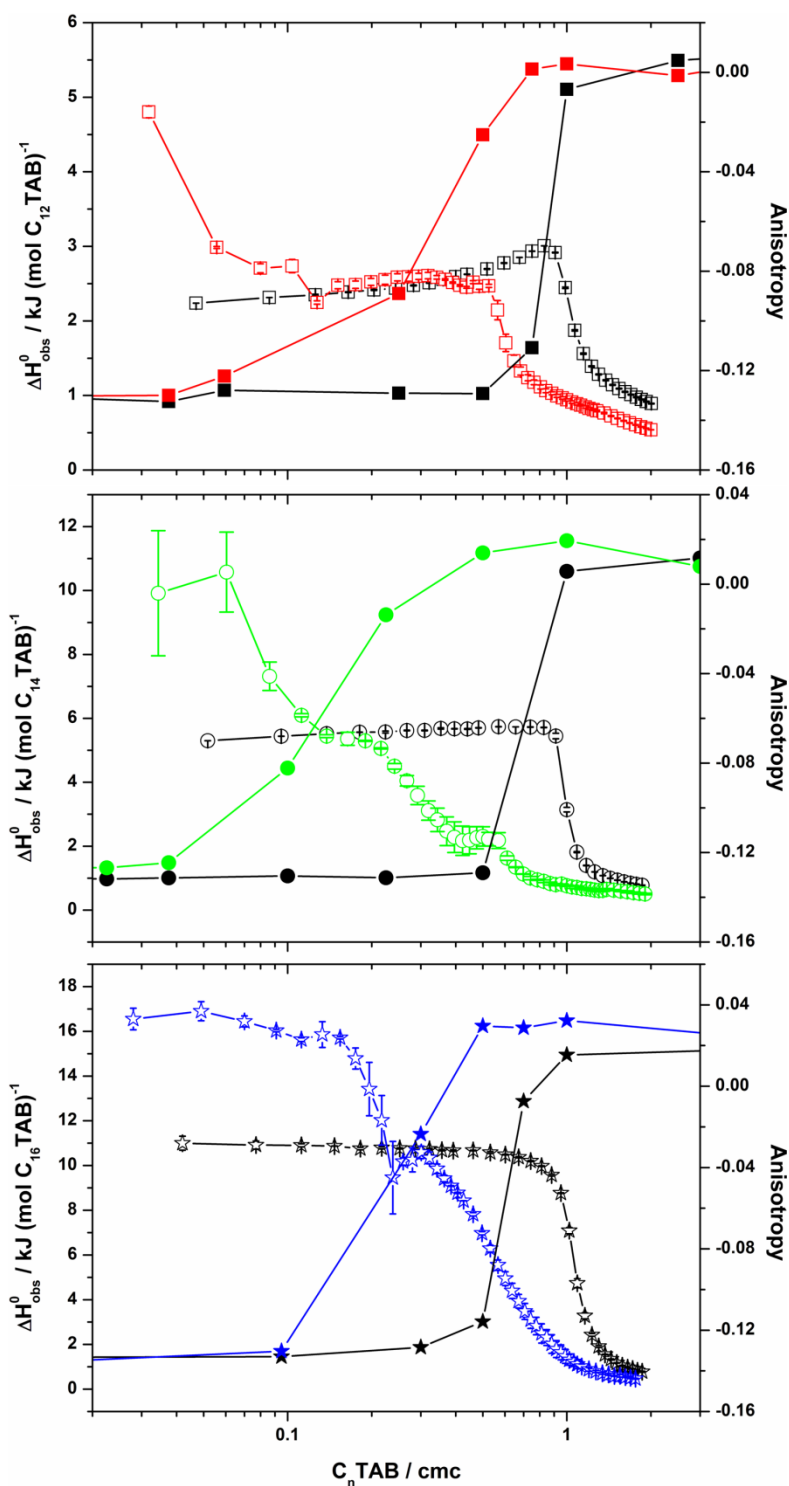
Figure 3.8 ANS fluorescence anisotropy (closed symbols) combined with ITC data (open symbols) obtained at 25 ºC for C$_{12}$TAB (red) and C$_{14}$TAB (green) and 28 ºC for C$_{16}$TAB (blue) in the presence of 0.1 wt% CNC dispersions. Black plots are the control (pure surfactant).

3.3.5 Electrophoretic Mobility Measurements

By measuring the electrophoretic mobility of all samples (Figure 3.9) the same S-shaped curves were obtained for all the three surfactants. At low surfactant concentration the values are all negative, followed by an abrupt rise in the mobility values over a narrow concentration range. When the surfactant concentration reaches half the *cmc* (where visual observation of flocculation starts) there is a signal inversion from negative to positive values, and after this point an increase in the surfactant concentration leads to more positive values. Considering a sulfate concentration of 0.23 mmol kg^{-1}CNC^{-1},[3] this point of charge inversion is close to the stoichiometry point of charge neutralization. Moreover, when comparing with ITC data, this matches the "bump" found on the ITC curves for the binding of C$_{16}$TAB (Figure 3.1).

Data presented in Figure 3.9 were plotted as a function of normalized surfactant concentration. Hence, considering that the same amount of CNC was used in all of the three experiments, and that the three surfactants display different *cmc* values, with C$_{16}$TAB presenting the smallest one, the absolute surfactant concentrations are different. Following this reasoning, charge neutralization should take place at a surfactant concentration of ca. 1/4 of that of C$_{16}$TAB for C$_{14}$TAB and 1/16 for C$_{12}$TAB, if the surfactants were fully bound to CNC. The observation that the three surfactants display charge inversion points at different absolute concentrations indicates that binding of the two less hydrophobic surfactants is not as complete as the one presented by C$_{16}$TAB. A similar observation was recently reported for studies comparing two different cationic surfactants C$_{16}$TAB and DMAB (didecyldimethylammonium bromide)[25] that display close charge neutralization points, but as their *cmc* values are also close, there is no clear discrimination of these effects.

Another interesting point related to the results presented in Figure 3.9 is that, although mixtures of C$_{n}$TAB-CNC display high positive charges at higher surfactant concentration, they do not fully redisperse, as has been observed for other colloidal coacervates formed by electrostatic interaction. Combining all the previous results, we suggest that a surface induced surfactant aggregation starts at a lower surfactant concentration for the more hydrophobic surfactants C$_{14}$TAB and C$_{16}$TAB; the negative electrophoretic values are in agreement with counterion adsorption in the formation of admicelles.[152] As for C$_{12}$TAB the initial interaction is due to an ion exchange mechanism between the CNC and the surfactant,[138,153] forming a surfactant monolayer

(hemimicelles)[152,154] with the alkyl chains towards the water, followed by surfactant aggregation at higher concentration. At this point, the mixture remains flocculated due to interaction of CNC rods with cationic surfactant admicelles, in a mechanism similar to physical cross-linking due to electrostatic interaction (see representation in Figure 3.10).
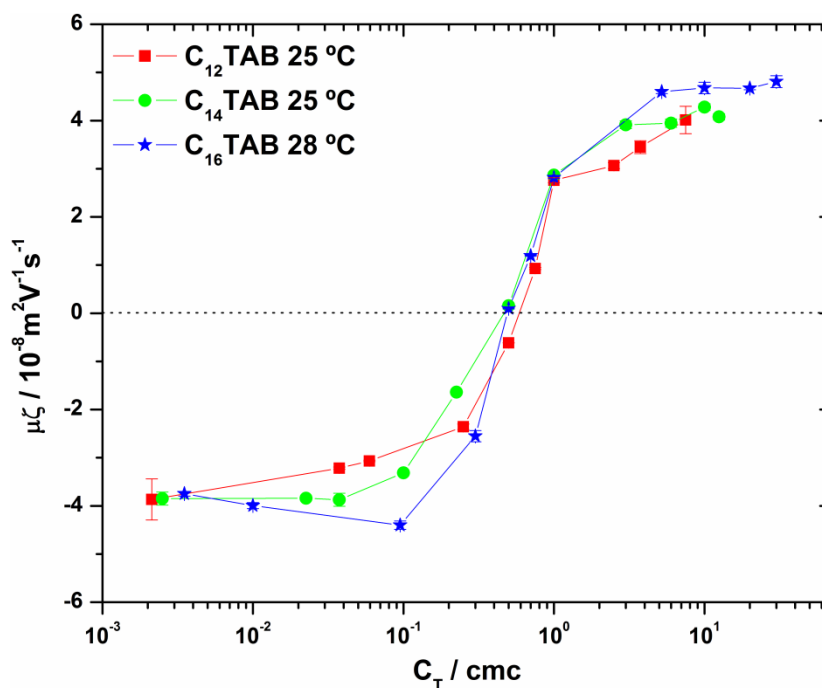
Figure 3.9 Electrophoretic mobility measurements at a fixed CNC concentration (0.1 wt%) as a function of normalized surfactants C_nTAB concentration at 25 ºC.
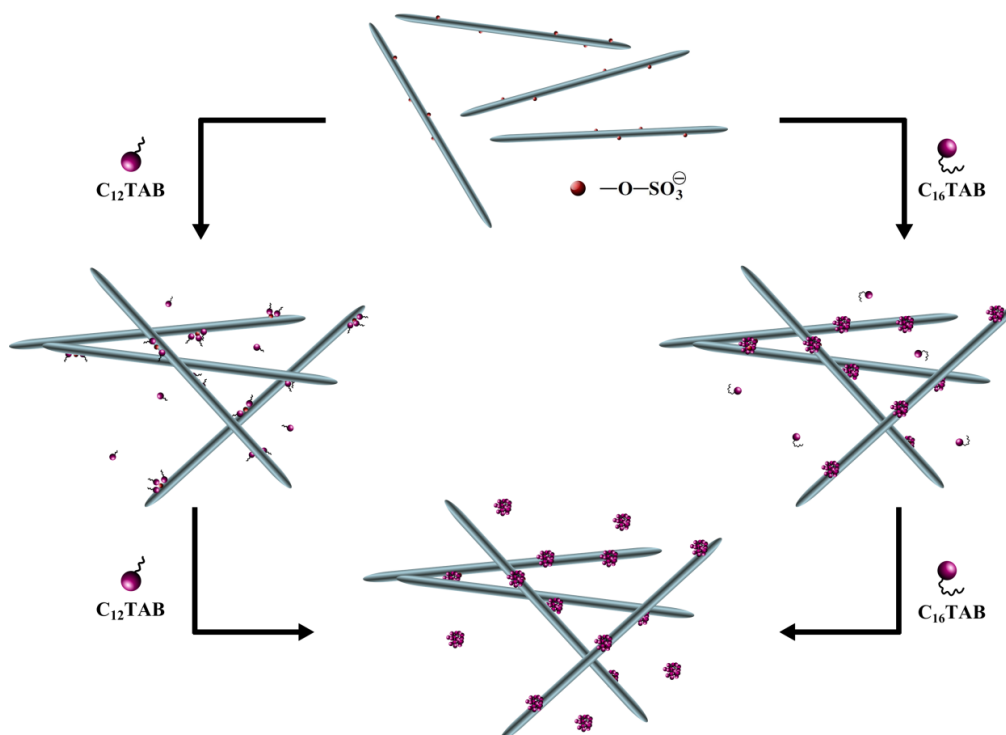
Figure 3.10 Binding mechanism for both C$_n$TAB – CNC (counterions are not shown for the sake of clarity) with an increase in the surfactant concentration. Pictorial representation of the formation of hemimicelles for C$_{12}$TAB (left) followed by the formation of admicelles (bottom and surfactant-CNC coacervates). C$_{16}$TAB only forms admicelles. Not drawn to scale.

We tried to further investigate the nature of these flocs using small-angle X-ray scattering measurements. The SAXS curves (Figures A.12 and A.13 in Appendix A) do not show any distinct evidence of ordering in the scale of dimensions probed with this q range, except for one broad and weak peak around q = 0.8 nm^{-1}. The presence of a peak in the curves for both surfactant-CNC mixtures that is not seen in those for pure CNC or pure surfactant may be interpreted as a result of some ordering of the scattering objects, and corresponds to a correlation distance around 8.0 nm, which is not far from the diameter of the CNC rods. If they are arranged as pictured in Figure 3.10, such a correlation distance may arise from the distance of between adjacent rods that are joined by adsorbed surfactant aggregates.

3.4 Discussion

Analyzing the results presented above, one can propose that the interaction between the less hydrophobic surfactant, $C_{12}TAB$, and CNC is electrostatic driven at low surfactant concentration.[36] ITC curves (Figure 3.1) show that after this initial process, there is a concentration range in which no significant changes occur followed by surface induced surfactant aggregation at a concentration around half of its *cmc* value. The predominantly electrostatic nature[138,155] of this initial interaction is confirmed by results obtained in the presence of electrolytes and with desulfated CNC, in which this initial part is suppressed.

The formation of surface induced aggregates is supported by the results of fluorescence anisotropy (Figure 3.8). It shows a change in anisotropy around the same concentration range, consistent with the incorporation of ANS into surfactant aggregates. For the more hydrophobic surfactant studied, $C_{16}TAB$, the major difference is that hydrophobic surfactant interactions start at a much lower surfactant concentration (even considering the relative values normalized by their *cmc*), with a less important contribution from electrostatic interactions. This is also revealed by studies with electrolytes, desulfated CNC and temperature variation, with the latter showing to have a higher impact on the more hydrophobic surfactant.[39,137] Overall, $C_{14}TAB$ displays an intermediate behavior.

Studies of electrophoretic mobility of the C_nTAB-CNC mixtures indicate that surfactant addition leads to CNC charge reversal but, interestingly, the point of charge inversion depends more on the surfactant tendency to self-associate. It occurs at concentrations near half their *cmc* values for the three surfactants, rather than to their absolute concentrations. This finding indicates that almost all of the added $C_{16}TAB$ binds to CNC, as indicated by the close agreement between the charge ratio estimated from CNC charges and surfactant concentration. However, an increasing surfactant fraction remains in water for the less hydrophobic surfactants. Again, this finding bears a close relationship with the formation of admicelles, which becomes more favorable with the increase in surfactant hydrophobicity.[138,155,156]

Another interesting feature derived from this study relates to the nature of the C_nTAB-CNC aggregates formed by these mixtures. It has been previously proposed that these coacervates (which appear as flocs at higher surfactant concentrations) are formed by linking several CNC rods cross-linked by the cationic adsorbed surfactant aggregates

(as represented in Figure 3.10). Our SAXS results indicate that no long-order surfactant structures are formed, by the absence of Bragg peaks. SAXS curves reveal, however, a broad and small peak suggesting a correlation distance around 8.0 nm for scattering objects. In such mixtures, considering that the scattering from surfactant micelles is found at higher q values, these objects are most likely the CNC rods, and this correlation distance is consistent with the pictorial representation in Figure 3.10. The nature of these aggregates is consistent with the findings that at high surfactant concentrations, where their electrophoretic mobilities suggest a significant excess of positive charges, no redispersion is observed. For these aggregates, addition of more cationic surfactants would increase the number of adsorbed micelles and possible cross-linking points for CNC rods.

3.5 Conclusions

In this paper the interaction between CNC and a homologous series of C_nTAB cationic surfactants (n = 12, 14, and 16) was studied by different techniques. The ITC results in the presence of CNC and at varied conditions clearly show that the electrostatic interactions are the driving force at low surfactant concentration for all mixtures and that the formation of hemimicelles (surfactant alkyl chains exposed towards the water) is predominant for the less hydrophobic homologue. This process is followed by hydrophobic interactions between the surfactant alkyl chains at higher concentrations, leading to the formation of admicelles. Electrophoretic mobility measurements indicate that this binding is associated with charge inversion with the concentration of zero charge for all the three surfactants coinciding with half of their *cmc* values, and not controlled by their absolute concentrations. This confirms that surfactant binding depends strongly on their hydrophobicity. These results, along with those from other techniques extend and complement earlier reports on surfactant interaction with CNC rods demonstrating important differences depending on the surfactant hydrophobicity. Moreover, the present results support the proposal that the coacervates formed by these mixtures consist of a bunch of CNC rods cross-linked by adsorbed cationic surfactant aggregates and, for this reason, no redispersion is observed even when they possess excess positive charge.

The observation of these properties is of great relevance for the separation and recovery of CNC rods by their surfactant induced flocculation, an important feature for

these particles to be used for the removal of contaminants, for instance.[131] Another point of potential relevance relates to use of CNC as vehicle for uptake or release of active compounds, such as in pharmaceutical formulations. For this reason, the present findings open the possibility of tuning CNC properties by changing not only concentrations, but also the nature (hydrophobicity) of the surfactant employed.

Chapter 4: Redispersion of poly (oligo (ethylene oxide) methacrylate) grafted cellulose nanocrystals in the presence of ionic surfactants‡

My contributions to this manuscript:

Performed all the experiments except HSDSC in the presence of surfactants, zeta potential, particle size and FTIR. TGA experiments were performed by a lab technician. The manuscript was written by me.

Abstract

Due to their negatively charged surfaces, cellulose nanocrystals (CNC) may undergo precipitation when interacting with cationic surfactants in aqueous solutions. Two different approaches were evaluated in this study as alternatives to avoid such behavior or to promote their redispersion. First, adding a nonionic nonylphenol etoxylate surfactant (NP) with 100 ethylene oxide (EO) units, which increased the binding of alkyltrimethylammonium bromide (C_nTAB) surfactants to CNC but could not avoid precipitation as seen by electrophoretic mobility and light scattering results. Second, surface grafting of CNC with a thermoresponsive poly (oxyethylene) (PEO) derived polymer, poly di (ethylene oxide) methyl ether methacrylate , (P(MEO$_2$MA), presenting a cloud point of approximately 25 ºC. Addition of excess dodecyltrimethylammonium bromide (C_{12}TAB) surfactant to the system, at a temperature above its cloud point, caused a non-reversible redispersion in the system due to surfactant binding to both the polymer and to the surface negative charges of the CNC. The addition of different concentrations of an anionic surfactant, sodium dodecylsulfate (SDS) caused an increase in the temperature of the phase transition of the polymer, as revealed by HSDSC measurements, a phenomenon that could be reversed by dialysis.

4.1 Introduction

Cellulose nanocrystals (CNC) are a class of nanobiomaterials derived from cellulose via sulfuric acid hydrolysis, presenting negative sulfate-ester groups that

---

‡ This chapter is adapted from the manuscript "Brinatti, C.; Akhlaghi, S.P.; Oliveira, R.P.; Berry, R.M.; Tam, K.C.; Loh, W. Redispersion of poly (oligo (ethylene oxide) methacrylate) grafted cellulose nanocrystals in the presence of ionic surfactants".

render an electrostatic stability for dispersions in water and polar solvents.[5,7,16] When in the presence of oppositely charged molecules such as cationic alkyltrimethylammonium bromide surfactants (C_nTAB) the electrostatic interaction between them is so strong they precipitate [36] when the surfactant concentration reaches around half of its critical micellar concentration (*cmc*) (Chapter 3).[157] To avoid such behavior, by changing the amount of cationic surfactant bound to CNC, two different approaches might be pursued. The first one is the addition of a nonionic surfactant, which could either increase or decrease the binding of cationic surfactants to CNC due to the synergy between both molecules. The second is surface modification of CNC by grafting a polymer that would increase the CNC surface area and could enhance the number of available binding sites.

Synergy between nonionic and ionic surfactants has been earlier reported by many research groups.[158–160] Interactions between hexadecyltrimethylammonium bromide (C_{16}TAB), a cationic surfactant and nonionic nonylphenol ethoxylated surfactants with varying the degree of ethoxylation (NP series) was studied by Desai & Dixit.[158] By increasing the ethoxylated moiety of the nonionic surfactant the shape of the micelles would change from spherical to rod-shaped attributed to interactions between the hydrophilic polar groups of both surfactants. In another study, Somasundaram and Huang observed that nonionic NP surfactants could only be adsorbed on alumina surfaces in the presence of tetradecyltrimethylammonium chloride (C_{14}TAC) and this feature was increased when the content of the cationic surfactant was increased in solution as seen by zeta potential results.[161]

Mészáros and coworkers performed extensive studies regarding the presence of nonionic surfactants in the interactions between ionic surfactants and oppositely-charged polyelectrolytes. They observed that this strong electrostatic interaction and non-equilibrium association that could lead to phase separation might be tuned by the nonionic/ionic surfactant ratio. The presence of nonionic surfactant could affect this non-equilibrium state by destabilizing the colloidal complexes formed at different surfactant/polyelectrolyte and nonionic/ionic surfactant ratios. At a low ratio the onset of phase separation is shifted towards lower ionic surfactant concentration; at a high ratio the ionic surfactant can be solubilised into mixed micelles and binding can be suppressed.[141] Interactions between the anionic surfactant sodium dodecylsulfate (SDS) and the cationic poly (diallyldimethylammonium chloride) (PDADMAC) was enhanced in the dilute regime in the presence of glucosidic nonionic surfactants.[162] Similarly the

same effect was observed when studying the binding of alkyltrimethylammonium bromide surfactants (C_nTAB) to poly (styrenesulfonate) (PSS), with a more pronounced effect for C_{12}TAB than for C_{16}TAB that was related to the surfactant hydrophobicity.[134]

Surface modification of cellulose and its derivatives such as CNC with stimuli-responsive polymers – especially pH and temperature responsive – have been drawing some attention since the past decade.[105,107,108] Ethoxylated polymers and derivatives present advantages of being water soluble, biocompatible and thermoresponsive. An important and yet relatively new class of EO derivatives is the one containing a methacrylate unit that could be polymerized, therefore broadening the possibility of its use in different fields.[118] Nho and Kwon [163] modified the surface of cellulose films by radiation grafting polymerization technique and used poly(ethylene oxide methacrylates) (PEOMA) with increasing hydrophilicity by increasing the number of ethylene oxide units from 2 to 9. The process was followed by amination and heparin immobilization in order to assess their improved compatibility with blood. Grishkewich et al.[108] observed that by adjusting the grafted molar ratio of $OEGMA_{300}$ (oligoethylene oxide methyl ether methacrylate) to MEO_2MA (diethylene oxide methyl ether methacrylate) onto CNC it is possible to tune the lower critical solution temperature (LCST) of the CNC-g-POEGMA nanoparticles from 23.8 to 63.8 ℃. They also observed a thermal hysteresis when cooling down the system, denoting a kinetic effect on the nanoparticles aggregation. Peng et al.[35] studied the interactions between a polymer-grafted CNC (CNC-g-M600, a polypropylene glycol (PPG) derivative) and different surfactants with alkyl chains containing 12 carbon atoms namely SDS (anionic), C_{12}TAB (cationic) and Brij 30 (nonionic). No interactions were observed between CNC-g-M600 and Brij 30; but it was found that SDS presented hydrophobic interactions with the grafted polymer chains while C_{12}TAB would bind electrostatically to the negatively charged sulfate-ester groups on the CNC surface.

In our study we investigated the binding of C_nTAB (n = 12 and 16) to CNC in the presence of the nonionic surfactant NP-100 containing 100 ethylene oxide (EO) units by measuring the electrophoretic mobility and transmittance of their mixtures. When CNC surface was modified by grafting P(MEO_2MA), we attempted to redisperse the CNC-g-P(MEO_2MA) with ionic surfactants SDS and C_nTAB at a temperature above its LCST. The surface-modified CNC was characterized by FTIR-ATR spectroscopy, thermal gravimetric analysis (TGA) and high sensitivity differential scanning calorimetry (HSDSC). The interactions between CNC-g-P(MEO_2MA) and ionic

surfactants were analysed by ITC, electrophoretic mobility, light scattering measurements and HSDSC at varied SDS concentrations.

4.2 Experimental Section

4.2.1 Chemicals

Cellulose nanocrystal (CNC) hydrolyzed from wood pulp was provided by CelluForce Inc. The nonionic surfactant used was ULTRANEX NP 1000, a nonylphenol etoxylate with an average of 100 EO units (NP-100) kindly donated by Oxiteno, Brazil. The ionic surfactants used were alkyltrimethylammonium bromide (C_nTAB, n = 12 and 16) and sodium dodecylsulfate (SDS) ($\geq$ 98% purity). All the surfactants were used without purification. The monomer di(ethylene glycol)methyl ether methacrylate (MEO$_2$MA, 95% purity, M_w = 188.22 g mol^{-1}) was purified by passing it through a basic alumina oxide column to remove the inhibitors. Cerium (IV) ammonium nitrate ($\geq$ 98% purity) was used without purification. All these chemicals were purchased from Sigma-Aldrich$^{®}$. Water used to prepare all solutions and dispersions was of Milli-Q grade (18.2 MΩ cm^{-1}).

4.2.2 Graft Polymerization

In a two-neck round bottom flask 0.5 g of CNC powder was dispersed in 50.0 mL of water by ultrasonication with Hielscher UP100H equipment (Germany), using a MS3 sonication probe. The dispersion was kept under stirring at room temperature and then purged for 20 min with nitrogen gas into the flask. The MEO$_2$MA with a ratio of 100:1 (based on the ration MEO$_2$MA/OH groups on the CNC surface) was added to the flask. To the CNC dispersion 1.0 mL of a solution containing 100 mg L^{-1} of cerium (IV) ammonium nitrate was added dropwise – the drops were only added after the yellow color from the cerium (IV) solution added to the flask disappeared. After this procedure the nitrogen purge was ceased and the two necks of the flask were sealed with a rubber stop and silicone glue. The reaction was kept under stirring for 20 h. The final product (white solid agglomerate) was dialyzed against deionised water for 1 week using a membrane with a M_W cut off: 12,000 g mol^{-1}. The product was then centrifuged at 3000 rpm for 20 min at least 6 times. This procedure was made to ensure the removal of

unreacted MEO$_2$MA monomers and unbound polymers that might be physically adsorbed to the CNC.[32]

4.2.3 CNC-*g*-P(MEO$_2$MA) Sample Preparation

Stock dispersions of CNC-*g*-P(MEO$_2$MA) 3.0 wt% were prepared by ultrasonication with Hielscher UP100H equipment (Germany), using a MS3 sonication probe, under ice bath for at least 20 min and stored in the refrigerator. All the experiments were performed with 1.0 wt% CNC-*g*-P(MEO$_2$MA) by simply diluting the stock dispersion.

4.2.4 FTIR-ATR spectroscopy

An Agilent Cary 630 FTIR spectrometer with diamond attenuated total reflectance (ATR) with a ZnSe beamsplitter crystal was used in order to characterize both pristine CNC and surface modified CNC-*g*-P(MEO$_2$MA). Each sample as analyzed over a frequency range of 400-4000 cm^{-1} and with a resolution of 4 cm^{-1}.

4.2.5 Thermogravimetric Analysis (TGA)

Thermogravimetric experiments were conducted using TA 20.50 equipment. The analyzed samples (pristine CNC powder, CNC-*g*-P(MEO$_2$MA) underflow and P(MEO$_2$MA) supernatant) were inserted into a platinum pan and heated up from 30 to 800 °C at a rate of 10 °C min^{-1} under a nitrogen flow rate of 30 mL min^{-1}.

4.2.6 High Sensitivity Differential Scanning Calorimetry (HSDSC)

A MicroCal VP-DSC (Northampton, MA, USA) calorimeter was used for the experiment. 1.0 wt% CNC-g-P(MEO$_2$MA) dispersion and its mixtures containing SDS (0.1, 1.0, 5.0, 20.0 and 40.0 mmol kg^{-1}) were added in a 0.5 mL reaction cell and they were scanned from 20 up to 110 °C. Scan rates were performed at 60 °C h^{-1}. For all experiments were performed three consecutive runs. The first one was considered to have erased the grafted polymer thermal history, so the other two were considered.

4.2.7 Transmittance Measurements

Transmittance measurements were carried out on a 8453 Spectrophotometer (Hewlett-Packard), equipped with a Peltier system, at a wavelength of 600 nm under stirring (500 rpm). For the nonionic surfactants experiments we fixed both the CNC concentration at 0.1 wt% and NP-100 concentration at 1.3 mmol L^{-1} while varying the cationic surfactants concentrations. The experiments were performed at 25 ºC for C_{12}TAB and 28 ºC for C_{16}TAB. For the determination of the cloud point of CNC-*g*-P(MEO$_2$MA) the dispersion was heated up from 15 to 40 ºC and then cooled down back to 15 ºC at a rate of 1.0 ºC min^{-1}. Three consecutive cycles were performed and the first cycle was intended to erase the thermal history of the polymer.

4.2.8 Isothermal Titration Calorimetry (ITC)

MicroCal VP-ITC (Northampton, MA, USA) was the calorimeter used for the experiments. Aliquots ranging from 3 to 10 μL were added stepwise by an automatic injection syringe containing 270 μL of a concentrated surfactant solution (at least twelve times above its *cmc* value) into the reaction cell of 1.43 mL containing either water or 1.0 wt% CNC-*g*-P(MEO$_2$MA) dispersions with a 5 min interval between injections. Two different temperatures were used in the experiments 15 ºC and 40 ºC, below and above the P(MEO$_2$MA) LCST, respectively. All the experiments were performed in duplicate. Data obtained were treated with the Origin$^{®}$ 7.0 software.

4.2.9 Electrophoretic Mobility and Particle Size Determination

Electrophoretic measurements were carried out using a NanoZS Zetasizer (Malvern Instruments). It uses an M3-PALS technique – a combination of phase analysis light scattering and laser Doppler velocimetry. For the nonionic surfactant experiments we fixed both the CNC concentration at 0.1 wt% and NP-100 concentration at 1.3 mmol L^{-1} while varying the cationic surfactants concentrations. The experiments were performed at 25 ºC for C_{12}TAB and 28 ºC for C_{16}TAB. The CNC-*g*-P(MEO$_2$MA) concentration was fixed at 1.0 wt% while varying the surfactant concentration. When measuring high concentrated surfactant solutions only the μζ sign is relevant, for there

is a contribution from both the C_nTAB-CNC complex and the bulk micelles.[141] The experiments were performed in triplicate for all the systems.

For particle size determination (detection angle of 173º), the apparent hydrodynamic diameter (d_{Happ}) was measured at 15.0 ± 0.1 ℃ and at 40 ± 0.1 ℃ for C_{12}TAB and SDS, respectively. All the experiments were performed in triplicate.

4.3 Results

4.3.1 Mixtures containing C_nTAB /NP-100/CNC

The nonionic/ionic surfactant ratio has an influence on the interactions with oppositely charged polyelectrolytes and/or particles.[134,141,158,159,161,162] Binding could be even suppressed by increasing this ratio. With that in mind, we decided to add the nonionic surfactant NP-100 to the C_nTAB/CNC mixture to evaluate the effect of this nonionic/ionic surfactant ratio. The surface area occupied by the NP-100 surfactant molecules is very large (15.6 nm)[164] so perhaps the adsorbed nonionic micelles on the CNC surface would also impart a significant contribution to sterical hindrance for the binding of cationic surfactants.

Following the results from our previous publication (Chapter 3),[157] we varied the cationic surfactant concentrations while fixing the CNC concentration at 0.1 wt% and NP-100 concentration at 1.3 mmol L^{-1}. The NP-100 concentration was chosen based on its *cmc* value of 0.68 mmol L^{-1} obtained by ITC experiments (Figure B.1 in Appendix B) so to ensure NP-100 micelles in solution. The mixtures are shown in Figure 4.1 where we have a comparison with the mixtures in the absence of NP-100 (mixtures containing C_{12}TAB are showed in Figure B.2 in Appendix B).

C$_{16}$TAB – CNC 0.1 wt%

| Zero | 3.5x10^{-6} | 10x10^{-6} | 95x10^{-6} | 0.5x10^{-3} | 1.0x10^{-3} | 5.0x10^{-3} | 10x10^{-3} | 20x10^{-3} | 30x10^{-3} |

C$_{16}$TAB + NP-100 1.3 mmol L^{-1} – CNC 0.1 wt%

| Zero | 3.5x10^{-6} | 10x10^{-6} | 95x10^{-6} | 0.3x10^{-3} | 0.5x10^{-3} | 0.7x10^{-3} | 1.0x10^{-3} | 5.0x10^{-3} | 10x10^{-3} | 20x10^{-3} | 30x10^{-3} |
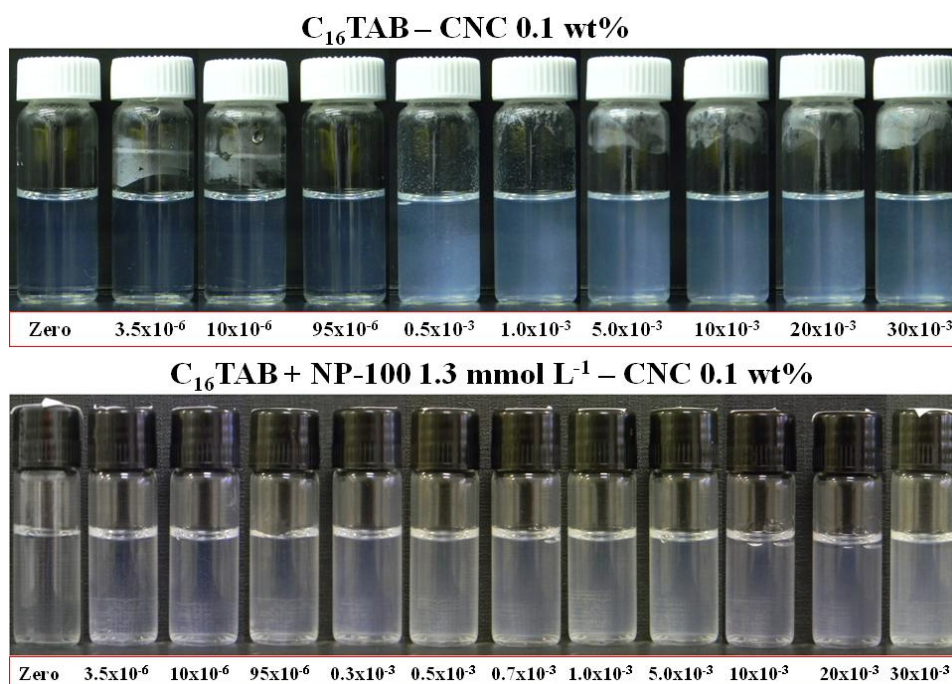
Figure 4.1 Comparison of mixtures containing C$_{16}$TAB and 0.1 wt% CNC dispersions in the absence (top)[157] and in the presence of 1.3 mmol L^{-1} NP-100 solution (bottom). C$_{16}$TAB concentrations are expressed in mol L^{-1}(at the bottom).

The samples in the presence of NP-100 (Figure 4.1 bottom) do not show any visible sign of phase separation/sedimentation throughout the whole concentration range when compared to the mixtures in the absence of NP-100 (Figure 4.1 top). With this promising result we performed transmittance and electrophoretic mobility experiments and the results are presented in Figure 4.2. We compared the new results with the ones obtained previously (Chapter 3).[157]
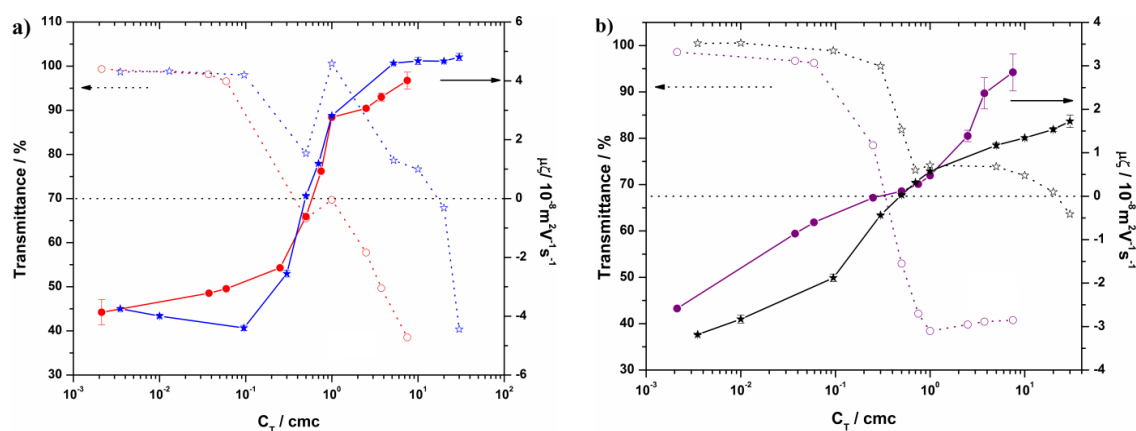
Figure 4.2 Transmittance (open symbols) and electrophoretic mobility (filled symbols) as a function of normalized surfactant concentration (C$_T$/cmc) for the mixtures containing: a) C$_n$TAB/CNC 0.1 wt% (C$_{12}$TAB circles and C$_{16}$TAB stars) and b) C$_n$TAB/NP-100/CNC 0.1

wt% (C$_{12}$TAB circles and C$_{16}$TAB stars) The experiments were performed at 25 ºC for C$_{12}$TAB (red symbols) and at 28 ºC for C$_{16}$TAB (blue symbols).

In the experiments with C$_n$TAB/CNC (Figure 4.2a) we see an S-shaped curve obtained for both surfactants when measuring electrophoretic mobility. There is a signal inversion at 0.5 *cmc* concentration for both surfactants, where flocculation starts. There is also a steep decrease at the same concentration range when performing transmittance experiments with both surfactants reaching 40% of their original values (Chapter 3).[157] A similar trend can be found in the experiments with C$_n$TAB/NP-100/CNC (Figure 4.2b). For the more hydrophilic surfactant C$_{12}$TAB the concentration of signal inversion decreased (from 0.5 to 0.25 *cmc*) and the net electrophoretic mobility values are reduced, while its transmittance values did not change significantly. For C$_{16}$TAB the point of signal inversion did not change (although the net values were narrowed as well) and the transmittance values reached 60% of its original value. Both systems containing C$_{12}$TAB and C$_{16}$TAB in the presence of NP-100 showed sedimentation after some time (approx. 5 h), showing that the nonionic surfactant NP-100 did not hinder the growth/agglomeration of the particles.

4.3.2 Mixtures containing CNC-*g*-P(MEO$_2$MA)/Surfactants

Because our attempt to prevent CNC agglomeration and/or redispersion by adding a nonionic surfactant as a sterical stabilizer failed, we turned our attention to chemically grafting a polymer on the CNC surface.

We aimed at applying a thermoresponsive polymer in order to be able to test this hypothesis. Below the LCST the polymer grafted CNC would have to remain dispersed in solution so it would not interfere with our analyses. Increasing the temperature of the system up to a point above the LCST would cause a visual phase separation that could be reversed by the addition of surfactants. By choosing ionic surfactants with the same alkyl chain length we could assess where they would be bound to, i.e. the polymer chain coil/globules and/or the CNC negative charges. This could be achieved by using oppositely charged surfactants, the cationic C$_{12}$TAB and the anionic SDS.

4.3.3 CNC-*g*-P(MEO$_2$MA) Characterization

4.3.3.1 FTIR-ATR

The FTIR-ATR spectra of both pristine CNC and CNC-*g*-P(MEO$_2$MA) are presented in Figure 4.3. Pristine CNC spectrum peaks are in accordance with previous studies.[32,106,108] The presence of a new peak at 1723 cm^{-1} at the CNC-*g*-P(MEO$_2$MA) spectrum is characteristic of a new C=O bond on the CNC surface due to a ring opening mechanism.[163,165]
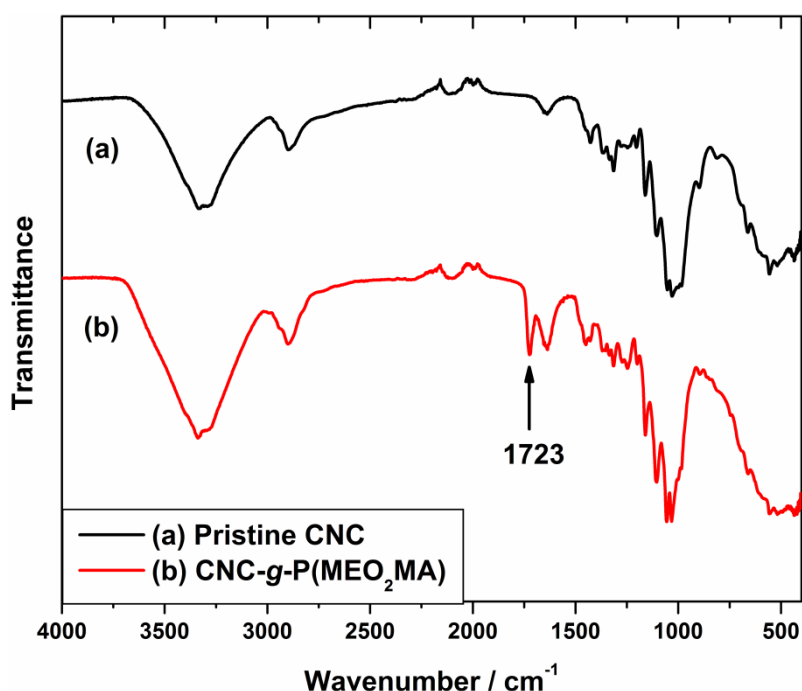
Figure 4.3 ATR spectra obtained for (a) Pristine CNC and (b) CNC-*g*-P(MEO$_2$MA).

4.3.3.2 TGA, HSDSC and Transmittance Experiments

Thermogravimetric analysis was used to characterize the surface modification of CNC with P(MEO$_2$MA). Figure 4.4 shows the decomposition curve obtained for pristine CNC, CNC-*g*-P(MEO$_2$MA) and the supernatant comprised mostly by P(MEO$_2$MA) loose polymer chains and unreacted monomers. Analyzing Figure 4.4 inset (derivative weight loss thermograms) we see that pristine CNC (black curve) and CNC-*g*- P(MEO$_2$MA) (red curve) profiles are superimposed and present a degradation process starting at 275 ºC, attributed to the presence of sulfuric groups on the surface

due to the acid hydrolysis of cellulose.[8,127,166] The higher temperature processes at 350 ºC and 600 ºC are attributed to a slow char residue formation.[8,166] However, CNC-*g*-P(MEO$_2$MA) presents an initial peak at a lower temperature of 185 ºC. This indicates a decrease on the CNC thermal stability after polymer grafting reaction.[127] In the proposed mechanism for cerium (IV) ammonium nitrate ion as a surface initiated "grafting-from" radical reaction[32,105] it is suggested that covalent bonds between C2 and C3 on the anhydroglucose units at the surface might break, thus weakening the crystalline structure.[32] We assumed that the supernatant (blue curve) does not show any considerable traces of CNC –there is only one transition temperature starting at 85 ºC throughout the entire temperature range.
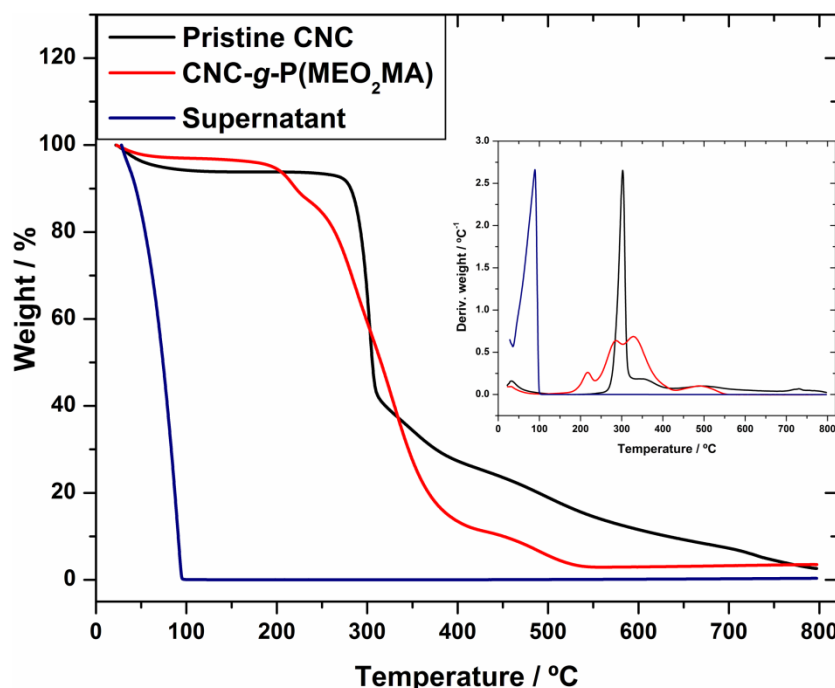
Figure 4.4 TGA thermograms obtained for Pristine CNC (—), CNC-*g*-P(MEO$_2$MA) (—), and Supernatant (—). Inset shows the derivative weight loss thermograms of the three samples.

In order to assess the LCST behavior for CNC-*g*-P(MEO$_2$MA) we performed a series of experiments using HSDSC (Figure 4.5) and UV-Vis transmittance (Figure 4.6). HSDSC results showed a temperature transition in the range of 24.3 to 35.4 ºC, with a maximum of 25.0 ºC and, after this maximum the curve kept decreasing and did not return to the base line, in a similar way as to proteins.[167] These results are in close

agreement with the ones obtained by UV-Vis transmittance measurements: temperature transition in the range of 20.3 to 34.8 °C, with a maximum at 23.0 °C. Similar results were obtained by Lutz et al.[118] and Grishkewich et al.[108]. Figure 4.6 also shows that the thermoresponsive behavior is reversible and presented some hysteresis for dehydration/aggregation (heating, red curve) and rehydration/redispersion (cooling, blue curve), the latter a slower process then the former.
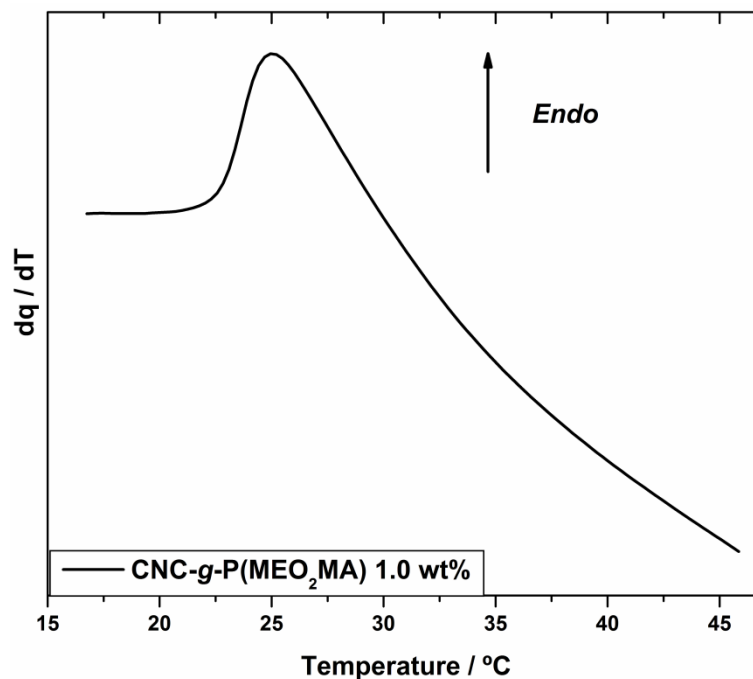
Figure 4.5 Thermogram obtained at a scan rate of 60 °C h⁻¹ for 1.0 wt% CNC-*g*-P(MEO₂MA) dispersion.
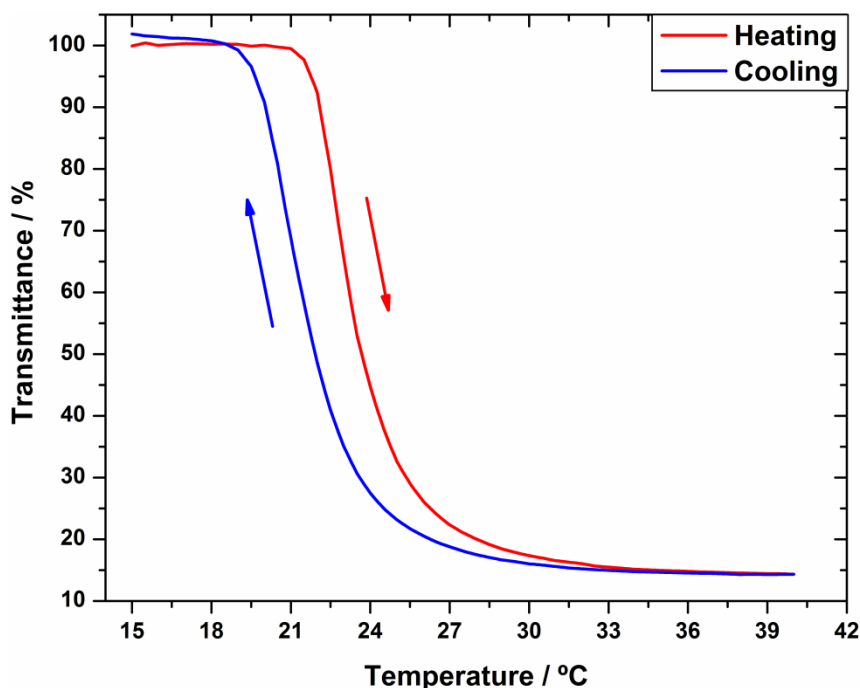
Figure 4.6 Hysteresis behavior for the second heating and cooling cycles of 1.0 wt% CNC-*g*-P(MEO$_2$MA) dispersion.

4.3.3.3 ITC Experiments

To examine the effects of the addition of ionic surfactants with different electrical charges to CNC-*g*-P(MEO$_2$MA), we performed a series of calorimetric titration experiments at two different temperatures, 15 and 40 ºC, below and above the LCST, respectively for both C$_{12}$TAB and SDS (Figure 4.7). Electrostatic interactions should not be affected by this temperature change, while hydrophobic interactions are expected to be significantly affected.[39] When using C$_{12}$TAB, an interaction with both the negative sulfate groups on the CNC surface and the grafted polymer chains is expected. However, cationic surfactants are known to interact less with hydrophilic polymers[137,140] due to the presence of the large trimethylammonium headgroup. Therefore, we would expect to see no significant interaction at 15 ºC and some interaction with the polymer chains at 40 ºC. Our hypothesis was confirmed when we analyzed the data in Figure 4.7 (left): at a lower surfactant concentration range from 0.5 up to 2.0 mmol kg^{-1} there is a small peak in the titration curves in the presence of CNC-*g*-P(MEO$_2$MA) attributed to electrostatic interaction, regardless of the temperature (Chapter 3).[157] Increasing the surfactant concentration (7.2 mmol kg^{-1}) we only observed one peak in the system at 40 ºC that is attributed to hydrophobic interactions

between the surfactants and the polymer chains – here we have a polymer induced micellization process known as critical aggregation concentration (*cac*) that has been observed in previous studies.[40,42,168]

When we compared these results with the ones obtained for SDS (Figure 4.7, right) our hypothesis became clear. SDS can only interact with the grafted polymer chains and this is reflected on the titration curves in the presence of CNC-*g*-P(MEO$_2$MA) as peaks corresponding to a polymer induced micellization (*cac*).

At 15 °C there is a small exothermic peak (-1.82 kJ mol^{-1}) at a surfactant concentration of 0.90 mmol kg^{-1}, while at 40 °C there is a much more pronounced peak (-18.24 kJ mol^{-1}). These values are obtained by simple subtraction of the maximum enthalpy value for the titration curves in the presence of CNC-*g*-P(MEO$_2$MA) from the enthalpy value obtained of the control samples (titration into water) at the same surfactant concentration.

This difference can be attributed to the hydration of the grafted polymer chains when interacting with SDS. At 40 °C the grafted polymer chains acquire a globular structure and are dehydrated, a phenomenon similar to what has been reported for poly (N-isopropylacrilamide), P(NIPAM).[95,169] When we added SDS to the system the surfactant was responsible for the formation of micellar aggregates involving the P(MEO$_2$MA) chains, and they assumed a coil fashion and were rehydrated.
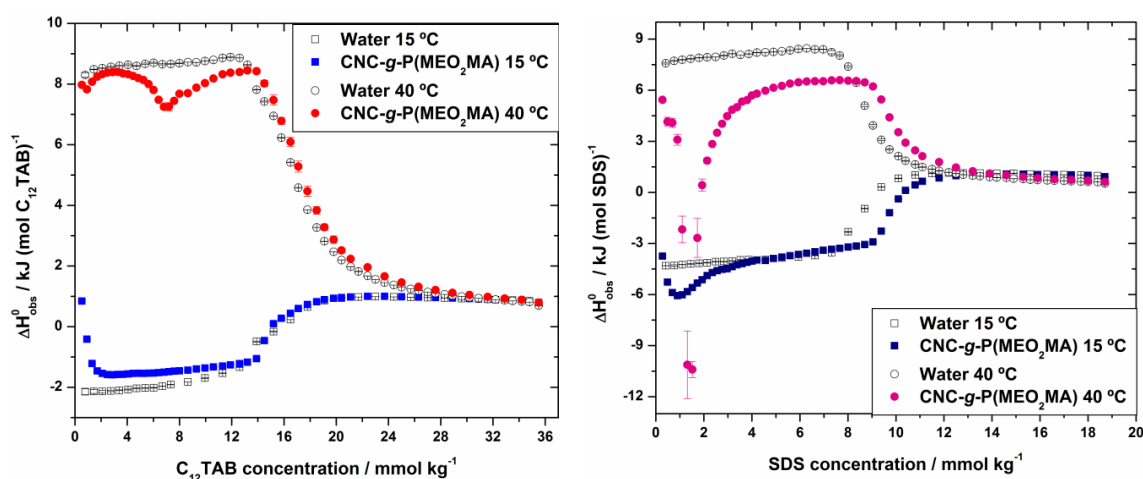
Figure 4.7 ITC curves at 15 and 40 °C for the titration of C$_{12}$TAB (left) and SDS (right) into water (empty symbols) and into 1.0 wt% CNC-*g*-P(MEO$_2$MA) dispersions.

4.3.3.4 Electrophoretic Mobility and Particle Size Measurements

By preparing mixtures containing a fixed CNC-*g*-P(MEO$_2$MA) concentration at 1.0 wt% while varying the surfactant concentration in the same range as studied by ITC, we could gather more information between the two different systems at the two different temperatures. Figure 4.8 shows electrophoretic mobility and particle size results for mixtures with C$_{12}$TAB and SDS.

For the mixtures containing CNC-*g*-P(MEO$_2$MA) and different C$_{12}$TAB concentrations (0, 0.5, 4.0, 7.0, 16.0 and 32.0 mmol kg^{-1})(Figure 4.8a) there is a charge inversion from negative to positive values at low surfactant concentration that corresponds to the first small ITC peak (0.5 mmol kg^{-1}), which can be associated to the charge neutralization on the CNC surface. Increasing the surfactant concentration lead to more positive electrophoretic mobility values, with the values obtained at 40 ℃ being more positive than the ones obtained at 15 ℃. For the very first two concentration points (0.5 and 4.0 mmol kg^{-1}) it was not possible to measure the particle size (Figure 4.8c), and again it is correlated to the small ITC peak observed. The CNC-*g*-P(MEO$_2$MA)/C$_{12}$TAB mixtures were turbid and agglomerated (Figures B.3 and B.4 in Appendix B). This is represented by a dashed line connecting the first point for pure CNC-*g*-P(MEO$_2$MA) to the point related to a surfactant concentration of 7.0 mmol kg^{-1}, where we have the second peak at 40 ℃ in the ITC experiments (Figure 4.7). We put this point to show how large the particles became (2.4 ± 0.3 μm) especially at 15 ℃ because of the aggregation/agglomeration of the CNC-*g*-P(MEO$_2$MA) particles. At high surfactant concentration the particle size at both temperatures decreased down to values of 610 ± 50 nm and the mixtures became transparent again (Figure B.3 in Appendix B). We can assume that the binding of C$_{12}$TAB to the CNC-*g*-P(MEO$_2$MA) particles occurs in a sequential manner: it first binds to the negatively charged sulfate ester groups as it was observed for pristine CNC before (Chapter 3),[36,157] followed by a polymer induced micellization (*cac*), which causes the now C$_{12}$TAB decorated CNC-*g*-P(MEO$_2$MA) particles to repel each other and to remain dispersed in solution.[38]

For the mixtures containing CNC-*g*-P(MEO$_2$MA) in the presence of different SDS concentrations (0, 0.3, 1.5, 4.0, 10.0 and 16.0 mmol kg^{-1}) the electrophoretic mobility values (Figure 4.8b) became more negative when increasing the surfactant concentration. Analyzing the particle size results (Figure 4.8d) we see that at 15 ℃ there

is only a slight variation regardless of the SDS concentration. When the mixtures were at 40 °C there was a considerable increase in the particle size (from 206 ± 1 nm to 410 ± 70 nm) at a surfactant concentration of 0.3 mmol kg^{-1} that is correlated to a polymer induced micellization process (*cac*) and observed as an ITC peak (Figure 4.7). Increasing the SDS concentration caused the particle size of the mixtures to decrease down to 230 ± 20 nm. Although there was this variation in the size of the mixtures, they became transparent and did not display visual agglomeration and/or aggregation (Figures B.5 and B.6 in Appendix B). When SDS was added to CNC-*g*-P(MEO$_2$MA) it would bind to the grafted polymer chains regardless of the temperature. At 40 °C, the increase in the particle size at low surfactant concentration was due to the SDS bound to entangle polymer chains from distinct CNC particles. Then a polymer-induced micellization would take place by increasing the surfactant concentration, which caused the polymer chains to disentangle one from another, and the system became redispersed, causing a decrease in the particle size.
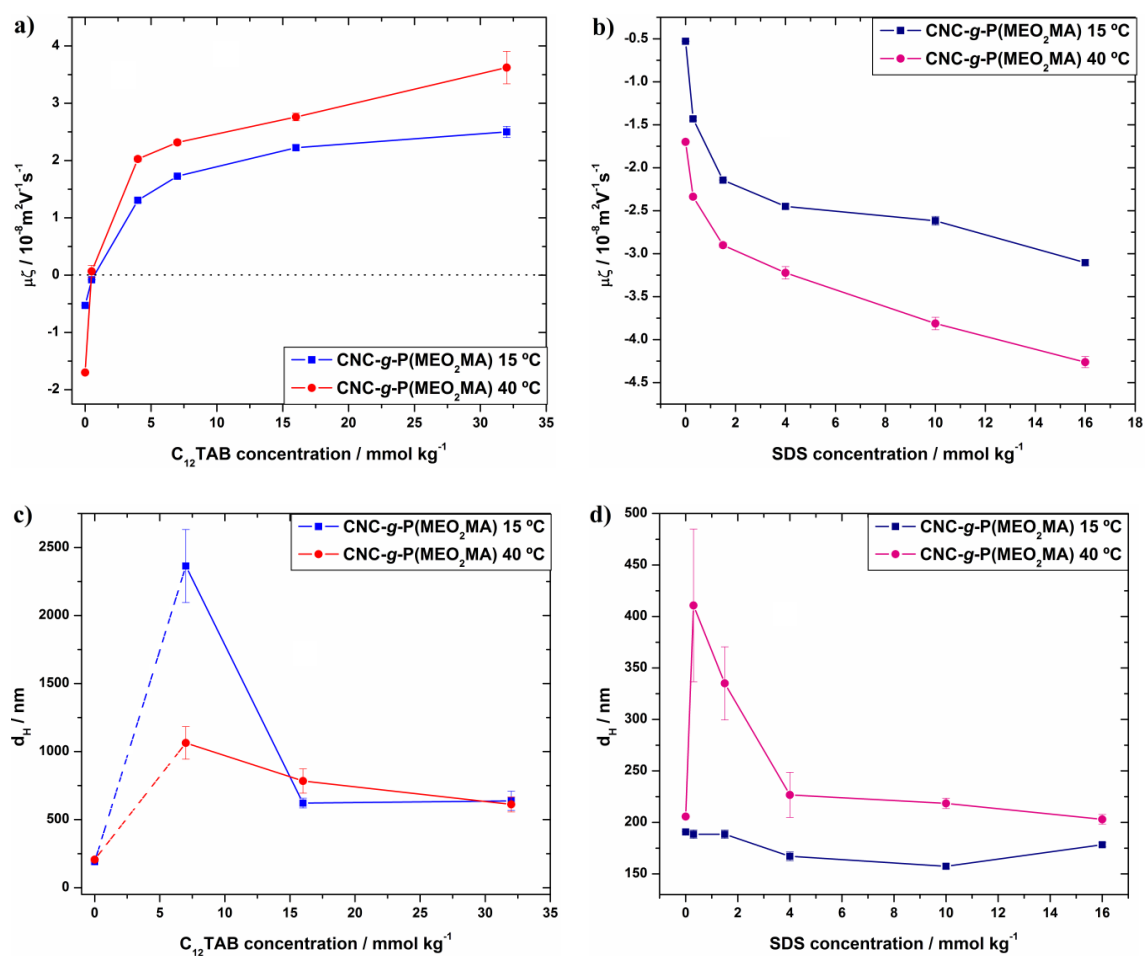
Figure 4.8 Electrophoretic mobility results obtained for C$_{12}$TAB (a) and SDS (b) and apparent hydrodynamic diameter (d$_{Happ}$) results obtained for C$_{12}$TAB (c) and SDS (d) as a function of surfactant concentration.

4.3.3.5 Influence of SDS on the redispersion of CNC-*g*-P(MEO$_2$MA)

As mentioned before the redispersion of the grafted P(MEO$_2$MA) chains was achieved by adding electrical charges to the system (either positive or negative) and therefore, enhancing their solubility in water.[169] We then attempted to reverse the phase transition of the mixtures in a "switch on"/"switch off" mechanism (measured by transmittance), by removing the added surfactant with dialysis against deionised water. Once all the surfactant was removed (or at least most of it) the system would undergo phase separation by increasing the temperature once again ("switch on") and it could be redispersed by adding more surfactant ("switch off").

The added C$_{12}$TAB (80.0 mmol kg^{-1}, 5 times its *cmc*) could not be removed from the mixture even after dialysing it 3 times a day during 1 week, due to its strong electrostatic interactions with the sulfate-ester groups on the CNC surface – some flocs would appear in solution, much similar to those found by Brinatti and co-workers (Chapter 3).[157](Figure B.7 in Appendix B) When adding SDS (40.0 mmol kg^{-1}, 5 times its *cmc*) however, the "switch on"/"switch off" mechanism worked at least partially. Dialysis water was exchanged 12 times within 2 days. For the time being no visual precipitation or turbidity was observed. The mixture was left in water for another week at room temperature. After this period of time some small flocs were found inside the dialysis tube and when DSC was performed, there was only one peak observed and it had shifted back to 25.0 ℃ with a much smaller intensity (inset in Figure 4.9). The reduced intensity of this DSC peak may indicate dilution of the dispersion and this may be the reason why no clear turbidity could be observed at higher temperature.

We decided to further investigate the LCST behavior in the presence of different SDS concentrations (Figure 4.9). The addition of increasing SDS concentrations caused a shift of the peak related to the P(MEO$_2$MA) transition to higher temperature values, up to the concentration of 20.0 mmol kg^{-1}. At a concentration of 40.0 mmol kg^{-1} (the same concentration used for the "switch on"/"switch off" mechanism) we could not

obtain a peak due to equipment limitations (the temperature is supposed to be above 120 ºC). Even the smallest concentration of SDS added to the system (0.1 mmol kg^{-1}) shifted the maximum of the curve from 23.6 to 28.9 ºC. At this surfactant concentration there is also the presence of a shoulder at a lower temperature around 25.2 ºC. Not only the peak related to P(MEO$_2$MA) is shifted to higher temperatures, but also another peak showed up at higher temperature than this one that is much smaller and broader than the first one. A similar behavior had been observed before when studying SDS in the presence of PNIPAM.[170]
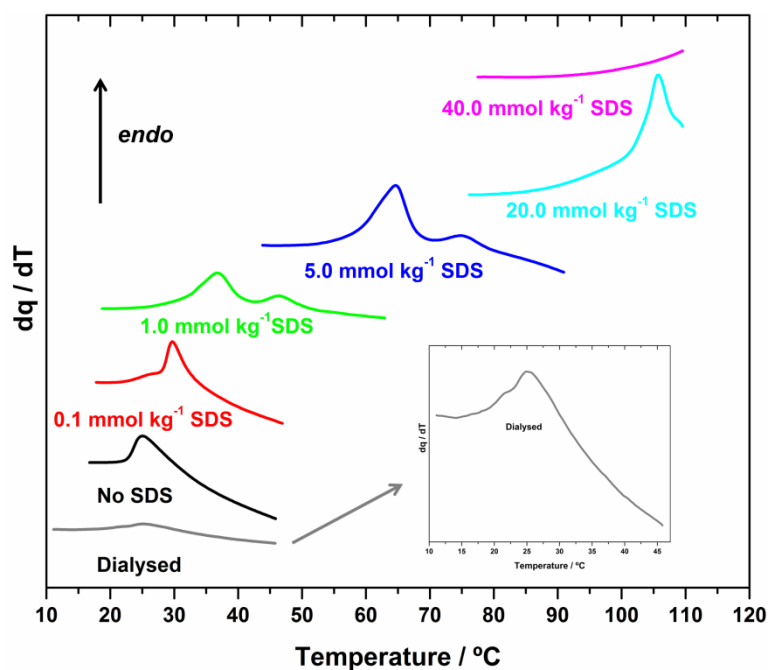
Figure 4.9 HSDSC curves for CNC-*g*-P(MEO$_2$MA) in the presence of different SDS concentrations. The dialysed mixture (grey line) contained originally 40.0 mmol kg^{-1} of SDS.

Table **4.1** shows the values of T_m (ºC) for the different SDS concentrations used. When plotting the T_m obtained for the first peaks against SDS concentration (Figure B.8 in Appendix B) we can see that LCST presented is an exponential growth, much similar to what was found by Schild & Tirrell[169] when studying sodium n-alkyl sulfates in the presence of PNIPAM.

Table 4.1 T_m (ºC) obtained by the HSDSC curves as a function of SDS concentration (mmol kg^{-1})

SDS concentration / mmol kg^{-1}	T_m / ºC	
0	25.0	
0.1	29.7	
1.0	36.7	46.3*
5.0	64.7	74.8*
20.0	105.8	—
40.0	—	
Dialysed	25.0	

*T_m obtained at the maximum of the second peak.

4.4 Discussion

The presence of the nonionic surfactant micelles NP-100 in mixtures containing cationic C_nTAB surfactants and CNC was able to change the concentration at which precipitation starts as seen by electrophoretic mobility and transmittance experiments (Figure 4.2). Charge neutralization was reduced from 0.5 to 0.25 *cmc* for C_{12}TAB and it did not change for C_{16}TAB, which reveals a larger influence on the more hydrophilic surfactant. Nonetheless, precipitation occurred for the mixtures after they were left to equilibrate for some time (5 h). These results pointed that even with the presence of a nonionic surfactant with a large headgroup it was not able to prevent the strong electrostatic interaction between the cationic C_nTAB and the negatively charged CNC.

Although C_nTAB is able to bind and decorate the pristine CNC rods and change its surface electrical charge (Figure 4.2, left), there are not enough binding sites accessible as the CNC surface modification by grafting P(MEO$_2$MA) helped us proving this concept. Using a thermoresponsive polymer that undergoes phase transition near room temperature (starting at 23.6 ºC, Figure 4.5) helps us visually observe this phenomenon. Below LCST, C_{12}TAB surfactant binds preferably to the negative sulfate-ester groups on the CNC and it can only bind to the P(MEO$_2$MA) at higher surfactant concentration. Above LCST there are enough hydrophobic domains due to the collapse of the polymer chains on the CNC surface and consequently intermolecular interactions between the rods, which causes the cationic surfactant to be able to readily bind to them

as seen by a peak on ITC results (Figure 4.7, left) and by the large particle size observed (Figure 4.8c). This interaction with the polymer chains is reversible (only hydrophobic interactions) and the surfactant bound to them can be removed by dialysis, while the surfactant bound to the negative charges cannot.

Considering SDS possesses the same electrical charge signal as CNC, the only possible interactions of SDS molecules are with the $P(MEO_2MA)$ chains. This can be seen by the presence of a peak on ITC results (Figure 4.7, right) regardless of the temperature and that becomes more prominent after LCST. As it happens for PEO in the presence of SDS, the polymer chains of $P(MEO_2MA)$ at a temperature above LCST can be rehydrated and incorporated into micellar aggregates.[171,172] It causes a continuous decrease to more negative values of electrophoretic mobility (Figure 4.8b) and to larger particle aggregates (Figure 4.8d) at the very concentration where we see a peak on ITC. Because the interactions between SDS and CNC-g-$P(MEO_2MA)$ are purely hydrophobic we expected to be able to remove the surfactant through dialysis and reverse the phase transition of the system (Figure 4.9 inset). There was only peak present and it was related to the polymer phase transition at 25.0 ℃ with a much lower intensity. This was attributed to a dilution of the CNC-g-$P(MEO_2MA)$ dispersion during the dialysis. The second peak related to aggregation was not observed, which confirmed that the "switch on"/"switch off" mechanism could be used to tune the thermal behavior of the system.

As we can see by DSC results (Figure 4.9) the presence of an increasing concentration of SDS was able to not only increase phase transition temperature by adding more electrical charge to the polymer chains and making it more soluble in water,[114] but also to delay the interpolymer chain aggregation to high temperatures by forming micellar aggregates around the polymer chains.[173]

4.5 Conclusions

The present study showed that although the presence of nonionic surfactant could enhance the binding between C_nTAB and CNC it was not sufficient to prevent precipitation. The surface modification of CNC with a thermoresponsive polymer $P(MEO_2MA)$ was confirmed by FTIR-ATR and TGA techniques, and its reversible phase transition was confirmed by performing DSC and transmittance experiments.

By grafting a thermoresponsive polymer on the CNC surface and with the addition of ionic surfactants to the system above its phase transition temperature we were able to cause the C_nTAB/CNC-*g*-P(MEO$_2$MA) mixtures to redisperse. $C_{12}TAB$ would bind to the P(MEO$_2$MA) polymer chains at 40 ℃ due to hydrophobic interactions, and would also strongly bind to the negative charges and could not be removed after one week of dialysis. However, even SDS that could only be bound to the polymer chains regardless of the temperature was not fully removed from the system after dialysis at either low or high temperature, and the reason for this phenomenon is still unknown. Increasing the SDS concentration could increase the phase transition temperature of CNC-*g*-P(MEO$_2$MA) that is attributed to the first peak, and delayed the intermolecular polymer aggregation to higher temperatures attributed to the presence of a second peak when performing DSC experiments. Dialysis was able to remove the present surfactant from the mixture and therefore could be used as a trigger to tune in the phase transition behavior. Overall, these results confirm the possibility of using similar systems in a reversible temperature responsive dispersion.

Chapter 5: Isothermal Titration Calorimetry Studies on the Interactions of Amine-modified Cellulose Nanocrystals with Ionic Surfactants§

My contributions to this paper

Performed all the experiments and wrote the manuscript.

Abstract

In this paper we present our findings on the study of the interactions between amine-modified cellulose nanocrystals (CNC-NH$_2$) and two ionic surfactants: sodium dodecyl sulfate (SDS) and dodecyltrimethylammonium bromide (C$_{12}$TAB), both with an alkyl chain with 12 carbon atoms. By varying the pH values from 4.1 up to 8.9 we could assess a decrease of electrostatic interactions between CNC-NH$_2$ and SDS, while an opposite phenomenon was observed for C$_{12}$TAB. Results obtained by isothermal titration calorimetry (ITC) and zeta potential measurements showed that electrostatic interactions were the driving force for the interactions with both surfactants. ITC studies also showed an exothermic process at low surfactant concentration for SDS in the presence of CNC-NH$_2$ (regardless of the pH and temperature), and an endothermic one for C$_{12}$TAB at high pH. This endothermic feature for C$_{12}$TAB in the presence of CNC-NH$_2$ disappeared when performing ITC experiments at higher temperatures, a phenomenon that could be attributed to a lower energy required releasing water molecules and counterions into the bulk solution.

5.1 Introduction

The interactions of oppositely charged molecules such as, surfactants with polymers and surfactants with particles have been studied for many decades now.[42,43,174–178] Mixtures of oppositely charged molecules at different concentrations are used for many practical applications, ranging from emulsions,[179] rheology modifiers,[180,181] flocculation,[182] to drug delivery systems.[183]

---

§ This chapter is adapted from the manuscript "Brinatti, C.; Berry, R.M.; Tam, K.C.; Loh, W Isothermal Titration Calorimetry Studies of Interactions of Amine-modified Cellulose Nanocrystals with Ionic Surfactants".

In the past decade, cellulose nanocrystals (CNC) have gained a lot of interest for being a non-toxic, renewable, environmentally friendly material obtained from the acid hydrolysis of cellulose.[122] There are many advantages in using CNC due to its high strength, modulus, surface area, the possibility of derivatization of its hydroxyl groups and the presence of negative charged sulfate-ester groups on its surface resulting from the sulfuric acid hydrolysis.[7,11,14,104,184] This last feature allows CNC to be able to interact with cationic surfactants in aqueous solutions (Chapter 3).[25,36,157] It was observed that the electrostatic interactions are so strong between CNC and alkyltrimethylammonium bromide surfactants (C_nTAB) that they cause flocculation and the mixture cannot be redispersed even at a high surfactant concentration.[36,157] The studies performed by Dhar et al. and Brinatti and co-workers have mainly used isothermal titration calorimetry (ITC) technique to obtain information regarding the mixtures containing surfactants and CNC at different temperatures and in the presence of electrolytes. This technique has been widely used to survey complex interactions in aqueous colloidal mixtures (surfactants, polymers, proteins, nanoparticles) in aqueous solutions.[40]

Surface modification of CNC by derivatization of the hydroxyl groups can broaden its applications in the presence of surfactants.[125,185] However, ITC has only been used to study a few systems with modified CNC in the presence of surfactants. Peng et al.[35] studied a CNC grafted with a poly (propylene glycol) derivative in the presence of ionic surfactants sodium dodecyl sulfate (SDS) and dodecyltrimethylammonium bromide (C_{12}TAB). The former interacted only with the polymer chains by hydrophobic interactions, and the latter only interacted with the negative charged groups on the CNC surface by electrostatic interactions. Brinatti and co-workers (Chapter 4) have studied the redispersion of a CNC grafted with a thermoresponsive polymer poly (oligo (ethylene oxide) methacrylate), CNC-*g*-P(MEO$_2$MA) with SDS and C_{12}TAB as well, at temperatures below and above the phase transition one. They found that SDS is able to interact with the polymer chains regardless of the temperature, while the interactions between C_{12}TAB and CNC-*g*-P(MEO$_2$MA) are also electrostatic with the negatively charged groups and they are temperature dependent with the polymer – they only occur when the polymer chains have collapsed at a temperature above that of its phase transition.

The surface modification of CNC with amine groups has been earlier performed by some groups [186–188] In an attempt to increase the amine content and to optimize the

reaction conditions, our group used a simple protocol to prepare CNC-NH$_2$ through a two-step process using an etherification reaction in an organic solution (Appendix E).[107] This CNC modification with amine groups could be a useful method for a second derivatization as well.[186] Modifications with different amine groups, such as (dimethylamino) ethyl methacrylate (DMAEMA) derivatives could be used as a gene delivery system[189] and in Pickering emulsion formulations.[26]

Here we present a study using ITC as the main technique to study the interactions of an amine-surface modified CNC (CNC-NH$_2$) with two ionic surfactants: SDS and C$_{12}$TAB. Three different pH values were investigated for both surfactants and, at the pH of strongest electrostatic interaction between CNC-NH$_2$ and the surfactant, experiments were performed at three different temperatures in order to better assess the hydrophobic contributions from the surfactants. Based on the ITC results, we performed measurements of transmittance, zeta potential and settling behavior at low temperature to provide a better understanding of the systems.

5.2 Experimental Section

5.2.1 Materials

Cellulose nanocrystal (CNC) hydrolyzed from wood pulp was kindly provided by CelluForce Inc. The synthesis, purification and characterization of amine-modified CNC (CNC-NH$_2$) is described elsewhere (Appendix E).[107] The NH$_2$ content is 0.62 mmol g^{-1}.[107] The chemicals used for the surface modification were epichlorohydrin (EPH), dimethylsulfoxide (DMSO) and tetrabutylammonium hydroxide (TBAH), all purchased from Sigma-Aldrich®, and ammonium hydroxide (28-30% NH$_3$ in water) was purchased from Acros Organics. The surfactants dodecyltrimethylammonium bromide (C$_{12}$TAB) and sodium dodecylsulfate (SDS) were purchased from Sigma-Aldrich® ($\geq$ 98% purity) and used without any purification. Water used to prepare all solutions and dispersions was of Milli-Q grade (18.2 MΩ cm^{-1}).

All the experiments were performed with 0.1 wt% CNC-NH$_2$ dispersions. The pH of all the samples (surfactant solution and CNC-NH$_2$ dispersions) was adjusted to 4.1, 7.5 and 8.9 by adding either 1.0 mol L^{-1} HCl or NaOH. For experiments performed at high temperatures the pH as adjusted at room temperature and the samples were heated inside the ITC cell.

5.2.2 Isothermal Titration Calorimetry

The calorimeter used was the MicroCal VP-ITC (Northampton, MA, USA). Aliquots ranging from 3 to 15 μL were added stepwise by an automatic injection syringe containing 270 μL of a concentrated surfactant solution (typically at least twelve times above its critical micellar concentration (*cmc*) value) into the reaction cell (1.43 mL) containing either water or 0.1 wt% CNC-NH$_2$ dispersion with a 5 min interval between each injection. To evaluate the charge effect on the interactions, three different pH values were used in the experiments: 4.1, 7.5 and 8.9. In order to evaluate the hydrophobic contributions, the experiments were performed at different temperatures of 25, 45 and 55 ºC. All the experiments were performed in duplicate. All obtained data were treated with the Origin® 7.0 software.

5.2.3 Transmittance Measurements

Transmittance measurements were carried out on a UV-Vis Cary Varian 100 Bio Spectrophotometer, equipped with a thermostat water bath. The results were obtained at a wavelength of 600 nm at 25 ºC.

5.2.4 Zeta Potential Measurements

Zeta potential measurements were carried out using a NanoZS Zetasizer (Malvern Instruments) that uses M3-PALS technique. The CNC-NH$_2$ concentration was fixed at 0.1 wt% while varying the surfactant concentration. All the experiments were performed at 25 ºC in duplicate.

5.2.5 Settling behavior measurements[**]

The samples were prepared containing a constant concentration of 0.1 wt% CNC-NH$_2$ dispersion while the surfactant concentration was increased following the ITC concentration range. The vials were manually shaken prior to the measurements, and the settling of the mixtures was measured for 30 min. The settling height was measured every 3 min. The white turbid region on the bottom of the vial represented the

---

[**] Some of the results described here were partially reported elsewhere [107]

flocculated CNC-NH$_2$/surfactant mixtures. The settling velocity was determined after 9 min by calculating the slope of the graph height (cm) as a function of time (min) (see Figures C.1 and C.2 in Appendix C).

5.3 Results

5.3.1 Isothermal Titration Calorimetry (ITC)

Figure 5.1 presents the ITC results obtained at 25 ºC for the titration of SDS (left) and C$_{12}$TAB (right) in water and in the presence of CNC-NH$_2$ at three different pH values. The critical micellar concentration (*cmc*) values did not change considerably for both surfactants regardless of the pH value (SDS 8.5 mmol kg^{-1}, C$_{12}$TAB 16.0 mmol kg^{-1}) and are in accordance with previous literature results.[145,157,190,191] *Cmc* values can be obtained by the first derivative method.[39,40]
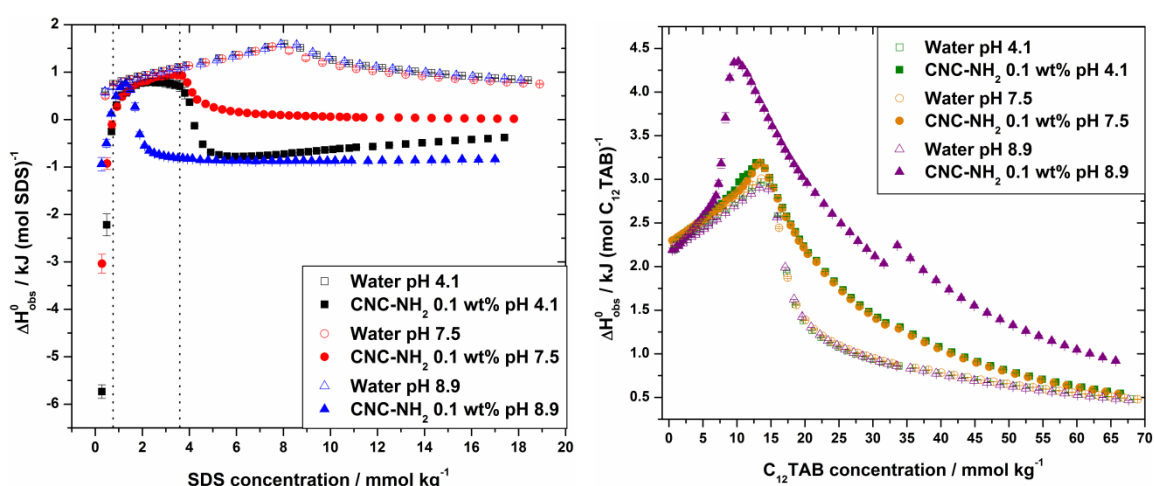
Figure 5.1 Calorimetric titration curves at 25 ºC for the titration of SDS (left) and C$_{12}$TAB (right) into water (open symbols) and into 0.1 wt% CNC-NH$_2$ dispersions (filled symbols) at three different pH values.

For the SDS/CNC-NH$_2$ mixtures (Figure 5.1, left) we observed that, regardless of the pH, the titration curves were similar and could be divided in three regions: first there was an exothermic process ($\Delta H^0_{obs} < 0$) at low surfactant concentration (0 to 1.3 mmol kg^{-1}) whose magnitude decreased as the pH increased (-5.73, -3.03 and -0.94 kJ mol^{-1}, for pH values of 4.1, 7.5 and 8.9, respectively). This process could be attributed to an electrostatic interaction between the negatively charged sulfate groups of the

surfactant (OSO_3^-) and the positively charged amine groups (NH_3^+) on the surface of the CNC. An increase in the pH of the system led to a deprotonation of the same amine groups ($NH_3^+ \rightarrow NH_2$) thus reducing the overall available positive charge for such interaction to occur with the surfactant, which was reflected on lower enthalpy values. By increasing the surfactant concentration the titration curves in the absence and in the presence of CNC-NH$_2$ dispersions superimpose each other. There was a plateau for the curves at pH 4.1 and 7.5, from 1.3 to 3.5 mmol kg^{-1}, while there was only a peak at the titration curve at pH 8.9, probably related to the surfactant binding continuously to the CNC-NH$_2$. Finally, the titration curves in the presence of CNC-NH$_2$ diverged from the dilution curves in water. To this phenomenon we attributed a surface induced micellization on the CNC-NH$_2$,[157] a process similar to a critical aggregation concentration (*cac*) observed for mixtures containing surfactants and polymers.[1353940] The saturation concentration (C_2) typically found for the similar systems was not reached in the surfactant concentration range of this study, for the curves in the presence and in the absence of CNC-NH$_2$ did not merge.

For the C$_{12}$TAB/CNC-NH$_2$ mixtures (Figure 5.1, right) the titration curves in the presence and absence of CNC-NH$_2$ were practically identical at the pH values of 4.1 and 7.5 due to the fact that they were all superimposed. CNC-NH$_2$ dispersions present residual positive charges (zeta potential values of +11.3 and +8.4 mV) at these pH values, respectively, which might have hindered the formation of micelle aggregates on the surface similar to the mixture with SDS. The repulsion between the NH_3^+ groups on the CNC surface and the headgroup of the cationic surfactant C$_{12}$TAB led to a broader concentration range from 15.0-65.0 mmol kg^{-1}, as it can be seen in Figure 5.1.

Only when the pH was increased to 8.9 the titration curve in the presence of CNC-NH$_2$ distinctly showed an endothermic process ($\Delta H_{obs}^0 > 0$) that started at surfactant concentration around 7.5 mmol kg^{-1}. In this peak region, surface induced micellization happened in a similar fashion as for SDS. This endothermic process might be associated to the dehydration of both the CNC-NH$_2$ and the surfactant polar group (trimethylammonium) due to the release of water molecules (Scheme 5.1) into the bulk solution. Water molecules have now a higher degree of freedom than before, which is entropically favorable and contributes for the interaction process. Therefore, the interactions between surfactant and CNC-NH$_2$ were mainly considered electrostatic. Here, the C_2 value was not reached in the surfactant concentration range studied. In an attempt to obtain the superimposition of the curves, a second titration experiment was

performed after the first titration was over. We did it by removing the overflown volume in the reaction cell (270 μL previously injected), filling the injection syringe with a $C_{12}TAB$ stock solution, and started the second experiment. By doing this, some of the mixture $C_{12}TAB/CNC-NH_2$ must have been removed in this procedure, which led to a discontinuity in the titration curve (▲) in Figure 5.1 at a surfactant concentration of 33.0 mmol kg^{-1}. The reasons for a higher surfactant concentration required for the surface induced micellization of $C_{12}TAB$ compared to SDS are not evident. One hypothesis might be that $C_{12}TAB$ could bind not only to the negative OSO_3^- groups, but also to the non-charged NH_2 groups, therefore having more available binding sites.

The results found here are much similar to the ones reported by Olofsson and Wang[192] when studying mixtures of tetradecyltrimethylammonium bromide ($C_{14}TAB$) and two ethyl(hydroxyethyl) cellulose (EHEC) polymers, one being hydrophobically modified. Micellization of $C_{14}TAB$ was affected in the presence of the less hydrophobic EHEC but with no distinct break that could be associated with a *cac* value, similar to what was observed in our study at lower pH values. When titrating $C_{14}TAB$ into the hydrophobically modified EHEC, the ITC curve showed a large endothermic peak.[192]
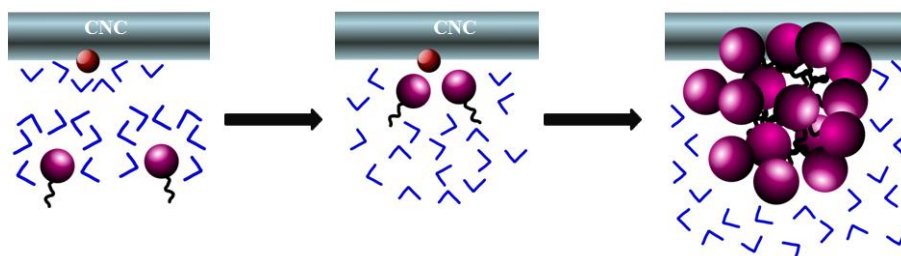
Scheme 5.1 Pictorial representation of the electrostatic interaction between $C_{12}TAB$ and CNC-NH$_2$, featured by an endothermic process of dehydration of water molecules as seen by ITC results (Figure 5.1).

5.3.2 Transmittance, Zeta Potential and Settling Measurements

The strong electrostatic interactions between ionic surfactants and oppositely charged particles could possibly lead to associative phase separation. CNC-NH$_2$ dispersions are pH-responsive and can acquire positive charge at low pH, thus a strong interaction with SDS is expected while at a high pH it interacts strongly with $C_{12}TAB$ (Scheme 5.2).

The presence of amine groups (NH_2) on the CNC surface is responsible for the pH-responsiveness of CNC-NH_2 (Appendix E).[107] At low pH values the surface acquires a positive charge due to the protonation of the amine groups ($NH_2 \rightarrow NH_3^+$). The opposite is true – by increasing the pH of the dispersion for the amine groups are expected to deprotonate, acquiring less positive values and, eventually, the surface will present a negative charge due to the sulfate groups (OSO_3^-). Zeta potential results obtained for the pure CNC-NH_2 dispersions at 25 ºC and different pH values were +11.3 mV (pH 4.1), +8.4 mV (pH 7.5) and +2.4 mV (pH 8.9), showing that even at high pH values there is a residual positive charge from protonated amine groups.
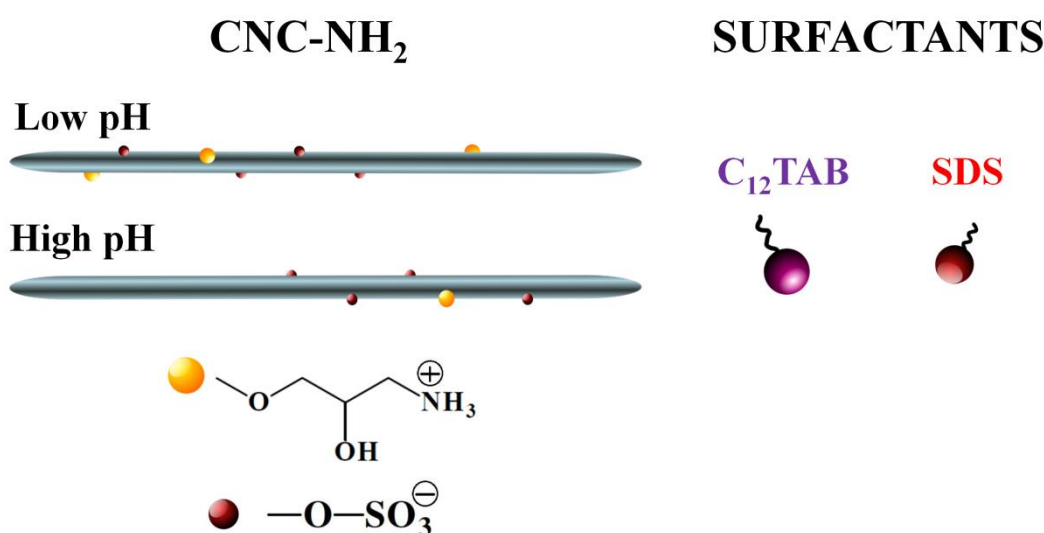
Scheme 5.2 Pictorial representation of CNC-NH$_2$ at low and high pH, and the representation of the C$_{12}$TAB and SDS surfactants.

Based on the ITC concentration range studied at different pH values (Figure 5.1), we prepared different samples by fixing the CNC-NH_2 concentration at 0.1 wt% and varying the surfactant concentration for both surfactants. Due to the fact that the pH had a large influence on the interactions between surfactants and the CNC-NH_2, we present here the results for SDS at pH 4.1 (Figure 5.2) and C12TAB at pH 8.9 (Figure 5.3). Some of the results for SDS have been already reported in an earlier publication, but are shown here for comparison (Appendix E).[107] We performed transmittance, zeta potential and settling measurements for CNC in the presence of both surfactants (Figure 5.4). The vertical lines are at the same concentration as the ones marked on Figure 5.1 showing the correlation between the results.
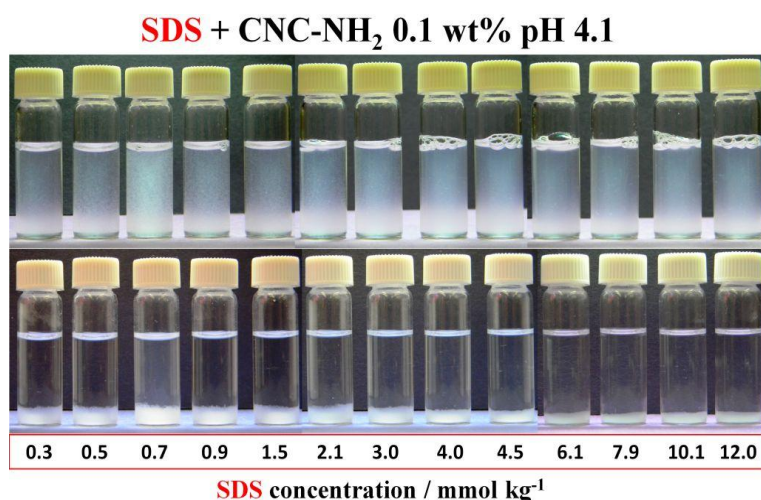
Figure 5.2 Mixtures containing 0.1 wt% CNC-NH₂ and SDS at 25 ºC. Top part shows the mixtures after mixing, and in the bottom after 30 min.
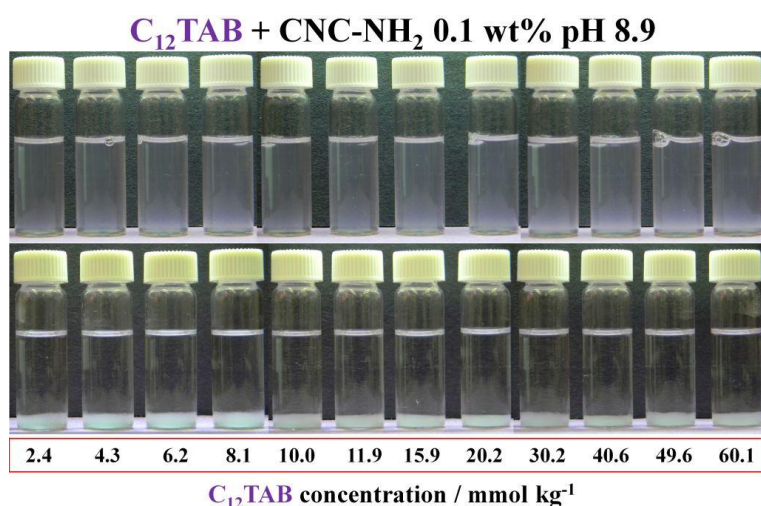
Figure 5.3 Mixtures containing 0.1 wt% CNC-NH₂ and C12TAB at 25 ºC. Top part shows the mixtures after mixing, and in the bottom after 30 min.

Zeta potential results for SDS (Figure 5.4, left) show a signal inversion from positive (+11.3 mV) to negative (-14.9 mV) values at a narrow surfactant concentration range (0 to 0.70 mmol kg^{-1}). In this concentration range the transmittance values decreased considerably to 26% of its original value, and the settling velocity presented the maximum value of 0.26 cm min^{-1}. These results could be correlated to the exothermic peak obtained by ITC (Figure 5.1) where we propose a strong electrostatic interaction between the surfactant and the CNC-NH₂. By increasing the surfactant concentration to values higher than 4.0 mmol kg^{-1}, the settling velocity approached zero

while the zeta potential and transmittance values remained practically constant possibly due to the decoration of the CNC-NH$_2$ by the surfactant and eventually the formation of surface induced micelles.

For C$_{12}$TAB (Figure 5.4, right) there were only two distinct regions. Up to a surfactant concentration of 12.0 mmol kg^{-1}, zeta potential values became more positive (+8.9 mV), transmittance values did not vary significantly and settling velocity presented its highest value similar to the results obtained for SDS (0.26 cm min^{-1}) (Figure 5.4, left). Here we assumed that a surface induced micellization was taking place, in accordance to the ITC results (Figure 5.1). Further increase in the surfactant concentration led to a decrease in the settling velocity values to zero, while the zeta potential and transmittance values remained constant.
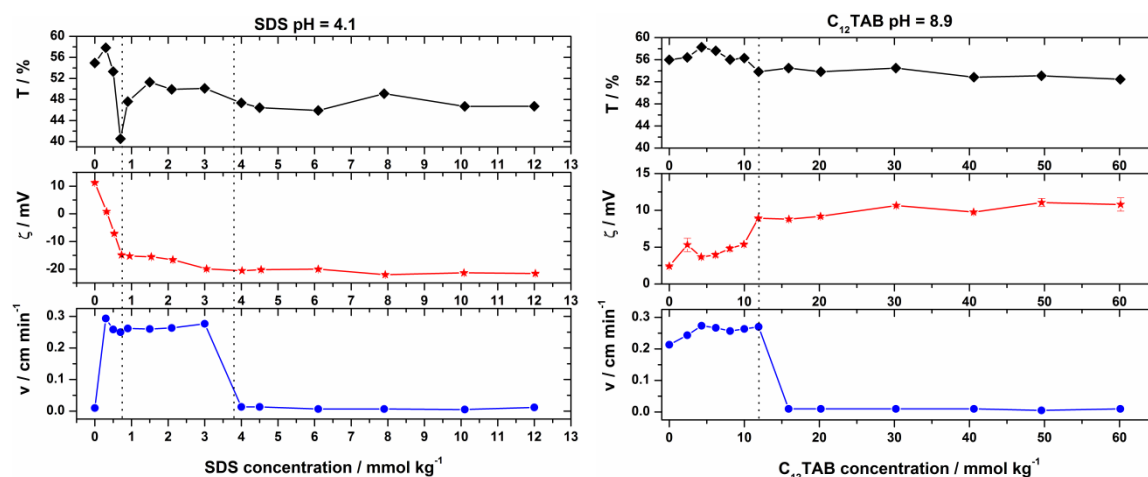
Figure 5.4 Transmittance (◆), zeta potential (★) and settling velocity (●) for the SDS/CNC-NH$_2$ mixtures at pH 4.1 (left) and C$_{12}$TAB/CNC-NH$_2$ mixtures at pH 8.9 (right). Results were obtained at 25 ºC.

5.3.3 Effect of Temperature

In an attempt to evaluate the magnitude of the hydrophobic contributions (Chapter 3),[39,157] the interactions between surfactants and CNC-NH$_2$ – alkyl chains of the surfactants (both with 12 carbon atoms) and the surface of CNC were studied at various temperatures –. ITC experiments were performed at higher temperatures of 45 and 55 ºC at the pH values of 4.1 for SDS and 8.9 for C$_{12}$TAB. At these pH values the long range electrostatic interactions between the surfactants and the CNC-NH$_2$ should remain the same.[39] The obtained results are shown in Figure 5.5.
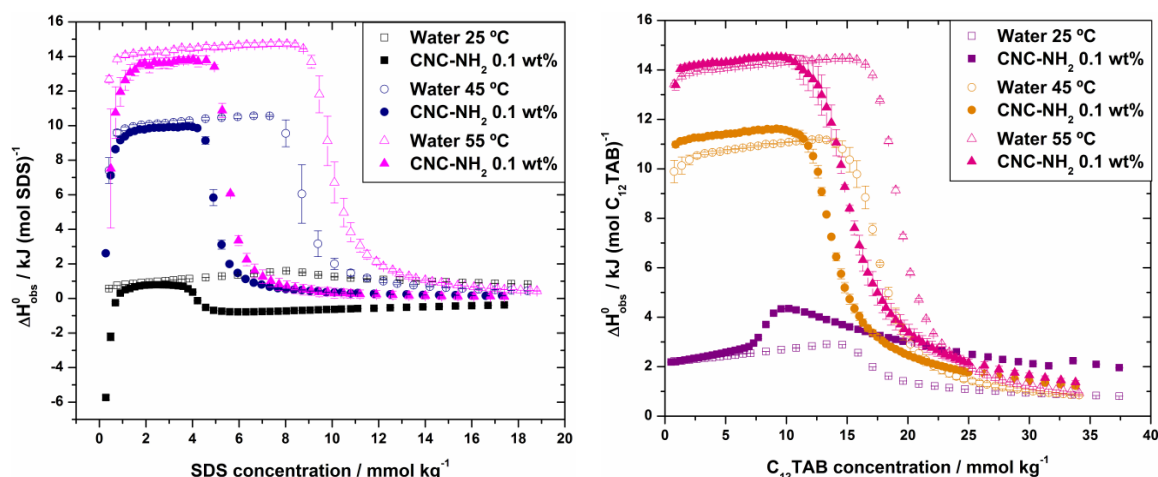
Figure 5.5 Calorimetric titration curves obtained at three different temperatures for the mixtures of SDS/CNC-NH$_2$ at pH 4.1 (left) and C$_{12}$TAB/CNC-NH$_2$ at pH 8.9 (right). The open symbols represent the titrations of surfactant in water and the filled symbols are the titration of surfactant into 0.1 wt% CNC-NH$_2$ dispersions.

For the mixture containing SDS (Figure 5.5, left) the titration curves in the presence of CNC-NH$_2$ at three different temperatures were similar. The electrostatic interaction was still present at low surfactant concentration, for the first injections the interaction curve remained below the dilution curves. Increasing the surfactant there was a plateau for a concentration range of 4.0 mmol kg^{-1} where both curves superimposed each other (dilution and interaction curves) that is related to the binding of the surfactant to the CNC-NH$_2$ surface. When the curves diverged we attributed it to a surface induced micellization. It is interesting to note that at higher temperatures (45 and 55 ºC) the curves merged at a high surfactant concentration, denoting a surface saturation concentration (C_2) of the CNC-NH$_2$ and the formation of free micelles in solution. This experiment clearly highlights the importance of electrostatic interactions between surfactants and CNC, which are the major driving forces for the interactions. This is because the calorimetric curves did not change when increasing the temperature. The curves at higher temperatures were shifted to more positive enthalpy values because micellization is a temperature dependent process[39] – it became exothermic and the *cmc* values were also slightly shifted to higher values (8.6 and 9.4 mmol kg^{-1} at 45 and 55 ºC, respectively).

The mixture containing C$_{12}$TAB (Figure 5.5, right) shows some interesting results. The *cmc* values shifted to higher values with an increase in the temperature

(17.3 and 19.1 mmol kg^{-1} at 45 and 55 ºC, respectively) as it were observed for SDS. Nonetheless, while increasing the temperature the initial endothermic peak observed at 25 ºC attributed to a surface induced micellization disappeared. At 45 ºC the titration curve in the presence of CNC-NH$_2$ was slightly more endothermic than the dilution curve, while at 55 ºC both curves were superimposed. As for the mixture containing SDS, the electrostatic interactions were not expected to be affected by temperature, but the hydration of both the surfactant and the CNC-NH$_2$ should be. There was an increase on the degrees of freedom of the water molecules and less energy was required for them to be released into the bulk solution (Scheme 5.1). This was demonstrated by Loh and coworkers[137,172] when studying interactions between SDS and PEO at higher temperatures.

5.4 Discussion

Electrostatic interactions are the driving force at low surfactant concentration for the interactions between both SDS and C$_{12}$TAB surfactants with CNC-NH$_2$, followed by surfactant hydrophobic interactions when surface-induced surfactant aggregation starts. For SDS at a very low surfactant concentration, the lower the pH values, the stronger the interactions as seen by the ITC curves (Figure 5.1) and zeta potential results (Figure 5.4, middle). This is followed by a maximum speed in the settling velocity graphic as well (Figure 5.4, bottom). From the ITC curves (Figure 5.1) we can also infer that with an increase in the pH values from 4.1 to 8.9, the amine groups on the CNC surface become gradually deprotonated (as observed by a decrease in the zeta potential values from +11.3 to +2.4 mV) therefore decreasing the number of available binding sites for electrostatic interaction as well. This is seen by a decrease in the enthalpy values at the very first addition of the surfactant into the reaction cell containing CNC-NH$_2$, and also a decrease in the plateau concentration range. By fixing the pH at 4.1, increasing the temperature of the system did not affect the initial electrostatic interactions between SDS and CNC-NH$_2$ (Figure 5.5). The ITC curves were only shifted to more positive values of enthalpy, following the micellization behavior.[39] The surfactant concentration at which the curves deviated from each other was not shifted, indicating that temperature did not have an impact on the interactions.

Due to the overall charge of CNC-NH$_2$ still being positive at the pH range studied, interaction with C$_{12}$TAB only occurred at pH 8.9, when zeta potential was close

to zero (+2.4 mV). Interestingly enough, ITC showed that the interaction between surfactant and CNC-NH$_2$ possessed an endothermic signature. However, the only possible interactions expected at low surfactant concentration were electrostatic and, as for SDS, exothermic. It is known that the interactions between cationic surfactants and modified polymers are much more pronounced especially when the polymer presents hydrophobic modifications, similar to what was observed by Olofsson & Wang[192] and by Loh and coworkers[137,172] when studying interactions between SDS and PEO at higher temperatures. The Scheme 5.2 is based on this information: dehydration plays a key role when it comes to the interactions of cationic surfactants and polymers.

Combining the results from ITC, zeta potential and transmittance measurements with the ones from the settling behavior experiment (Figure 5.4, bottom) we could assess that the velocity is maximum until surface induced micellization takes place at a concentration of 4.0 mmol kg^{-1} for SDS and 12 mmol kg^{-1} for C$_{12}$TAB.

5.5 Conclusions

We presented in this paper a calorimetric study of the interactions between an amine -modified CNC (CNC-NH$_2$) and two ionic surfactants, SDS and C$_{12}$TAB, both possessing the same alkyl chain length, at different pH values and temperatures. By increasing the pH of the medium from 4.1 to 8.9 we were able to tune the electrical charge on the CNC-NH$_2$ surface and consequently, decrease the interactions with SDS while increasing the interactions with C$_{12}$TAB. This was confirmed by fixing the pH value at the most energetic interaction for each surfactant (pH= 4.1 for SDS and 8.9 for C$_{12}$TAB) and increasing the temperature of the system. Although the initial driving force was the electrostatic interaction between surfactants and CNC-NH$_2$, the process was exothermic for SDS and endothermic for C$_{12}$TAB, which was associated with the parallel dehydration of both the surfactant headgroups and the CNC-NH$_2$ surface.

Surface-modification of CNC with pH-responsive groups/polymers might be very useful for different applications such as controlled delivery and formation of Pickering emulsions that could be tailored just by tuning the pH of the environment/system. The complete understanding on how it behaves in the presence of different concentrations of ionic surfactants may lead to new and improved formulations.

Chapter 6: General Discussions and Conclusions

Isothermal titration calorimetry (ITC) was the main technique used throughout this thesis for studying the interactions of pristine and modified CNC with surfactants in aqueous dispersions. It is the only technique in which one can directly obtain the enthalpy of reaction (ΔH^0) and also derive several thermodynamic parameters, such as critical micellar concentration (*cmc*), equilibrium constant (K_{eq}) and Gibbs free energy (ΔG^0) in a single experiment. Moreover, we have confirmed that ITC results also provide relevant, and in some cases unique, information on how the interaction process evolves and on its mechanism.

ITC was always chosen as the starting point for our experiments because we could see "the big picture" due to the obtaining of all the aforementioned parameters. As any other titration technique the concentrations at each injection of both components of our mixtures were known. After performing the control experiments (pure surfactant titrated into water), any deviation or difference observed by titrating the same surfactant (titrant) into CNC and its derivatives (analyte) would provide us with valuable information. However, ITC alone cannot and should not be used to fully interpret and draw conclusions from an interaction process between the titrant and analyte. New experiments have to be designed by using ancillary techniques such as light and/or X-ray scattering techniques, electrophoretic mobility, surface tension, spectroscopy and visual observations. The combination of all the data obtained by these techniques was pivotal in understanding many of the observed features for mixtures containing CNC and surfactants.

Although pristine CNC itself displays colloidal stability in water due to the presence of negative charges, this phenomenon could be disrupted by adding enough cationic surfactant (C_nTAB) to the dispersion. The electrostatic interactions are the driving force for this process to happen and, they are so strong that the mixture precipitates when the surfactant concentration reaches near half its *cmc* value, regardless of the surfactant alkyl chain length. At this point the surfactant is able to form micelles onto the CNC rods. Nonetheless, the longer the surfactant alkyl chain length, the more important the hydrophobic interactions became and more surfactant could be bound to the CNC. Still, after the negative CNC rods are covered by cationic micelles and assume a high positive electrical charge (as observed by electrophoretic mobility

experiments) this was not enough to cause CNC redispersion, probably because C_nTAB micelles acted as transient cross-linking agents among the CNC rods.

The addition of a nonionic surfactant with a large polymer-like headgroup such as NP-100 could provide an additional sterical hindrance to CNC/ cationic surfactant mixtures by interacting and adsorbing to its surface via hydrogen bonds. There could be an increase or decrease in the binding of the cationic surfactants to CNC depending on the ratio of the two surfactants. An increase of C_nTAB binding to CNC rods was indeed observed by electrophoretic mobility measurements, and yet again precipitation still occurred, with no redispersion. Another way of avoiding such behavior was to increase even further the sterical hindrance of CNC by grafting a polymer to its surface. With a grafted polymer there were more available binding sites not only for C_nTAB to bind, but also for an anionic surfactant such as SDS, to bind to it as well. A way of accomplishing this was to graft a thermoresponsive polymer, $P(MEO_2MA)$, with a phase transition temperature near room temperature. On one hand C_nTAB would preferably bind to the negative charges on the CNC surface regardless of the temperature, and it could only bind to the polymer chains when there is enough hydrophobicity – either at high surfactant concentration or at a temperature above the polymer phase transition. On the other hand, SDS could only interact with $P(MEO_2MA)$ chains regardless of the temperature. When the system was dialysed the surfactant was removed and the phase transition could be reversed, similar to a "switch on"/"switch off" mechanism.

The surface modification of CNC with amine groups (NH_2) that present a pH-responsive behavior was of much interest because it allowed the possibility to tune the interactions with oppositely charged surfactant molecules by adjusting the pH of the dispersion. When fixing the alkyl length of the surfactant while changing the electrical charge of its polar headgroup (from anionic to cationic) it was possible to gather more information at different experimental conditions of pH and temperature. The very same molecule that presented strong electrostatic interactions at low pH, such as SDS will have its interactions reduced when the pH was increased. A cationic surfactant $C_{12}TAB$ which has a large hydrated headgroup had its interactions with the negative charges on CNC and the NH_2 groups to be much more affected by a temperature change.

The results summarized above add a new body of experimental information on the interactions of CNC with surfactants. Although CNC has a high surface area, the lack or reduced number of available binding sites on its surface might be responsible for its associative phase separation when interacting with cationic surfactants. This

aforementioned hypothesis was confirmed by grafting a polymer which its hydrophilicity can be tuned by a change in temperature such as P(MEO$_2$MA) and does not affect the CNC colloidal stability. We were able to redisperse the CNC-*g*-P(MEO$_2$MA) in the presence of ionic surfactants with different electrical charges. This finding broadens the applications of CNC derivatives and ergo, the possibilities of different matrices they could be applied to.

We hope to have unraveled some issues regarding the colloidal stability of CNC and its derivatives in the presence of ionic surfactants at different experimental conditions. We also hope to have raised a few (or a lot) more questions on a fascinating topic that we are certain will still come up with many wonders in the near future in the most diverse possible applications.

References

(1)   Espinosa, S. C.; Kuhnt, T.; Foster, E. J.; Weder, C. Isolation of Thermally Stable Cellulose Nanocrystals by Phosphoric Acid Hydrolysis. *Biomacromolecules* **2013**, *14*, 1223–1230.

(2)   Habibi, Y.; Lucia, L. A.; Rojas, O. J. Cellulose Nanocrystals: Chemistry, Self-Assembly, and Applications. *Chem. Rev.* **2010**, *110*, 3479–3500.

(3)   Beck, S.; Bouchard, J.; Berry, R. Dispersibility in Water of Dried Nanocrystalline Cellulose. *Biomacromolecules* **2012**, *13*, 1486–1494.

(4)   Lin, N.; Huang, J.; Dufresne, A. Preparation, Properties and Applications of Polysaccharide Nanocrystals in Advanced Functional Nanomaterials: A Review. *Nanoscale* **2012**, *4*, 3274.

(5)   Moon, R. J.; Martini, A.; Nairn, J.; Simonsen, J.; Youngblood, J. Cellulose Nanomaterials Review: Structure, Properties and Nanocomposites. *Chem. Soc. Rev.* **2011**, *40*, 3941–3994.

(6)   Guo, J.; Catchmark, J. M. Surface Area and Porosity of Acid Hydrolyzed Cellulose Nanowhiskers and Cellulose Produced by Gluconacetobacter Xylinus. *Carbohyd. Polym.* **2012**, *87*, 1026–1037.

(7)   Dufresne, A. Nanocellulose: A New Ageless Bionanomaterial. *Mater. Today* **2013**, *16*, 220–227.

(8)   Roman, M.; Winter, W. T. Effect of Sulfate Groups from Sulfuric Acid Hydrolysis on the Thermal Degradation Behaviour of Bacterial Cellulose. *Biomacromolecules* **2004**, *5*, 1671–1677.

(9)   Eichhorn, S. J. Cellulose Nanowhiskers: Promising Materials for Advanced Applications. *Soft Matter* **2011**, *7*, 303.

(10)   Yang, H.; Tejado, A.; Alam, N.; Antal, M.; Van De Ven, T. G. M. Films Prepared from Electrosterically Stabilized Nanocrystalline Cellulose. *Langmuir* **2012**, *28*, 7834–7842.

(11)   Lagerwall, J. P. F.; Schütz, C.; Salajkova, M.; Noh, J.; Hyun Park, J.; Scalia, G.; Bergström, L. Cellulose Nanocrystal-Based Materials: From Liquid Crystal Self-Assembly and Glass Formation to Multifunctional Thin Films. *NPG Asia Mater.* **2014**, *6*, e80.

(12)   De Souza Lima, M. M.; Borsali, R. Rodlike Cellulose Microcrystals: Structure, Properties, and Applications. *Macromol. Rapid. Comm.* **2004**, *25*, 771–787.

(13) Mu, X.; Gray, D. G. Formation of Chiral Nematic Films from Cellulose Nanocrystal Suspensions Is a Two-Stage Process. *Langmuir* **2014**, *30*, 9256–9260.

(14) Lahiji, R. R.; Xu, X.; Reifenberger, R.; Raman, A.; Rudie, A.; Moon, R. J. Atomic Force Microscopy Characterization of Cellulose Nanocrystals. *Langmuir* **2010**, *26*, 4480–4488.

(15) Elazzouzi-Hafraoui, S.; Putaux, J. L.; Heux, L. Self-Assembling and Chiral Nematic Properties of Organophilic Cellulose Nanocrystals. *J. Phys. Chem. B* **2009**, *113*, 11069–11075.

(16) Abitbol, T.; Kloser, E.; Gray, D. G. Estimation of the Surface Sulfur Content of Cellulose Nanocrystals Prepared by Sulfuric Acid Hydrolysis. *Cellulose* **2013**, *20*, 785–794.

(17) Lokanathan, A. R.; Uddin, K. M. A.; Rojas, O. J.; Laine, J. Cellulose Nanocrystal-Mediated Synthesis of Silver Nanoparticles: Role of Sulfate Groups in Nucleation Phenomena. *Biomacromolecules* **2014**, *15*, 373–379.

(18) Abitbol, T.; Palermo, A.; Moran-Mirabal, J. M.; Cranston, E. D. Fluorescent Labeling and Characterization of Cellulose Nanocrystals with Varying Charge Contents. *Biomacromolecules* **2013**, *14*, 3278–3284.

(19) Lu, P.; Hsieh, Y.-L. Preparation and Properties of Cellulose Nanocrystals: Rods, Spheres, and Network. *Carbohyd. Polym.* **2010**, *82*, 329–336.

(20) Kim, J.; Montero, G.; Habibi, Y.; Hinestroza, J. P.; Genzer, J.; Argyropoulos, D. S.; Rojas, O. J. Dispersion of Cellulose Crystallites by Nonionic Surfactants in a Hydrophobic Polymer Matrix. *Polym. Eng. Sci.* **2009**, *49*, 2054–2061.

(21) Siqueira, G.; Bras, J.; Dufresne, A. Cellulose Whiskers versus Microfibrils: Influence of the Nature of the Nanoparticle and Its Surface Functionalization on the Thermal and Mechanical Properties of Nanocomposites. *Biomacromolecules* **2009**, *10*, 425–432.

(22) Kalashnikova, I.; Bizot, H.; Cathala, B.; Capron, I. Modulation of Cellulose Nanocrystals Amphiphilic Properties to Stabilize Oil/water Interface. *Biomacromolecules* **2012**, *13*, 267–275.

(23) Zoppe, J. O.; Venditti, R. A.; Rojas, O. J. Pickering Emulsions Stabilized by Cellulose Nanocrystals Grafted with Thermo-Responsive Polymer Brushes. *J. Colloid Interface Sci.* **2012**, *369*, 202–209.

(24) Capron, I.; Cathala, B. Surfactant-Free High Internal Phase Emulsions Stabilized

by Cellulose Nanocrystals. *Biomacromolecules* **2013**, *14*, 291–296.

(25) Hu, Z.; Ballinger, S.; Pelton, R.; Cranston, E. D. Surfactant-Enhanced Cellulose Nanocrystal Pickering Emulsions. *J. Colloid Interface Sci.* **2015**, *439*, 139–148.

(26) Tang, J.; Lee, M. F. X.; Zhang, W.; Zhao, B.; Berry, R. M.; Tam, K. C. Dual Responsive Pickering Emulsion Stabilized by Poly[2- (Dimethylamino)ethyl Methacrylate] Grafted Cellulose Nanocrystals. *Biomacromolecules* **2014**, *15*, 3052–3060.

(27) Akhlaghi, S. P.; Tiong, D.; Berry, R. M.; Tam, K. C. Comparative Release Studies of Two Cationic Model Drugs from Different Cellulose Nanocrystal Derivatives. *Eur. J. Pharm. Biopharm.* **2014**, *88*, 207–215.

(28) Dong, S.; Cho, H. J.; Lee, Y. W.; Roman, M. Synthesis and Cellular Uptake of Folic Acid-Conjugated Cellulose Nanocrystals for Cancer Targeting. *Biomacromolecules* **2014**, *15*, 1560–1567.

(29) Espino-Pérez, E.; Bras, J.; Ducruet, V.; Guinault, A.; Dufresne, A.; Domenek, S. Influence of Chemical Surface Modification of Cellulose Nanowhiskers on Thermal, Mechanical, and Barrier Properties of Poly(lactide) Based Bionanocomposites. *Eur. Polym. J.* **2013**, *49*, 3144–3154.

(30) Rescignano, N.; Fortunati, E.; Montesano, S.; Emiliani, C.; Kenny, J. M.; Martino, S.; Armentano, I. PVA Bio-Nanocomposites: A New Take-off Using Cellulose Nanocrystals and PLGA Nanoparticles. *Carbohyd. Polym.* **2014**, *99*, 47–58.

(31) Petersson, L.; Kvien, I.; Oksman, K. Structure and Thermal Properties of Poly(lactic Acid)/cellulose Whiskers Nanocomposite Materials. *Compos. Sci. Technol.* **2007**, *67*, 2535–2544.

(32) Kedzior, S. A.; Graham, L.; Moorlag, C.; Dooley, B. M.; Cranston, E. D. Poly(methyl Methacrylate)-Grafted Cellulose Nanocrystals: One-Step Synthesis, Nanocomposite Preparation, and Characterization. *Can. J. Chem. Eng.* **2016**, *94*, 811–822.

(33) Cranston, E. D.; Gray, D. G. Morphological and Optical Characterization of Polyelectrolyte Multilayers Incorporating Nanocrystalline Cellulose. *Biomacromolecules* **2006**, *7*, 2522–2530.

(34) Wu, X.; Chabot, V. L.; Kim, B. K.; Yu, A.; Berry, R. M.; Tam, K. C. Cost-Effective and Scalable Chemical Synthesis of Conductive Cellulose Nanocrystals for High-Performance Supercapacitors. *Electrochim. Acta* **2014**, *138*, 139–147.

(35)   Peng, B.; Han, X.; Liu, H.; Berry, R. C.; Tam, K. C. Interactions between Surfactants and Polymer-Grafted Nanocrystalline Cellulose. *Colloid Surface A* **2013**, *421*, 142–149.

(36)   Dhar, N.; Au, D.; Berry, R. C.; Tam, K. C. Interactions of Nanocrystalline Cellulose with an Oppositely Charged Surfactant in Aqueous Medium. *Colloid Surface A* **2012**, *415*, 310–319.

(37)   Hu, Z.; Cranston, E. D.; Ng, R.; Pelton, R. Tuning Cellulose Nanocrystal Gelation with Polysaccharides and Surfactants. *Langmuir* **2014**, *30*, 2684–2692.

(38)   Peng, B.; Han, X.; Liu, H.; Tam, K. C. Binding of Cationic Surfactants to a Thermo-Sensitive Copolymer below and above Its Cloud Point. *J. Colloid Interface Sci.* **2013**, *412*, 17–23.

(39)   Brinatti, C.; Mello, L. B.; Loh, W. Thermodynamic Study of the Micellization of Zwitterionic Surfactants and Their Interaction with Polymers in Water by Isothermal Titration Calorimetry. *Langmuir* **2014**, *30*, 6002–6010.

(40)   Loh, W.; Brinatti, C.; Tam, K. C. Use of Isothermal Titration Calorimetry to Study Surfactant Aggregation in Colloidal Systems. *Biochim. Biophys. Acta - Gen. Subj.* **2015**, *1860*, 999–1016.

(41)   Mészaros, R.; Varga, I.; Gilanyi, T. Effect of Polymer Molecular Weight on the Polymer/surfactant Interaction. *J. Phys. Chem. B* **2005**, *109*, 13538–13544.

(42)   Sidhu, J.; Bloor, D. M.; Couderc-Azouani, S.; Penfold, J.; Holzwarth, J. F.; Wyn-Jones, E. Interactions of Poly(amidoamine) Dendrimers with the Surfactants SDS, DTAB, and $C_{12}EO6$: An Equilibrium and Structural Study Using a SDS Selective Electrode, Isothermal Titration Calorimetry, and Small Angle Neutron Scattering. *Langmuir* **2004**, *20*, 9320–9328.

(43)   Tam, K. C.; Wyn-Jones, E. Insights on Polymer Surfactant Complex Structures during the Binding of Surfactants to Polymers as Measured by Equilibrium and Structural Techniques. *Chem. Soc. Rev.* **2006**, *35*, 693–709.

(44)   Diab, C.; Winnik, F. M.; Tribet, C. Enthalpy of Interaction and Binding Isotherms of Non-Ionic Surfactants onto Micellar Amphiphilic Polymers (Amphipols). *Langmuir* **2007**, *23*, 3025–3035.

(45)   Levitz, P. E. Adsorption of Non Ionic Surfactants at the Solid/water Interface. *Colloid Surface A* **2002**, *205*, 31–38.

(46)   Hamberger, A.; Landfester, K. Influence of Size and Functionality of Polymeric Nanoparticles on the Adsorption Behavior of Sodium Dodecyl Sulfate as

Detected by Isothermal Titration Calorimetry. *Colloid Polym. Sci.* **2011**, *289*, 3–14.

(47) Paria, S.; Khilar, K. C. A Review on Experimental Studies of Surfactant Adsorption at the Hydrophilic Solid-Water Interface. *Adv. Colloid Interface Sci.* **2004**, *110*, 75–95.

(48) Loh, W.; Brinatti, C. Calorimetry Is Not Color-Blind. Molecular Insights on Association Processes in Surfactant-Polymer Mixtures Derived from Calorimetric Experiments. *Sci. China Chem.* **2011**, *54*, 2024–2027.

(49) Bouchemal, K. New Challenges for Pharmaceutical Formulations and Drug Delivery Systems Characterization Using Isothermal Titration Calorimetry. *Drug Discov. Today* **2008**, *13* (21–22), 960–972.

(50) Grolier, J.-P. E.; Del Río, J. M. Isothermal Titration Calorimetry: A Thermodynamic Interpretation of Measurements. *J. Chem. Thermodyn.* **2012**, *55*, 193–202.

(51) Ahola, S.; Turon, X.; Osterberg, M.; Laine, J.; Rojas, O. J. Enzymatic Hydrolysis of Native Cellulose Nano Brils and Other Cellulose Model Films: Effect of Surface Structure. *Langmuir* **2008**, *24*, 11592–11599.

(52) Aulin, C.; Ahok, S.; Josefsson, P.; Nishino, T.; Hirose, Y.; Österberg, M.; Wågberg, L. Nanoscale Cellulose Films with Different Crystallinities and Mesostructures - Their Surface Properties and Interaction with Water. *Langmuir* **2009**, *25*, 7675–7685.

(53) Hidayat, B. J.; Felby, C.; Johansen, K. S.; Thygesen, L. G. Cellulose Is Not Just Cellulose: A Review of Dislocations as Reactive Sites in the Enzymatic Hydrolysis of Cellulose Microfibrils. *Cellulose* **2012**, *19*, 1481–1493.

(54) Hirrien, M.; Desbrières, J.; Rinaudo, M. Physical Properties of Methylcelluloses in Relation with the Conditions for Cellulose Modification. *Carbohyd. Polym.* **1996**, *31*, 243–252.

(55) Kalia, S.; Dufresne, A.; Cherian, B. M.; Kaith, B. S.; Avérous, L.; Njuguna, J.; Nassiopoulos, E. Cellulose-Based Bio- and Nanocomposites: A Review. *Int. J. Polym. Sci.* **2011**, *2011*, 1–35.

(56) Lavoine, N.; Desloges, I.; Dufresne, A.; Bras, J. Microfibrillated Cellulose - Its Barrier Properties and Applications in Cellulosic Materials: A Review. *Carbohyd. Polym.* **2012**, *90*, 735–764.

(57) Medronho, B.; Romano, A.; Miguel, M. G.; Stigsson, L.; Lindman, B.

Rationalizing Cellulose (In)solubility: Reviewing Basic Physicochemical Aspects and Role of Hydrophobic Interactions. *Cellulose* **2012**, *19*, 581–587.

(58) Pääkkö, M.; Vapaavuori, J.; Silvennoinen, R.; Kosonen, H.; Ankerfors, M.; Lindström, T.; Berglund, L. A.; Ikkala, O. Long and Entangled Native Cellulose I Nanofibers Allow Flexible Aerogels and Hierarchically Porous Templates for Functionalities. *Soft Matter* **2008**, *4*, 2492–2499.

(59) Pinto, L. F. V; Kundu, S.; Brogueira, P.; Cruz, C.; Fernandes, S. N.; Aluculesei, a.; Godinho, M. H. Cellulose-Based Liquid Crystalline Photoresponsive Films with Tunable Surface Wettability. *Langmuir* **2011**, *27*, 6330–6337.

(60) Visakh, P. M.; Thomas, S. Preparation of Bionanomaterials and Their Polymer Nanocomposites from Waste and Biomass. *Waste and Biomass Valorization* **2010**, *1*, 121–134.

(61) Xu, W. Z.; Zhang, X.; Kadla, J. F. Design of Functionalized Cellulosic Honeycomb Films: Site-Specific Biomolecule Modification Via "click Chemistry." *Biomacromolecules* **2012**, *13*, 350–357.

(62) Zugenmaier, P. Conformation and Packing of Various Crystalline Cellulose Fibers. *Prog. Polym. Sci.* **2001**, *26*, 1341–1417.

(63) Nelson, D. L.; Cox, M. M. *Lehninger Principles of Biochemistry*, 5th ed.; W.H. Freeman and Company: New York, 2008.

(64) Krässig, H.; Schurz, J.; Steadman, R. G.; Schliefer, K.; Albrecht, W.; Mohring, M.; Schlosser, H. Cellulose. In *Ullmann's Encyclopedia of Industrial Chemistry*; Wiley-VCH Verlag GmbH & Co. KGaA: Weinheim, Germany, 2004; pp 279–327.

(65) Horii, F. Structure of Cellulose: Recent Developments in Its Characterization. In *Wood and Cellulosic Chemistry*; Hon, D. N.-S., Shiraishi, N., Eds.; Marcell Dekker Inc.: New York, 1991; pp 83–108.

(66) Rinaudo, M.; Reguant, J. Polysaccharide Derivatives. In *Natural Polymers and Agrofibers Composites*; Frollini, E., Leão, A. L., Mattoso, L. H. C., Eds.; Embrapa Instrumentação Agropecuária: São Carlos, 2000.

(67) Liu, Z.; Choi, H.; Gatenholm, P.; Esker, A. R. Quartz Crystal Microbalance with Dissipation Monitoring and Surface Plasmon Resonance Studies of Carboxymethyl Cellulose Adsorption onto Regenerated Cellulose Surfaces. *Langmuir* **2011**, *27*, 8718–8728.

(68) Henriksson, M.; Henriksson, G.; Berglund, L. A.; Lindström, T. An

Environmentally Friendly Method for Enzyme-Assisted Preparation of Microfibrillated Cellulose (MFC) Nanofibers. *Eur. Polym. J.* **2007**, *43*, 3434–3441.

(69)   Sakakibara, A.; Sano, Y. Chemistry of Ligning. In *Wood and Cellulosic Chemistry*; Hon, D. N.-S., Shiraishi, N., Eds.; Marcell Dekker Inc.: New York, 1991; pp 109–174.

(70)   Williams, L. The Problem with Cellulosic Ethanol https://www.olcf.ornl.gov/2011/09/12/the-problem-with-cellulosic-ethanol/ (accessed Oct 20, 2012).

(71)   Hansen, N. M. L.; Plackett, D. Sustainable Films and Coatings from Hemicelluloses: A Review. *Biomacromolecules* **2008**, *9*, 1493–1505.

(72)   U.S. DOE. Titan Supercomputer Being Used to Probe Biofuel Barriers https://solarthermalmagazine.com/2016/02/17/titan-supercomputer-being-used-probe-biofuel-barriers/ (accessed Jun 12, 2016).

(73)   Arola, S.; Tammelin, T.; Setälä, H.; Tullila, A.; Linder, M. B. Immobilization-Stabilization of Proteins on Nanofibrillated Cellulose Derivatives and Their Bioactive Film Formation. *Biomacromolecules* **2012**, *13*, 594–603.

(74)   Camino, N. a.; Pérez, O. E.; Sanchez, C. C.; Patino, J. M. R.; Pilosof, A. M. R. Hydroxypropylmethylcellulose Surface Activity at Equilibrium and Adsorption Dynamics at the Air-Water and Oil-Water Interfaces. *Food Hydrocolloid* **2009**, *23*, 2359–2368.

(75)   Hedin, J.; Löfroth, J. E.; Nydén, M. Adsorption Behavior and Cross-Linking of EHEC and HM-EHEC at Hydrophilic and Hydrophobic Modified Surfaces Monitored by SPR and QCM-D. *Langmuir* **2007**, *23*, 6148–6155.

(76)   Joabsson, F.; Rosén, O.; Thuresson, K.; Piculell, L.; Lindman, B. Phase Behavior of a "clouding" Nonionic Polymer in Water. Effects of Hydrophobic Modification and Added Surfactant on Phase Compositions. *J. Phys. Chem. B* **1998**, *102*, 2954–2959.

(77)   Amim, J.; Kosaka, P. M.; Petri, D. F. S.; Maia, F. C. B.; Miranda, P. B. Stability and Interface Properties of Thin Cellulose Ester Films Adsorbed from Acetone and Ethyl Acetate Solutions. *J. Colloid Interface Sci.* **2009**, *332*, 477–483.

(78)   Orelma, H.; Filpponen, I.; Johansson, L. S.; Laine, J.; Rojas, O. J. Modification of Cellulose Films by Adsorption of Cmc and Chitosan for Controlled Attachment of Biomolecules. *Biomacromolecules* **2011**, *12*, 4311–4318.

(79) Sato, T.; Ali, M. M.; Pelton, R.; Cranston, E. D. DNA Stickers Promote Polymer Adsorption onto Cellulose. *Biomacromolecules* **2012**, *13*, 3173–3180.

(80) Xu, F. J.; Zhu, Y.; Liu, F. S.; Nie, J.; Ma, J.; Yang, W. T. Comb-Shaped Conjugates Comprising Hydroxypropyl Cellulose Backbones and Low-Molecular-Weight Poly(n-Isopropylacryamide) Side Chains for Smart Hydrogels: Synthesis, Characterization, and Biomedical Applications. *Bioconjugate Chem.* **2010**, *21*, 456–464.

(81) Van Vlierberghe, S.; Dubruel, P.; Schacht, E. Biopolymer-Based Hydrogels as Scaffolds for Tissue Engineering Applications: A Review. *Biomacromolecules* **2011**, *12*, 1387–1408.

(82) Fujita, M.; Harada, H. Ultrastructure and Formation of Wood Cell Wall. In *Wood and Cellulosic Chemistry*; Hon, D. N.-S., Shiraishi, N., Eds.; Marcell Dekker Inc.: New York, 1991; pp 1–49.

(83) Liao, R.; Zhu, M.; Zhou, X.; Zhang, F.; Yan, J.; Zhu, W.; Gu, C. Molecular Dynamics Study of the Disruption of H-Bonds By Water Molecules and Its Diffusion Behavior in Amorphous Cellulose. *Mod. Phys. Lett. B* **2012**, *26*, 1250088.

(84) Stephens, C. H.; Whitmore, P. M.; Morris, H. R.; Bier, M. E. Hydrolysis of the Amorphous Cellulose in Cotton-Based Paper. *Biomacromolecules* **2008**, *9*, 1093–1099.

(85) Li, Q.; Matuana, L. M. Surface of Cellulosic Materials Modified with Functionalized Polyethylene Coupling Agents. *J. Appl. Polym. Sci.* **2003**, *88*, 278–286.

(86) Edgar, C. D.; Gray, D. G. Smooth Model Cellulose I Surfaces from Nanocrystal Suspensions. *Cellulose* **2003**, *10*, 299–306.

(87) Nishiyama, Y.; Sugiyama, J.; Chanzy, H.; Langan, P. Crystal Structure and Hydrogen Bonding System in Cellulose Iα from Synchrotron X-Ray and Neutron Fiber Diffraction. *J. Am. Chem. Soc.* **2003**, *125*, 14300–14306.

(88) De Mesquita, J. P.; Donnici, C. L.; Teixeira, I. F.; Pereira, F. V. Bio-Based Nanocomposites Obtained through Covalent Linkage between Chitosan and Cellulose Nanocrystals. *Carbohyd. Polym.* **2012**, *90*, 210–217.

(89) Habibi, Y.; Hoeger, I.; Kelley, S. S.; Rojas, O. J. Development of Langmuir - Schaeffer Cellulose Nanocrystal Monolayers and Their Interfacial Behaviors. *Langmuir* **2010**, *26*, 990–1001.

(90)   Wahba, M. Moisture Relationships of Cellulose. I. The Heat of Wetting in Water and in Certain Organic Liquids. *J. Phys. Chem-US* **1948**, *52*, 1197–1208.

(91)   Nakai, Y.; Fukuoka, E.; Nakajima, S.; Hasegawa, J. Crystallinity and Physical Characteristics of Microcrystalline Cellulose. *Chem. Pharm. Bull.* **1977**, *25*, 96–101.

(92)   Glasser, W. G.; Atalla, R. H.; Blackwell, J.; Brown, M. M.; Burchard, W.; French, A. D.; Klemm, D. O.; Nishiyama, Y. About the Structure of Cellulose: Debating the Lindman Hypothesis. *Cellulose* **2012**, *19*, 589–598.

(93)   Takahashi, M.; Shimazaki, M.; Yamamoto, J. Thermoreversible Gelation and Phase Separation in Aqueous Methyl Cellulose Solutions. *J. Polym. Sci. Part B Polym. Phys.* **2001**, *39*, 91–100.

(94)   Li, L.; Shan, H.; Yue, C. Y.; Lam, Y. C.; Tam, K. C.; Hu, X. Thermally Induced Association and Dissociation of Methylcellulose in Aqueous Solutions. *Langmuir* **2002**, *18*, 7291–7298.

(95)   Schild, H.; Tirrell, D. Microcalorimetric Detection of Lower Critical Solution Temperatures in Aqueous Polymer Solutions. *J. Phys. Chem.* **1990**, *94*, 4352–4356.

(96)   Qiu, X.; Hu, S. "Smart" materials Based on Cellulose: A Review of the Preparations, Properties, and Applications. *Materials (Basel).* **2013**, *6*, 738–781.

(97)   Safari, S.; Sheikhi, A.; van de Ven, T. G. M. Electroacoustic Characterization of Conventional and Electrosterically Stabilized Nanocrystalline Celluloses. *J. Colloid Interface Sci.* **2014**, *432*, 151–157.

(98)   Dong, X. M.; Kimura, T.; Gray, D. G. Effects of Ionic Strength on the Isotropic - Chiral Nematic Phase Transition of Suspensions of Cellulose Crystallites. *Langmuir* **1996**, *12*, 2076–2082.

(99)   Favier, V.; Chanzy, H.; Cavaille, J. Y. Polymer Nanocomposites Reinforced by Cellulose Whiskers. *Macromolecules* **1995**, *28*, 6365–6367.

(100)   Morandi, G.; Heath, L.; Thielemans, W. Cellulose Nanocrystals Grafted with Polystyrene Chains through Surface-Initiated Atom Transfer Radical Polymerization (SI-ATRP). *Langmuir* **2009**, *25*, 8280–8286.

(101)   Yang, X.; Cranston, E. D. Chemically Cross-Linked Cellulose Nanocrystal Aerogels with Shape Recovery and Superabsorbent Properties. *Chem. Mater.* **2014**, *26*, 6016–6025.

(102)   Khouri, S.; Shams, M.; Tam, K. C. Determination and Prediction of Physical

Properties of Cellulose Nanocrystals from Dynamic Light Scattering Measurements. *J. Nanoparticle Res.* **2014**, *16*, 1–14.

(103) Habibi, Y. Key Advances in the Chemical Modification of Nanocelluloses. *Chem. Soc. Rev.* **2014**, *43*, 1519–1542.

(104) Eyley, S.; Thielemans, W. Surface Modification of Cellulose Nanocrystals. *Nanoscale* **2014**, *6*, 7764–7779.

(105) Kan, K. H. M.; Li, J.; Wijesekera, K.; Cranston, E. D. Polymer-Grafted Cellulose Nanocrystals as pH-Responsive Reversible Flocculants. *Biomacromolecules* **2013**, *14*, 3130–3139.

(106) Akhlaghi, S. P.; Berry, R. M.; Tam, K. C. Surface Modification of Cellulose Nanocrystal with Chitosan Oligosaccharide for Drug Delivery Applications. *Cellulose* **2013**, *20*, 1747–1764.

(107) Akhlaghi, S. P.; Zaman, M.; Mohammed, N.; Brinatti, C.; Batmaz, R.; Berry, R.; Loh, W.; Tam, K. C. Synthesis of Amine Functionalized Cellulose Nanocrystals: Optimization and Characterization. *Carbohyd. Res.* **2015**, *409*, 48–55.

(108) Grishkewich, N.; Akhlaghi, P.; Zhaoling, Y.; Berry, R.; Tam, K. C. Cellulose Nanocrystal-Poly(oligo(ethylene Glycol) Methacrylate) Brushes with Tunable LCSTs. *Carbohyd. Polym.* **2016**, *144*, 215–222.

(109) Yi, J.; Xu, Q.; Zhang, X.; Zhang, H. Temperature-Induced Chiral Nematic Phase Changes of Suspensions of poly(N,N-Dimethylaminoethyl Methacrylate)-Grafted Cellulose Nanocrystals. *Cellulose* **2009**, *16*, 989–997.

(110) Goussé, C.; Chanzy, H.; Excoffier, G.; Soubeyrand, L.; Fleury, E. Stable Suspensions of Partially Silylated Cellulose Whiskers Dispersed in Organic Solvents. *Polymer* **2002**, *43*, 2645–2651.

(111) Nagalakshmaiah, M.; El Kissi, N.; Dufresne, A. Ionic Compatibilization of Cellulose Nanocrystals with Quaternary Ammonium Salt and Their Melt Extrusion with Polypropylene. *ACS Appl. Mater. Interfaces* **2016**, *8*, 8755–8764.

(112) Araki, J.; Wada, M.; Kuga, S. Steric Stabilization of a Cellulose Microcrystal Suspension by Poly (Ethylene Glycol) Grafting. *Cellulose* **2001**, *17*, 21–27.

(113) Walter, R.; Rička, J.; Quellet, C.; Nyffenegger, R.; Binkert, T. Coil - Globule Transition of Poly (N-Isopropylacrylamide): A Study of Polymer - Surfactant Association. *Macromolecules* **1996**, *29*, 4019–4028.

(114) Tiktopulo, E. I.; Bychkova, V. E.; Ricka, J.; Ptitsyn, O. B. Cooperativity of the Coil-Globule Transition in a Homopolymer : Microcalorimetric Study of Poly (

N-Isopropylacrylamide). *Macromolecules* **1994**, *27*, 2879–2882.

(115) Beezer, A.; Loh, W.; Mitchell, J.; Royall, P. An Investigation of Dilute Aqueous Solution Behavior of Poly (Oxyethylene)+ Poly (Oxypropylene)+ Poly (Oxyethylene) Block Copolymers. *Langmuir* **1994**, *10*, 4001–4005.

(116) Howley, C.; Marangoni, D. G.; Kwak, J. C. T. Association and Phase Behavior of Hydrophobically Modified Photoresponsive Poly(acrylamide)s in the Presence of Ionic Surfactant. *Colloid Polym. Sci.* **1997**, *275*, 760–768.

(117) Seuring, J.; Agarwal, S. Polymers with Upper Critical Solution Temperature in Aqueous Solution. *Macromol. Rapid Commun.* **2012**, *33*, 1898–1920.

(118) Lutz, J. F. Polymerization of Oligo(ethylene Glycol) (Meth)acrylates: Toward New Generations of Smart Biocompatible Materials. *J. Polym. Sci. Part A Polym. Chem.* **2008**, *46*, 3459–3470.

(119) Li, J.; Stöver, H. D. H. Doubly pH-Responsive Pickering Emulsion. *Langmuir* **2008**, *24*, 13237–13240.

(120) Yi, C.; Liu, N.; Zheng, J.; Jiang, J.; Liu, X. Dual-Responsive Poly(styrene-Alt-Maleic Acid)-Graft-poly(N-Isopropyl Acrylamide) Micelles as Switchable Emulsifiers. *J. Colloid Interface Sci.* **2012**, *380*, 90–98.

(121) Tan, B. H.; Tam, K. C. Review on the Dynamics and Micro-Structure of pH-Responsive Nano-Colloidal Systems. *Adv. Colloid Interface Sci.* **2008**, *136*, 25–44.

(122) Zhou, J.; Butchosa, N.; Jayawardena, H. S. N.; Park, J.; Zhou, Q.; Yan, M.; Ramström, O. Synthesis of Multifunctional Cellulose Nanocrystals for Lectin Recognition and Bacterial Imaging. *Biomacromolecules* **2015**, *16*, 1426–1432.

(123) Akhlaghi, S. P.; Zaman, M.; Peng, B.; Tam, K. C. Cationic Cellulose and Chitin Nanocrystals for Novel Therapeutic Applications. In *Cationic Polymers in Regenerative Medicine*; Samal, S., Dubruel, P., Eds.; RSC Polymer Chemistry Series, 2015; pp 197–227.

(124) Yi, J.; Xu, Q.; Zhang, X.; Zhang, H. Chiral-Nematic Self-Ordering of Rodlike Cellulose Nanocrystals Grafted with Poly(styrene) in Both Thermotropic and Lyotropic States. *Polymer* **2008**, *49*, 4406–4412.

(125) Salajková, M.; Berglund, L. A.; Zhou, Q. Hydrophobic Cellulose Nanocrystals Modified with Quaternary Ammonium Salts. *J. Mater. Chem.* **2012**, *22*, 19798–19805.

(126) Akhlaghi, S. P.; Berry, R. M.; Tam, K. C. Modified Cellulose Nanocrystal for

Vitamin C Delivery. *Am. Assoc. Phamaceutical Sci.* **2014**, *16*, 306–314.

(127) Bitinis, N.; Verdejo, R.; Bras, J.; Fortunati, E.; Kenny, J. M.; Torre, L.; López-Manchado, M. A. Poly(lactic Acid)/natural Rubber/cellulose Nanocrystal Bionanocomposites Part I. Processing and Morphology. *Carbohyd. Polym.* **2013**, *96*, 611–620.

(128) McKee, J. R.; Appel, E. a.; Seitsonen, J.; Kontturi, E.; Scherman, O. a.; Ikkala, O. Healable, Stable and Stiff Hydrogels: Combining Conflicting Properties Using Dynamic and Selective Three-Component Recognition with Reinforcing Cellulose Nanorods. *Adv. Funct. Mater.* **2014**, *24*, 2706–2713.

(129) Podsiadlo, P.; Sui, L.; Elkasabi, Y.; Burgardt, P.; Lee, J.; Miryala, A.; Kusumaatmaja, W.; Carman, M. R.; Shtein, M.; Kieffer, J.; et al. Layer-by-Layer Assembled Films of Cellulose Nanowires with Antireflective Properties. *Langmuir* **2007**, *23*, 7901–7906.

(130) Ma, H.; Burger, C.; Hsiao, B. S.; Chu, B. Nanofibrous Microfiltration Membrane Based on Cellulose Nanowhiskers. *Biomacromolecules* **2012**, *13*, 180–186.

(131) Batmaz, R.; Mohammed, N.; Zaman, M.; Minhas, G.; Berry, R. M.; Tam, K. C. Cellulose Nanocrystals as Promising Adsorbents for the Removal of Cationic Dyes. *Cellulose* **2014**, *21*, 1655–1665.

(132) Hansson, P.; Almgren, M. Interaction of Alkyltrimethylammonium Surfactants with Polyacrylate and Poly(styrenesulfonate) in Aqueous Solution: Phase Behavior and Surfactant Aggregation Numbers. *Langmuir* **1994**, *10*, 2115–2124.

(133) Wang, H.; Wang, Y. Studies on Interaction of Poly(sodium Acrylate) and Poly(sodium Styrenesulfonate) with Cationic Surfactants: Effects of Polyelectrolyte Molar Mass, Chain Flexibility, and Surfactant Architecture. *J. Phys. Chem. B* **2010**, *114*, 10409–10416.

(134) Fegyver, E.; Mészáros, R. Complexation between Sodium Poly(styrenesulfonate) and Alkyltrimethylammonium Bromides in the Presence of Dodecyl Maltoside. *J. Phys. Chem. B* **2015**, *119*, 5336–5346.

(135) Olofsson, G.; Loh, W. On the Use of Titration Calorimetry to Study the Association of Surfactants in Aqueous Solutions. *J. Brazil Chem. Soc.* **2009**, *20*, 577–593.

(136) Lapitsky, Y.; Parikh, M.; Kaler, E. W. Calorimetric Determination of Surfactant/Polyelectrolyte Binding Isotherms. *J. Phys. Chem. B* **2007**, *111*, 8379–8387.

(137) Loh, W.; Teixeira, L. A. C.; Lee, L.-T. Isothermal Calorimetric Investigation of the Interaction of Poly (N -Isopropylacrylamide) and Ionic Surfactants. *J. Phys. Chem. B* **2004**, *108*, 3196–3201.

(138) Alila, S.; Boufi, S.; Belgacem, M. N.; Beneventi, D. Adsorption of a Cationic Surfactant onto Cellulosic Fibers I. Surface Charge Effects. *Langmuir* **2005**, *21*, 8106–8113.

(139) Ghoreishi, S. M.; Fox, G. A.; Bloor, D. M.; Holzwarth, J. F.; Wyn-Jones, E. EMF and Microcalorimetry Studies Associated with the Binding of the Cationic Surfactants to Neutral Polymers. *Langmuir* **1999**, *15*, 5474–5479.

(140) Wang, G.; Olofsson, G. Ethyl(hydroxyethyl)cellulose and Ionic Surfactants in Dilute Solution. Calorimetric and Viscosity Study of the Interaction with SDS and Some Cationic Surfactants. *J. Phys. Chem. B* **1995**, *99*, 5588–5596.

(141) Fegyver, E.; Mészáros, R. Fine-Tuning the Nonequilibrium Behavior of Oppositely Charged Macromolecule/Surfactant Mixtures via the Addition of Nonionic Amphiphiles. *Langmuir* **2014**, *30*, 15114–15126.

(142) Wang, X.; Li, Y.; Li, J.; Wang, J.; Wang, Y.; Guo, Z.; Yan, H. Salt Effect on the Complex Formation between Polyelectrolyte and Oppositely Charged Surfactant in Aqueous Solution. *J. Phys. Chem. B* **2005**, *109*, 10807–10812.

(143) Sen, S.; Sukul, D.; Dutta, P.; Bhattacharyya, K. Fluorescence Anisotropy Decay in Polymer - Surfactant Aggregates. *J. Phys. Chem. A* **2001**, *105*, 7495–7500.

(144) Mata, J.; Varade, D.; Bahadur, P. Aggregation Behavior of Quaternary Salt Based Cationic Surfactants. *Thermochim. Acta* **2005**, *428*, 147–155.

(145) Stodghill, S. P.; Smith, A. E.; O'Haver, J. H. Thermodynamics of Micellization and Adsorption of Three Alkyltrimethylammonium Bromides Using Isothermal Titration Calorimetry. *Langmuir* **2004**, *20*, 11387–11392.

(146) Tong, W.; Zheng, Q.; Shao, S.; Lei, Q.; Fang, W. Critical Micellar Concentrations of Quaternary Ammonium Surfactants with Hydroxyethyl Substituents on Headgroups Determined by Isothermal Titration Calorimetry. *J. Chem. Eng. Data* **2010**, *55*, 3766–3771.

(147) Majhi, P. R.; Moulik, S. P. Energetics of Micellization: Reassessment by a High-Sensitivity Titration Microcalorimeter. *Langmuir* **1998**, *14*, 3986–3990.

(148) Courtois, J.; Berret, J.-F. Probing Oppositely Charged Surfactant and Copolymer Interactions by Isothermal Titration Microcalorimetry. *Langmuir* **2010**, *26*, 11750–11758.

(149) Vitorazi, L.; Ould-Moussa, N.; Sekar, S.; Fresnais, J.; Loh, W.; Chapel, J.-P.; Berret, J.-F. Evidence of a Two-Step Process and Pathway Dependency in the Thermodynamics of Poly(diallyldimethylammonium Chloride)/poly(sodium Acrylate) Complexation. *Soft Matter* **2014**, *10*, 9496–9505.

(150) Borsali, R.; Nguyen, H.; Pecora, R. Small-Angle Neutron Scattering and Dynamic Light Scattering from a Polyelectrolyte Solution: DNA. *Macromolecules* **1998**, *31*, 1548–1555.

(151) Valeur, B. *Molecular Fluorescence - Principles and Applications (Online)*; Wiley-VCH, 2001; Vol. 8.

(152) Yeskie, M. A.; Harwell, J. H. On the Structure of Aggregates of Adsorbed Surfactants: The Surface Charge Density at the Hemimicelle/Admicelle Transition. *J. Phys. Chem.* **1988**, *92* (8), 2346–2352.

(153) Konop, A. J.; Colby, R. H. Role of Condensed Counterions in the Thermodynamics of Surfactant Micelle Formation with and without Oppositely Charged Polyelectrolytes. *Langmuir* **1999**, *15*, 58–65.

(154) Gao, Y.; Du, J.; Gu, T. Hemimicelle Formation of Cationic Surfactants at the Silica Gel-Water Interface. *J. Chem. Soc. Faraday Trans. 1* **1988**, *83*, 2671–2679.

(155) Atkin, R.; Craig, V. S. J.; Wanless, E. J.; Biggs, S. The Influence of Chain Length and Electrolyte on the Adsorption Kinetics of Cationic Surfactants at the Silica-Aqueous Solution Interface. *J. Colloid Interface Sci.* **2003**, *266*, 236–244.

(156) Velegol, S. B.; Fleming, B. D.; Biggs, S.; Wanless, E. J.; Tilton, R. D. Counterion Effects on Hexadecyltrimethylammonium Surfactant Adsorption and Self-Assembly on Silica. *Langmuir* **2000**, *16*, 2548–2556.

(157) Brinatti, C.; Huang, J.; Berry, R. M.; Tam, M. K.; Loh, W. Structural and Energetic Studies on the Interaction of Cationic Surfactants and Cellulose Nanocrystals. *Langmuir* **2016**, *32*, 689–698.

(158) Desai, T. R.; Dixit, S. G. Interaction and Viscous Properties of Aqueous Solutions of Mixed Cationic and Nonionic Surfactants. *J. Colloid Interface Sci.* **1996**, *177*, 471–477.

(159) Zhang, R.; Somasundaran, P. Advances in Adsorption of Surfactants and Their Mixtures at Solid/solution Interfaces. *Adv. Colloid Interface Sci.* **2006**, *123–126*, 213–229.

(160) Binks, B. P.; Rodrigues, J. A.; Frith, W. J. Synergistic Interaction in Emulsions

Stabilized by a Mixture of Silica Nanoparticles and Cationic Surfactant. *Langmuir* **2007**, *23*, 3626–3636.

(161) Somasundaran, P.; Huang, L. Adsorption/aggregation of Surfactants and Their Mixtures at Solid-Liquid Interfaces. *Adv. Colloid Interface Sci.* **2000**, *88*, 179–208.

(162) Fegyver, E.; Mészáros, R. The Impact of Nonionic Surfactant Additives on the Nonequilibrium Association between Oppositely Charged Polyelectrolytes and Ionic Surfactants. *Soft Matter* **2014**, *10*, 1953–1962.

(163) Nho, Y. C.; Kwon, O. H. Blood Compatibility of AAc, HEMA, and PEGMA-Grafted Cellulose Film. *Radiat. Phys. Chem.* **2003**, *66*, 299–307.

(164) Santos, F. K. G.; Neto, E. L. B.; Moura, M. C. P. A.; Dantas, T. N. C.; Neto, A. A. D. Molecular Behavior of Ionic and Nonionic Surfactants in Saline Medium. *Colloid Surface A* **2009**, *333*, 156–162.

(165) Belfer, S.; Fainchtain, R.; Purinson, Y.; Kedem, O. Surface Characterization by FTIR-ATR Spectroscopy of Polyethersulfone Membranes-Unmodified, Modified and Protein Fouled. *J. Memb. Sci.* **2000**, *172*, 113–124.

(166) Wang, N.; Ding, E.; Cheng, R. Thermal Degradation Behaviors of Spherical Cellulose Nanocrystals with Sulfate Groups. *Polymer* **2007**, *48*, 3486–3493.

(167) Privalov, P. L.; Dragan, A. I. Microcalorimetry of Biological Macromolecules. *Biophys. Chem.* **2007**, *126*, 16–24.

(168) Courdec-Azouani, S.; Sidhu, J.; Georgiou, T. K.; Charalambous, D. C.; Vamvakaki, M.; Patrickios, C. S.; Bloor, D. M.; Penfold, J.; Holzwarth, J. F.; Wyn-Jones, E. Binding of Sodium Dodecyl Sulfate to Linear and Star Homopolymers of the Nonionic Poly(methoxyhexa(ethylene Glycol) Methacrylate) and the Polycation Poly(2-(Dimethylamino)ethyl Methacrylate): Electromotive Force, Isothermal Titration Calorimetry, Surface Tension, and Small-Angle Neutron Scattering Measurements. *Langmuir* **2004**, *20*, 6458–6469.

(169) Schild, H. G.; Tirrell, D. A. Interaction of poly(N-Isopropylacrylamide) with Sodium N-Alkyl Sulfates in Aqueous Solution. *Langmuir* **1991**, *7*, 665–671.

(170) Teixeira, L. A. de C. Calorimetric Investigation of the Interaction of Poly (N-Isopropylacrylamide) and Ionic Surfactants. M.S. Thesis, University of Campinas, Brazil, May 2004.

(171) Dai, S.; Tam, K. C. Isothermal Titration Calorimetry Studies of Binding Interactions between Polyethylene Glycol and Ionic Surfactants. *J. Phys. Chem.*

B **2001**, *105*, 10759–10763.

(172) Da Silva, R. C.; Loh, W.; Olofsson, G. Calorimetric Investigation of Temperature Effect on the Interaction between Poly(ethylene Oxide) and Sodium Dodecylsulfate in Water. *Thermochim. Acta* **2004**, *417*, 295–300.

(173) Mylonas, Y.; Staikos, G.; Lianos, P. Investigation of the Poly(N - Isopropylacrylamide)-Sodium Dodecyl Sulfate Complexation with Viscosity, Dialysis, and Time-Resolved Fluorescence-Quenching Measurements. *Langmuir* **1999**, *15*, 7172–7175.

(174) Piculell, L.; Lindman, B. Association and Segregation in Aqueous Polymer/polymer, Polymer/surfactants, and Surfactants/surfactant Mixtures: Similarities and Differences. *Adv. Colloid Interf. Sci.* **1992**, *41*, 149–178.

(175) Holmberg, K.; Jönsson, B.; Kronberg, B.; Lindman, B. *Surfactants and Polymers in Aqueous Solution*, Second.; John Wiley & Sons, LTD, 2002.

(176) Janiak, J.; Piculell, L.; Olofsson, G.; Schillén, K. The Aqueous Phase Behavior of Polyion-Surfactant Ion Complex Salts Mixed with Nonionic Surfactants. *Phys. Chem. Chem. Phys.* **2011**, *13*, 3126–3138.

(177) Percebom, A. M.; Janiak, J.; Schillén, K.; Piculell, L.; Loh, W. Micellization of Water-Soluble Complex Salts of an Ionic Surfactant with Hairy Polymeric Counterions. *Soft Matter* **2013**, 515–526.

(178) Vitorazi, L.; Berret, J. F.; Loh, W. Self-Assembly of Complex Salts of Cationic Surfactants and Anionic-Neutral Block Copolymers. Dispersions with Liquid-Crystalline Internal Structure. *Langmuir* **2013**, *29*, 14024–14033.

(179) Cui, Y.; Threlfall, M.; van Duijneveldt, J. S. Optimizing Organoclay Stabilized Pickering Emulsions. *J. Colloid Interface Sci.* **2011**, *356*, 665–671.

(180) Hoffmann, I.; Heunemann, P.; Prévost, S.; Schweins, R.; Wagner, N. J.; Gradzielski, M. Self-Aggregation of Mixtures of Oppositely Charged Polyelectrolytes and Surfactants Studied by Rheology, Dynamic Light Scattering and Small-Angle Neutron Scattering. *Langmuir* **2011**, *27*, 4386–4396.

(181) Piculell, L.; Egermayer, M.; Sjöström, J. Rheology of Mixed Solutions of an Associating Polymer with a Surfactant. Why Are Different Surfactants Different? *Langmuir* **2003**, *19*, 3643–3649.

(182) Binks, B. P.; Rodrigues, J. A. Enhanced Stabilization of Emulsions due to Surfactant-Induced Nanoparticle Flocculation. *Langmuir* **2007**, *23*, 7436–7439.

(183) Mahmud, A.; Xiong, X.-B.; Aliabadi, H. M.; Lavasanifar, A. Polymeric Micelles

for Drug Targeting. *J. Drug Target.* **2007**, *15*, 553–584.

(184) Wu, Q.; Meng, Y.; Wang, S.; Li, Y.; Fu, S.; Ma, L.; Harper, D. Rheological Behavior of Cellulose Nanocrystal Suspension: Influence of Concentration and Aspect Ratio. *J. Appl. Polym. Sci.* **2014**, *131*, 40525.

(185) Holt, B.; Stoyanov, S.; Pelan, E.; Paunov, V. Novel Anisotropic Materials from Functionalised Colloidal Cellulose and Cellulose Derivatives. *J. Mater. Chem.* **2010**, *20*, 10058–10070.

(186) Dong, S.; Roman, M. Fluorescently Labeled Cellulose Nanocrystals for Bioimaging Applications. *J. Am. Chem. Soc.* **2007**, *129*, 13810–13811.

(187) Nielsen, L. J.; Eyley, S.; Thielemans, W.; Aylott, J. W. Dual Fluorescent Labelling of Cellulose Nanocrystals for pH Sensing. *Chem. Commun.* **2010**, *46*, 8929–8931.

(188) Hemraz, U. D.; Boluk, Y.; Sunasee, R. Amine-Decorated Nanocrystalline Cellulose Surfaces: Synthesis, Characterization, and Surface Properties. *Can. J. Chem.* **2013**, *91*, 974–981.

(189) Samsonova, O.; Pfeiffer, C.; Hellmund, M.; Merkel, O. M.; Kissel, T. Low Molecular Weight pDMAEMA-Block-pHEMA Block-Copolymers Synthesized via RAFT-Polymerization: Potential Non-Viral Gene Delivery Agents. *Polymers* **2011**, *3*, 693–718.

(190) Dai, S.; Tam, K. C. Isothermal Titration Calorimetric Studies on the Temperature Dependence of Binding Interactions between Poly (Propylene Glycol)S and Sodium Dodecyl Sulfate. *Langmuir* **2004**, *20*, 2177–2183.

(191) Prasad, M.; Palepu, R.; Moulik, S. P. Interaction between Sodium Dodecyl Sulfate (SDS) and Polyvinylpyrrolidone (PVP) Investigated with Forward and Reverse Component Addition Protocols Employing Tensiometric, Conductometric, Microcalorimetric, Electrokinetic, and DLS Techniques. *Colloid Polym. Sci.* **2006**, *284*, 871–878.

(192) Olofsson, G.; Wang, G. Interactions between Surfactants and Uncharged Polymers in Aqueous Solution Studied by Microcalorimetry. *Pure Appl. Chem.* **1994**, *66*, 527–532.

Appendices

Appendix A-Supplements to Chapter 3

ITC results at 45 ºC
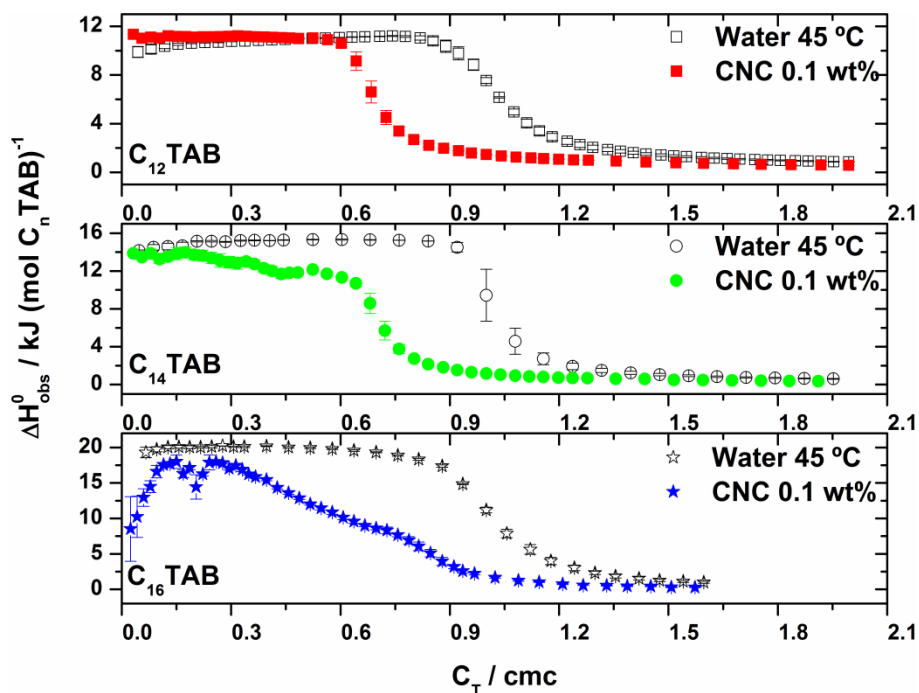
Figure A.1 Calorimetric titration curves obtained at 45 ºC for the titration of C_nTAB into water (empty symbols) and into 0.1 wt% CNC dispersion (filled symbols), as a function of normalized surfactant concentration (C_T/cmc).

ITC results with 0.01 wt% CNC dispersions
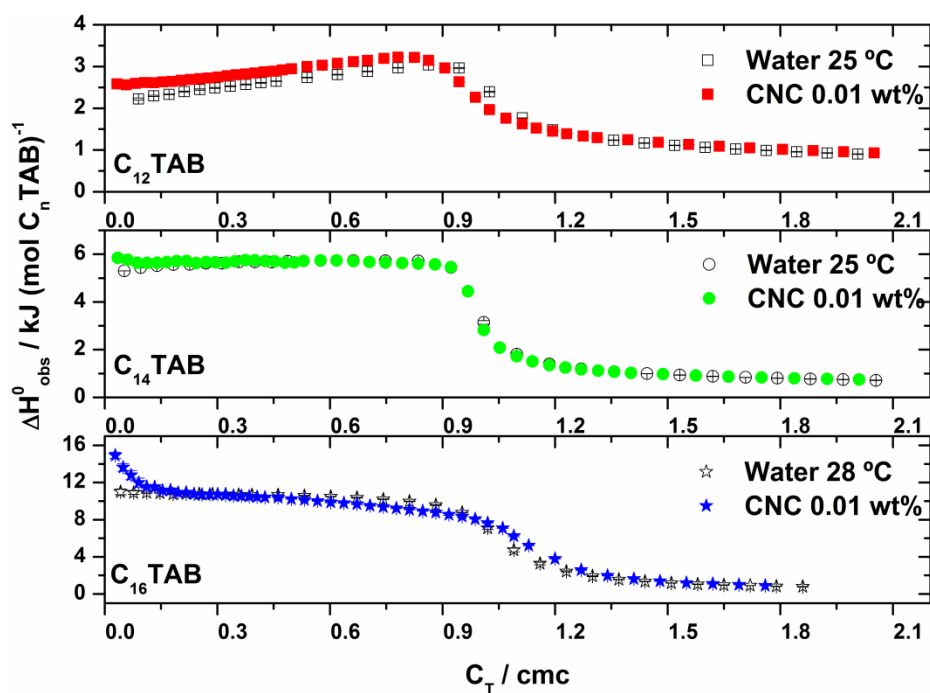
Figure A.2 Calorimetric titration curves obtained for the titration of C_nTAB into water (empty symbols) and into 0.01 wt% CNC dispersion (filled symbols) at 25 °C for $C_{12}TAB$ and $C_{14}TAB$, and 28 °C for $C_{16}TAB$, as a function of normalized surfactant concentration (C_T/cmc).

ITC comparison between $C_{16}TAB$ and $C_{16}PyB$
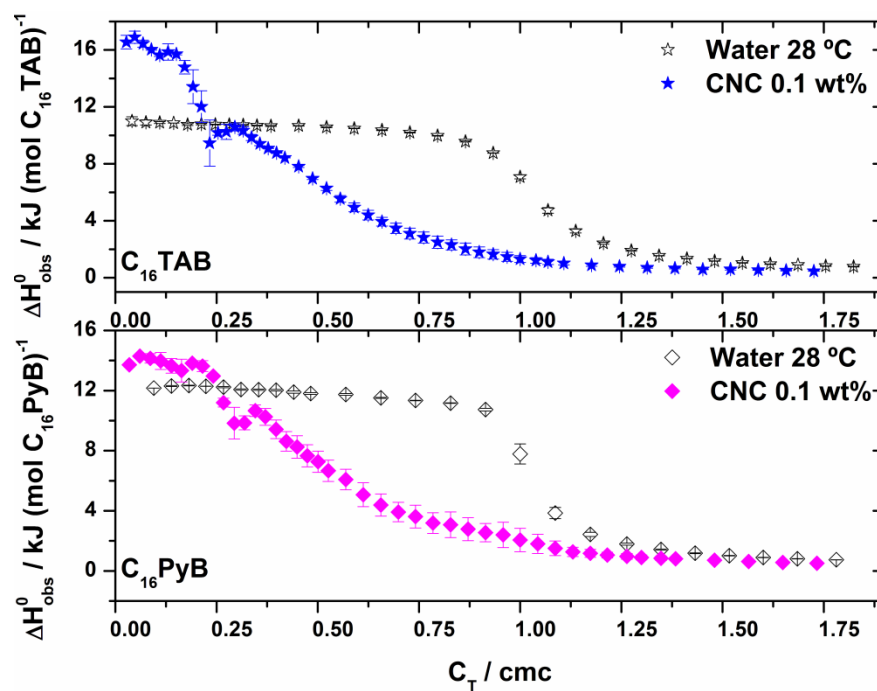
Figure A.3 Calorimetric titration curves obtained for the titration of $C_{16}TAB$ and $C_{16}PyB$ into water (empty symbols) and into 0.1 wt% CNC dispersion (filled symbols) at 28 °C, as a function of normalized surfactant concentration (C_T/cmc).

ITC comparison between C$_{16}$TAB and C$_{16}$TAC
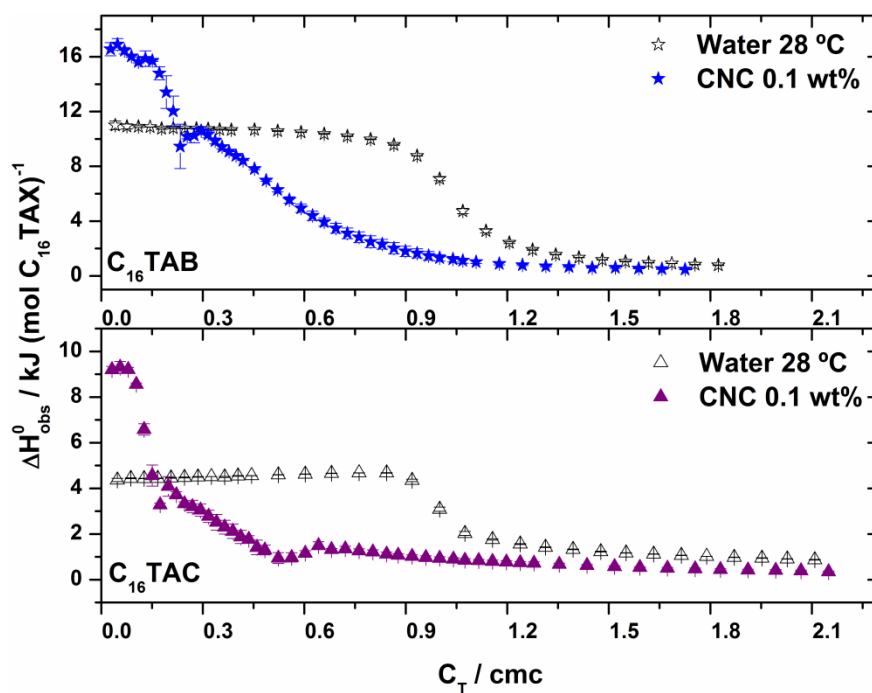
Figure A.4 Calorimetric titration curves obtained for the titration of C$_{16}$TAB and C$_{16}$TAC into water (empty symbols) and into 0.1 wt% CNC dispersion (filled symbols) at 28 ºC, as a function of normalized surfactant concentration (C$_T$/cmc).

Visual observation of mixtures containing 0.1 wt% CNC dispersions and $C_{12}TAB$ and $C_{16}TAB$, in the absence and in the presence of 25 mmol L^{-1} NaBr solutions
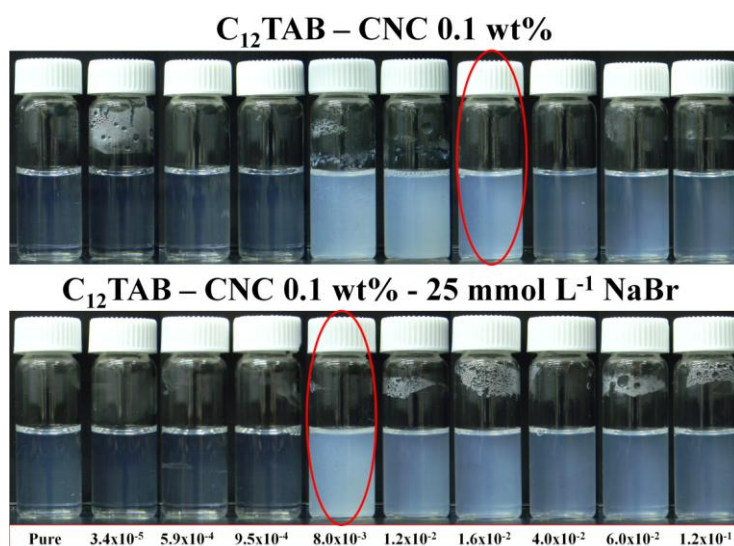
Figure A.5 Comparison of mixtures containing $C_{12}TAB$ and 0.1 wt% CNC dispersions in the absence (top) and in the presence of 25 mmol L^{-1} NaBr solution (bottom). The red circles represent the cmc concentration. The $C_{12}TAB$ concentrations are expressed in mol L^{-1}.
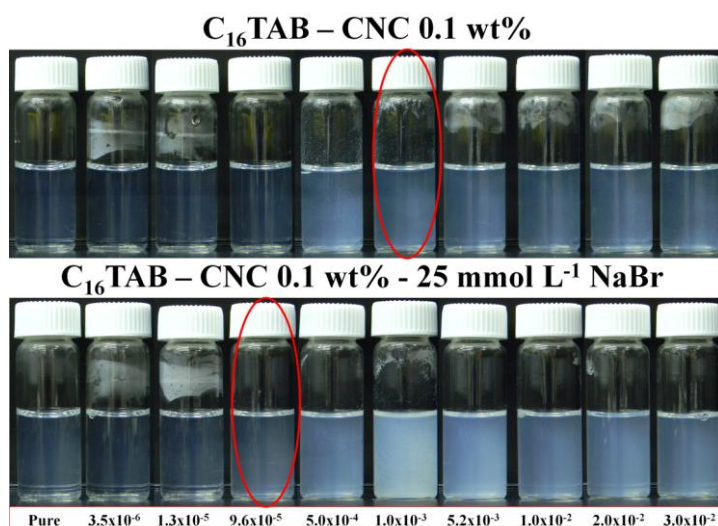
Figure A.6 Comparison of mixtures containing $C_{16}TAB$ and 0.1 wt% CNC dispersions in the absence (top) and in the presence of 25 mmol L^{-1} NaBr solution (bottom). The red circles represent the cmc concentration. The $C_{16}TAB$ concentrations are expressed in mol L^{-1}.

Settling behavior of mixtures containing 0.1 wt% CNC dispersion and C$_{12}$TAB and C$_{16}$TAB, after 1 week and 2 months

| 3.4x10^{-5} | 5.9x10^{-4} | 9.5x10^{-4} | 8.0x10^{-3} | 1.2x10^{-2} | 1.6x10^{-2} | 4.0x10^{-2} | 6.0x10^{-2} | 1.2x10^{-1} |

Figure A.7 Comparison of mixtures containing C$_{12}$TAB and 0.1 wt% CNC. The pictures were taken after preparation (top), after 1 week (middle), and after 2 months (bottom). The C$_{12}$TAB concentrations are expressed in mol L^{-1}.

| 3.5x10^{-6} | 1.3x10^{-5} | 9.6x10^{-5} | 5.0x10^{-4} | 1.0x10^{-3} | 5.2x10^{-3} | 1.0x10^{-2} | 2.0x10^{-2} | 3.0x10^{-2} |

Figure A.8 Comparison of mixtures containing C$_{16}$TAB and 0.1 wt% CNC. The pictures were taken after preparation (top), after 1 week (middle), and after 2 months (bottom). The C$_{16}$TAB concentrations are expressed in mol L^{-1}.

Visual observation of the settling behavior of mixtures containing 0.1 wt% CNC dispersion and C_{12}TAB and C_{16}TAB
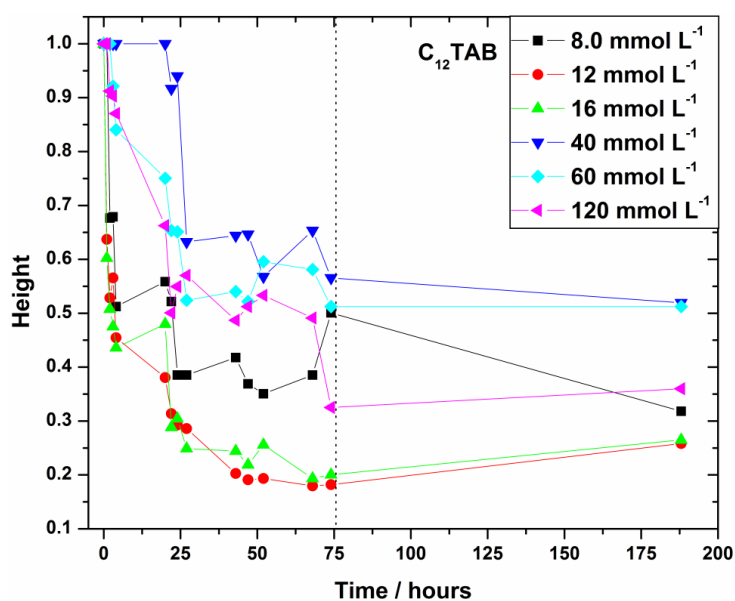
Figure A.9 Settling behavior for mixtures containing 0.1 wt% CNC dispersions and C_{12}TAB with increasing concentration, starting from 1/2 the cmc value.
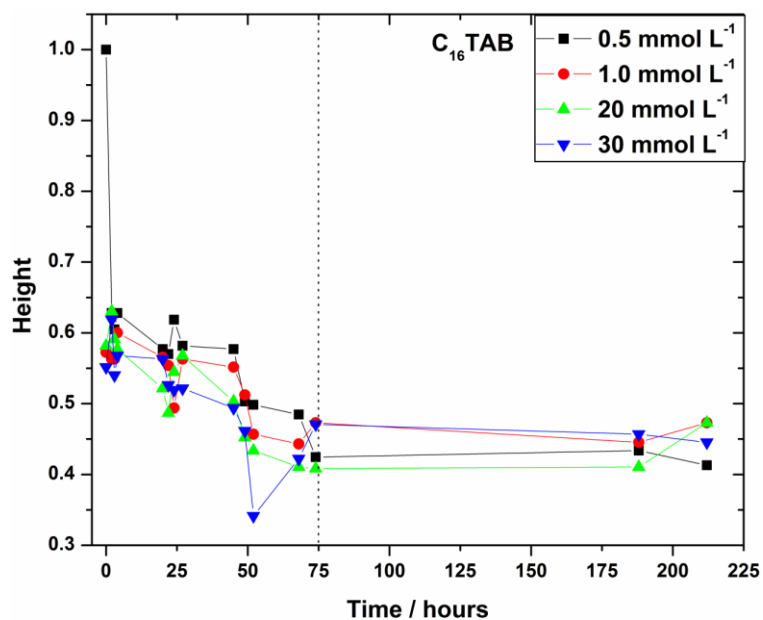
Figure A.10 Settling behavior for mixtures containing 0.1 wt% CNC dispersions and C_{16}TAB with increasing concentration, starting from 1/2 the cmc value.

Viscosity Measurements

The experiments were performed using a Haake RS1 rheometer equipped with a water bath and a cup Z20 Din sensor (d = 20 mm). The temperature was set at 25.0 ± 0.1 ℃ for $C_{12}TAB$ and 28.0 ± 0.1 ℃ for $C_{16}TAB$.

The results show a slight increase in the viscosity values for the mixtures containing surfactant (colored symbols) in comparison with pure CNC (black symbols). It is within an order of magnitude, therefore depicting no significant changes.
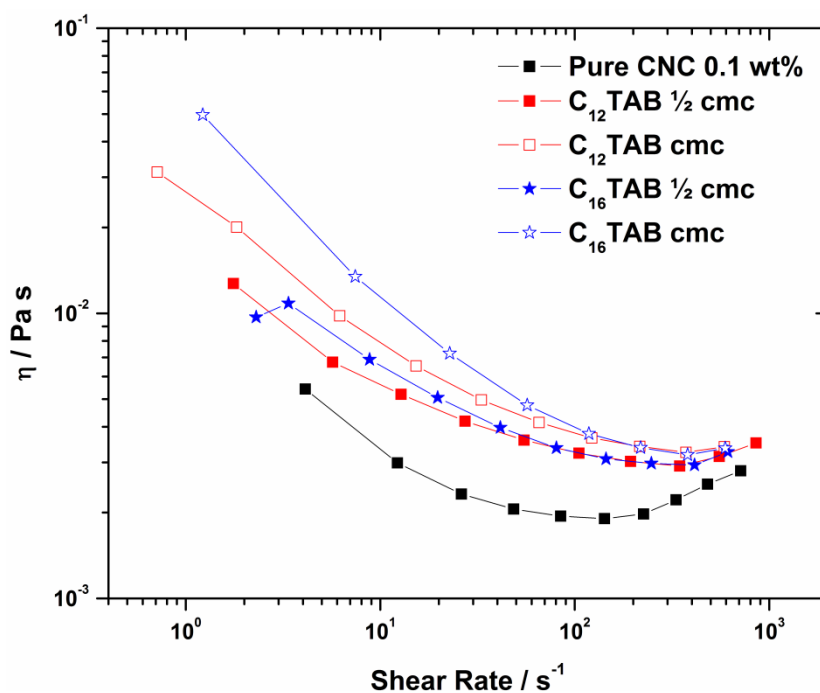
Figure A.11 Viscosity measurements performed for mixtures containing 0.1 wt% CNC dispersions and C_nTAB at 1/2 the cmc concentration (filled colored symbols) and at the cmc concentration (open colored symbols).

SAXS results for mixtures containing 0.1 wt% CNC dispersion and $C_{12}TAB$ and $C_{16}TAB$

Small angle X-ray scattering (SAXS): The measurements were performed at the SAXS1 beamline of the Brazilian Synchrotron National Laboratory, LNLS, in Campinas, Brazil. The samples were positioned in a cell with two flat mica windows and a thermal bath was used for temperature control. The wavelength of X-rays was 1.608 Å and the used sample-to-detector distance was around 0.6 m. The obtained CCD images were integrated and treated with the software Fit2D.[††]
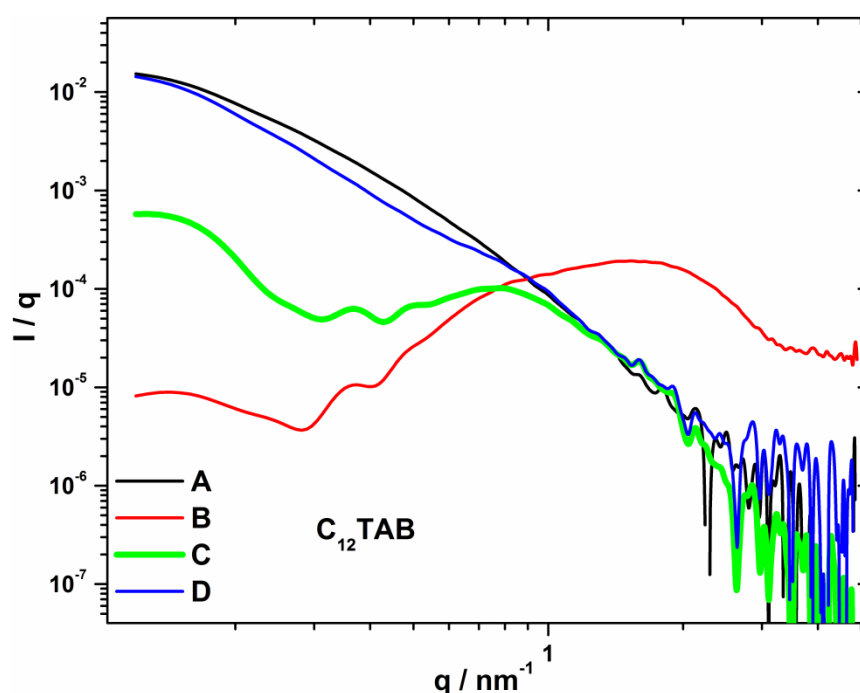
Figure A.12 SAXS curves for mixtures $C_{12}TAB$ and 0.1 wt% CNC dispersions. A (—) Pure 0.1 wt % CNC dispersion; B (—) pure $C_{12}TAB$ 120 mmol L^{-1}; C (—) mixture containing $C_{12}TAB$ 120 mmol L^{-1} and 0.1 wt % CNC subtracting water; D (—) mixture containing $C_{12}TAB$ 120 mmol L^{-1} and 0.1 wt % CNC subtracting curve B. The experiments were performed at 25 ºC.

[††] Hammersley, A. FIT2D: An Introduction and Overview, European Synchrotron Radiation Facility Internal Report, 1997.
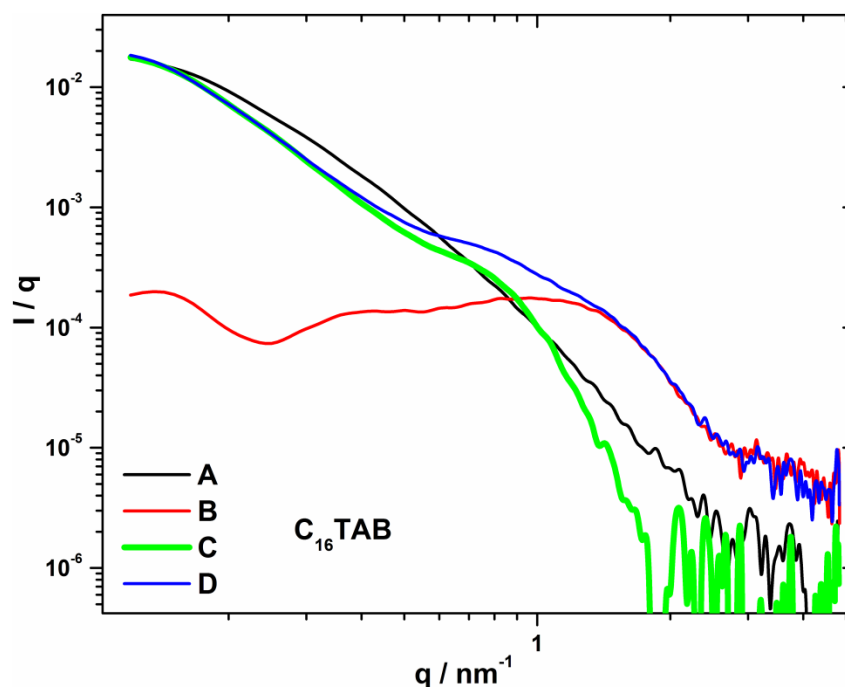
Figure A.13 SAXS curves for mixtures C_{16}TAB and 0.1 wt% CNC dispersions. A (—) Pure 0.1 wt% CNC dispersion; B (—) pure C_{16}TAB 30 mmol L^{-1}; C (—) mixture containing C_{16}TAB 30 mmol L^{-1} and 0.1 wt % CNC subtracting water; D (—) mixture containing C_{16}TAB 30 mmol L^{-1} and 0.1 wt % CNC subtracting curve B. The experiments were performed at 28 ºC.

The SAXS interpretation of the data as well its comparison with other techniques is presented in the Manuscript. The curves do not show a peak corresponding to the free micelle formation in water for C_{12}TAB in the q range of 1.2 nm^{-1}, even though the concentration is extremely high (120 mmol L^{-1}). This is only observed for C_{16}TAB (30 mmol L^{-1}), where the blue curve presents two broad peaks, one at q value around 0.8 nm^{-1} and the other at 1.2 nm^{-1}. This second peak might correspond to the saturation of the CNC rods, as it was observed with ITC experiments (both curves in the absence and in the presence of CNC are superimposed).

Appendix B-Supplements to Chapter 4

ITC results for NP-100 and CNC at 25 ºC
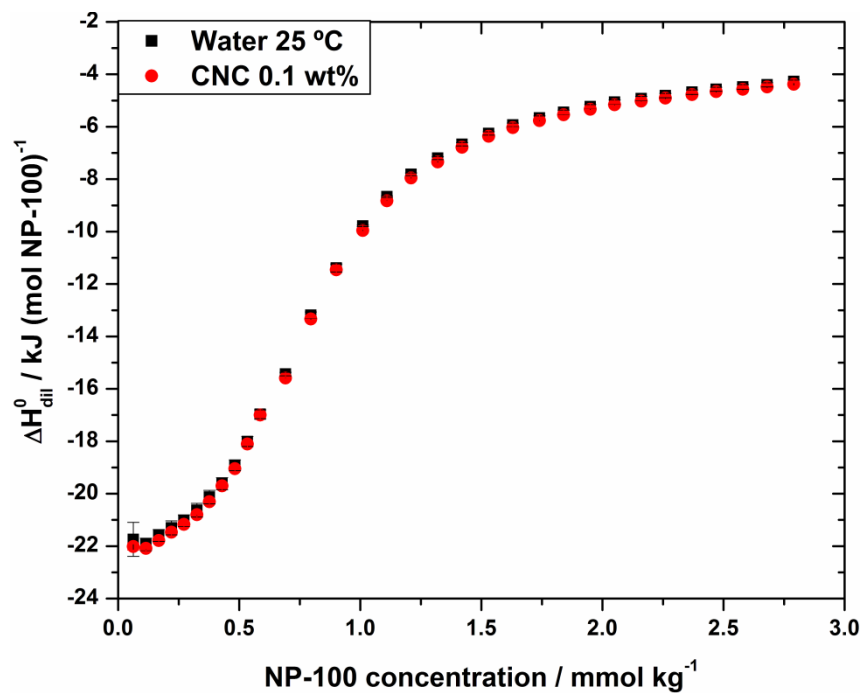
Figure B.1 Calorimetric titration curves obtained at 25 ºC for the titration of NP-100 into water (■) and into 0.1 wt% CNC dispersion (●), as a function of NP surfactant concentration in mmol kg^{-1}.

Visual observation of mixtures containing 0.1 wt% CNC dispersions and C_{12}TAB in the presence of 1.3 mmol L-1 NP-100

C_{12}TAB – CNC 0.1 wt%

| Pure | 3.4×10^{-5} | 6.0×10^{-4} | 9.5×10^{-4} | 8.0×10^{-3} | 12×10^{-3} | 16×10^{-3} | 40×10^{-3} | 60×10^{-3} | 120×10^{-3} |

C_{12}TAB + NP-100 1.3 mmol L^{-1} – CNC 0.1 wt%

| Pure | 3.4×10^{-5} | 6.0×10^{-4} | 9.5×10^{-4} | 4.0×10^{-3} | 8.0×10^{-3} | 12×10^{-3} | 16×10^{-3} | 40×10^{-3} | 60×10^{-3} | 120×10^{-3} |
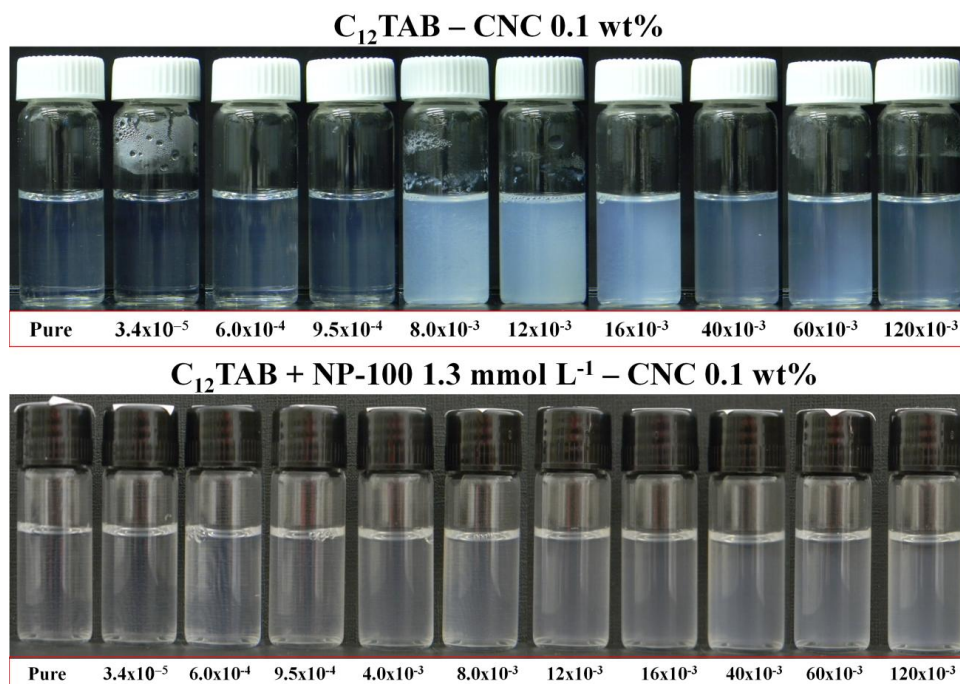
Figure B.2 Comparison of mixtures containing C_{12}TAB and 0.1 wt% CNC dispersions in the absence (top)[157] and in the presence of 1.3 mmol L^{-1} NP-100 solution (bottom). C_{12}TAB concentrations are expressed in mol L^{-1}(inside the red squares at the bottom).

Mixtures containing 1.0 wt% CNC-g-P(MEO$_2$MA) dispersions and surfactants prepared according to ITC results
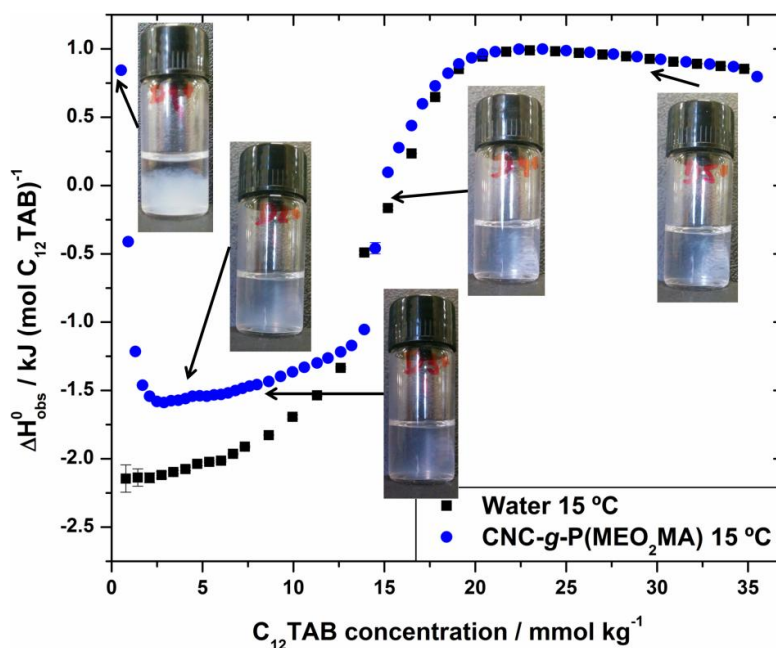
Figure B.3 ITC results for the system 1.0 wt% CNC-*g*-P(MEO$_2$MA) and varying C$_{12}$TAB concentration obtained at 15 ºC. Mixtures were prepared for electrophoretic mobility and particle size measurements according to the concentrations pointed by arrows on the graphic. At low C$_{12}$TAB concentration the first three mixtures are turbid and precipitate.
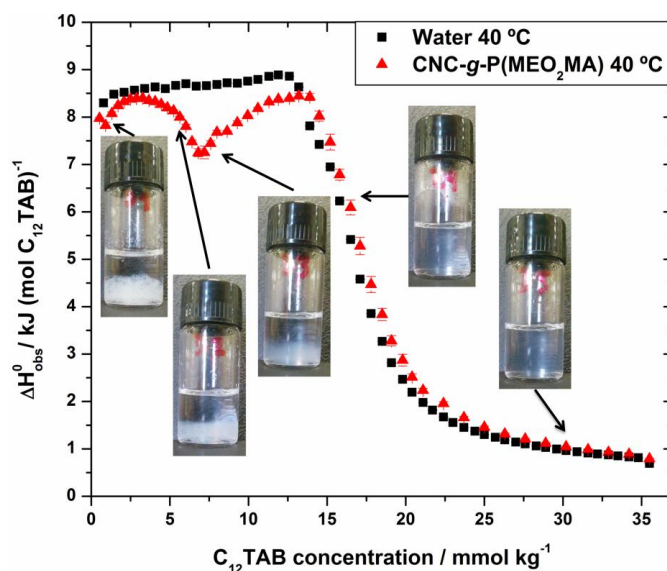
Figure B.4 ITC results for the system 1.0 wt% CNC-*g*-P(MEO$_2$MA) and varying C$_{12}$TAB concentration obtained at 40 ºC. Mixtures were prepared for electrophoretic mobility and particle size measurements according to the concentrations pointed by arrows on the graphic. At low C$_{12}$TAB concentration the first three mixtures are turbid and precipitate.
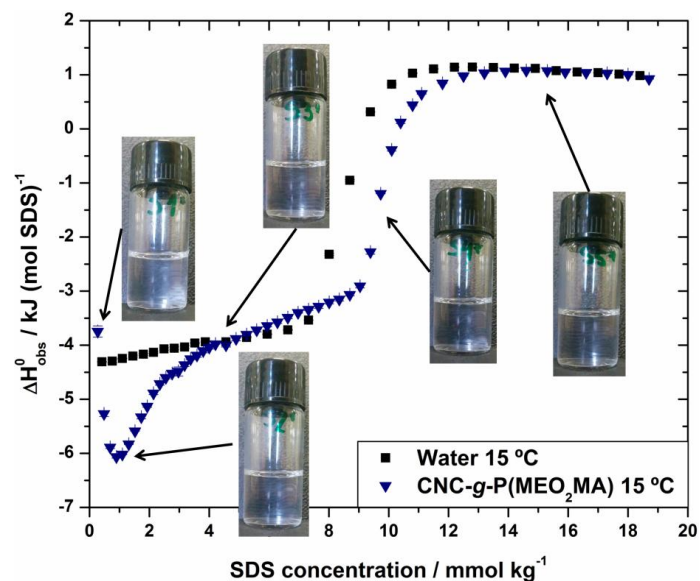
Figure B.5 ITC results for the system 1.0 wt% CNC-*g*-P(MEO₂MA) and varying SDS concentration obtained at 15 ºC. Mixtures were prepared for electrophoretic mobility and particle size measurements according to the concentrations pointed by arrows on the graphic. All the mixtures are transparent after mixing.
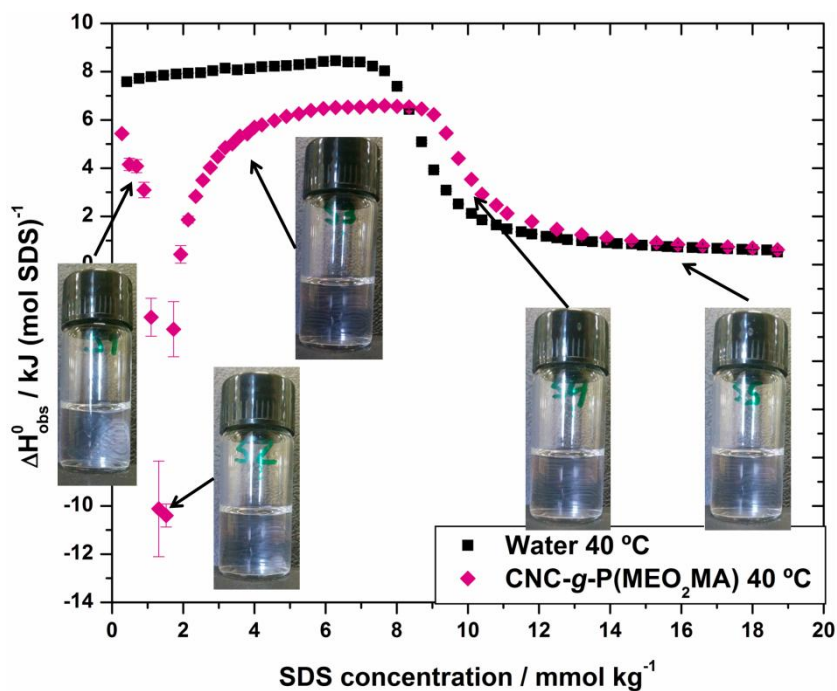
Figure B.6 ITC results for the system 1.0 wt% CNC-*g*-P(MEO₂MA) and varying SDS concentration obtained at 40 ºC. Mixtures were prepared for electrophoretic mobility and particle size measurements according to the concentrations pointed by arrows on the graphic. All the mixtures are transparent after mixing.

Dialysis tube containing CNC-g-P(MEO$_2$MA) and C$_{12}$TAB after 1 week of dialysis

Figure B.7 Dialysis tube containing 1.0 wt% CNC-*g*-P(MEO$_2$MA) and C$_{12}$TAB 80.0 mmol kg^{-1}. Result obtained after 1week of dialysis, replacing the water three times a day.

LCST behavior for CNC-g-P(MEO₂MA) in the presence of SDS
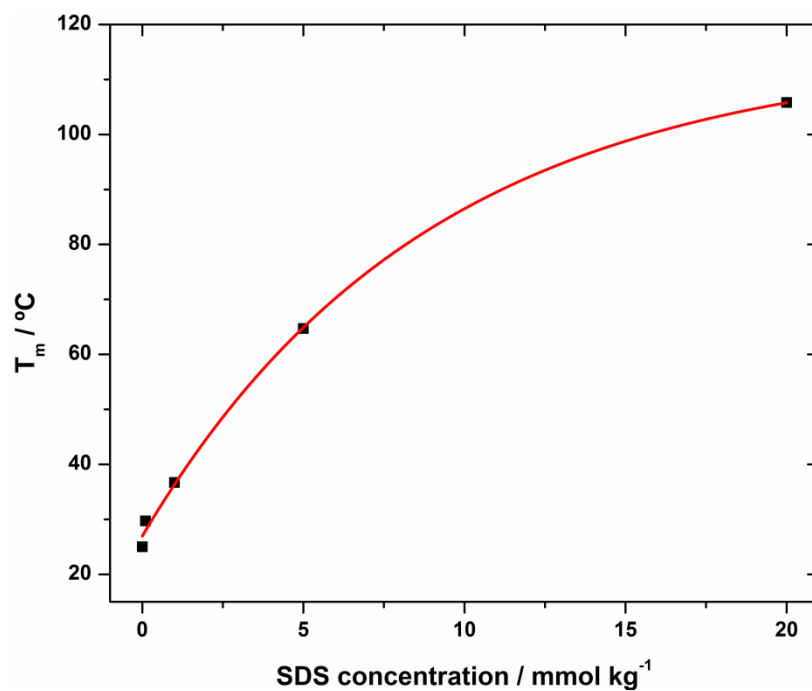
Figure B.8 Graphic of T_m obtained for the mixtures containing 1.0 wt% CNC-*g*-P(MEO₂MA) as a function of SDS concentration. The data was fitted just to help the reader.

Appendix C-Supplements to Chapter 5

Visual observation of the settling behavior of mixtures containing 0.1 wt% CNC-NH$_2$ dispersion and SDS (pH = 4.1) and C$_{12}$TAB (pH = 8.9)
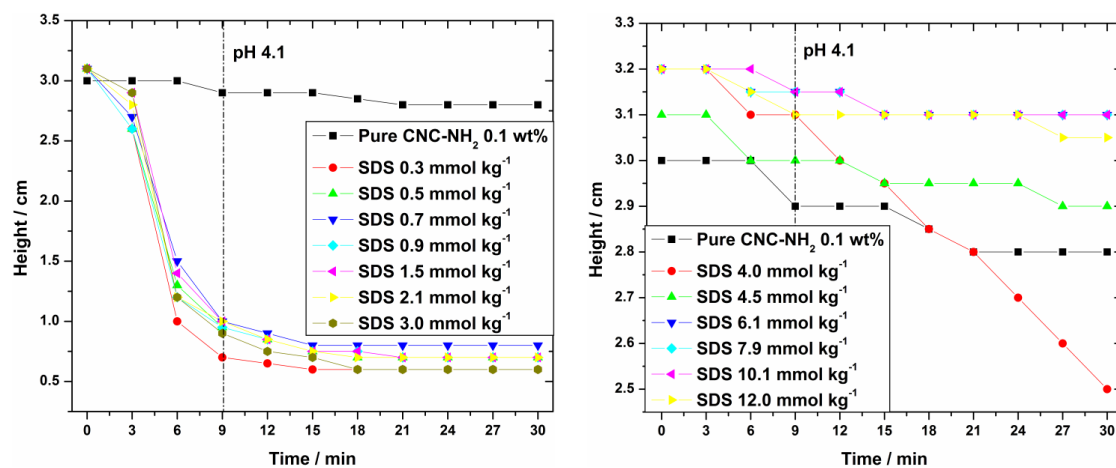
Figure C.1 Settling behavior for mixtures containing 0.1 wt% CNC-NH$_2$ dispersions and SDS with increasing surfactant concentration, at pH = 4.1.
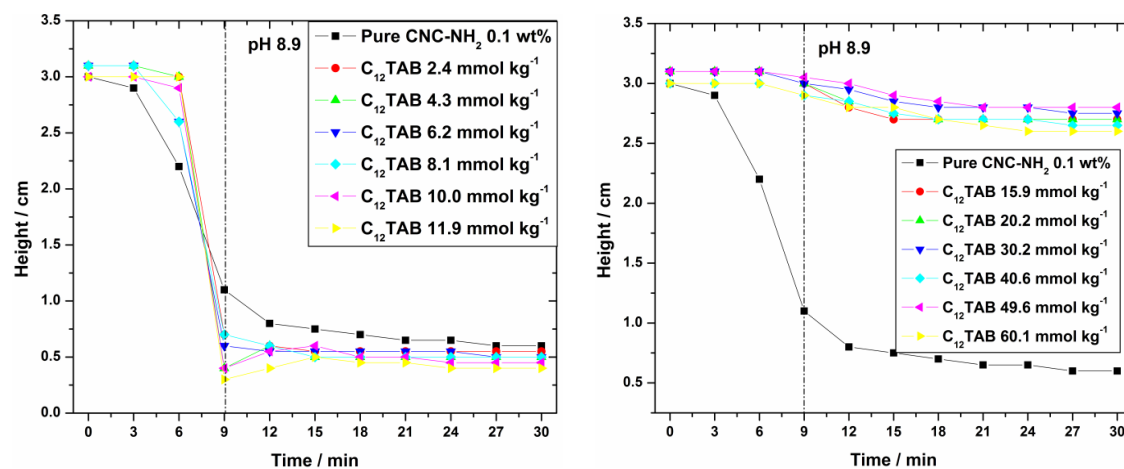
Figure C.2 Settling behavior for mixtures containing 0.1 wt% CNC-NH$_2$ dispersions and C$_{12}$TAB with increasing surfactant concentration, at pH = 8.9.

Appendix D- Use of isothermal titration calorimetry to study surfactant aggregation in colloidal systems

My contributions to the paper:

Wrote sections 2 to 2.4; assembled the different sections of the paper; references, figures and tables; final corrections.
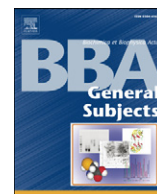
Use of isothermal titration calorimetry to study surfactant aggregation in colloidal systems ☆

Watson Loh [a,*], César Brinatti [a], Kam Chiu Tam [b]

[a] Institute of Chemistry, University of Campinas (UNICAMP), CP 6154, CEP 13083-970, Campinas, SP, Brazil
[b] Department of Chemical Engineering and Waterloo Institute for Nanotechnology, University of Waterloo, 200 University Avenue West, Waterloo, ON N2L 3G1, Canada

ARTICLE INFO

ABSTRACT

Background: Isothermal titration calorimetry (ITC) is a general technique that allows for precise and highly sensitive measurements. These measurements may provide a complete and accurate thermodynamic description of association processes in complex systems such as colloidal mixtures.

Scope of the review: This review will address uses of ITC for studies of surfactant aggregation to form micelles, with emphasis on the thermodynamic studies of homologous surfactant series. We will also review studies on surfactant association with polymers of different molecular characteristics and with colloidal particles.

General significance: ITC studies on the association of different homologous series of surfactants provide quantitative information on independent contribution from their apolar hydrocarbon chains and polar headgroups to the different thermodynamic functions associated with micellization (Gibbs energy, enthalpy and entropy). Studies on surfactant association to polymers by ITC provide a comprehensive description of the association process, including examples in which particular features revealed by ITC were elucidated by using ancillary techniques such as light or X-ray scattering measurements. Examples of uses of ITC to follow surfactant association to biomolecules such as proteins or DNA, or nanoparticles are also highlighted. Finally, recent theoretical models that were proposed to analyze ITC data in terms of binding/association processes are discussed.

Major conclusions: This review stresses the importance of using direct calorimetric measurements to obtain and report accurate thermodynamic data, even in complex systems. These data, whenever possible, should be confirmed and associated with other ancillary techniques that allow elucidation of the nature of the transformations detected by calorimetric results, providing a complete description of the process under scrutiny. This article is part of a Special Issue entitled Microcalorimetry in the BioSciences — Principles and Applications, edited by Fadi Bou-Abdallah.

1. Introduction

Calorimetry has evolved significantly since its early beginning and with the most recent technological evolution established itself as a unique technique to monitor chemical or biological events mostly because of its high sensitivity, allied to the fact that nearly all processes are associated with some form of thermal activity. One of the issues that is not resolved involving calorimetry can be summarized in the statement that "heat bears no color", to reinforce that it is not always straightforward to ascribe the origin of the heat detected during an event to a specific molecular process, as compared, for instance, with spectroscopic techniques (hence the mention to color). This issue has been recently commented by some of us [1] and we will provide a few examples in this article on how this could be overcome specifically to investigate self-assembling in complex colloidal systems.

Surfactants are molecules that tend to self-associate to form a variety of aggregates, starting with the simplest spherical micelles, which occur above a specific concentration denoted as the critical micelle concentration (*cmc*), to more complex tridimensional structures such as cubic, hexagonal or lamellar phases. They are commonly found in a variety of industrial products, for instance, for household cleaning, pharmaceutical or cosmetic purposes. Surfactants are also vital in biological process, including the composition of cell membranes (in this case, normally referred to as lipids), but also in digestion (bile salts) or in ensuring proper functioning of our lungs. In most cases, surfactants are found or formulated in mixtures containing polymers, which normally take part in the association process leading to aggregates with different properties. Again, biological examples of surfactant mixtures with proteins are common.

In a special issue devoted to calorimetry, there is no need to stress the importance of this technique as there are many examples described in the accompanying reviews. This review will focus only on one of the most common calorimetric techniques, called titration calorimetry, in which the system composition is varied by addition of one or more

components followed by measurement of heat exchange (see, for instance, reference [2] for more complete thermodynamic description of this procedure). These experiments are typically run under isothermal conditions; hence it is most commonly referred to as Isothermal Titration Calorimetry (ITC). Typically, experiments are performed at different temperatures to provide a more complete description of the process under investigation, and various examples described here will demonstrate.

Titration calorimetry is becoming one of the most used techniques for investigating surfactant association in solution phase. Phase transitions in the surfactant mesophase domain, however, due to the high viscosity of the phases involved, are more commonly investigated using scanning calorimetry techniques that allow the determination of transition enthalpies and temperatures. However this is outside the scope of the present review. A literature survey using the Web of Knowledge® (ISI) databank reveals over 600 articles published with the terms: (titration calorimetr*) and (surfact* OR lipid*) and (micelle* OR aggregat*), which represent the topic of this review. During the 1990's there were fewer than 10 articles published per year, which turned into around 30 during 2000's and, in the last two years reaching closer to 50 papers per year. These numbers double when the topic searched is broadened to remove the requirement of (surfact* OR lipid*), and which includes studies with polymers, especially biopolymers such as proteins and DNA.

ITC is not only advantageous for providing direct access to all the information necessary to determine the most important thermodynamic functions associated with micellization, namely the variations in Gibbs energy (ΔG), enthalpy (ΔH) and, from these two, the changes in entropy (ΔS), in only one experiment. Combination of ITC experiments at varying temperatures allows the determination of changes in heat capacity (ΔC_p), which is an important parameter for the evaluation of hydrophobic contributions [3,4]. The ITC technique allows simple experiments with advanced instrumentation that provides sensitivity for monitoring most processes in the micromolar concentration range. In addition, it has been extensively demonstrated, see for instance contributions from El Seoud [5–7] and Moulik's [8,9] research groups, that the van't Hoff approach is not capable of accounting for parallel changes in the surfactant aggregates with temperature and, therefore, does not provide exact values for enthalpy and entropy changes upon micellization.

In addition, an important fact that will most likely be stressed in other reviews in this special issue is that direct calorimetric measurements of enthalpy values provide greater accuracy in the derived thermodynamic data, as shown in the simulation of associated uncertainties shown in Table 1, as presented by Beezer et al. [10] This Table illustrates the error propagation when using the van't Hoff approach to derive all thermodynamic parameters (ΔH, ΔS and ΔC_p) in different temperature ranges and varying the number of *cmc* measurements obtained within each temperature range, when considering that one can assume $cmc = 1/K_{mic}$.

In general, ITC experiments display an uncertainty of less than 1% when obtaining enthalpy of micellization. Therefore, the derived thermodynamic parameters, ΔS and ΔC_p, are associated with uncertainties

smaller than a few %. In conclusion, the use of ITC to investigate the thermodynamics of certain processes could achieve high accuracy in the reported data and, in some cases, avoiding its use may render the results of a certain study inappropriate to allow correct comparisons and conclusions.

There are a few review articles already published on issues that will be analyzed in this review. Among them we would like to acknowledge contributions from Olofsson and co-workers [11], Tam and Wyn-Jones [12], Bouchemal [13] among others, all dealing with the use of calorimetry to investigate surfactant solutions. There are other more specific reviews that overlap with the present one, such as a recent one by Chiappisi and Gradzielski [14] on chitosan–surfactant mixtures, including the use of ITC. The first series of review articles came out a few years ago and we feel that there is room to update those revisions, as well as to expand them by adding relevant recent information on surfactant association with other colloidal systems.

In this review we will present and discuss recent studies using ITC to investigate surfactant association to form micelles and their interaction with other colloidal systems. The first section of this review addresses the issue of surfactant micellization, describing results on how ITC could be used to measure the most important thermodynamic functions associated with this process, and how this information could bring insights on the structure of the resulting micelles. Specific emphasis is focused on studies involving homologous series of surfactants that allow estimates of the independent contributions from the surfactant apolar and headgroups. A compilation of relevant literature data is presented in an attempt to derive information on interactions occurring in these micelles. Finally, studies on the interaction between surfactants and lipid assemblies are also reported.

The second section deals with surfactant association with polymers of different chemical structures, compositions and molecular architectures. Discussion is divided into systems of nonionic polymers and those in which electrostatic interaction between surfactant and polymer occurs, with emphasis on oppositely charged systems. Emphasis will be given to information on the mechanism of interaction that can be derived from features of enthalpy changes along the association, as well as on complementary information that should be obtained from ancillary techniques.

Finally, a section is devoted to reporting studies on the interaction of surfactants with other colloidal systems, mostly nanoparticles of different nature. We conclude with a summary of the studies using ITC and a perspective on the future directions regarding the use of ITC for these studies.

2. Obtaining thermodynamic parameters from ITC curves

When studying the aggregation behavior of colloidal systems, ITC is the only technique where one can directly obtain different important thermodynamic parameters in a single experiment such as: the *cmc* and the enthalpy of micellization ($\Delta H_{mic}^0 \leq$) [11,12,15]. Automated global analysis of data peaks and their integration is also possible through software other than the ones provided by the calorimeters manufacturers, among which we would like to mention the free software NITPIC [16–18]. A typical micellization experiment consists of titrating a concentrated surfactant solution (10–15 times above the *cmc* value) stepwise into the reaction cell, containing water or buffer solution, at a constant temperature. Integrating the titration peaks provides an energy value (q_i), that when normalized by the moles of titrant injected gives ΔH_{dil}^0.

ITC curves can be analyzed using two different models [11,19–29], namely the pseudo-phase separation model and the mass-action law model. The pseudo-phase separation model assumes that *cmc* is a dominant cooperative process and micelles are a separate phase, i.e. after *cmc* is reached the increase in surfactant concentration affects only the concentration of micelles and not the concentration of free unimers. Though it is a simple approximate model, when the system possesses

Table 1
Estimates of error propagation for the derivation of thermodynamic parameters (ΔH, ΔS and ΔC_p) of micellization from *cmc* values, using the van't Hoff approach at different temperature ranges and different number of data points. (adapted from reference [10]).

Temp. range/K	293–303		273–323		278–323	
N° of *cmc* measurements	5		5		10	
Uncertainty in log **cmc**	±0.02	±0.001	±0.02	±0.001	±0.02	±0.001
Deviation in ΔH/kJ mol^{-1}	±4	±0.2	±0.8	±0.04	±0.8	±0.04
Deviation in ΔS/J mol^{-1} K^{-1}	±14	±0.7	±3	±0.1	±1	±0.07
Deviation in ΔC_p/J mol^{-1} K^{-1}	±2700	±140	±110	±5	±120	±6

a large aggregation number (N_{agg}) it shows a steep change in ΔH^0_{dil} values at the *cmc* range as seen in ITC, thus fitting the model. However, it assumes the degree of counterions bound to the micelles to be one ($\beta = 1$), which affects the determination of ΔH^0_{mic} for ionic surfactants. The symbols α (ionization degree) and β (degree of counterion condensation) can be used interchangeably, but they are not numerically equal. The relationship between them is $\alpha = (1 - \beta)$. The mass-action law model assumes an existing equilibrium between free surfactant unimers and micelles at *cmc* and it takes into account the fraction of counterions bound to the micelles. It works for systems possessing a low aggregation number and it is also used to calculate thermodynamic parameters ($\Delta G^0_{mic}, T\Delta S^0_{mic}$). The equilibrium of micelle formation can be described for both nonionic and ionic surfactants by Eqs. (1) and (2):

$$nS \rightleftharpoons S_n \quad K = [S_n]/[S^n] \qquad (1)(\text{nonionic surfactants})$$

$$nS^- + (n\beta)B^+ \rightleftharpoons S_n^{(1-\beta)n} \quad K = [S_n]^{(1-\beta)}/\left([S^-]^n[B^+]^{n\beta}\right)$$
$$(2) \ (\text{ionic surfactants})$$
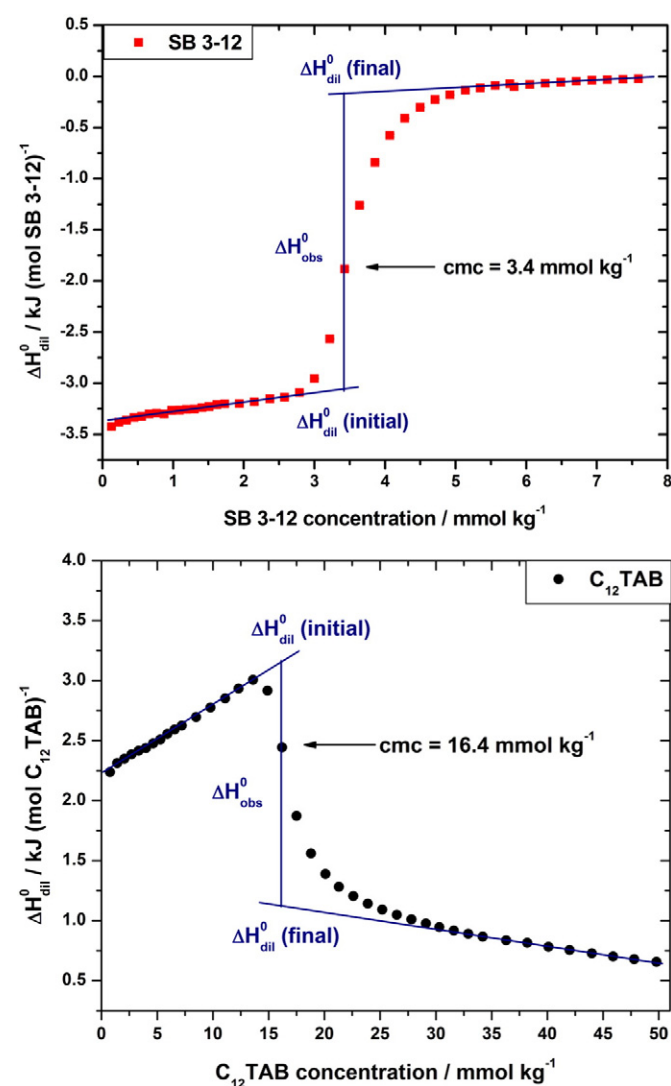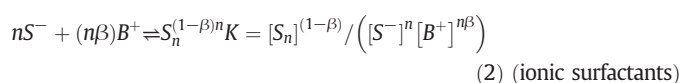
Fig. 1. Calorimetric titration curves obtained for two different surfactants: zwitterionic surfactant SB 3-12 (■) and a cationic surfactant C_{12}TAB (●) at 25 °C. The arrows are pointing at the *cmc* value obtained by the first derivative method. The initial surfactant concentration on the syringe (C_T) was 30.6 mmol kg^{-1} for SB 3-12 and 186.6 mmol kg^{-1} for C_{12}TAB (see text on how to properly obtain ΔH^0_{mic}).

Fig. 1 presents two calorimetric titration curves for two different surfactants at 25 °C with an alkyl chain of 12 carbon atoms: a zwitterionic sulfobetaine SB 3-12 (top, reference [15]), and a cationic dodecyltrimethylammonium bromide C_{12}TAB (bottom, unpublished data). The shape and profile of the curves are dependent on different factors such as, surfactant concentration, aggregation number, counterion binding, solvation–desolvation, temperature, and micellar shape [6, 19,30–32]. Both graphs can be divided into three different concentration regions — a pre-micellar region at low surfactant concentration where the measured enthalpy is related to the breakup of micelles in addition to the dilution of monomers added into the reaction cell; a post-micellar region at high surfactant concentration where the measured enthalpy is related to the dilution of both micelles and monomers added into the reaction cell; and the transition concentration region in which *cmc* can be obtained, where only a fraction of micelles is dissociated into unimers, while the rest remain in the micellar form. The *cmc* value is taken as the inflection point using the first derivative method [11,12,15,30,33,34,], $(\partial(\Delta H^0_{dil})/\partial C)$ for both ionic and nonionic surfactants, according to the mass-action law model (shown by an arrow in Fig. 1). At this concentration, the probability of an added monomer to remain in the bulk or to enter a micelle is 0.5. The measured *cmc* values are *3.4 mmol kg^{-1}* for SB 3-12 and *16.4 mmol kg^{-1}* for C_{12}TAB.

By using the mass-action law model (Eqs. (1) and (2)), the ΔG^0_{mic} can be derived from the *cmc* values for both types of surfactants:

$$\Delta G^0_{mic} = RT \ln \chi_{cmc} \qquad (3)(\text{nonionic surfactants})$$

$$\Delta G^0_{mic} = (2-\alpha)RT \ln \chi_{cmc}$$
$$(4)(\text{ionic surfactants in water and/or low ionic strength})$$

χ_{cmc} is the mole fraction of monomers at the *cmc*. The entropic term $T\Delta S^0_{mic}$ can then be derived using the Gibbs equation:

$$T\Delta S^0_{mic} = \Delta H^0_{mic} - \Delta G^0_{mic} \qquad (5)$$

It is noteworthy to mention that although both surfactants have the same alkyl chain length with 12 carbon atoms, they present entirely different ΔH^0_{dil} profiles at the same temperature when titrating into water. On one hand, SB 3-12 presents only negative values of ΔH^0_{dil} with a steep increase around the *cmc* region, denoting a strong cooperative micellization process, which can be modeled by both aforementioned models. The low *cmc* value and the fact the curve presents ΔH^0_{dil} in the pre and post-micellar region almost parallel to one another (resembling a sigmoidal curve) means that we can assume the system to have a large aggregation number and the solutions in the syringe and the reaction cell to be considered ideal, with their concentrations equal to their activities [6,11,31]. On the other hand, C_{12}TAB presents only positive values of ΔH^0_{dil} that slowly decrease for a broader range around the *cmc* region, denoting a more continuous and less cooperative micellization process with a low aggregation number. The positive slope on its ΔH^0_{dil} at low surfactant concentration is related to the known effect of an ion-pair interaction between surfactant unimers [11,25,35] due to a high surfactant concentration added at each injection, and the slope of ΔH^0_{dil} at high surfactant concentration is attributed to a decrease in concentration of free surfactant unimers (product $([S^-]^n[B^+]^{n\beta})$ in Eq. (2) remains constant) [11].

In order to obtain ΔH^0_{mic} values, two steps must be performed. First, we have to extrapolate the pre-micellar region towards the *cmc* value and the post-micellar region backwards to the *cmc* value using straight lines (blue lines shown in Fig. 1). At this point we have ΔH^0_{dil}(initial) and

ΔH_{dil}^0(final) respectively, and by taking the difference of their values we obtain ΔH_{obs}^0 [7,11,20,28,30,33,34,36–38]. This value is defined by a simple mathematical expression given by Eq. (6):

$$\Delta H_{obs}^0 = \Delta H_{dil}^0(\text{final}) - \Delta H_{dil}^0(\text{initial}) \tag{6}$$

Second and most importantly, even though the initial concentration is much greater than the *cmc* concentration, it is mandatory to consider the monomer fraction in the titrant solution [11,28]. To do this, we must take into account the total surfactant concentration in the syringe (C_T) that is titrated into the reaction cell and the *cmc* value:

$$\Delta H_{mic}^0 = -\Delta H_{demic}^0 = \Delta H_{obs}^0 x C_T / (C_T - cmc) \tag{7}$$

In ITC experiments we are titrating a concentrated surfactant solution containing micelles into water or buffer solution, so the observed heats are related to a demicellization process (ΔH_{demic}^0), which is the same as the micellization process but with an opposite sign. The correct values of ΔH_{mic}^0 are:

$$SB\,3-12 : (\Delta H_{dil}^0(\text{final}) = -0.16\,\text{kJ}\,\text{mol}^{-1}; \Delta H_{dil}^0(\text{initial})$$
$$= -3.04\,\text{kJ}\,\text{mol}^{-1}, C_T = 30.6\,\text{mmol}\,\text{kg}^{-1}, cmc$$
$$= 3.4\,\text{mmol}\,\text{kg}^{-1}) = +3.2\,\textbf{kJmol}^{-1}$$

$$C_{12}TAB : (\Delta H_{dil}^0(\text{final}) = +1.10\,\text{kJ}\,\text{mol}^{-1}; \Delta H_{dil}^0(\text{initial}) = +3.17\,\text{kJ}\,\text{mol}^{-1},$$
$$C_T = 190.0\,\text{mmol}\,\text{kg}^{-1}, cmc = 16.4\,\text{mmol}\,\text{kg}^{-1})$$
$$= -2.3\,\textbf{kJmol}^{-1}$$

While for the zwitterionic surfactant micellization is an *endothermic* process, for the cationic surfactant the same process is *exothermic*.

The thermodynamics of micellization of two commercially available alkyl phenol ethoxylates (APEs), i.e. octyl phenol ethoxylate (Triton X-series) and nonyl phenol ethoxylate (Tergitol NP-series), at various temperatures were quantified using the ITC technique. [30] Their titration curves display a classical sigmoidal shaped (Fig. 2), where ΔH_{mic}^0 and *cmc* can be readily obtained. It was observed that the values of these two thermodynamic parameters are directly linked to the length of the hydrophilic poly (ethylene glycol) (PEG) segments. However, increasing the size of the hydrophobic alkyl segments leads to a sharp decrease in the *cmc*.
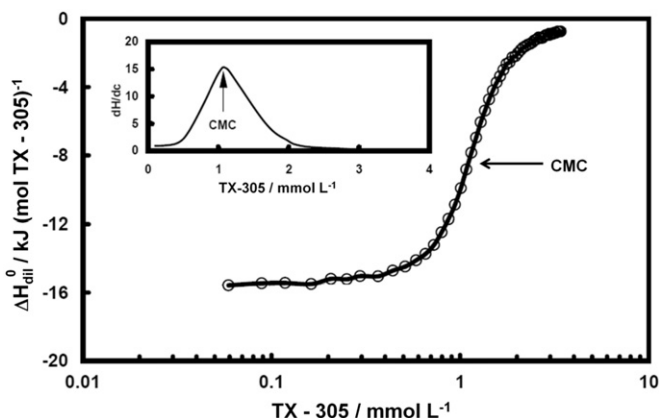
Fig. 2. Sigmoidal micellization curve obtained for an octyl phenol ethoxylate TX − 305 at 25 °C. Inset shows determination of cmc by the first derivative method. Adapted from reference [30].

2.1. Determination of aggregation number (N_{agg}) using ITC

We have already mentioned that the aggregation number (N_{agg}) has an influence, among other factors, on the shape of micellization curves in ITC, more precisely the slope of the curve. N_{agg} does not vary at the *cmc* region, and the values obtained are usually smaller than the ones gathered by spectroscopic and light scattering techniques that are performed at a high surfactant concentration (much higher than the *cmc* value) [34,39,40]. Because of this, studies were conducted using ITC by modeling the curves using some variations of the mass-action law model to ascertain the aggregation number as a rough estimate for systems at the *cmc* transition region.

Paula et al. [23] observed a strong dependence of N_{agg} with temperature and the alkyl chain length of different systems when comparing two bile salts sodium cholate (NaC) and sodium deoxycholate (NaDC) with sodium dodecylsulfate (SDS), an anionic surfactant, and octyl glucoside (OG), a nonionic surfactant. A much broader *cmc* transition range was observed for the bile salts rather than for SDS and OG. For bile salts are described as having hydrophobic and hydrophilic surfaces, this is directly related to a much smaller aggregation number and a less cooperative process.

Experiments were performed by Garidel et al. [21,22] with NaC and NaDC in 0.1 mol L^{-1} NaCl at pH 7.5. They considered the fact that bile salts present a small aggregation number [23] that varies with temperature and is dependent on the amount of counterion bound to the aggregates (β). In their analysis they allowed several parameters to be adjusted by taking into consideration N_{agg} and ΔG_{mic}^0 into Eq. (2) (N_{agg} and ΔG_{mic}^0 are responsible for the steepness of the ITC curves), while fixed β values (obtained from literature) were used in order to obtain reasonable results regarding N_{agg}. It should be mentioned that they found similar results for N_{agg} by using both models (pseudo-phase and mass action). Following the same reasoning, Olesen et al. [24,25] have proposed a method of extracting N_{agg} from the ITC data for a series of 6 bile salts and SDS. They described an accurate way of modeling the curves based on the mass-action law model. Their model considers that at the *cmc*, only unimers and surfactant micelles are in equilibrium in the presence of a large amount of counterions. Therefore $[(n\beta)B^+] \gg [nS^-]$, and so Eq. (2) becomes an approximation of Eq. (1).

A homologous series of alkyltrimethylammonium bromide surfactants C_nTAB (n = 12, 14 and 16) in the presence of 0.1 mol L^{-1} NaCl solution at pH 6.4 was studied by Beyer et al. [28] They reported small N_{agg} values (20−30) for the whole series at 25 °C. This could be because they used fixed values of β previously reported in the literature [43] at a constant temperature and in pure water.

Lah et al. [26] combined calorimetric data from both ITC and Differential Scanning Calorimetry (DSC) with Small Angle X-ray Scattering (SAXS) for an ethoxylated surfactant derivative C_8EO_γ. They observed a good correlation between the N_{agg} and ΔG_{mic}^0 obtained by calorimetry and Small Angle X-ray Scattering measurements, as pointed out by Garidel et al. [21,22]

2.2. Contributions of the headgroup (HG) and the alkyl chain ($-CH_2-$) on the micellization thermodynamic parameters

It is possible to calculate the contributions of both moieties of a surfactant, i.e. the headgroup (HG) and the alkyl chain ($-CH_2-$) on the micellization process when we consider the pseudo-phase separation model, where micelles are a different phase within an aqueous environment. This can be attained by considering that a measured thermodynamic parameter is a linear sum of contributions from the headgroup and the alkyl chain [5,6,16,31], known as the additivity relationship, as shown by the following equation:

$$\Delta X_{mic}^0 = \Delta X_{mic}^0 HG + n\Delta X_{mic}^0 CH_2 \tag{8}$$

ΔX^0_{mic} is the measured thermodynamic parameter (ΔG^0_{mic}, ΔH^0_{mic} or $T\Delta S^0_{mic}$), $\Delta X^0_{mic}HG$ is the contribution of the headgroup on the parameter, n is the number of carbon atoms present in the alkyl chain, and x is the individual contribution of each methylene unit on the parameter.

In this review we assume an equal contribution from the terminal methyl unit ($-CH_3$) and the methylene units ($-CH_2-$). Therefore, the slope of the curve provides information on the transfer of the alkyl chain from water to the interior of the micelle, and the intercept is related to the confinement of the headgroup at the surface of the micelle. Moreover, information from several studies on a homologous series of surfactants by ITC had provided sufficient information for us to apply Eq. (8) on their data.

Tables 2–6 present data for *cationic* (bromide is the most common counterion), *imidazolium derivatives* (chloride is the most common counterion), *zwitterionic* (sulfobetaines and sulfobetaine derivatives), *nonionic* (phosphine oxides, glucoside and ethoxylated derivatives) and *anionic surfactants*. We decided to split the imidazolium derivatives (also known as ionic liquids) from the regular cationic surfactants due to the presence of an imidazolium ring in their headgroup, although when in water they behave in the same way as cationic surfactants [42]. All data presented in the tables were obtained with at least three points, i.e. a homologous series with at least three alkyl chain lengths, unless mentioned otherwise. All the data presented in the Tables are in kJ mol^{-1}.

There is a similar trend for all the classes of surfactants analyzed when considering the contributions from the alkyl chains on different thermodynamic parameters ($\Delta X^0_{mic}CH_2$). $\Delta H^0_{mic}CH_2$ is the sum of energies related to the desolvation process and the confinement of the alkyl chains and their interactions inside the micelle. The value of this parameter is always negative, around -1.5 kJ mol^{-1}. As for the term $\Delta G^0_{mic}CH_2$ it is related to the transfer of an organic compound from a polar environment (in these cases water) to a nonpolar environment (the interior of the micelle), and they present a value of -3.0 kJ mol^{-1} in agreement with other literature values [5,6,15,31,36, 53,54,56]. The term $T\Delta S^0_{mic}CH_2$ is always positive denoting an increase in the degrees of freedom of the water molecules involved in the salvation of these alkyl chains when they are transferred from water to the interior of the micelles.

Investigation on the contributions of the headgroups on micellization ($\Delta X^0_{mic}HG$) leads to more interesting results. $\Delta G^0_{mic}HG$ reveals no observable trend and also the larger spread within the same series (from -0.4 to 3.7 kJ mol^{-1} in Table 2, and 0.3 to 11.9 kJ mol^{-1} in Table 3) for cationic and imidazolium surfactant derivatives, respectively. This may be attributed to how the values of α (or β) were obtained and their accuracy; there is a direct dependency when calculating ΔG^0_{mic} (Eq. (4)), as seen by the large discrepancy between the results from references [44] (3.7 kJ mol^{-1}) and [45] (0.9 kJ mol^{-1}) for cationic surfactants presenting a diminute difference in temperature of 3 degrees among them, and references [5] and [48] for imidazolium surfactant derivatives (0.3 and 2.1 kJ mol^{-1} respectively). In the case of other series of surfactants, zwitterionics and alkyldimethylphosphine oxides they present the largest values (16.1 kJ mol^{-1} and 18.0 kJ mol^{-1}) followed by glucoside derivatives (3.8 kJ mol^{-1}) and ethoxylated derivatives (2.7 kJ mol^{-1}).

As for the contributions from $\Delta H^0_{mic}HG$ on the micellization process the highest to the lowest values are: ethoxylated derivatives present the highest value of all: 35.3 kJ mol^{-1} for C_nEO_6 — it shows us the huge dehydration penalty of transferring six EO units from water to the surface of the micelle; zwitterionic and phosphine oxide derivatives present a similar value close to 23.0 kJ mol^{-1}, due to a dipolar moment present on both their headgroups; cationic and imidazolium surfactant derivatives present the second lowest value around 16.5 kJ mol^{-1}, pointing that the presence of an imidazole ring in the surfactant headgroup does not render a major influence on the thermodynamics within the cationic homologues; the glucoside surfactant derivatives C_nG_m displaying a contribution of 16.1 kJ mol^{-1}, probably due to the fact that the energy expended in dehydrating the glucoside rings is compensated by an energy gain when hydrogen bonds are formed between the hydroxyl groups at the surface of the micelle; and anionic surfactants, presenting the lowest value of 7.4 kJ mol^{-1}, probably due to the presence of the smallest counterions for all ionic surfactants.

An interesting observation can be derived when analyzing the data presented in Tables 2 and 3. Exchanging the counterion from chloride (Cl^-) to bromide (Br^-) for the imidazolium surfactant derivatives has caused a large reduction in $\Delta G^0_{mic}HG$ from a positive and unfavorable process (2.1 kJ mol^{-1}) [5] to a negative and favorable process (-2.7 kJ mol^{-1}) [49]. A similar behavior was observed when comparing $\Delta H^0_{mic}HG$ values: the process has changed from *endothermic* (15.0 kJ mol^{-1}) to *exothermic* (-0.8 kJ mol^{-1}). Comparing the data for cationic surfactants we observe that the presence of chloride as the counterion does not favor micellization. Though we have collected data from two different sources (references [43] and [47]) to calculate $\Delta H^0_{mic}HG$ for C_nTAC, it shows the highest value among all surfactants (22.6 kJ mol^{-1} against 18.2 kJ mol^{-1} for the highest value for C_nTAB). This shows a higher affinity between polarizable anions and positive charged surfactants according to the Hofmeister series [57–59].

2.3. ITC as a tool in studying membranes and vesicles

In this section, we will briefly comment on some of the astounding contributions of ITC in the field of biomolecules self-assembly — the study of vesicle formation and membrane-protein reconstitution in real time [60], membrane translocation with ionic surfactants [61,62], and membrane refolding using a fluorinated surfactant [63]. Jahnke et al. [60] have demonstrated the use of ITC to monitor and obtain a phase-diagram for bilayer self-assembly. They performed titration experiments by injecting a mixture of an *E.coli* extracted lipid and a nonionic detergent octyl-β-D-glucopyranoside (OG) in the absence (Fig. 3 top) and in the presence of a homotetrameric K$^+$ channel KcsA (Fig. 3 bottom). Their results show a large influence of the surfactant concentration on two boundaries, namely solubilization and saturation boundaries.

Table 2
Contributions of thermodynamic parameters of micellization from both headgroup and alkyl chain for cationic surfactants.

Surfactant	Temperature/K	Headgroup			Alkyl chain			Reference
		ΔG^0_{mic}	ΔH^0_{mic}	$T\Delta S^0_{mic}$	ΔG^0_{mic}	ΔH^0_{mic}	$T\Delta S^0_{mic}$	
C_nTAB	298.15		16.9			−1.6		[43]
C_nTAB	298.15	3.7	9.3	5.5	−3.2	−1.0	2.2	[44]
C_nTAB	301.15	0.9	16.3	15.8	−3.1	−1.6	1.5	[45]
C_nTAB^a	298.15	−2.9	16.2	19.1	−2.6	−1.2	1.4	[28]
C_nDHAB	298.15	0.4	16.6	16.2	−3.5	−1.7	1.8	[46]
C_nHDAB	298.15	0.4	18.2	17.8	−3.5	−1.7	1.7	[46]
C_nTAC^b	298.15		22.6			−1.5		[43,47]
C_nPyC	298.15	1.9	10.6	8.8	−3.1	−0.7	2.3	[5]

[a] Experiments performed in 0.1 mol L^{-1} NaCl.
[b] Data obtained by combining two different sources.

Table 3

Contributions of thermodynamic parameters of micellization from both headgroup and alkyl chain for imidazolium derivative surfactants.

Surfactant	Temperature/K	Headgroup			Alkyl Chain			Reference
		ΔG^0_{mic}	ΔH^0_{mic}	$T\Delta S^0_{mic}$	ΔG^0_{mic}	ΔH^0_{mic}	ΔH^0_{mic}	
$C_n mimCl$	298.15	0.3	15.9	18.5	−2.5	−1.2	1.1	[48]
$C_n mimCl$	298.15	2.1	13.0	10.9	−3.2	−1.0	2.2	[5]
$C_n mimCl$	308.15	11.9	11.5	1.8	−3.7	−1.3	2.3	[37]
$C_n mimBr$	298.15	−2.7	−0.8	1.9	−3.4	−0.2	3.1	[49]
$C_n BzMe_2Cl$	298.15	6.1	19.2	13.1	−3.7	−1.5	2.2	[31]
$C_n AEtBzMe_2Cl$	298.15	0.4	17.1	16.9	−3.4	−1.6	1.8	[5]
$C_n ABzMe_2Cl$	298.15	1.2	16.4	15.2	−3.4	−1.6	1.8	[31]

Using a basic principle of a simple surface partition equilibrium and the Gouy–Chapman theory, Keller and Heerklotz [61] reported ITC as a method to monitor transmembrane movement of charged surfactants by performing uptake and release experiments (flip-flop) in buffer conditions They used SDS and a zwitterionic phospholipid 1-palmitoyl-2-oleoyl-sn-glycero-3-phosphocholine (POPC) membrane at two different temperatures of 25 and 65 °C. The uptake experiments consisted in titrating POPC into an SDS solution, while for release experiments a mixture of POPC and SDS was titrated into the reaction cell containing buffer. In addition to the fact that SDS is used for membrane solubilization studies, they have shown that it can slowly permeate lipid bilayers at room temperature while presenting a rapid flip-flop above 50 °C.

At the temperature of 25 °C for both uptake and release experiments, a 5 min interval between each injections was more than enough for the electrical signal to return to the baseline level and a good correlation was obtained when assuming no measurable flip-flop during the whole titration experiment. However, a different result was obtained when doing experiments at higher temperature (65 °C). A much longer interval of 20 min was necessary for the electrical signal to return to the baseline level at the first injections in both uptake and release experiments, denoting a much slower process. This difference in equilibration time was attributed to binding (uptake experiment) and desorption (release experiment), again with a very good data fitting. The calorimetry results were in agreement with experiments performed with radiolabels and fluorescence experiments, with the advantage of being much faster (within hours) and label-free [62]. Still on the idea of transmembrane movement, Frotscher et al. [63] showed that a fluorinated octyl maltoside surfactant derivative, which is known from being hydrophobic and lipophobic, can migrate between phospholipid vesicles (POPC) and does not compromise the vesicle order/structure at high temperatures (60 °C).

2.4. Micellar shape transitions followed by ITC

ITC can be also used to monitor further shape transitions starting from the spherical aggregates. In some cases, depending on the surfactant packing, their aggregates may attain anisometric shapes. This sphere-to-rod transition is normally observed for ionic surfactants upon the addition of salts [64] due to the screening of electrostatic forces that allow a more efficient approximation of the surfactant headgroups, reducing the aggregate curvature and leading to its growth in one direction. For some surfactants, this transition is also observed at higher surfactant concentration, and for this reason, it is sometimes

referred to as the "second *cmc*", a term we believe is not appropriate, and should be replaced by sphere-to-rod transition.

Interestingly, for ionic surfactants, there are only a few studies on such transition using ITC, this transition being more commonly investigated using other techniques such as conductometry [65], spectroscopic probes [66] and scattering techniques. [67] For nonionic surfactants, however, there are more reports on the sphere-to-rod transition using calorimetry but since this process may be driven by temperature changes, DSC is the calorimetric technique of choice [68,69].

One of the few reports where ITC is used in this case in combination with conductometry and fluorescence measurements for investigating the sphere-to-rod transition of an ionic surfactant, benzethonium chloride is attributed to Karumbamkandathil and co-workers [66]. They present results without a clear indication from calorimetry that could be ascribed to this transition. In a more systematic investigation on the aggregation of $C_n TAB$, Ray and co-workers [44] reported results that constitute a clearer indication that ITC curves could be used to determine the sphere-to-rod transition. More recently, Du et al. [70] also reported a study on the aggregation of a gemini surfactant with another imidazolium derivative, where this second shape transition was observed using a variety of techniques, including ITC. In this case, the calorimetric curves revealed a clear description of the second transition at higher temperatures, although it is not clear whether the second transition refers to a rod-like or elongated micelle.

A very similar calorimetric curve (Fig. 4) was reported by Ito et al. for tetradecyltrimethylammonium bromide ($C_{14}TAB$) — salicylate mixtures, but in this case they clearly refer to a specific shape transition associated with the formation of elongated or worm-like micelles [71]. These are micron-sized cylindrical aggregates that appear in very specific conditions (depending on co-solute type, concentration and temperature range). ITC results, in conjunction with viscometry, light scattering and rheology clearly indicate the presence of a second shape transition, but the formation of this special aggregate is finely dependent on the co-solute/surfactant mole ratio where upon addition of excess co-solute, the elongated aggregates start to dissociate, reversing the micellar growth. Some features from the ITC curves such as a strong cooperative transition, associated with a large and negative enthalpy change, seem to be a characteristic of the process associated with the formation of elongated (worm-like) micelles, as described in Fig. 4.

Another example of this fine balance resulting in the packing of mixed aggregates leading to sphere-to-rod transition was reported for mixtures of an EO-PO-EO block copolymer and a nonionic surfactant

Table 4

Contributions to thermodynamic parameters of micellization from both headgroup and alkyl chain for zwitterionic surfactants.

Surfactant	Temperature/K	Headgroup			Alkyl Chain			Reference
		ΔG^0_{mic}	ΔH^0_{mic}	$T\Delta S^0_{mic}$	ΔG^0_{mic}	ΔH^0_{mic}	$T\Delta S^0_{mic}$	
SB 3-X[a]	298.15	18.6	25.2	6.6	−2.8	−1.8	1.0	[36]
SB 3-X	298.15	20.3	22.4	2.0	−2.9	−1.6	1.3	[15]
SB 3-X[a]	298.15	16.6	18.0	1.4	−2.6	−1.3	1.3	[50]
$C_n N1C$[a]	298.15	16.9	32.2	15.3	−2.7	−2.3	0.4	[36]
ASB 3-X	298.15	11.4	8.1	2.8	−3.1	−0.9	1.9	[51]
$C_n C6Tri$	298.15	12.7	11.5	−1.2	−1.9	−1.1	0.8	[50]

[a] Values obtained with two data points.

Table 5

Contributions to thermodynamic parameters of micellization from both headgroup and alkyl chain for nonionic surfactants.

Surfactant	Temperature/K	Headgroup			Alkyl chain			Reference
		ΔG^0_{mic}	ΔH^0_{mic}	$T\Delta S^0_{mic}$	ΔG^0_{mic}	ΔH^0_{mic}	$T\Delta S^0_{mic}$	
C_nDPO[a]	298.15	18.1	24.0	6.0	−3.2	−1.3	1.9	[52]
C_nDPO[b]	298.15	17.8	23.6	5.8	−3.1	−1.4	1.8	[52]
C_mG_1	298.15	5.0	16.1	11.1	−3.0	−1.1	1.9	[53]
C_mG_2	298.15	2.6	8.4	5.0	3.0	−1.2	1.8	[53]
C_nEO_6	298.15	2.1	35.3	33.2	−2.9	−2.0	0.9	[54]

[a] Experiments performed in D_2O.
[b] Data considered for n = 10, 11, 12.

[68], whose complex behavior was elucidated by comparing ITC and DSC results, with the aid of scattering techniques. As will be discussed later, this example also reveals that ITC results may convey important kinetic information.

3. Use of ITC for studies on the association of surfactants and polymers

3.1. Interaction with nonionic polymers

Two of the review articles cited in the Introduction section [11,12] describe a tutorial approach on how to conduct ITC experiments to examine the association of surfactants in the presence of polymers, and on how to derive the most important parameters for this interaction. In short, Fig. 5 depicts a typical calorimetric curve for the interaction of an ionic surfactant with a nonionic polymer [72].

This interaction can be assessed in terms of the Gibbs energy difference per surfactant molecule between micelles and the surfactant-induced aggregates, ΔG^0_{PS} as follows:

$$\Delta G^0_{PS} = RTln(cac/cmc) \qquad (9)$$

cac is denoted as the critical aggregation concentration. Above this concentration starts a polymer-induced aggregation, as indicated in Fig. 5.

A result from a molecular dynamics (MD) simulation investigation provides a representative picture on how to understand the polymer effect on the surfactant aggregate, as summarized in Fig. 6 [73]. In this representation, polymer chains — in this case hydrophilic poly (ethylene oxide) (PEO) locate themselves at the micelle surface, reducing the unfavorable contacts between water and the surfactant alkyl chains due to roughness and imperfect surfactant headgroup packing at this surface. This leads to a clear stabilization of the mixed aggregate that can be ascribed to the entropic hydrophobic effect associated with this process.

From Eq. (9) one can derive that larger reduction of aggregation concentration in the presence of polymer (cac) with respect to aggregation in water (cmc) is a consequence of more favorable interaction, as ΔG^0_{PS} becomes more negative. Typically, this interaction becomes more favorable the more hydrophobic the surfactant and the polymer [74]. As for the surfactant, this trend reveals that a more hydrophobic environment is provided at the aggregates formed around (or including) the polymer chains. As for the polymer, this binding process may be visualized as a competition between surfactant and water (solvent) molecules for the polymer chain. More hydrophobic polymers are more resilient to replace hydration molecules by surfactants, hence resulting in a more favorable interaction with surfactants. This picture is supported by the fact that

this interaction is endothermic in the beginning, in agreement with the need for polymer dehydration at low temperatures, but becomes less endothermic as temperature is raised due to a less intense polymer hydration (see, for instance, references [74] and [75]). This endothermic (dehydration) process associated with the beginning of polymer-induced surfactant aggregation must be controlled by entropy, which agrees with findings that water molecules are also restricted in their degrees of freedom in the presence of solvating hydrophilic polymers such as PEO [76,77]. In addition, the presence of the polymer chain among the surfactant headgroups diminish the electrostatic repulsion for ionic surfactants [12]. This is probably the reason for the weak interaction between nonionic surfactants and polymers, which do not display significant polymer-induced aggregation as opposed to that observed for ionic surfactants.

As the surfactant concentration increases, there are two limiting behaviors as revealed by ITC, according to Fig. 7: for more hydrophilic polymers (such as poly (ethylene oxide), PEO, or poly (vinylpyrrolidone), PVP) [75,78] the endothermic process is followed by an exothermic one, while for more hydrophobic polymers (such as poly (propylene oxide), PPO, or poly (N-isopropylacrylamide), PNIPAM) [74,78], this exothermic process does not appear. The fact that the areas under the endo and exo peaks are close, almost canceling each other, which suggests that as surfactant concentration increases, the hydrophilic polymers become more exposed to water, being rehydrated, is consistent with the picture depicted in Fig. 6, while the hydrophobic ones remain less exposed to water. This proposal finds partial support from results derived from Small Angle Neutron Scattering (SANS) measurements, in addition to the MD simulation that led to Fig. 6, but these were only investigated at high surfactant concentration in the experimental case due to the difficulty connected to low concentration regime. The fact that ITC can provide information at such low concentrations reinforces its utility as a very sensitive monitoring technique.

As indicated from this discussion, it is important to emphasize that ITC curves provide more information than just the determination of critical concentrations such as cac, saturation concentration (C_2), but it also offers information on the evolution of the interaction process, which may render important insights on its mechanism. One of these examples was described for the interaction of ionic surfactants with EO-PO-EO block copolymers. ITC results, shown in Fig. 8, clearly indicate that the interaction occurs as a sum of two almost independent processes, as confirmed from the comparison of the ITC results for surfactant addition into a mixture of EO and PO homopolymers of the same chain length as in the block copolymer. The surfactant interaction starts with the more hydrophobic block (PO), as described above is associated with a lower cac value, and then proceeds to the more hydrophilic block (EO).

Table 6

Contributions to thermodynamic parameters of micellization from both headgroup and alkyl chain for anionic surfactants.

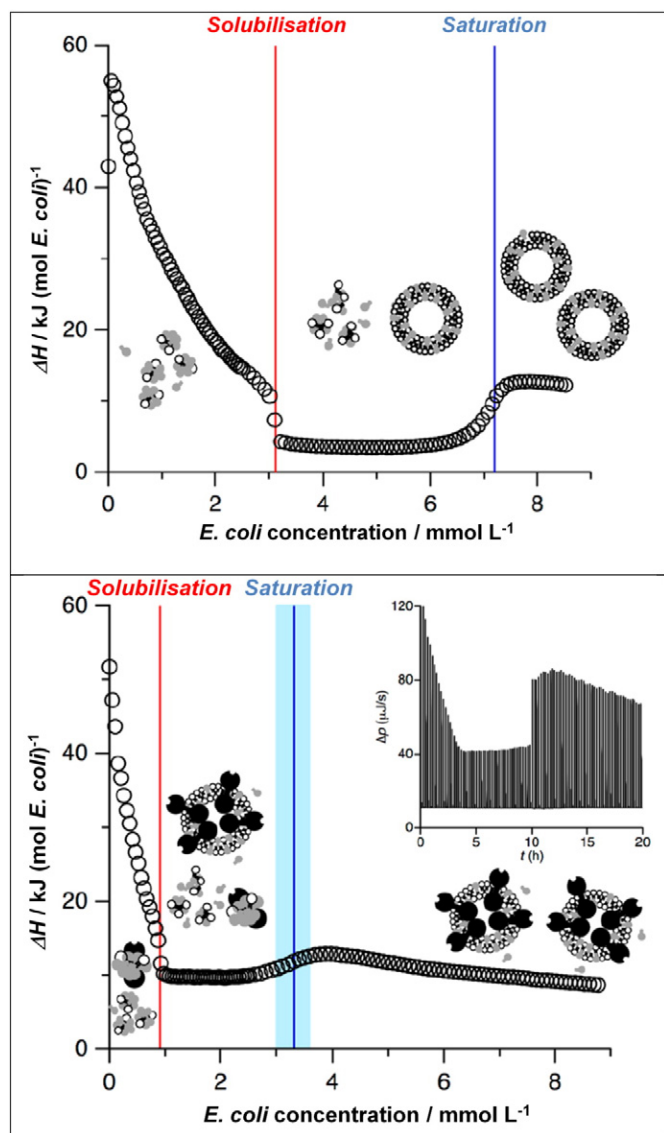| Surfactant	Temperature/K	Headgroup			Alkyl chain			Reference
		ΔG^0_{mic}	ΔH^0_{mic}	$T\Delta S^0_{mic}$	ΔG^0_{mic}	ΔH^0_{mic}	$T\Delta S^0_{mic}$	
SC_nS	308.15	19.1	7.4	−11.6	−3.4	−1.1	2.3	[55]

Fig. 3. Calorimetric titration curves of a mixture containing *E. coli* (50 mM) and octyl-β-D-glucopyranoside (35 mmol L^{-1}) in the absence (top) and in the presence (bottom) of KcsA tetramer (1.5 μmol L^{-1}), at 8 °C. Inset at the bottom depicts the raw data (thermogram) obtained from ITC. The difference in the peaks size at 10 h correspond to a different volume injection.
Adapted from reference [60].

Fig. 4. Process of formation of worm-like micelles (ΔH^0_{WLM}) measured by ITC at 25 °C. The experiment consists in titrating a 14 mmol L^{-1} solution of C$_{14}$TAB into 1.5 mmol L^{-1} solution of 2-hydroxybenzoate.
Adapted from reference [71].

Other features of polymer architecture affecting this interaction have been reported for star-shaped polymers [80] or for polymer with pendant groups [55,81], especially with the latter being hydrophobic, or electrically charged (more important for oppositely charged ones). ITC was also recently used to characterize polymer–surfactant mixtures proposed as nanoreactors to mimic enzyme catalysis [82]. In that study, the presence of surfactant aggregates, an important feature for the proposed kinetic mechanism of phosphates hydrolysis was confirmed from ITC results, as discussed above.

Another important feature that sometimes does not receive enough attention is that ITC can provide kinetic information, as long as the system under evaluation involves processes that are slower than the thermal response of the equipment (or that this instrumental contribution can be accounted for). It is important to stress that the theory behind kinetic analysis depends on the principle under which the equipment works, most commonly heat-flux or power compensation, with the latter more common in the most recent instruments. One example of thermodynamic and kinetic study involving surfactants using a heat-flux instrument was reported by Nilsson et al. [83] on the association of bolaform surfactants with CD. Bolaform surfactants contain two polar

Another case in which the shape of the ITC curves revealed important information is for the interaction of SDS with PEO of different molar masses. First, from ITC results it was clear that there is a minimum PEO polymer molar mass (M around 1500 g mol^{-1}) only above which polymer-induced surfactant aggregation occurs, and this is associated with a *cac* value lower than the surfactant *cmc*, and then endo/exo peaks described above appear (as described in references [72] and [75]). As PEO molar mass increases, there is not much change in the profile of the ITC curves, except for the interval of molar masses around 8000–11,000 g mol^{-1}, for which, as depicted in Fig. 9, two minima are observed, differently from the other curves. This behavior reverts to the one depicted in Fig. 5 at larger molar masses (above 20,000 g mol^{-1}). These two minima were interpreted as the result of two surfactant aggregates being formed around the same PEO chain as a result of electrostatic repulsion (an endothermic process) associated with the aggregate growth. For PEO of longer chains, these aggregates could be formed apart, without mutual interference, hence the undisturbed ITC curve.
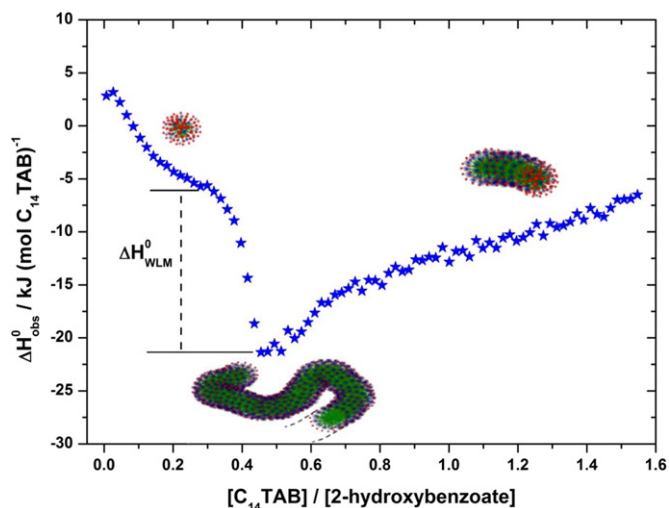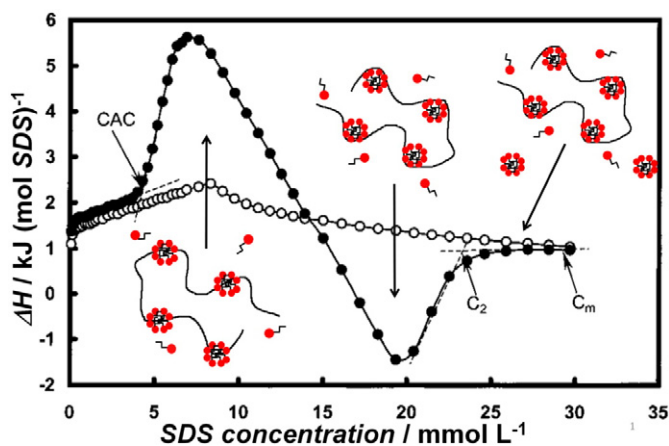

Fig. 5. Titration of a 0.2 mol L^{-1} SDS solution into water (○) and into a 0.1 wt.% PEG solution (●) at 25 °C. The cartoons depict the attributed interactions to different regions.
Adapted from reference [72].
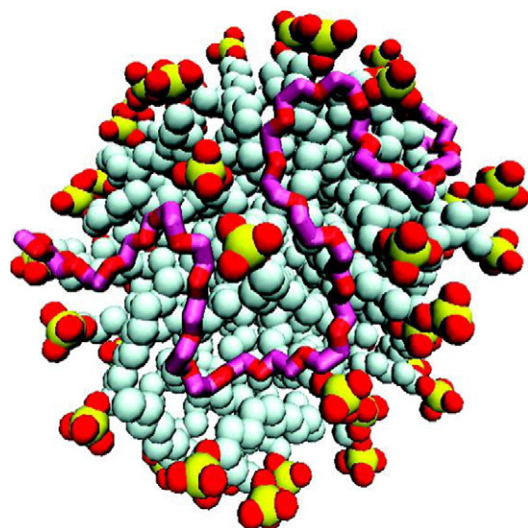
Fig. 6. Interaction between a nonionic polymer PEO and an anionic surfactant SDS at the micelle surface. Water and counterions were omitted for the sake of clarity.
Taken from reference [73].

headgroups connected by one alkyl chain, in this case with bulky trimethylammonium headgroups. This study showed that these surfactants are indeed incorporated into the hydrophobic cavities of CD, and
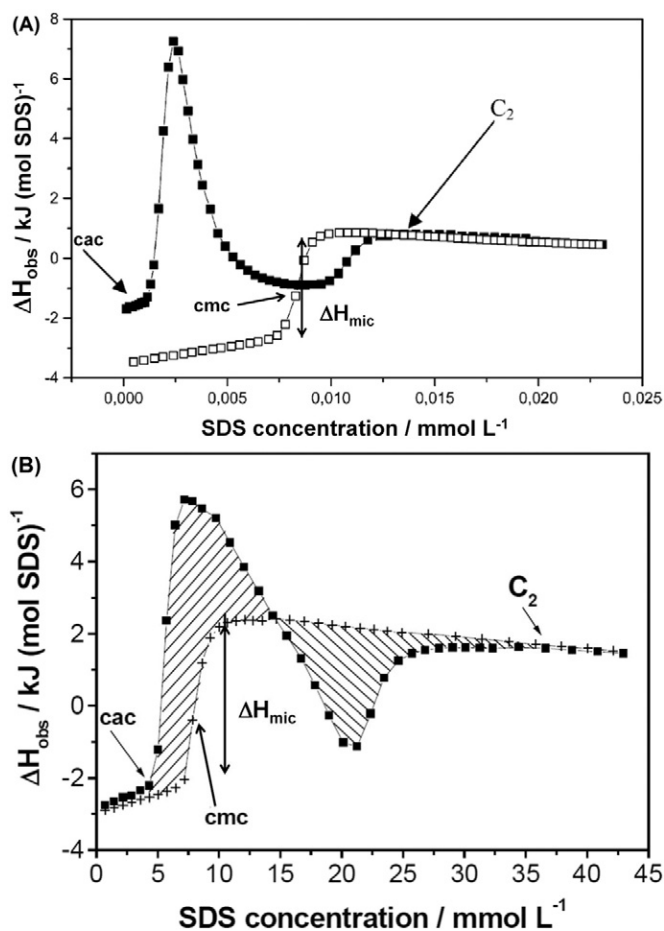
Fig. 7. Interaction between SDS and two different polymer solutions. (A) dilution of SDS into water (□) and into 0.1 wt.% solution of PNIPAM (■), at 17 °C; (B) dilution of SDS into water (+) and into 0.1 wt.% solution of PEO (■), at 15 °C.
Adapted from references [75] and [74].
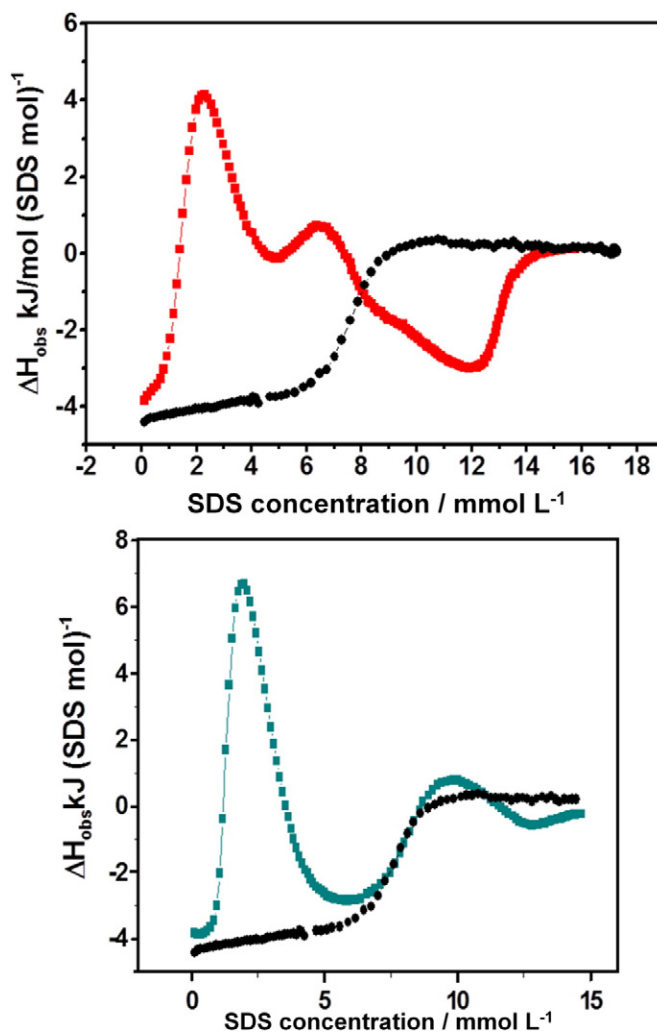
Fig. 8. ITC curves obtained at 25 °C for 10 wt% SDS solution titrated into water (●) and into 0.1 wt% solution of block-copolymer EO_{52}-PO_{35}-EO_{52} (F77) (□) and into a 0.1 wt.% mixture containing PEO 2000 (EO_{52}) and PPO 2000 (PO_{35}) (□).
Adapted from reference [79].

the kinetic of this process is controlled by the slow passage of the bulky surfactant headgroup through the CD cavity, with significant differences between alpha and beta CD (alpha, with the smaller cavity,
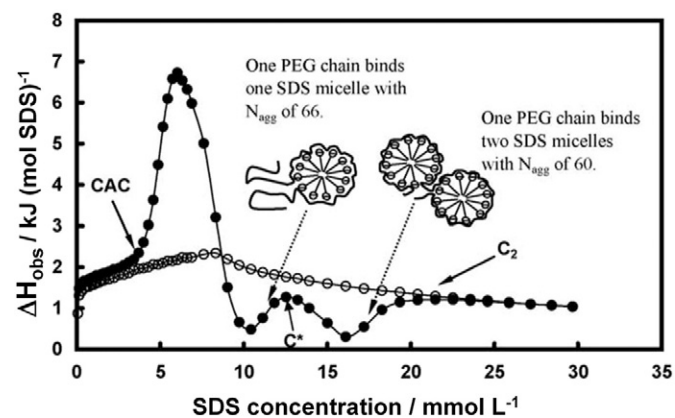
Fig. 9. Calorimetric titration curves obtained for the addition of SDS into water (○) and into 0.1 wt% solution of PEG 7000 (●) at 25 °C. The cartoon shows the two aggregate structures formed at high surfactant concentration.
Adapted from reference [80].

displaying the slower incorporation). This analysis was performed in a quantitative way in order to allow the estimation of rate constants for the association in a simple kinetic model.

Following this line, in using a power-compensation calorimeter, Loh and co-workers [11,79] elucidated a complex combination of shape transitions of block copolymer micellar aggregates from spherical to rod-shaped, induced by the incorporation of a nonionic surfactant. In this case, the phase transition was only qualitatively assessed, but confirmed with use of scattering techniques, and observed to take ca. 30 min to complete after the surfactant incorporation. This transition was only observed within a limited combination of temperature and surfactant/copolymer mole ratios, as revealed by a combination of DSC and ITC measurements. In addition to exemplifying the subtle balance between molecular packing governing aggregate curvature and, consequently, its shape, this example stresses that attention must be paid to the raw calorimetric results because they convey important information also on the kinetics of the processes under study.

3.2. Polyelectrolyte-surfactant systems

In many systems, such as water-borne coatings, personal care products, pharmaceutical incipients, food formulations, and drilling fluids, mixtures of water-soluble polymers and surfactants are commonly found in these formulations [84,85]. As a result, interactions between polymers and surfactant molecules have a large impact on their bulk properties and performance. These mixtures produce many interesting and unique properties, which have attracted significant attention in corporate research laboratories and academic institutions. In most polyelectrolyte-surfactant systems, in addition to short-range hydrophobic interactions, electrostatic forces play a dominant role in the binding interaction between charged macromolecules and ionic surfactants. Association of charged surfactants onto polyelectrolyte chains results in the conformational change of macromolecular chains.

Mixtures of charged surfactants and polyelectrolytes display aggregation properties that are totally different from their individual components in aqueous solution. The interactions depend greatly on the characteristics of the polymer chains and the surfactant molecules. For oppositely charged polymers and surfactants, long range electrostatic attractions between these opposite charged pairs of polymers and surfactants dominate the polymer/surfactant interactions at low surfactant concentrations resulting in phase separation at the isoelectric point (IEP) [85]. When all the charged groups are neutralized, hydrophobic interaction begins to dominate resulting in the structural reorganization at high surfactant concentration.

Many techniques have been used to study the interactions between polyelectrolyte and surfactant, such as surface tension, turbidity, light scattering, electromotive force, conductometry, and calorimetry. For example, Harada and Nozakura used turbidity and microscopy to elucidate the interaction of polyelectrolytes and ionic surfactants [86]. By mixing solutions of poly (vinyl sulfate) (PVS) and hexadecyltrimethylammonium bromide ($C_{16}TAB$), the turbidity exhibited a sharp maximum at the mole ratio of 1:1, indicating quantitative binding between PVS and $C_{16}TAB$. Electron micrographs revealed a multilayer structure, and a single strand structure at the mole ratio of PVS:$C_{16}TAB$ of 2:1 and 1:1 respectively. In addition, computer simulation has been used to understand the binding of polyelectrolyte and surfactants. Using MD simulation, Shang and co-workers [87] examined the effects of hydrophilicity or hydrophobicity of the polyelectrolyte chains on their interaction with oppositely charged surfactants. They observed that the interaction between surfactants and hydrophilic polyelectrolytes is significantly different from hydrophobic polyelectrolyte. In the hydrophilic polyelectrolyte system, the complex evolve from "bottle brush" to "necklace" and, finally to rod-like micelle wrapped with polyelectrolyte chains as the surfactant concentration is increased. For hydrophobic polyelectrolytes, with increasing surfactant concentration, spherical micelle is initially formed with the polyelectrolyte chains penetrating into the hydrophobic core of the micellar complexes.
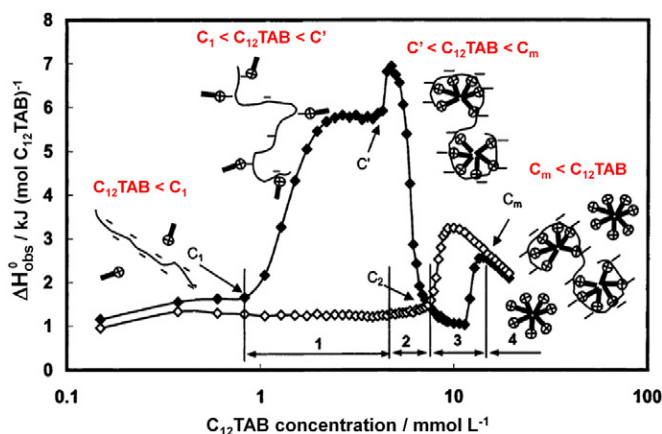

Fig. 10. Classification of binding regimes and schematic binding mechanism of the PA/$C_{12}TAB$ system: (■) binding isotherm in 0.1 mol L^{-1} NaCl solution; (■) dilution curve in 0.1 mol L^{-1} NaCl solution.
Adapted from reference [88].

Recently, Wang and Tam used ITC to study the binding interactions between $C_{12}TAB$ and anionic polymers (neutralized poly (acrylic acid) (PAA) and methacrylic acid/ethyl acrylate (MAA/EA) copolymers [88–90]. At low $C_{12}TAB$ concentration, the cationic headgroups of surfactant bind electrostatically to the anionic carboxylate groups on the polymer chains (Fig. 10). At a surfactant concentration of C′, micellization of polymer-bound surfactant occurs to produce insoluble polymer/surfactant complexes. Thermodynamic analyses suggest that the electrostatic binding is an endothermic process driven by a positive entropy value that is related to the recovery of translational entropy of released counterions by the bound surfactant. In increasing salt conditions, screening of the electrostatic repulsion weakens the binding of surfactant onto the polymers, which favors the formation of free micelles.

The interaction of a hydrophobically modified polyelectrolyte (D40OCT30) and oppositely charged surfactants n-alkyl sodium sulfates (SC_nS) in aqueous solution was studied by ITC [55,80]. A dextran polymer having 28.1% pendant N-(2-hydroxypropyl)-N,N-dimethyl-N-octylammonium chloride groups distributed along its backbone was complexed with anionic surfactants comprising of sodium octyl sulfate (SC_8S) and sodium tetradecyl sulfate ($SC_{14}S$). The complexation is controlled by electrostatic and hydrophobic forces, and the strength of association is proportional to the length of the alkyl chains of the surfactant hydrophobes.

The binding interactions between polysaccharides (methylcellulose (MC), chitosan (CS), and κ-Carrageenan (KC) corresponding to neutral and positively, and negatively charged polysaccharides, respectively) with SDS and $C_{16}TAB$ were examined [91]. Polymer–surfactant combinations, such as MC–SDS, MC–$C_{16}TAB$, CS–SDS, CS–$C_{16}TAB$, KC–SDS, and KC–$C_{16}TAB$ were evaluated using ITC. MC–SDS displayed strong hydrophobic and weak ion–dipole interactions, while KC–SDS exhibited weaker hydrophobic interaction compared to MC–SDS. CS–SDS displayed strong ionic interaction and moderate hydrophobic interaction. Similar interactions were also observed for $C_{16}TAB$ surfactant.

McClements and co-workers reported on the binding interactions between a highly potent food-grade antimicrobial lauric arginate (LAE) and cationic surfactant with an anionic biopolymer (high methoxyl pectin, HMP) [92,93]. ITC measurements revealed the binding of LAE to pectin resulting in either soluble or insoluble complexes, depending on solution composition as determined by turbidity measurements. The LAE–pectin binding contribution interaction is exothermic, driven by the electrostatic attraction between the cationic surfactant and anionic biopolymer.

The binding interactions are divided into 4 regions as shown in Fig. 11. In "**A**", the binding enthalpy between LAE and pectin is exothermic,
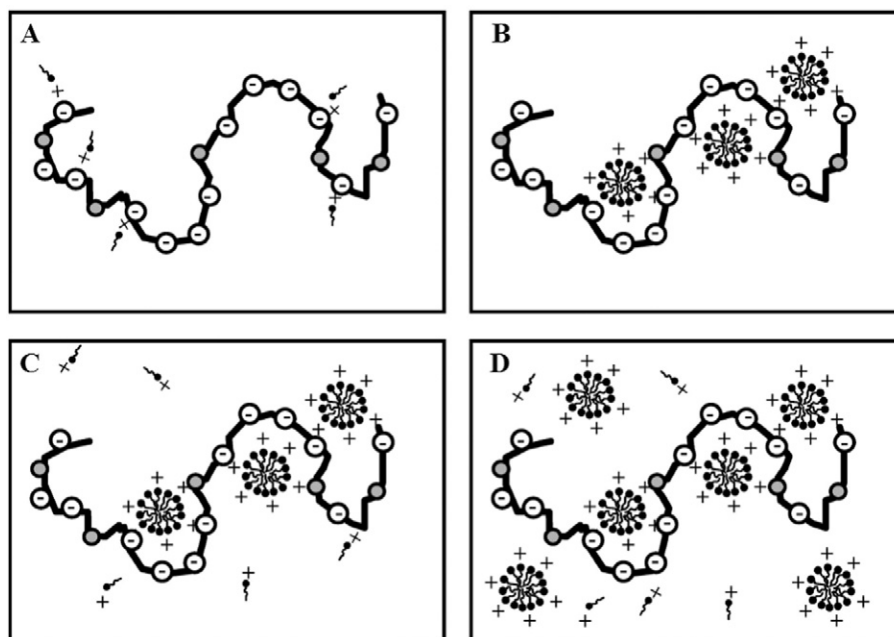
Fig. 11. Schematic representation of the interaction between cationic LAE and anionic pectin.
Adapted from reference [92].

where the positive head groups of LAE molecules are bound to negative carboxylic acid groups on the pectin molecules via electrostatic attraction. In "**B**", micelle-like surfactant clusters are formed on the polymer to shield the hydrophobic LAE tails from water. It was observed that the surfactant binding capacity to pectin ($=C_{micelle}/C_{pectin}$) is about 1.3 g of surfactant per 1 g of pectin. In "**C**", pectin chains are saturated with LAE micelles, and any additional LAE micelles titrated to the reaction cell will dissociate into monomers as the free surfactant concentration is below the *cmc*. In "**D**", where the surfactant concentration is above the *cmc*, any additional LAE micelles titrated into the reaction cell remain as micelles resulting in negligible heat produced. They have also studied the interactions between chitosan and an anionic surfactant [94], and Yang et al. [95] reported the binding of SDS to sodium alginate in dilute solution, where binding interactions were observed at low pH.

Wyn-Jones and co-workers have published results from several studies on the interactions between various types of polyelectrolytes such as PVP and poly (ethyleneimines) (PEI), and surfactant molecules [96–101]. Using a combination of electromotive force and ITC, the interactions between surfactants and various polyelectrolyte systems were elucidated. The effect of pH, surfactant types, surfactant alkyl chain length and the polymer characteristics were examined. The typical phase transformation comprises of complex formation resulting in phase separation and resolubilisation with increasing amounts of surfactant added. It was observed that the number of surfactant molecules bound per mole of polymer is independent of pH. Further studies on the binding interactions between linear and branched PEIs with SDS was reported by Yan and co-workers [102]. The pH-dependent interactions between polyampholytes and SDS were examined by Koetz and co-workers [103], where a rather complex interaction mechanism consisting of non-cooperative, electrostatic and cooperative hydrophobic interactions were identified.

Extension of the study to gemini surfactants and hydrophobically modified poly (acrylamides) (PAM) revealed stronger binding interaction for the gemini compared to single-chain surfactants [104]. Wang and co-workers [105] used ITC, turbidity, and steady-state fluorescence measurements to study the interaction of cationic ammonium gemini surfactant ($C_{12}C_6C_{12}Br_2$) and $C_{12}TAB$ with anionic PSS and poly (sodium acrylate) (PA). Significant binding was observed, where the gemini surfactant possessed stronger interactions with PSS and PA.

Wang and Tam examined the interaction between a monodispersed PAA ($M_w = 5670$ g mol^{-1}, $M_w/M_n = 1.02$) and SDS using ITC, ISE, and dynamic light scattering (DLS) measurements [106]. Using the ITC technique, the interaction between SDS and PAA at a degree of neutralization α of PAA lower than 0.2 was observed for the first time (Fig. 12). The dodecyl chains of SDS cooperatively bind to apolar segments of PAA driven by hydrophobic interaction, which is both enthalpy and entropy driven (ΔH is negative but ΔS is positive). The onset of binding (i.e., *cac*) is ~2.4 mmol L^{-1} and the C_2 is ~13.3 mmol L^{-1} at $\alpha = 0$. As the carboxylic acid functional groups are deprotonated with increasing α, the binding is hindered by strong electrostatic repulsion between negatively charged SDS and PAA chains. At low α, mixed micelles are formed on uncharged PAA chains that expand and dissociate into single PAA chains, stabilized by bound SDS micelles in solution.
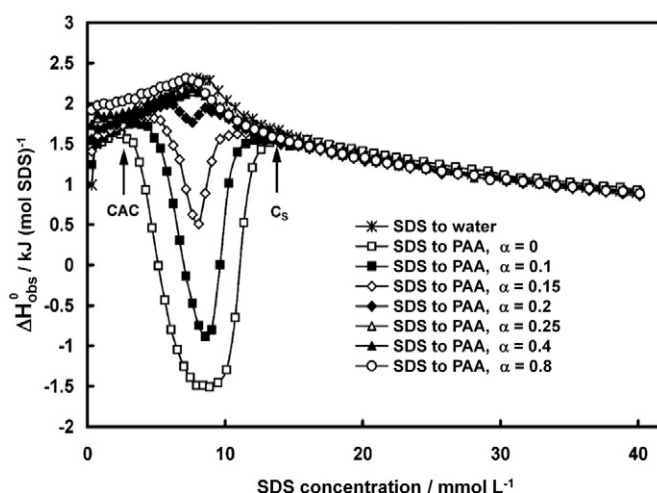

Fig. 12. Differential enthalpy curves for titrating 200 mmol L^{-1} SDS into 0.05 wt.% solutions of PAA at different α values.
Adapted from reference [106].

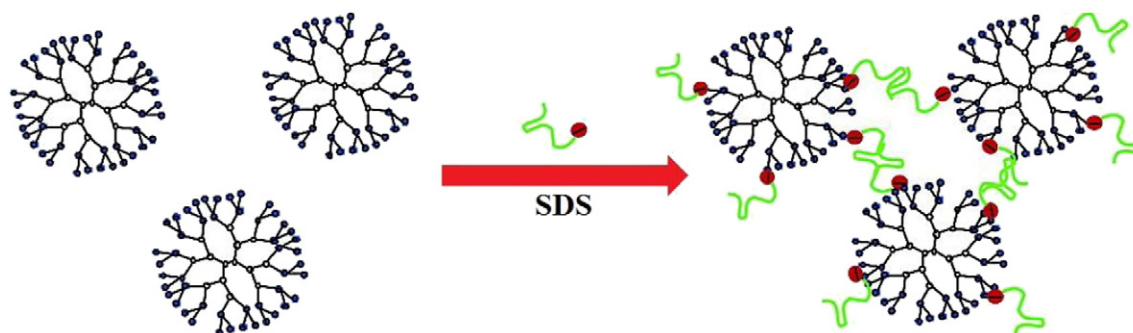W. Loh et al. / Biochimica et Biophysica Acta 1860 (2016) 999–1016

Fig. 13. Schematic showing the binding and complexation of SDS and amine terminated dendrimers.
Adapted from reference [110].

Wyn-Jones and workers first reported the interaction of surfactants and dendrimers using various physical techniques, including ITC [107]. Tam and co-workers [108,109] used both ITC and DLS to elucidate the spontaneous supramolecular complexation between an amine and hydroxyl terminated PAMAM dendrimers (G3[EDA] PAMAM-NH$_2$, G3[EDA] PAMAM-OH) and SDS (Fig. 13). At low pH, SDS molecules bound electrostatically to protonated amines on the surface of G3[EDA] PAMAM-NH$_2$ that led to the formation of PAMAM/SDS supramolecular complex via hydrophobic association of surface bound SDS molecules on the dendrimers. The size of the complex increased progressively with SDS concentration and precipitation occurred when the SDS concentration exceeded 15 mmol L^{-1}. At high pH, the primary amines are deprotonated and the electrostatic binding ceased. The stability of the dendrimer/surfactant complexes can be enhanced by the grafting of EO chains on the surface of the dendrimers [110].

Biological polyelectrolytes such as proteins and DNA constitute another important set of examples in which ITC has been used to follow their interaction with surfactants. Moulik and co-workers [111] had studied the interaction of C$_{16}$TAB and SDS with various polyelectrolytes, such as gelatin (Gn), lysozyme (Lz) and DNA using ITC. The polymer-induced aggregation consisting of binding of surfactant molecules to the polymer chain, and subsequent reorganization of bound aggregates. The group of Westh [112,113] allied ITC and spectroscopic techniques to study interaction of SDS with proteins and glycoproteins. By using a simple partitioning assumption, their ITC data allowed estimates of binding isotherms that were interpreted to derive a comprehensive view of the binding processes. Wettig et al. [114] used ITC and scattering techniques to compare the interaction of gemini surfactants with their similar ones containing pyrenyl units with DNA. Their results showed that the possibility of pyrene intercalation into DNA changes completely their mechanism of interaction. As a final example on this issue, there is a recent report by Tanaka and co-workers [115] in which ITC was one of the many techniques used to confirm a lipid triggered protein metamorphosis into a haemolytic transmembrane pore.

Models to account for ITC binding curves to produce thermodynamic and, sometimes, structural information from the calorimetric results are very important, and constitute an area with significant latest developments. Lapitsky and co-workers [116] used both surfactant ion-specific electrodes (ISE) and ITC to examine the interactions between two surfactant/polyelectrolyte mixtures: (**A**) sodium perfluorooctanoate (FC7) and N,N,N-trimethylammonium derivatized hydroxyethyl cellulose (UCARE Polymer JR-400), and (**B**) C$_{12}$TAB and poly (sodium 4-styrenesulfonate) (PSS). Cooperative surfactant adsorption onto the polyelectrolyte chains was observed, and fitting of the calorimetric data revealed that mixture **A** followed the two-binding-state Satake–Yang adsorption model, while mixture **B** deviates dramatically from the Satake–Yang model. Based on the calorimetric results, a physical mechanism describing the binding interactions is proposed (Fig. 14). At low surfactant concentration, a plateau corresponding uncooperative binding occurs prior to the *cac* (see Fig. 14). The peak corresponds to the stronger binding driven by

favorable hydrophobic interactions between cooperatively bound surfactant molecules and the polyelectrolyte chains. At high surfactant concentration, the enthalpy approaches zero when the polyelectrolyte chains become saturated and no further binding occurs.

It has been reported that some ITC curves for the binding between oppositely charged surfactants and polymers display a bump superimposed to the typical sigmoidal binding curve, as represented in Fig. 15 for the interaction of a cationic polymer with polyacrylate. More recently, it was confirmed that this is a more general behavior observed in other binding processes involving oppositely charged colloids such as polyelectrolytes [117] or nanoparticles [118]. Vitorazi and co-workers [117] proposed that this bump is associated with a second process, referred to as coacervation, that follows the electrostatic binding, occurring close to charge neutralization, which involves the rearrangement of these colloidal objects (for surfactants these will be their micelles) to maximize contacts of their opposite charges. Moreover, they have shown that the ITC curves could be deconvoluted to allow for independent analyses of the two processes (binding + rearrangement), and confirmed that this process is strongly dependent on the polyelectrolyte molar mass, for instance, confirming its kinetic nature.

Recently, Chiappisi and co-workers [119] reported on an improved and thermodynamically consistent analysis of ITC data for surfactants binding to polymers, and they validated their analysis according to the Satake–Yang model. This approach can be used and adapted to analyze most thermodynamic data related to polymer–surfactant interactions, with the advantage of taking into account the surfactant association
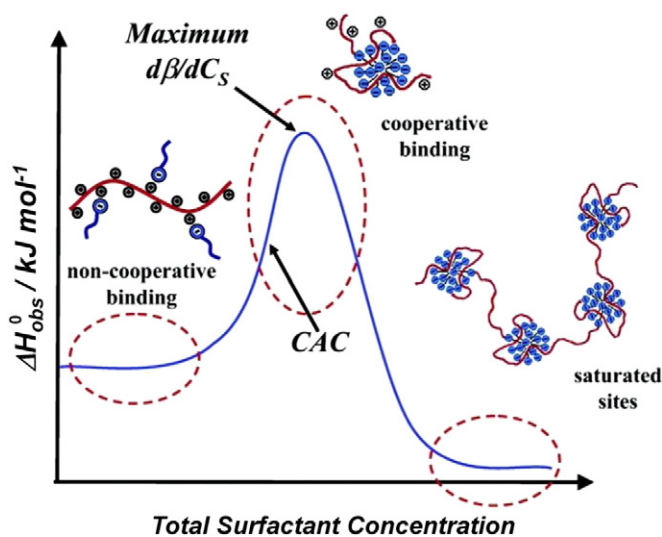

Fig. 14. Schematic representation of the ITC curve obtained from a generic surfactant/polyelectrolyte binding process.
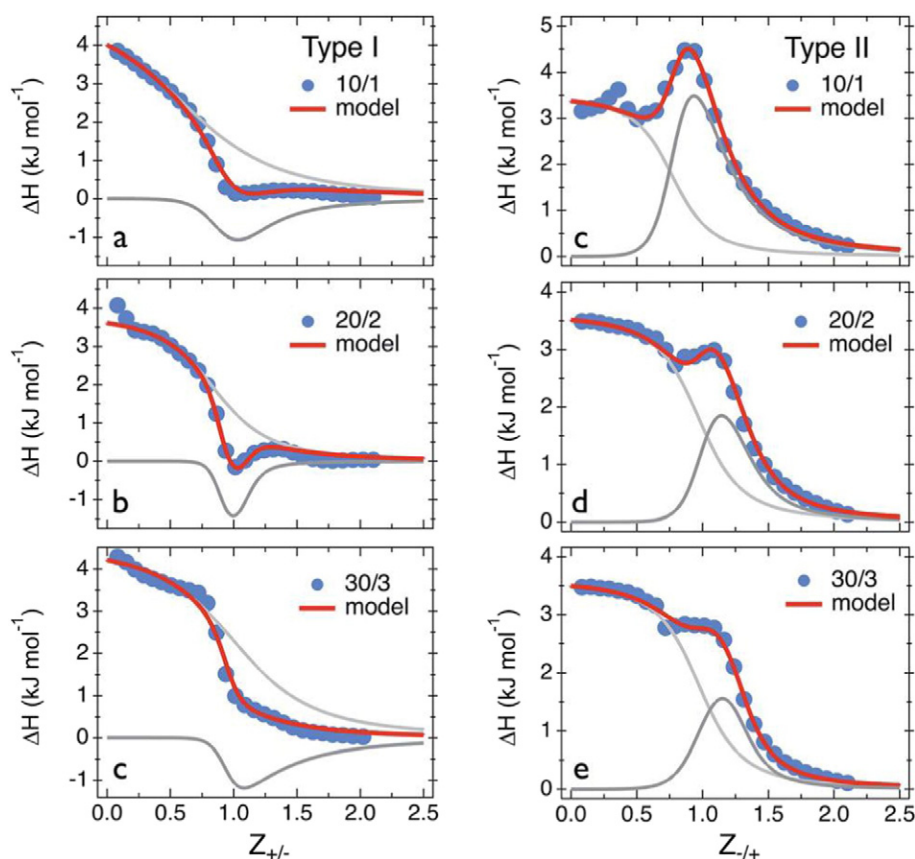Adapted from reference [116].

Fig. 15. ITC results for the titration of: (Type I) a cationic poly (diallyldimethylammonium chloride) PDADMAC into anionic PA; (Type II) PA into PDADMAC. (●) ITC data, (—) total enthalpy, (—) primary process, (—) secondary process.
Adapted from reference [117].

that follows its binding to the polymer. Another recent proposal for modeling binding from ITC data was reported by Herrera and Winnik [120]. This is more general differential binding model, which includes Wiseman isotherms [121], and that could be applied to a variety of processes, possibly including surfactant binding.

We would also like to point to a recent publication by Pethica [122], which alerts to possible misuses of ITC data due to inappropriate thermodynamic simplifications sometimes used to account for biological molecules that will render wrong interpretation.

4. Colloids-surfactant systems

Surfactants are very important in the preparation stability of colloidal particles because they can produce particles of different sizes and shapes, hence with varied chemical properties [123]. Moreover, the kinetic stability of these nanoparticles aqueous dispersions may be determined by their surfactant coverage and, in the case of biomaterials, they can also influence the fate of these particles in living bodies [124]. For some of these processes, the control of nanoparticles properties may require the detailed knowledge on aspects such as the mode of packing of the surfactant layer [125]. Surfactant binding to and associating at nanoparticles surface may be viewed as a combination of the two processes discussed earlier in this review, with many similarities to polymer-induced surfactant aggregation [126].

Using SAXS, Chu and co-workers examined the phase transition of slightly cross-linked positively charged gels of PDADMAC when SC_nS (n = 8,9,10,11 and 12) were added to the aqueous solution [127]. The polyelectrolyte–surfactant complexes existed as crystalline nanostructures, which melted at higher temperatures (62 and ~70 °C for PDADMAC–$SC_{10}S$ and PDADMAC–SC_9S complexes, respectively).

These crystalline structures were produced via a combination of electrostatic and hydrophobic interactions.

Interactions of block copolymers with oppositely charged surfactants display similar trends. Uchman and co-workers [128] presented a nice example of a combined investigation that allied ITC to other techniques for a comprehensive thermodynamic, kinetic and structural investigation of dispersions with liquid-crystalline cores.

Hydrophobically modified alkali-soluble emulsions (HASE) latex exists as a milky dispersion at low pH, but it becomes transparent with the addition of SDS [129]. Fig. 16 (inset) shows the dependence of the
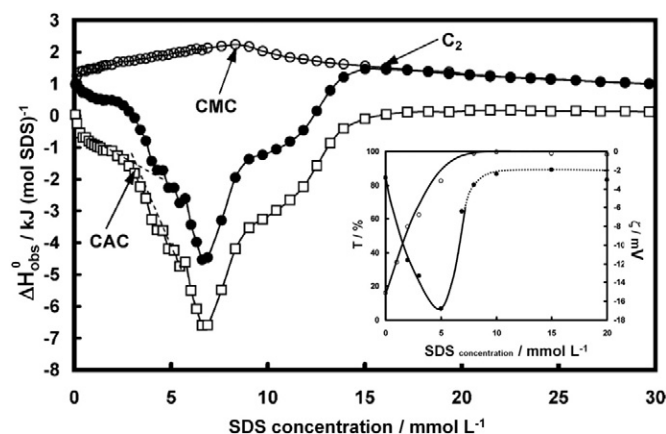

Fig. 16. ITC curves for titration of 0.2 mmol L^{-1} SDS into water (○) and 0.1 wt.% HASE (●) at 25 °C and 1 atm. The open square (□) is the difference curve between SDS into HASE latex and that into water.
Adapted from reference [129].

transmittance of HASE latex on SDS concentration, where it approaches a maximum transmittance when the SDS concentration exceeds 5 mmol L^{-1} SDS. The binding of SDS molecules onto HASE latex dissociates the polymer chains within the HASE latex.

The interaction between SDS and HASE latex can be observed from the differential enthalpy curve for the titrations of SDS into HASE latex. The binding of SDS molecules on the HASE latex is exothermic, which is attributed to the hydrophobic interaction between SDS and HASE latex. In addition, it may also include the contribution from hydrogen bonding. A sharp transition occurs at ~4 mmol L^{-1} SDS, which corresponds to the *cac* of the SDS/HASE latex system, while at ~15 mmol L^{-1} SDS, the polymer–surfactant interaction ceases, as defined by C_2. The ITC results indicate that the interaction between SDS and HASE latex is dominated by the solubilization of HASE latex into the SDS mixed micellar core.

Due to the fact that SDS is an anionic surfactant, the binding process is accompanied by surface charge fluctuations, which is defined by the dependence of ζ-potential on SDS concentration as described by the inset in Fig. 16. Pure HASE latex possesses a slightly negative charge (-3.0 mV). When anionic surfactant SDS was added, the surface of the latex becomes more negative, and this is related to the non-cooperatively binding of SDS monomers onto the HASE latex. The ζ-potential exhibits a minimum of -18 mV at ~5 mmol L^{-1} SDS. When the SDS concentration exceeds ~5 mmol L^{-1}, the HASE containing SDS mixed micelles are cooperatively formed in solution, which solubilizes the HASE latex into the hydrophobic micellar core. During the latex-induced micellization process, the accompanying counterion condensation could give rise to a reduction in the total surface charge and a corresponding increase in the ζ-potential. In addition, increasing the salt concentration not only decreases the thickness of the double layer but also decreases the ζ-potential, which also contributes to the increase in ζ-potential at higher SDS concentration. Beyond SDS concentration of 8 mmol L^{-1}, both the double-layer and latex structure HASE have been fully destroyed, and thus reliability of the ζ-potential value decreases, approaching zero at large SDS concentration.

Another example on the use of ITC to follow surfactant binding to polymeric particles was reported by Lamberger and Landfester [130] who used latexes of different properties and, combining ITC and surface tension measurements, derived a comprehensive picture on how the latexes surface properties affect their interaction with SDS stressing the capacity of calorimetric studies to provide insights into interaction mechanisms.

Interaction of surfactant with other colloidal objects such as cellulose nanocrystals (CNC) was also reported. These are anisometric nanoparticles with dimensions in the range of tens to a few hundred nanometers [131–133] that, depending of their extraction procedures, may bear interfacial carboxylic, sulfate or phosphoric groups rendering negative charges that stabilize their dispersions in water [134–136]. Due to their interesting physico-chemical properties and renewable nature, CNC has gained increasing interest for many applications that involve reinforcement of composites, rheological modifiers, water purification or for actives controlled delivery [137–140]. In some
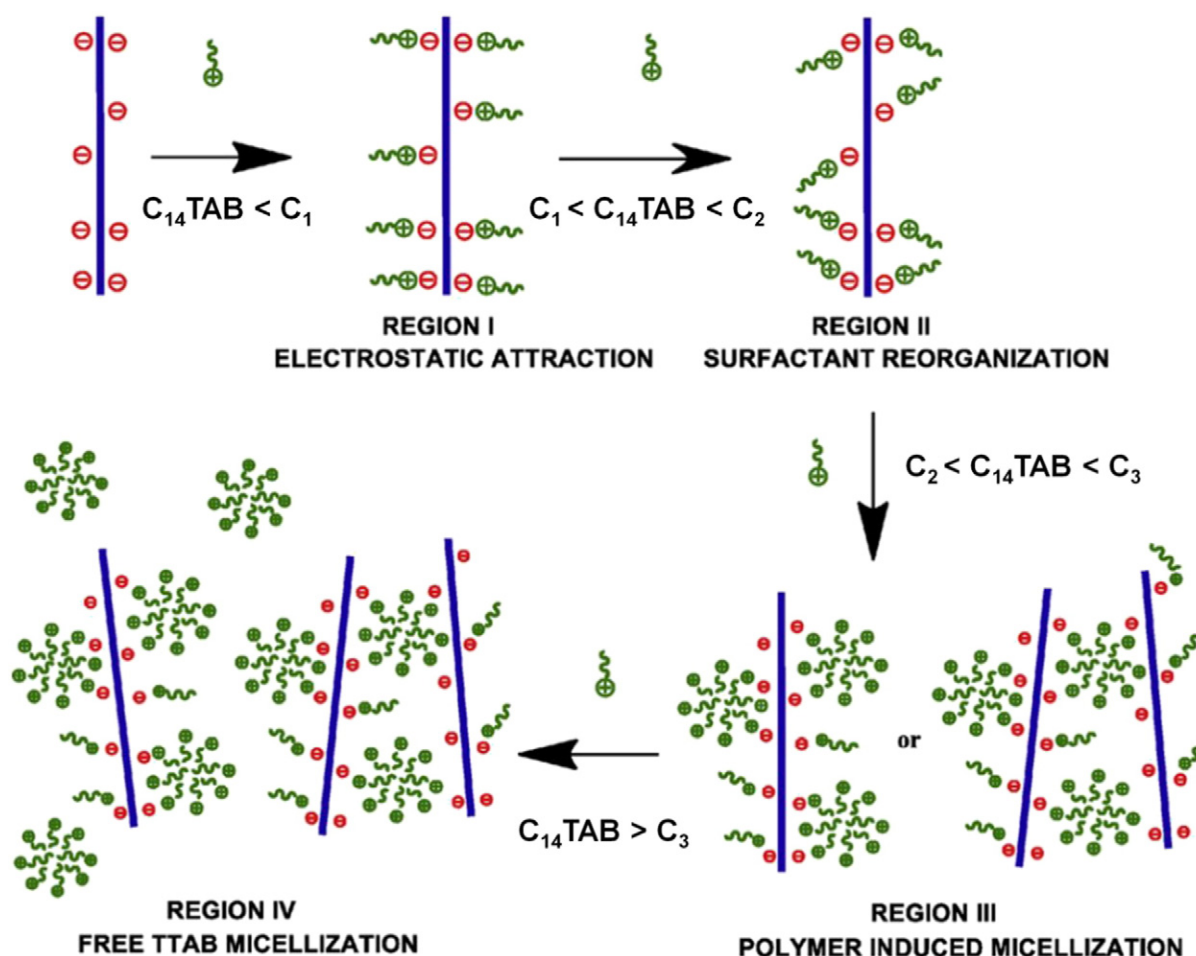

Fig. 17. Interaction mechanism between C_{14}TAB and CNC mixtures derived from ITC data. Adapted from reference [142].

cases, such as cosmetic or pharmaceutical formulations, these colloidal objects may be formulated with surfactants, especially cationic ones, which may alter significantly their colloidal properties. Dhar et al. [141] reported a study on the interaction of $C_{14}TAB$ with sulfated CNC, using ITC, surface tension and light scattering techniques to propose a mechanism for the complex association process (see Fig. 17) in which the surfactant first binds electrostatically to the CNC surface and, as surfactant concentration increases, they aggregate and, eventually, provide means for physical cross-linking between these particles forming flocs. Recently [142], this study was extended to shorter/less hydrophobic (C_{12}) and longer/more hydrophobic (C_{16}) cationic surfactant homologues, again using ITC in combination with light scattering measurements. The less hydrophobic surfactant binds to CNC and forms a monolayer, while for the more hydrophobic surfactant the initial electrostatic binding is overlapped with hydrophobic surface-induced aggregation, as indicated by their different ITC profiles.

5. Conclusions and perspectives

In this review we tried to summarize examples of the most important applications of ITC to investigate association of surfactants involving colloidal systems. The presented survey confirms that ITC is expanding its use for study of surfactant association (micellization and other further shape transitions) and, most importantly, for the most complex association processes that involve polymers (in many cases biomolecules such as proteins or nucleic acids) or colloidal particles. This involves expansion of ITC use to new colloidal systems (such as the field of metallic nanoparticles), and in models to interpret the calorimetric results. From the pass of publications in these directions it is also clear that a new reviewing update will be needed soon.

We hope to have made clear that in many cases the use of ITC is not only convenient, but it is an indispensible tool to obtain an accurate description of the processes under investigation, especially when aiming at the determination of thermodynamic properties associated with aggregation processes. Based on the reports reviewed above and on the results presented it seems clear that direct calorimetric determination of enthalpy values, mostly via ITC, is necessary and this research field has reached a maturity level in which other less accurate approaches should be avoided, including indirect van't Hoff estimates. ITC is now widespread and a little effort from researchers should be enough to achieve access to calorimetric measurements for this purpose.

Another point that we tried to stress with this review relates to the benefits of using ancillary techniques to clearly identify the nature of the processes identified by calorimetry. The use of analytical techniques such as selective electrodes to monitor surfactant monomer concentrations, or structural techniques such as light or X-ray scattering ones, among others, is necessary to provide a full description of the process under investigation. It is very frustrating to read a report pointing out to what seems an interesting phenomenon detected by calorimetric techniques, without an extra effort attempting to fully describe it. In this sense, the high sensitivity of calorimetric techniques can be complemented by additional information overcoming the unspecific nature of heat exchange to provide detailed molecular information on the process under scrutiny.

We would like to invite our research colleagues in this field to reflect about these two proposals, either in our roles as authors, reviewers or editors for scientific publications because we feel that great improvement can be achieved with respect to our publication standards that will certainly help advancing our understanding of these usually complex colloidal systems.

Transparency document

The Transparency document associated with this article can be found, in the online version.

References

[1] W. Loh, C. Brinatti, Calorimetry Is Not Color-Blind Molecular Insights on Association Processes in Surfactant-Polymer Mixtures Derived from Calorimetric Experiments, Sci. China: Chem. 54 (12) (2011) 2024–2027.

[2] J.P.E. Grolier, J.M. Del Río, Isothermal Titration Calorimetry: A Thermodynamic Interpretation of Measurements, J. Chem. Thermodyn. 55 (2012) 193–202.

[3] S.J. Gill, S.F. Dec, G. Olofsson, I. Wadsö, Anomalous Heat Capacity of Hydrophobic Solvation, J. Phys. Chem. 89 (23) (1985) 3758–3761.

[4] P.L Privalov, Thermodynamic Problems in Structural Molecular Biology, Pure Appl. Chem. 79 (8) (2007) 1445–1462.

[5] P.D. Galgano, O.A. El Seoud, Surface Active Ionic Liquids: Study of the Micellar Properties of 1-(1-Alkyl)-3-Methylimidazolium Chlorides and Comparison with Structurally Related Surfactants, J. Colloid Interface Sci. 361 (1) (2011) 186–194.

[6] S. Shimizu, P.A.R. Pires, O.A. El Seoud, Thermodynamics of Micellization of benzyl(2-Acylaminoethyl)dimethylammonium Chloride Surfactants in Aqueous Solutions: A Conductivity and Titration Calorimetry Study, Langmuir 20 (22) (2004) 9551–9559.

[7] P.D. Galgano, O.A. El Seoud, Micellar Properties of Surface Active Ionic Liquids: A Comparison of 1-Hexadecyl-3-Methylimidazolium Chloride with Structurally Related Cationic Surfactants, J. Colloid Interface Sci. 345 (1) (2010) 1–11.

[8] P.R. Majhi, S.P. Moulik, Energetics of Micellization: Reassessment by a High-Sensitivity Titration Microcalorimeter, Langmuir 14 (15) (1998) 3986–3990.

[9] S.P. Moulik, D. Mitra, Amphiphile Self-Aggregation: An Attempt to Reconcile the Agreement-Disagreement between the Enthalpies of Micellization Determined by the Van't Hoff and Calorimetry Methods, J. Colloid Interface Sci. 337 (2) (2009) 569–578.

[10] A.E. Beezer, R.J. Miles, B.F. Perry, Transfer Thermodynamics, in: A.M. James (Ed.), Thermal and Energetic Studies of Cellular Biological Systems, Wright: Bristol 1987, pp. 167–181.

[11] G. Olofsson, W. Loh, On the Use of Titration Calorimetry to Study the Association of Surfactants in Aqueous Solutions, J. Braz. Chem. Soc. 20 (4) (2009) 577–593.

[12] K.C. Tam, E. Wyn-Jones, Insights on Polymer Surfactant Complex Structures during the Binding of Surfactants to Polymers as Measured by Equilibrium and Structural Techniques, Chem. Soc. Rev. 35 (8) (2006) 693–709.

[13] K. Bouchemal, New Challenges for Pharmaceutical Formulations and Drug Delivery Systems Characterization Using Isothermal Titration Calorimetry, Drug Discov. Today 13 (21) (2008) 960–972.

[14] L. Chiappisi, M. Gradzielski, Co-Assembly in Chitosan–surfactant Mixtures: Thermodynamics, Structures, Interfacial Properties and Applications, Adv. Colloid Interface Sci. 220 (2015) 92–107.

[15] C. Brinatti, L.B. Mello, W. Loh, Thermodynamic Study of the Micellization of Zwitterionic Surfactants and Their Interaction with Polymers in Water by Isothermal Titration Calorimetry, Langmuir 30 (21) (2014) 6002–6010.

[16] T.H. Scheuermann, C.A. Brautigam, High-Precision Automated Integration of Multiple Isothermal Titration Calorimetric Thermograms: New Features of NITPIC, Methods 76 (2015) 87–98.

[17] C.A. Brautigam, Fitting Two- and Three-Site Binding Models to Isothermal Titration Calorimetric Data, Methods 76 (2015) 124–136.

[18] S. Keller, C. Vargas, H. Zhao, G. Piszczek, C.A. Brautigam, P. Schuck, High-Precision Isothermal Titration Calorimetry with Automated Peak-Shape Analysis, Anal. Chem. 84 (11) (2012) 5066–5073.

[19] A. Chatterjee, S.P. Moulik, S.K. Sanyal, B.K. Mishra, P.M. Puri, Thermodynamics of Micelle Formation of Ionic Surfactants: A Critical Assessment for Sodium Dodecyl Sulfate, Cetyl Pyridinium Chloride and Dioctyl Sulfosuccinate (Na Salt) by Microcalorimetric, Conductometric, and Tensiometric Measurements, J. Phys. Chem. B 105 (51) (2001) 12823–12831.

[20] N.M. van Os, G.J. Daane, G. Haandrikman, The Effect of Chemical Structure upon the Thermodynamics of Micellization of Model Alkylarenesulfonates: III. Determination of the Critical Micelle Concentration and the Enthalpy of Demicellization by Means of Microcalorimetry and a Comparison with the Phase Separation Model, J. Colloid Interface Sci. 141 (1) (1991) 199–217.

[21] P. Garidel, A. Hildebrand, R. Neubert, A. Blume, Thermodynamic Characterization of Bile Salt Aggregation as a Function of Temperature and Ionic Strenght Using Isothermal Titration Calorimetry, Langmuir 16 (12) (2000) 5267–5275.

[22] P. Garidel, A. Hildebrand, Thermodynamic Properties of Association Colloids, J. Therm. Anal. Calorim. 82 (2) (2005) 483–489.

[23] S. Paula, W. Süs, J. Tuchtenhagen, A. Blume, Thermodynamics of Micelle Formation as a Function of Temperature: A High Sensitivity Titration Calorimetry Study, J. Phys. Chem-US 99 (30) (1995) 11742–11751.

[24] N.E. Olesen, P. Westh, R. Holm, Determination of Thermodynamic Potentials and the Aggregation Number for Micelles with the Mass-Action Model by Isothermal Titration Calorimetry: A Case Study on Bile Salts, J. Colloid Interface Sci. 453 (2015) 79–89.

[25] N.E. Olesen, R. Holm, P. Westh, Determination of the Aggregation Number for Micelles by Isothermal Titration Calorimetry, Thermochim. Acta 588 (2014) 28–37.

[26] J. Lah, M. Bester-Rogac, T.-M. Perger, G. Vesnaver, Energetics in Correlation with Structural Features: The Case of Micellization, J. Phys. Chem. B 110 (46) (2006) 23279–23291.

[27] A.D. Tsamaloukas, A. Beck, H. Heerklotz, Modeling the Micellization Behavior of Mixed and Pure N-Alkyl-Maltosides, Langmuir 25 (8) (2009) 4393–4401.

[28] K. Beyer, D. Leine, A. Blume, The Demicellization of Alkyltrimethylammonium Bromides in 0.1 M Sodium Chloride Solution Studied by Isothermal Titration Calorimetry, Colloids Surf., B 49 (2006) 31–39.

[29] K. Matsuoka, Y. Moroi, M. Saito, Thermodynamics of Micelle Formation of 1 - Dodecanesulfonic Acid, J. Phys. Chem. 97 (49) (1993) 13006–13010.

[30] S. Dai, K.C. Tam, Isothermal Titration Calorimetric Studies of Alkyl Phenol Ethoxylate Surfactants in Aqueous Solutions, Colloids Surf., A 229 (1) (2003) 157–168.

[31] S. Shimizu, P.A.R. Pires, W. Loh, O.A. El Seoud, Thermodynamics of Micellization of Cationic Surfactants in Aqueous Solutions: Consequences of the Presence of the 2-Acylaminoethyl Moiety in the Surfactant Head Group, Colloid Polym. Sci. 282 (9) (2004) 1026–1032.

[32] Z. Király, I. Dekány, A Thermometric Titration Study on the Micelle Formation of Sodium Decyl Sulfate in Water, J. Colloid Interface Sci. 242 (1) (2001) 214–219.

[33] T.P. Golub, A. de Keizer, Calorimetric Study on the Temperature Dependence of the Formation of Mixed Ionic/nonionic Micelles, Langmuir 20 (22) (2004) 9506–9512.

[34] G.J.M. Koper, C.B. Minkenberg, I.S. Upton, J.H. van Esch, E.J.R. Sudhölter, Quantitatively Interpreting Thermal Behavior of Self-Associating Systems, J. Phys. Chem. B 113 (47) (2009) 15597–15601.

[35] I. Johnsson, G. Olofsson, B. Jönsson, Micelle Formation of Ionic Amphiphiles, J. Chem. Soc. Faraday Trans. 1 83 (11) (1987) 3331–3344.

[36] J. Zajac, C. Chorro, M. Lindheimer, S. Partyka, Thermodynamics of Micellization and Adsorption of Zwitterionic Surfactants in Aqueous Media, Langmuir 13 (6) (1997) 1486–1495.

[37] G. Bai, A. Lopes, M. Bastos, Thermodynamics of Micellization of Alkylimidazolium Surfactants in Aqueous Solution, J. Chem. Thermodyn. 40 (10) (2008) 1509–1516.

[38] A. Heintz, J.K. Lehmann, S.A. Kozlova, E.V. Balantseva, A.B. Bazyleva, D. Ondo, Micelle Formation of Alkylimidazolium Ionic Liquids in Water and in Ethylammonium Nitrate Ionic Liquid: A Calorimetric Study, Fluid Phase Equilib. 294 (1) (2010) 187–196.

[39] F.M. Winnik, S.T.A. Regismond, Fluorescence Methods in the Study of the Interactions of Surfactants with Polymers, Colloid Surface A 118 (1) (1996) 1–39.

[40] V. Mosquera, J.M. del Río, D. Attwood, M. García, M.N. Jones, G. Prieto, M.J. Suarez, F. Sarmiento, A Study of the Aggregation Behavior of Hexyltrimethylammonium Bromide in Aqueous Solution, J. Colloid Interface Sci. 206 (1) (1998) 66–76.

[41] C. Treiner, M.H. Mannebach, Counter Ion Condensation on Mixed Cationic/nonionic Micellar Systems: Bjerrum's Electrostatic Condition, Colloid Polym. Sci. 268 (1) (1990) 88–95.

[42] N.A. Smirnova, A.A. Vanin, E.A. Safonova, I.B. Pukinsky, Y.A. Anufrikov, A.L. Makarov, Self-Assembly in Aqueous Solutions of Imidazolium Ionic Liquids and Their Mixtures with an Anionic Surfactant, J. Colloid Interface Sci. 336 (2) (2009) 793–802.

[43] G. Wang, G. Olofsson, Ethyl(hydroxyethyl)cellulose and Ionic Surfactants in Dilute Solution Calorimetric and Viscosity Study of the Interaction with SDS and Some Cationic Surfactants, J. Phys. Chem. B 99 (15) (1995) 5588–5596.

[44] G.B. Ray, I. Chakraborty, S. Ghosh, S.P. Moulik, R. Palepu, Self-Aggregation of Alkyltrimethylammonium Bromides (C10-, C12-, C14-, and C16TAB) and Their Binary Mixtures in Aqueous Medium : A Critical and Comprehensive Assessment of Interfacial Behavior and Bulk Properties with Reference to Two Types Of Micelle Formation, Langmuir 21 (24) (2005) 10958–10967.

[45] S.P. Stodghill, A.E. Smith, J.H. O'Haver, Thermodynamics of Micellization and Adsorption of Three Alkyltrimethylammonium Bromides Using Isothermal Titration Calorimetry, Langmuir 20 (26) (2004) 11387–11392.

[46] W. Tong, Q. Zheng, S. Shao, Q. Lei, W. Fang, Critical Micellar Concentrations of Quaternary Ammonium Surfactants with Hydroxyethyl Substituents on Headgroups Determined by Isothermal Titration Calorimetry, J. Chem. Eng. Data 55 (9) (2010) 3766–3771.

[47] B. Šarac, M. Bešter-Rogač, Temperature and Salt-Induced Micellization of Dodecyltrimethylammonium Chloride in Aqueous Solution: A Thermodynamic Study, J. Colloid Interface Sci. 338 (2009) 216–221.

[48] J. Łuczak, C. Jungnickel, M. Joskowska, J. Thöming, J. Hupka, Thermodynamics of Micellization of Imidazolium Ionic Liquids in Aqueous Solutions, J. Colloid Interface Sci. 336 (1) (2009) 111–116.

[49] F. Geng, J. Liu, L. Zheng, L. Yu, Z. Li, G. Li, C. Tung, Micelle Formation of Long-Chain Imidazolium Ionic Liquids in Aqueous Solution Measured by Isothermal Titration Microcalorimetry, J. Chem. Eng. Data 55 (1) (2010) 147–151.

[50] Y. Wang, X. Huang, Y. Li, J. Wang, Y. Wang, Aggregation Properties of Zwitterionic Surfactants with Different Ionic Head groups Hydrophobic Chain Length and Inter-Charge Spacers, Colloids Surf. A 333 (1) (2009) 108–114.

[51] M.G. D'Andrea, C.C. Domingues, S.V.P. Malheiros, F.G. Neto, L.R.S. Barbosa, R. Itri, F.C.L. Almeida, E. De Paula, M.L. Bianconi, Thermodynamic and Structural Characterization of Zwitterionic Micelles of the Membrane Protein Solubilizing Amidosulfobetaine Surfactants ASB-14 and ASB-16, Langmuir 27 (13) (2011) 8248–8256.

[52] G.C. Kresheck, A Calorimetric Determination of the Standard Enthalpy and Heat Capacity Changes That Accompany Micelle Formation for Four Long Chain Alkyldimethylphosphine Oxides in H$_2$O and D$_2$O Solution from 15 to 79 °C, J. Am. Chem. Soc. 120 (42) (1998) 10964–10969.

[53] R.G. Angarten, W. Loh, Thermodynamics of Micellization of Homologous Series of Alkyl Mono and Di-Glucosides in Water and in Heavy Water, J. Chem. Thermodyn. 73 (2014) 218–223.

[54] J.M. Corkill, J.F. Goodman, J.R. Tate, Calorimetric Determination of the Heats of Micelle Formation of Some Non-Ionic Detergents, Trans. Faraday Soc. 60 (1964) 996.

[55] G. Bai, M. Nichifor, A. Lopes, M. Bastos, Thermodynamic Characterization of the Interaction Behavior of a Hydrophobically Modified Polyelectrolyte and Oppositely Charged Surfactants in Aqueous Solution: Effect of Surfactant Alkyl Chain Length, J. Phys. Chem. B 109 (1) (2005) 518–525.

[56] J.M. Corkill, J.F. Goodman, S.P. Harrold, Thermodynamics of Micellization of Non-Ionic Detergents, Trans. Faraday Soc. 60 (1964) 202.

[57] E. Leontidis, Hofmeister Anion Effects on Surfactant Self-Assembly and the Formation of Mesoporous Solids, Curr. Opin. Colloid Interface Sci. 7 (1) (2002) 81–91.

[58] L. Abezgauz, K. Kuperkar, P.A. Hassan, O. Ramon, P. Bahadur, D. Danino, Effect of Hofmeister Anions on Micellization and Micellar Growth of the Surfactant Cetylpyridinium Chloride, J. Colloid Interface Sci. 342 (1) (2010) 83–92.

[59] N. Jiang, P. Li, Y. Wang, J. Wang, H. Yan, R.K. Thomas, Aggregation Behavior of Hexadecyltrimethylammonium Surfactants with Various Counterions in Aqueous Solution, J. Colloid Interface Sci. 286 (2) (2005) 755–760.

[60] N. Jahnke, O.O. Krylova, T. Hoomann, C. Vargas, S. Fiedler, P. Pohl, S. Keller, Real-Time Monitoring of Membrane-Protein Reconstitution by Isothermal Titration Calorimetry, Anal. Chem. 86 (1) (2014) 920–927.

[61] S. Keller, H. Heerklotz, A. Blume, Monitoring Lipid Membrane Translocation of Sodium Dodecyl Sulfate by Isothermal Titration Calorimetry, J. Am. Chem. Soc. 128 (4) (2006) 1279–1286.

[62] A.D. Tsamaloukas, S. Keller, H. Heerklotz, Uptake and Release Protocol for Assessing Membrane Binding and Permeation by Way of Isothermal Titration Calorimetry, Nat. Protoc. 2 (3) (2007) 695–704.

[63] E. Frotscher, B. Danielczak, C. Vargas, A. Meister, G. Durand, S. Keller, A Fluorinated Detergent for Membrane-Protein Applications, Angew. Chem. Int. Ed. 54 (2015) 5069–5073.

[64] G.V. Jensen, R. Lund, J. Gummel, T. Narayanan, J.S. Pedersen, Monitoring the Transition from Spherical to Polymer-like Surfactant Micelles Using Small-Angle X-Ray Scattering, Angew. Chem. 126 (43) (2014) 11708–11712.

[65] A.J.M. Valente, J.J.L. Cascales, A.J.F. Romero, Thermodynamic Analysis of Unimer-Micelle and Sphere-to-Rod Micellar Transitions of Aqueous Solutions of Sodium Dodecylbenzenesulfonate, J. Chem. Thermodyn. 77 (2014) 54–62.

[66] A. Karumbamkandathil, S. Ghosh, U. Anand, P. Saha, M. Mukherjee, S. Mukherjee, Micelles of Benzethonium Chloride Undergoes Spherical to Cylindrical Shape Transformation: An Intrinsic Fluorescence and Calorimetric Approach, Chem. Phys. Lett. 593 (2014) 115–121.

[67] L.M. Bergström, A. Tehrani-Bagha, G. Nagy, Growth Behavior, Geometrical Shape, and Second CMC of Micelles Formed by Cationic Gemini Esterquat Surfactants, Langmuir 31 (16) (2015) 4644–4653.

[68] D. Löf, A. Niemiec, K. Schillén, W. Loh, W and G. Olofsson, A Calorimetry and Light Scattering Study of the Formation and Shape Transition of Mixed Micelles of EO$_{20}$PO$_{68}$EO$_{20}$ Triblock Copolymer (P123) and Nonionic Surfactant (C$_{12}$EO$_6$), J. Phys. Chem. B 111 (21) (2007) 5911–5920.

[69] H. Heerklotz, A. Tsamaloukas, K. Kita-Tokarczyk, P. Strunz, T. Gutberlet, Structural, Volumetric, and Thermodynamic Characterization of a Micellar Sphere-to-Rod Transition, J. Am. Chem. Soc. 126 (50) (2004) 16544–16552.

[70] C. Du, D. Cai, M. Qin, P. Zheng, Z. Hao, T. Yin, J. Zhao, W. Shen, Thermodynamics of Mixed Surfactant Solutions of N, N′-Bis(dimethyldodecyl)-1,2-Ethanediammoniumdibromide with 1-Dodecyl-3-Methylimidazolium Bromide, J. Phys. Chem. B 118 (4) (2014) 1168–1179.

[71] T.H. Ito, R.K. Rodrigues, W. Loh, E. Sabadini, Calorimetric and Light Scattering Investigations of the Transition from Spherical to Wormlike Micelles of C$_{14}$TAB Triggered by Salicylate, Langmuir 31 (22) (2015) 6020–6026.

[72] S. Dai, K.C. Tam, Isothermal Titration Calorimetry Studies of Binding Interactions between Polyethylene Glycol and Ionic Surfactants, J. Phys. Chem. B 105 (44) (2001) 10759–10763.

[73] B.Z. Shang, Z. Wang, R.G. Larson, Effect of Headgroup Size, Charge, and Solvent Structure on Polymer-Micelle Interactions Studied by Molecular Dynamics Simulations, J. Phys. Chem. B 113 (46) (2009) 15170–15180.

[74] W. Loh, L.A.C. Teixeira, L.-T. Lee, Isothermal Calorimetric Investigation of the Interaction of Poly(N-Isopropylacrylamide) and Ionic Surfactants, J. Phys. Chem. B 108 (10) (2004) 3196–3201.

[75] R.C. da Silva, W. Loh, G. Olofsson, Calorimetric Investigation of Temperature Effect on the Interaction between Poly(ethylene Oxide) and Sodium Dodecylsulfate in Water, Thermochim. Acta 417 (2) (2004) 295–300.

[76] M. Spitzer, E. Sabadini, W. Loh, Entropically Driven Partitioning of Ethylene Oxide Oligomers and Polymers in Aqueous/ Organic Biphasic Systems, J. Phys. Chem. B 106 (48) (2002) 12448–12452.

[77] E.E. Dormidontova, Role of Competitive PEO-Water and Water-Water Hydrogen Bonding in Aqueous Solution PEO Behavior, Macromolecules 35 (3) (2002) 987–1001.

[78] G. Olofsson, G. Wang, Interactions between Surfactants and Uncharged Polymers in Aqueous Solution Studied by Microcalorimetry, Pure Appl. Chem. 66 (3) (1994) 527–532.

[79] A. Niemiec, W. Loh, Interaction of Ethylene Oxide-Propylene Oxide Copolymers with Ionic Surfactants Studied by Calorimetry: Random versus Block Copolymers, J. Phys. Chem. B 112 (3) (2008) 727–733.

[80] S. Dai, K.C. Tam, Isothermal Titration Calorimetric Studies on the Interaction between Sodium Dodecyl Sulfate and Polyethylene Glycols of Different Molecular Weights and Chain Architectures, Colloids Surf. A 289 (1) (2006) 200–206.

[81] G. Bai, G.; L.M.N.B.F. Santos, M. Nichifor, A. Lopes and M. Bastos, Thermodynamics of the Interaction between a Hydrophobically Modified Polyelectrolyte and Sodium Dodecyl Sulfate in Aqueous Solution, J. Phys. Chem. B 108 (1) (2004) 405–413.

[82] R.S. Mello, E.S. Orth, W. Loh, H.D. Fiedler, F. Nome, Polymers Containing Hydroxamate Groups: Nanoreactors for Hydrolysis of Phosphoryl Esters, Langmuir 27 (24) (2011) 15112–15119.

[83] M. Nilsson, A.J.M. Valente, G. Olofsson, O. Söderman, M. Bonini, Thermodynamic and Kinetic Characterization of Host-Guest Association between Bolaform Surfactants and α- and β-Cyclodextrins, J. Phys. Chem. B 112 (36) (2008) 11310–11316.

[84] K. Holmberg, B. Jönsson, B. Kronberg, B. Lindman, Surfactants and Polymers in Aqueous Solution, 2nd ed. John Wiley & Sons, LTD, 2002.

[85] J.C.T. Kwak, Polymer-Surfactant System, 1st ed. Marcel Dekker Inc., New York, 1998.

[86] A. Harada, S. Nozakura, Formation of Organized Structures in Systems of Polyelectrolyte-Ionic Surfactants, Polym. Bull. 11 (2) (1984) 175–178.

[87] Z. Liu, Y. Shang, J. Feng, C. Peng, H. Liu, Y. Hu, Effect of Hydrophilicity or Hydrophobicity of Polyelectrolyte on the Interaction between Polyelectrolyte and Surfactants: Molecular Dynamics Simulations, J. Phys. Chem. B 116 (18) (2012) 5516–5526.

[88] C. Wang, K.C. Tam, New Insights on the Interaction Mechanism within Oppositely Charged Polymer/Surfactant Systems, Langmuir 18 (17) (2002) 6484–6490.

[89] C. Wang, K.C. Tam, Interaction between Polyelectrolyte and Oppositely Charged Surfactant: Effect of Charge Density, J. Phys. Chem. B 108 (26) (2004) 8976–8982.

[90] C. Wang, K.C. Tam., R.D. Jenkins and C.B. Tan, Interactions between Methacrylic Acid/Ethyl Acrylate Copolymers and Dodecyltrimethylammonium Bromide, J. Phys. Chem. B 107 (19) (2003) 4667–4675.

[91] H. Bao, L. Li, L.H. Gan, H. Zhang, Interactions between Ionic Surfactants and Polysaccharides in Aqueous Solutions, Macromolecules 41 (23) (2008) 9406–9412.

[92] D. Asker, J. Weiss, D.J. McClements, Analysis of the Interactions of a Cationic Surfactant (Lauric Arginate) with an Anionic Biopolymer (Pectin): Isothermal Titration Calorimetry, Light Scattering, and Microelectrophoresis, Langmuir 25 (1) (2009) 116–122.

[93] D.J. McClements, Isothermal Titration Calorimetry Study of Pectin-Ionic Surfactant Interactions, J. Agric. Food Chem. 48 (11) (2000) 5604–5611.

[94] M. Thongngam, D.J. McClements, Characterization of Interactions between Chitosan and an Anionic Surfactant, J. Agric. Food Chem. 52 (4) (2004) 987–991.

[95] J. Yang, Z. Zhao, Y. Fang, Calorimetric Study of the Interaction between Sodium Alginate and Sodium Dodecyl Sulfate in Dilute Solutions at Different pH Values, Carbohydr. Res. 343 (4) (2008) 719–725.

[96] D.M. Bloor, J.F. Holzwarth, E. Wyn-Jones, Polymer/Surfactant Interactions. The Use of Isothermal Titration Calorimetry and Emf Measurements in the Sodium Dodecyl Sulfate/Poly (N-Vinylpyrrolidone) System, Langmuir 11 (6) (1995) 2312–2313.

[97] Y. Li, S.M. Ghoreishi, J. Warr, D.M. Bloor, J.F. Holzwarth, E. Wyn-Jones, Interactions between a Nonionic Copolymer Containing Different Amounts of Covalently Bonded Vinyl Acrylic Acid and Surfactants: EMF and Microcalorimetry Studies, Langmuir 15 (7) (1999) 6326–6332.

[98] Y. Li, S.M. Ghoreishi, J. Warr, D.M. Bloor, J.F. Holzwarth, E. Wyn-Jones, Binding of Sodium Dodecyl Sulfate to Some Polyethyleneimines and Their Ethoxylated Derivatives at Different pH Values Electromotive Force and Microcalorimetry Studies, Langmuir 16 (7) (2000) 3093–3100.

[99] Y. Li, R. Xu, D.M. Bloor, J. Penfold, J.F. Holzwarth, E. Wyn-Jones, Moderation of the Interactions between Sodium Dodecyl Sulfate and Poly (vinylpyrrolidone) Using the Nonionic Surfactant Hexaethyleneglycol Mono-n-Dodecyl Ether $C_{12}EO_6$: An Electromotive Force, Microcalorimetry, and Small-Angle Neutron Scattering Study, Langmuir 16 (23) (2000) 8677–8684.

[100] Y. Li, R. Xu, S. Couderc, D.M. Bloor, J. Warr, J. Penfold, J.F. Holzwarth, E. Wyn-Jones, Structure of the Complexes Formed between Sodium Dodecyl Sulfate and a Charged and Uncharged Ethoxylated Polyethyleneimine: Small-Angle Neutron Scattering, Electromotive Force, and Isothermal Titration Calorimetry Measurements, Langmuir 17 (18) (2001) 5657–5665.

[101] S. Courdec-Azouani, J. Sidhu, T.K. Georgiou, D.C. Charalambous, M. Vamvakaki, C.S. Patrickios, D.M. Bloor, J. Penfold, J.F. Holzwarth, E. Wyn-Jones, Binding of Sodium Dodecyl Sulfate to Linear and Star Homopolymers of the Nonionic Poly(methoxyhexa(ethylene glycol) methacrylate) and the Polycation Poly(2-(dimethylamino)ethyl methacrylate): Electromotive Force, Isothermal Titration Calorimetry, Surface Tension, and Small-Angle Neutron Scattering Measurements, Langmuir 20 (15) (2004) 6458–6469.

[102] H. Wang, Y. Wang, H. Yan, J. Zhang, R.K. Thomas, Binding of Sodium Dodecyl Sulfate with Linear and Branched Polyethyleneimines in Aqueous Solution at Different pH Values, Langmuir 22 (4) (2006) 1526–1533.

[103] M. Fechner, S. Kosmella, J. Koetz, pH-Dependent Polyampholyte SDS Interactions, J. Colloid Interface Sci. 345 (2) (2010) 384–391.

[104] G. Bai, Y. Wang, H. Yan, R.K. Thomas, J.C.T. Kwak, Thermodynamics of Interaction between Cationic Gemini Surfactants and Hydrophobically Modified Polymers in Aqueous Solutions, J. Phys. Chem. B 106 (9) (2002) 2153–2159.

[105] H. Wang, Y. Wang, Studies on Interaction of Poly (sodium Acrylate) and Poly (sodium Styrenesulfonate) with Cationic Surfactants: Effects of Polyelectrolyte Molar Mass, Chain Flexibility, and Surfactant Architecture, J. Phys. Chem. B 114 (32) (2010) 10409–10416.

[106] C. Wang, K.C. Tam, Interactions between Poly(acrylic Acid) and Sodium Dodecyl Sulfate: Isothermal Titration Calorimetric and Surfactant Ion-Selective Electrode Studies, J. Phys. Chem. B 109 (11) (2005) 5156–5161.

[107] J. Sidhu, D.M. Bloor, S. Couderc-Azouani, J. Penfold, J.F. Holzwarth, E. Wyn-Jones, Interactions of Poly (amidoamine) Dendrimers with the Surfactants SDS, DTAB, and $C_{12}EO_6$: An Equilibrium and Structural Study Using a SDS Selective Electrode,

[108] Isothermal Titration Calorimetry, and Small Angle Neutron Scattering, Langmuir 20 (21) (2004) 9320–9328.

[108] C. Wang, E. Wyn-Jones, J. Sidhu, K.C. Tam, Supramolecular Complex Induced by the Binding of Sodium Dodecyl Sulfate to PAMAM Dendrimers, Langmuir 23 (4) (2007) 1635–1639.

[109] C. Wang, E. Wyn-Jones, K.C. Tam, Complexation between Amine- and Hydroxyl-Terminated PAMAM Dendrimers and Sodium Dodecyl Sulfate, Colloids Surf. A 364 (1) (2010) 49–54.

[110] A.H. Lim, K.C. Tam, Stabilization of Polyamidoamine (PAMAM) Dendrimers/sodium Dodecyl Sulfate Complexes via PEGylation, Colloid Surface A 380 (1) (2011) 47–52.

[111] A. Chatterjee, S.P. Moulik, P.R. Majhi, S.K. Sanyal, Studies on Surfactant–biopolymer Interaction. I. Microcalorimetric Investigation on the Interaction of Cetyltrimethylammonium Bromide (CTAB) and Sodium Dodecylsulfate (SDS) with Gelatin (Gn), Lysozyme (Lz) and Deoxyribonucleic Acid (DNA), Biophys. Chem. 98 (3) (2002) 313–327.

[112] A.D. Nielsen, L. Arleth, P. Westh, Analysis of Protein-Surfactant Interactions - A Titration Calorimetric and Fluorescence Spectroscopic Investigation of Interactions between *Humicola Insolens* Cutinase and an Anionic Surfactant, BBA - Proteins Proteom. 1752 (2) (2005) 124–132.

[113] H.L. Bagger, S.V. Hoffmann, C.C. Fuglsang, P. Westh, Glycoprotein-Surfactant Interactions: A Calorimetric and Spectroscopic Investigation of the Phytase-SDS System, Biophys. Chem. 129 (2) (2007) 251–258.

[114] S.D. Wettig, R. Deubry, J. Akbar, T. Kaur, H. Wang, T. Sheinin, J.W. Joseph, R.A. Slavcev, Thermodynamic Investigation of the Binding of Dissymmetric Pyrenyl-Gemini Surfactants to DNA, Phys. Chem. Chem. Phys. 12 (18) (2010) 4821–4826.

[115] K. Tanaka, J.M.M. Caaveiro, K. Morante, J.M. González-Mañas, K. Tsumoto, Structural Basis for Self-Assembly of a Cytolytic Pore Lined by Protein and Lipid, Nat. Commun. 6 (2015) 6337.

[116] Y. Lapitsky, M. Parikh, E.W. Kaler, Calorimetric Determination of Surfactant/Polyelectrolyte Binding Isotherms, J. Phys. Chem. B 111 (29) (2007) 8379–8387.

[117] L. Vitorazi, N. Ould-Moussa, S. Sekar, J. Fresnais, W. Loh, J.-P. Chapel, J.-F. Berret, Evidence of a Two-Step Process and Pathway Dependency in the Thermodynamics of Poly(diallyldimethylammonium Chloride)/poly(sodium Acrylate) Complexation, Soft Matter 10 (47) (2014) 9496–9505.

[118] L. Vitorazi, Association Structures of Complex Salts of Block Copolymer and Surfactants, Polyelectrolytes and Nanoparticles, PhD dissertation, University of Campinas, Campinas, 2013.

[119] L. Chiappisi, D. Li, N.J. Wagner, M. Gradzielski, An Improved Method for Analyzing Isothermal Titration Calorimetry Data from Oppositely Charged Surfactant Polyelectrolyte Mixtures, J. Chem. Thermodyn. 68 (2014) 48–52.

[120] I. Herrera, M.A. Winnik, Differential Binding Models for Isothermal Titration Calorimetry: Moving beyond the Wiseman Isotherm, J. Phys. Chem. B 117 (29) (2013) 8659–8672.

[121] T. Wiseman, S. Williston, J.F. Brandts, L.-N. Lin, Rapid Measurement of Binding Constants and Heats of Binding Using a New Titration Calorimeter, Anal. Biochem. 179 (1) (1989) 131–137.

[122] B.A. Pethica, Misuse of Thermodynamics in the Interpretation of Isothermal Titration Calorimetry Data for Ligand Binding to Proteins, Anal. Biochem. 472 (2015) 21–29.

[123] R.A. Sperling, W.J. Parak, Surface Modification, Functionalization and Bioconjugation of Colloidal Inorganic Nanoparticles, Philos. Trans. R. Soc. London A Math. Phys. Eng. Sci. 368 (1915) (2010) 1333–1383.

[124] A.E. Gulyaev, S.E. Gelperina, I.N. Skidan, A.S. Antropov, G.Y. Kivman, J. Kreuter, Significant Transport of Doxorubicin into the Brain with Polysorbate 80-Coated Nanoparticles, Pharm. Res. 16 (10) (1999) 1564–1569.

[125] B. Nikoobakht, M.A. El-Sayed, Evidence for Bilayer Assembly of Cationic Surfactants on the Surface of Gold Nanorods, Langmuir 17 (20) (2001) 6368–6374.

[126] R. Atkin, V.S.J. Craig, E.J. Wanless, S. Biggs, Mechanism of Cationic Surfactant Adsorption at the Solid-Aqueous Interface, Adv. Colloid Interface Sci. 103 (3) (2003) 219–304.

[127] E. Sokolov, F. Yeh, A. Khokhlov, V.Y. Grinberg, B. Chu, Nanostructure Formation in Polyelectrolyte-Surfactant Complexes, J. Phys. Chem. B 102 (37) (1998) 7091–7098.

[128] M. Uchman, M. Gradzielski, B. Angelov, Z. Tošner, J. Oh, T. Chang, M. Štěpánek, K. Procházka, Thermodynamic and Kinetic Aspects of Coassembly of PEO—PMAA Block Copolymer and DPCl Surfactants into Ordered Nanoparticles in Aqueous Solutions Studied by ITC, NMR, and Time-Resolved SAXS Techniques, Macromolecules 46 (6) (2013) 2172–2181.

[129] S. Dai, K.C. Tam, Microstructure of Un-Neutralized Hydrophobically Modified Alkali-Soluble Emulsion Latex in Different Surfactant Solutions, Langmuir 21 (16) (2005) 7136–7142.

[130] A. Hamberger, K. Landfester, Influence of Size and Functionality of Polymeric Nanoparticles on the Adsorption Behavior of Sodium Dodecyl Sulfate as Detected by Isothermal Titration Calorimetry, Colloid Polym. Sci. 289 (1) (2011) 3–14.

[131] M.M. de Souza Lima, R. Borsali, Rodlike Cellulose Microcrystals: Structure, Properties, and Applications, Macromol. Rapid. Comm. 25 (7) (2004) 771–787.

[132] Y. Habibi, L.A. Lucia, O.J. Rojas, Cellulose Nanocrystals: Chemistry, Self-Assembly, and Applications, Chem. Rev. 110 (6) (2010) 3479–3500.

[133] R.R. Lahiji, X. Xu, R. Reifenberger, A. Raman, A. Rudie, R.J. Moon, Atomic Force Microscopy Characterization of Cellulose Nanocrystals, Langmuir 26 (6) (2010) 4480–4488.

[134] H. Yang, A. Tejado, N. Alam, M. Antal, T.G.M. van De Ven, Films Prepared from Electrosterically Stabilized Nanocrystalline Cellulose, Langmuir 28 (20) (2012) 7834–7842.

[135] T. Abitbol, A. Palermo, J.M. Moran-Mirabal, E.D. Cranston, Fluorescent Labeling and Characterization of Cellulose Nanocrystals with Varying Charge Contents, Biomacromolecules 14 (9) (2013) 3278–3284.
[136] S.C. Espinosa, T. Kuhnt, E.J. Foster, C. Weder, Isolation of Thermally Stable Cellulose Nanocrystals by Phosphoric Acid Hydrolysis, Biomacromolecules 14 (4) (2013) 1223–1230.
[137] S.P. Akhlaghi, R.C. Berry, K.C. Tam, Surface Modification of Cellulose Nanocrystal with Chitosan Oligosaccharide for Drug Delivery Applications, Cellulose 20 (4) (2013) 1747–1764.
[138] E.D. Cranston, D.G. Gray, Morphological and Optical Characterization of Polyelectrolyte Multilayers Incorporating Nanocrystalline Cellulose, Biomacromolecules 7 (9) (2006) 2522–2530.
[139] Z. Hu, E.D. Cranston, R. Ng, R. Pelton, Tuning Cellulose Nanocrystal Gelation with Polysaccharides and Surfactants, Langmuir 30 (10) (2014) 2684–2692.
[140] R. Batmaz, N. Mohammed, M. Zaman, G. Minhas, R.M. Berry, K.C. Tam, Cellulose Nanocrystals as Promising Adsorbents for the Removal of Cationic Dyes, Cellulose 21 (3) (2014) 1655–1665.
[141] N. Dhar, D. Au, R.C. Berry, K.C. Tam, Interactions of Nanocrystalline Cellulose with an Oppositely Charged Surfactant in Aqueous Medium, Colloids Surf., A 415 (2012) 310–319.
[142] C. Brinatti, J. Huang, R.C. Berry, K.C., W. Loh, Structural and Energetic Aspects of the Interactions of Cationic Surfactants with Cellulose Nanocrystals, 2015 unpublished results.

Appendix E- Synthesis of amine functionalized cellulose nanocrystals: optimization and characterization

My contributions to the paper:

Performed the settling behavior experiments and proofread the manuscript.

Synthesis of amine functionalized cellulose nanocrystals: optimization and characterization

Seyedeh Parinaz Akhlaghi [a], Masuduz Zaman [a], Nishil Mohammed [a], César Brinatti [b], Rasim Batmaz [a], Richard Berry [c], Watson Loh [b], Kam Chiu Tam [a, *]

[a] Dept. of Chemical Engineering, Waterloo Institute for Nanotechnology, University of Waterloo, 200 University Avenue West, Waterloo, Ontario N2L 3G1, Canada
[b] Chemistry Institute, University of Campinas, PO Box 6154, 13083-970 Campinas, SP, Brazil
[c] CelluForce Inc., 625, Président-Kennedy Avenue, Montreal, QC H3A 1K2, Canada

ARTICLE INFO

ABSTRACT

A simple protocol was used to prepare amine functionalized cellulose nanocrystals (CNC–NH$_2$). In the first step, epichlorohydrin (EPH) was reacted with ammonium hydroxide to produce 2-hydroxy-3-chloro propylamine (HCPA). In the next step, HCPA was grafted to CNC using the etherification reaction in an organic solution media. Various reaction parameters, such as time, temperature, and reactant molar ratio were performed to determine the optimal reaction conditions. The final product (CNC–NH$_2$(T)) was dialyzed for a week. Further purification via centrifugation yielded the sediment (CNC–NH$_2$(P)) and supernatant (POLY–NH$_2$). The presence of amine groups on the surface of modified CNC was confirmed by FTIR and the amine content was determined by potentiometric titration and elemental analysis. A high amine content of 2.2 and 0.6 mmol amine/g was achieved for CNC–NH$_2$(T) and CNC–NH$_2$(P), respectively. Zeta potential measurements confirmed the charge reversal of amine CNC from positive to negative when the pH was increased from 3 to 10. The flocculation of amine functionalized CNC due to its interactions with a negatively charged surfactant namely, sodium dodecyl sulfate (SDS) was investigated at pH 4. It showed promising results for applications, such as in flocculation of fine dispersions in water treatment. This simple and versatile synthetic method to produce high amine content CNC can be used for further conjugation as required for various applications.

© 2015 Elsevier Ltd. All rights reserved.

1. Introduction

Cellulose nanocrystals (CNC)—rigid rod-like nanoparticles obtained by acid hydrolysis of pulp fibers have received increasing interests over the last 10 years. The non-toxicity, biocompatibility, and biodegradability of CNC along with its robust physical properties, such as large surface area, mechanical strength, and the presence of abundant surface hydroxyl groups offer interesting opportunity for their use in different fields.[1] In addition, further surface modification of CNC expands its usefulness in many product formulations. The primary hydroxyl groups could be converted to aldehyde, carboxylic acid and amine functionalities. Cationic modification of cellulose and its derivatives is of interest due to their utility in several key industrial sectors, such as water

treatment.[2] In a recent study, the surface of CNC was cationically modified with 4-(1-bromoethyl/bromomethyl) benzoic acid, pyridine in organic media. It was reported that a high degree of substitution leading to a zeta potential of +59.0 mV was observed.[3]

Modification of the surface of CNC with primary amine groups not only introduces cationic charge on the surface of CNC in acid medium, but it can also be used for the conjugation of biomolecules to CNC for biomedical applications.[4] The importance of polysaccharides with amine functional groups in biological systems has led to an increase in research activity in this field.[5,6]

Different forms of cellulose have been modified with amine groups via several synthetic methods. In one study, a three-step procedure was used to prepare 6-deoxy-6-amino cellulose derivatives. First, cellulose was tosylated and reacted with sodium azide, where the azide was reduced to amine using CoBr$_2$/2,2′-bypridine/NaBH$_4$ system.[7] Amine cellulose esters were also prepared by reactions involving lactam ring opening in the presence of N-methyl-2-pyrolidone and p-toluenesulphonic acid chloride.[8] In

another study, polyampholytic amino cellulose sulfates were prepared by the tosylation of C-6 carbon followed by the introduction of sulfate groups using trioxide/pyridine complex. Further nucleophilic displacement of tosyl groups by different amines yielded various types of cellulose with different types of amine functional groups.[9]

In recent years, amine functionalized CNCs have been produced via different synthetic routes. In one study, researchers decorated the surface of CNC with epoxide groups via reaction with epichlorohydrin (EPH) in sodium hydroxide at 60 °C. After dialyzing the reaction mixture, amine groups were introduced on the surface of CNC by opening the epoxide rings using ammonium hydroxide at 60 °C. The final product was obtained after dialysis until a pH of 7.[10] In another study, amine groups were introduced on the surface of CNC by esterification and consecutive thiol-ene click reaction.[11] Click-chemistry was also applied to prepare amine functionalized CNC. Firstly, azide groups were introduced to the surface of CNC via etherification of 1-azido-2,3-epoxy- propane in a mixture of isopropanol/basic water at room temperature. In the next step, pH-responsive amine decorated CNC was achieved by reacting the azide groups with propargyl amine via copper catalyzed azide-alkyne cycloaddition.[12] In a recent study, amine functionalized CNC was obtained via a two-step procedure in aqueous media at ambient temperature. In the first step, the primary hydroxyl groups on the surface of CNC were converted to carboxylic acid via TEMPO-mediated oxidation. In the next step, peptidic coupling reaction between carboxylic acids and amines on bifunctional amines of small alkyl chain length was conducted.[4] Amine groups have also been introduced on the surface of CNC by grafting with chitosan oligosaccharide.[13]

In this study, we develop and optimize the functionalization of CNC with primary amines in aqueous solution in a simple reaction protocol. The synthetic protocols previously used for the synthesis of amine functionalized CNC was modified and different reaction parameters, such as time, temperature, ratios of CNC and reagents, and the effect of reflux were optimized leading to a higher content of surface amine groups. The pH-responsive properties of amine functionalized CNC was investigated by viscosity measurements. We also investigated one of the potential applications of amine CNC as a flocculating agent in water treatment by interacting it with a negatively charged surfactant.

2. Experimental

2.1. Materials

Spray-dried cellulose nanocrystal (CNC) sample was supplied by Celluforce Inc. Epichlorohydrin (EPH), dimethylsulfoxide (DMSO), tetrabutylammonium hydroxide (TBAH), sodium dodecylsulfate (99%) (SDS) were purchased from Sigma–Aldrich. Ammonium hydroxide (28–30% NH_3 in water) was purchased from Acros organics. Millipore de-ionized (D.I.) water was used for all experiments and sample preparations.

2.2. Synthesis and optimization of amine functionalized cellulose nanocrystals

In the first step, epichlorohydrin (1.46 ml) was added to ammonium hydroxide (3.78 ml) and heated to 65 °C for 2 h. In the second step, CNC (1.00 g) was dispersed in DMSO (66.66 ml) and different amounts of TBAH were added to the mixture in a round bottom flask (molar ratio of TBAH/AGU: 0.1-1.0). Contents from the reaction in step 1 were removed using a syringe and added to the second mixture in a drop-wise manner. The reaction mixture

was stirred for various time intervals (0.5–8 h) and heated at different temperatures (25–85 °C) for studies on determining the optimal reaction conditions. The reaction mixture was purified by dialysis (M_W cut off: 12,000 g/mol) against D.I. water for at least one week until the conductivity of the dialysis medium remained constant yielding a final product designated as CNC–NH_2(T). Further purification of the reaction mixture was obtained by lowering the pH to ~2, which induced the agglomeration of amine CNC nanoparticles between positive NH_3^+ and negative OSO_3^- groups. The agglomerated amine CNC was separated by centrifugation at 10,000 rpm for 1 h. The sediment was redispersed in an alkaline aqueous solution, and the process was repeated once, where the purified product comprised of the sediment (CNC–NH_2(P)) and supernatant (POLY–NH_2).

2.3. Potentiometric titration

The amine content of the amine functionalized CNC was determined by potentiometric titration. A Metrohm 809 Titando automatic titrator was used and the pH and conductivity were measured simultaneously. The titrator is equipped with a Tiamo software that doses µL of titrants. All measurements were performed in a closed jacketed vessel at 25 °C and the stirrer was set at a medium rate. 50 ml of 0.1 wt % CNC suspension were prepared in D.I. water. The pH of the suspension was adjusted to ~3 using 1 M HCl. In order to remove the dissolved CO_2 and avoid the formation of carbonic acid, the purified amine CNC suspension was degassed by bubbling argon gas into the solution. The suspensions were titrated using 0.1 M NaOH under argon blanket and stirring. The conductivity and pH of the suspensions were measured simultaneously until the pH of the samples approached ~11. Finally, the pH and conductivity values were plotted against the volume of NaOH (in mL), which were used to determine the content of amine groups.

2.4. FTIR

FTIR spectra of the dried KBr pellets of pristine CNC, CNC–NH_2(T), CNC–NH_2(P), and POLY–NH_2 were determined using a Bruker Tensor 27 spectrometer with resolution of 4 cm^{-1} and a number of scans of 32 from 400 to 4000 cm^{-1}. KBr pellets were prepared by grinding approximately 2% of the samples in KBr and compressed into a pellet. The FTIR Spectra were monitored and analyzed using the OPUS software.

2.5. Elemental analysis

The percent of carbon (C), hydrogen (H), nitrogen (N) and sulfur (S) contents (%) of pristine CNC, CNC–NH_2(T), CNC–NH_2(P) and POLY–NH_2 were determined by a CHNS, Vario Micro Cube, Elemental Analyzer. The freeze-dried samples were combusted at 1000 °C and the combustion products were detected by a thermal conductivity detector for quantitative analysis.

2.6. TEM

Transmission electron microscopic (TEM) images of pristine CNC, CNC–NH_2(T), and CNC–NH_2(P), were recorded using a Philips CM10 TEM with 60 keV acceleration voltages. Approximately 10 µL of 0.01 wt % aqueous suspensions of the samples were deposited on a carbon-formvar film on 200 mesh copper grids. In order to minimize possible agglomeration of the particles, excess solvent was removed from the grids placed on a filter paper. Then the grids were allowed to dry over night.

2.7. Zeta potential measurements

Zeta potential measurements for the various CNC systems at different pH values were measured using the ZetaPALS Analyzer (Brookhaven Instruments Corp., USA). The concentration of the samples was maintained at 0.01 wt% and the experiments were conducted at 25 °C, and the reported values are an average of 10 measurements.

2.8. Viscosity measurements

The relative viscosity of 0.1 wt% CNC–NH_2(P) suspension, at different pH values was determined using an automated kinematic viscometer, MiniPV (Cannon Instrument Company), at 25 °C. The sample was automatically drawn by a vacuum pump to the upper glass bulb, and the sensors placed at the top and bottom of the glass bulb measured the time taken for a known volume of liquid to flow through the capillary tube. Repeated tests were performed and once the measured times were within 1% of each other, the relative viscosity was then calculated.

2.9. Settling behavior measurements

The interactions between positively charged amine CNC and negatively charged compounds can lead to phase separation. To demonstrate this effect, the flocculation of amine CNC with an anionic surfactant, SDS (sodium dodecylsulfate) was studied. The samples were prepared containing a constant concentration of CNC–NH_2(P) (0.1 wt%), with surfactant concentration ranging from 0 to 3 mmol kg^{-1}. The pH was set to 4 to ensure the protonation of all amine groups resulting in a higher affinity for the surfactant. The vials were shaken prior to the measurements, and the height of the mixture was quantified as a function of time. The white turbid region represents the flocculated amine CNC/SDS complexes.

3. Results and discussion

3.1. Two-step synthesis of amine functionalized cellulose nanocrystals

Cellulose nanocrystals have previously been functionalized with amine groups by various research groups.[4,10] However, in most of the studies, the amine content was found to be relatively low, thus it would be desirable to increase the amine content by improving the synthetic protocol. In the synthesis method adopted by Hemraz et al.[4] and Mahmoud et al.[14] the low amine content could be attributed to the alkaline hydrolysis of epoxide group on epichlorohydrin[15] resulting in a lower grafting onto CNC. In the current study, a two-step synthesis protocol was developed to increase and enhance the grafting of amine functional groups onto CNC. In the first step, 2-hydroxy, 3-chloro propylamine was produced by opening the epoxide group of epichlorohydrin with ammonium hydroxide. This reaction is highly explosive in a closed container as the heating of ammonium hydroxide solution results in the evolution of gaseous ammonia in the reaction chamber. As the ammonia content in the air exceeds 15% by volume it forms an explosive mixture. Therefore, in order to keep the gaseous ammonia below the explosion limit, a cooling water reflux system was used, which also increased the reaction yield. In the next step, to minimize side reactions and undesirable hydrolytic reactions we dispersed CNC in DMSO. TBAH was then gradually added to activate the hydroxyl groups on the surface of CNC. TBAH acts as a catalyst in the S_N2 substitution reaction and favors the stretching of surface hydroxyl groups of CNC, forming nucleophiles for S_N2 substitution reaction with 2-hydroxy-3-chloropropylamine. Finally, the drop-
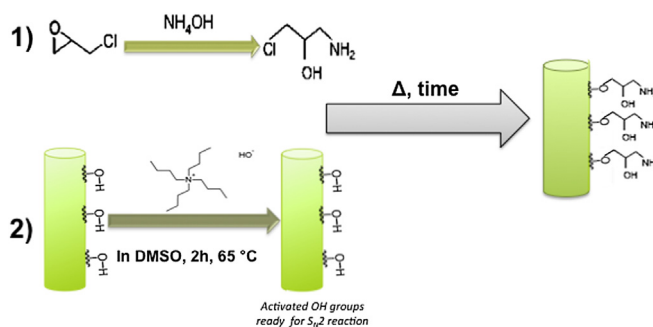
Scheme 1. Two-step amine functionalization of CNC.

wise addition of mixture 1 to 2 (Scheme 1) resulted in the amine functionalized CNC.

3.2. Effect of reaction parameters

In our attempt to optimize the reaction, different parameters were varied and their effects were investigated. Four reaction variables were selected for the reaction optimization study, which include: (1) reaction time, (2) temperature, (3) TBAH to AGU molar ratio, and (4) EPH to CNC molar ratio. One variable was varied at a time while the other three were kept constant. The amine content of the samples was determined by potentiometric titration. As shown in Fig. 1a, the amine content of modified CNC increased with reaction time and reached an optimum at 3 h. However, prolonging the reaction time resulted in a marginal reduction in amine content, and this could be attributed to degradation of functional groups and polymer fragments under alkaline condition.[16,17] The optimum temperature for reacting mixture 1 and 2 was found to be 50 °C (Fig. 1b). The reduction in amine content at high temperature could also be due to the enhanced degradation of functional groups and polymer fragments in amine CNC[18] under alkaline conditions. As shown in Fig. 1c, the amine content of modified CNC increased with molar ratio of TBAH to AGU due to the favorable activation of hydroxyl groups in the presence of TBAH. Fig. 1d shows the effect of EPH to CNC molar ratio on the amine content of CNC. At higher EPH content in the reaction system, a larger amount of HCPA was available at the surface of the CNC (near the glucose molecules), therefore, favoring the etherification reaction.[19] However, beyond a critical EPH content, the amine content of modified CNC was found to decrease, and the optimum EPH to CNC molar ratio was found to be 3.5:1. In step 1 of the protocol, the amount of NH_4OH was also increased in proportion to EPH so as to maintain a constant molar ratio of epoxy to ammonium groups. This has led to a larger proportion of water in both reaction mixture 1 and 2, which could have enhanced the undesirable hydrolytic reaction resulting in the reduction in the amine content above the EPH/CNC molar ratio of 3.5.[15] Under refluxing in the first step, we were able to increase the total amine content from 0.45 to 2.2 mmol/g.

3.3. Purification

EPH has also been used in the preparation of various kinds of polymers[20,21] and hence we anticipated the possibility of side reactions forming polyfunctional amines that may necessitate additional purification of the final products. Initially, we purified the sample using a dialysis tube (M_W cut off: 12,000 g/mol) against D.I. water. The dialysis was performed for more than a week until the conductivity of the dialysis medium remained constant. This purified sample was designated as CNC–NH_2(T), which we believed contained amine functionalized CNC (CNC–NH_2(P)) and polyfunctional amines (POLY–NH_2). In order to separate CNC–NH_2(P) from
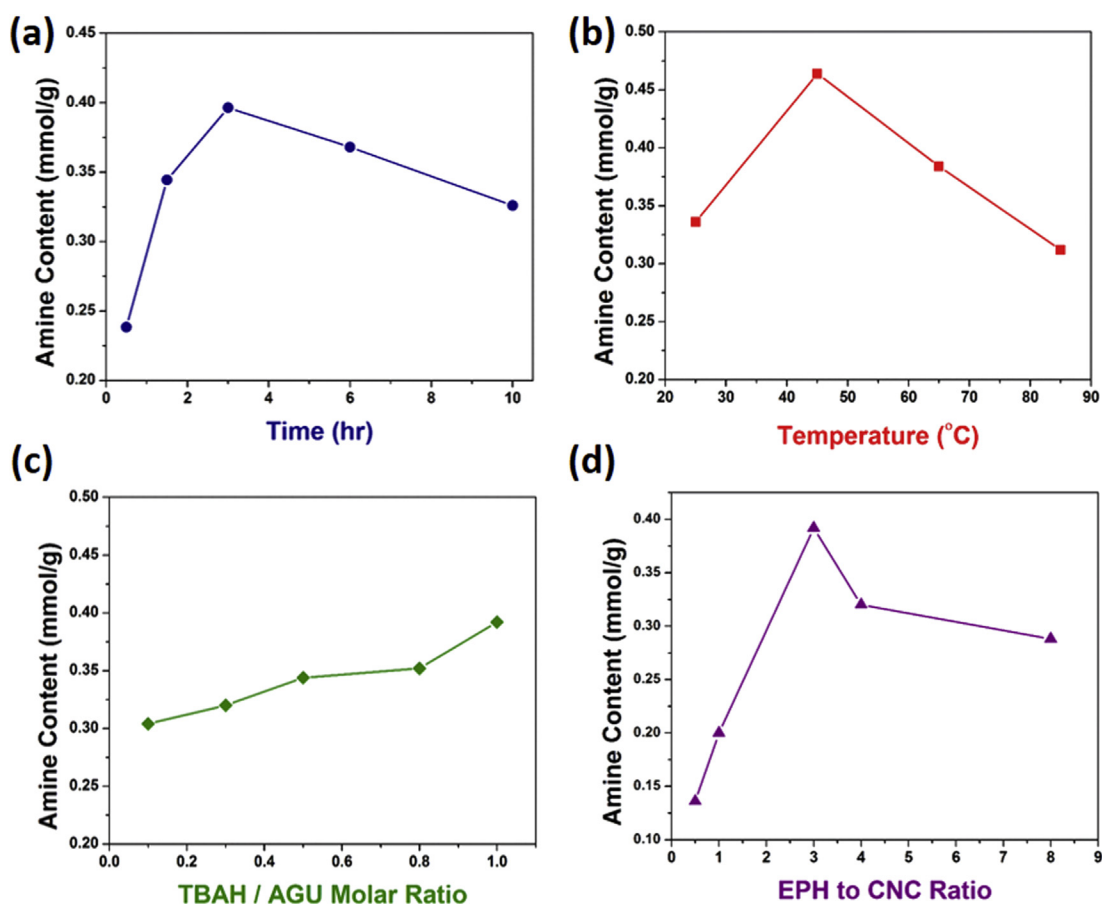
Fig. 1. Optimization of amine-CNC synthesis by varying different reaction parameters (a) time, (b) temperature, (c) TBAH/AGU ratio, and (d) EPH/CNC ratio.

POLY–NH$_2$, the reaction mixture was subjected to centrifugation. First, the pH of CNC–NH$_2$(T) dispersion was adjusted to 2 to promote the electrostatic interaction between positively charged amine groups and negatively charged sulfate ester groups on the surface of CNC, which induced the aggregation of the CNC nanoparticles. Next, centrifugation was performed at 10,000 rpm for 1 h. The supernatant was decanted and the sediment was redispersed in basic pH condition, and this step was repeated a second time. The sediment containing predominantly CNC–NH$_2$(P) dispersion was recovered and used in subsequent studies. Depending on the desired application either CNC–NH$_2$(T) with high amine content or CNC–NH$_2$(P) could be used.

3.4. Potentiometric titration

The amine content of unmodified CNC, CNC–NH$_2$(T), CNC–NH$_2$(P) and POLY–NH$_2$ was determined by potentiometric and conductometric titrations and the results are shown in Fig. 2. The suspensions were first treated with excess of HCl and then titrated with 0.1 M NaOH. The titration curve for CNC did not reveal the presence of amine groups whereas the three samples after the modification reactions clearly showed the presence of amine groups. The potentiometric plots of the modified samples displayed three regions, namely (1) reaction of NaOH with excess HCl, (2) deprotonation of amine groups, and (3) titration of excess NaOH. The region between the 2 equiv lines corresponded to the deprotonation of the amine groups. Based on Fig. 2, the amine content of CNC–NH$_2$(T), CNC–NH$_2$(P) and POLY–NH$_2$ were determined to be 2.20, 0.62, 1.58 mmol/g respectively. The amine content of our

CNC–NH$_2$(P) has been noticeably enhanced compared to the majority of previously reported values by Dong et al.[10] and Mahmoud et al.[14] (0.12–0.15 mmol/g), Nielsen et al.[11] (0.19 mmol/g), and Pahimanolis et al. (0.15 mmol/g).[12] The amine content of CNC–NH$_2$(T) is also comparable to the amine content obtained from the peptidic coupling reaction.[4] The high amine content of CNC–NH$_2$(T) might be useful in applications in which direct grafting of amine groups to CNC surface is not required.

3.5. Elemental analysis

The elemental composition of unmodified CNC, CNC–NH$_2$(T), CNC–NH$_2$(P) and POLY–NH$_2$ was evaluated from elemental analyses. As seen in Table 1, unmodified CNC contained no nitrogen, whereas the amine CNC samples revealed the presence of atomic nitrogen confirming the successful surface modification of CNC with amines. The presence of atomic nitrogen in POLY–NH$_2$ suggested the presence of polyfunctional amines. The sulfur content of the amine CNC is lower than the unmodified CNC, which is possibly attributed to the hydrolysis of sulfate ester groups at high pH during the purification step.[22]

The degree of surface substitution (DS) was determined by the nitrogen content evaluated by elemental analysis based on Eq. 1 and the method reported in the literature.[23,24]

$$DS = \frac{162 \times \%N}{1400 - 108.56 \times \%N} \tag{1}$$

The DS of our CNC–NH$_2$(T) and CNC–NH$_2$(P) after reflux was calculated to be 0.11 and 0.35, respectively. These results suggested
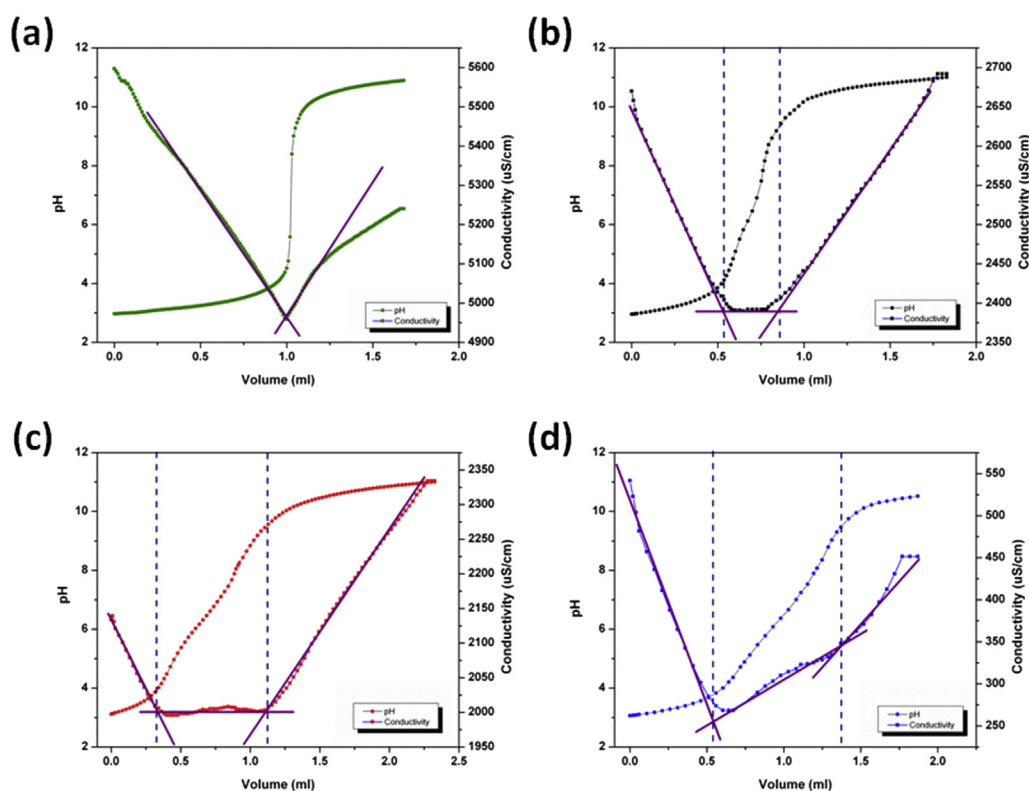
Fig. 2. Potentiometric titration plots of (a) unmodified CNC, (b) CNC−NH$_2$(P), (c) POLY−NH$_2$, and (d) CNC−NH$_2$(T).

Table 1
Elemental analysis of unmodified CNC, CNC−NH$_2$(P), POLY−NH$_2$, and CNC−NH$_2$(T)

Sample	%C	%H	%N	%S
Unmodified CNC	40.98	5.534	0	0.858
CNC−NH$_2$(P)	18.85	2.998	0.9	0.591
POLY−NH$_2$	4.16	0.858	1.42	0.431
CNC−NH$_2$(T)	42	6.19	2.55	0.801

that the amine functionalization protocol reported in this study yielded amine content that is significantly higher than previous reported studies, such as Dong et al.[10] and Mahmoud et al.[14] (DS=0.02), Nielsen et al.[11] (DS=0.03), and Pahimanolis et al. (DS=0.08).[12] The DS of CNC−NH$_2$(T) was also comparable to the DS reported by Hemraz et al. (N%=2.1, DS=0.32).[4] However, they have only used elemental analysis to determine the amine content and

they did not have complementary measurement, such as potentiometric and conductometric titration. Moreover, they have used diamine molecules in their modification, which could result in higher N% in elemental analysis.

3.6. FTIR

FTIR spectra of unmodified CNC, CNC−NH$_2$(T), CNC−NH$_2$(P) and POLY−NH$_2$ are shown in Fig. 3. The absence of characteristic peaks of the sample in the supernatant confirmed that no CNC was present in the supernatant. The new absorption band in Fig. 3b and d, at 1540 cm^{-1} corresponded to amide I, which is an indicator of successful surface functionalization with amine groups. The typical two weak bands for N−H of primary amines not observed in the FTIR spectra as they overlapped with the strong O−H band in the region of 3500 cm^{-14}
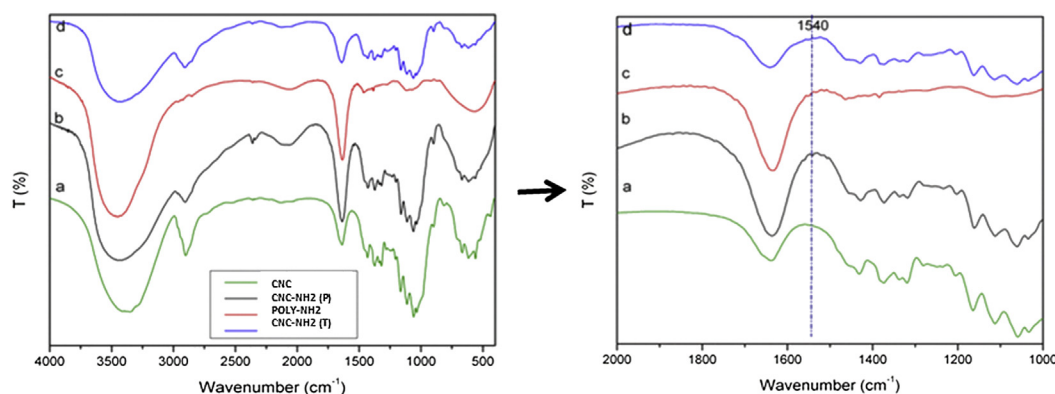

Fig. 3. FTIR spectra of (a) unmodified CNC, (b) POLY−NH$_2$, (c) CNC−NH$_2$(P), and (d) CNC−NH$_2$(T).
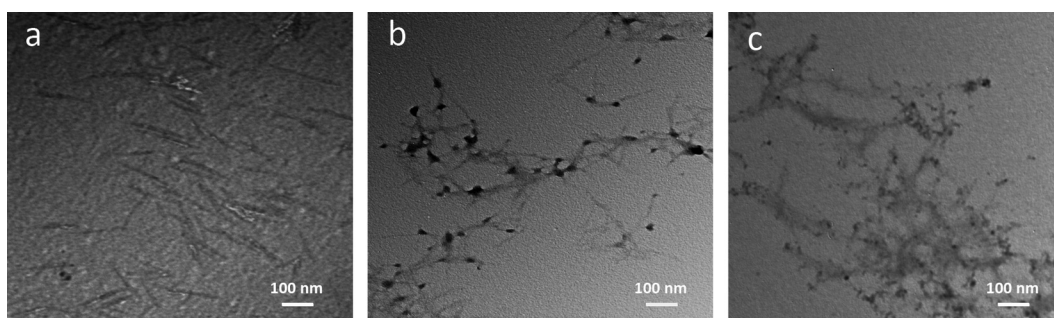
Fig. 4. TEM images of (a) unmodified CNC, (b) CNC—NH₂(T), and (c) CNC—NH₂(P).

3.7. TEM

The TEM images of unmodified CNC, CNC—NH₂(T), and CNC—NH₂(P) are shown in Fig. 4 a—c respectively. As evident, surface functionalization did not alter the rod like structure of the nanocrystals. However, slight agglomeration was observed after surface amine functionalization due to the electrostatic and enhanced hydrogen bond interactions. Similar results were observed previously.[4] Fig. 4b and c revealed that there were much less agglomerated polymer chains in CNC—NH₂(P) than in CNC—NH₂(T).

3.8. Zeta potential measurements

The zeta potential values of unmodified CNC, CNC—NH₂(T) and CNC—NH₂(P) at different pH values are shown in Fig. 5A. At all the pH values, unmodified CNC possessed negative zeta potentials. In acidic pH values, the negative charge is due to the presence of sulfate ester groups (OSO_3^-) arising from the sulfuric acid hydrolysis. With increasing pH, the ionization of the small amount of carboxylic acid groups present on the surface of CNC ($COOH \rightarrow COO^-$), increased the magnitude of the zeta potential as a result of the increasing proportion of negative charges. At high pH values, the negative OSO_3^- groups were hydrolyzed, leading to less negative zeta potential.[22] The successful amine surface modification of CNC could be confirmed by zeta potential measurements. As revealed by Fig. 5 both CNC—NH₂(T) and CNC—NH₂(P) possessed positive zeta potentials at low pH due to the protonation of the amine groups. The more positive zeta potential of CNC—NH₂(T) is due to the presence of more amine groups. As the pH increased, the amine groups became deprotonated, and beyond a pH of 9, the amine groups were completely deprotonated resulting in a negative zeta potential. In addition, hydrolysis of the sulfate ester groups on the surface of CNC resulting in a less negative zeta potential occurred at pH greater than 10.

The successful surface functionalization of CNC with amine groups and the enhanced grafting of amine groups by refluxing the reaction mixture was confirmed by the zeta potential measurements shown in Fig. 5B. In this figure unmodified CNC, CNC—NH₂(T) before and after reflux displayed negative zeta potentials at pH 12 due to the presence of sulfate ester groups. At low pH (pH=2), unmodified CNC was negatively charged whereas CNC—NH₂(T) possessed a substantial positive charge due to the presence of protonated amine groups. The higher zeta potential value observed for CNC—NH₂(T) after reflux illustrates the higher amine content leading to a more positive zeta potential value.

3.9. Viscosity measurements

The relative viscosity of unmodified CNC and CNC—NH₂(T) at low and high pH was measured (Fig. 6A). The higher relative viscosity at low pH for CNC—NH₂(T) is due to the formation of aggregates due to the electrostatic interaction between the positive charge of the protonated amine groups and the negatively charged sulfate ester groups. At high pH, the additional electrostatic interaction was removed due to the deprotonation of the amine groups leading to a reduction in the relative viscosity as reported previously.[12]
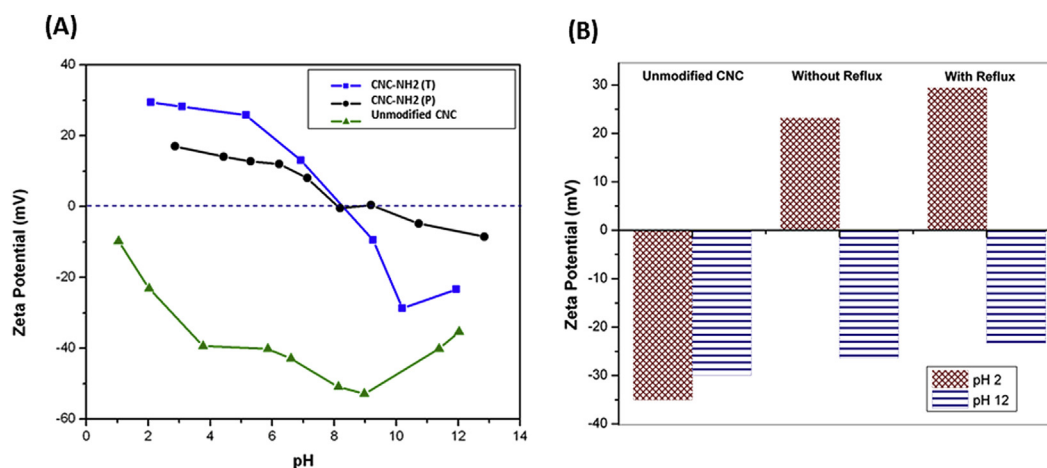

Fig. 5. (A): Zeta potential values of unmodified CNC, CNC—NH₂(T) and CNC—NH₂(P) at different pH values, (B): Comparison of zeta potential values of unmodified CNC, CNC—NH₂(T) before reflux and after reflux at low and high pH.
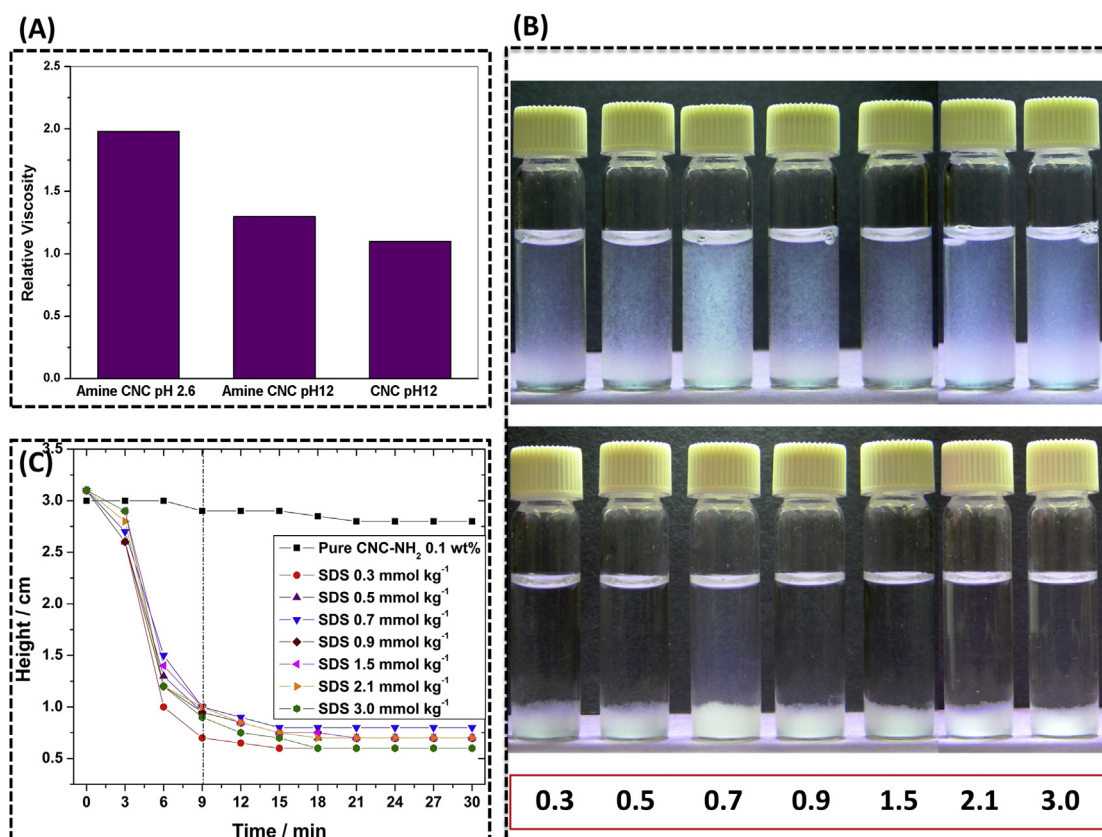
Fig. 6. Relative viscosity of unmodified CNC and CNC–NH₂(T) before reflux at low and high pH, (B): Aqueous suspensions of CNC–NH₂(P) and SDS after mixing (top) and after phase separation (bottom), (C): Height (cm) as function of time (min) for pure CNC–NH₂(P), and CNC–NH₂(P) with various SDS concentrations in mmolkg⁻¹, at 25 °C.

3.10. Settling behavior measurements

The presence of amine groups on the surface of the CNC imparts a pH-responsive characteristic to the nanoparticle. At low pH values (~4) the amine groups were protonated and exhibited a positive charge. Therefore, the CNC–NH₂(P) could be used as a flocculating agent. When mixed with oppositely charged molecules, such as surfactants, electrostatic interactions prevailed, and phase separation occurred (Fig. 6B). Two clear phases were observed where the white turbid phase corresponded to the concentrated flocculated amine CNC/SDS complex. It could be seen in Fig. 6C that the pure CNC–NH₂(P) dispersion was stable after 30 min due to the excessive positive charge present on the surface. However, after adding a negatively charged surfactant (SDS), regardless of the surfactant concentration, all mixtures were flocculated after ~9 min. This clearly shows the strong electrostatic interactions between oppositely charged systems leading to phase separation. The interactions of cationic CNC negative surfactants are relevant in many personal care formulations involving surface active agents, and the present study demonstrates the importance of understanding the mechanism of interactions of surfactants and various types of functional CNC.

4. Conclusions

In this paper, a simple protocol to functionalize the surface of CNC with amine groups is presented. The synthetic process was optimized by varying different parameters such as reaction time, temperature and reactant ratios. Refluxing of the reaction mixture enhanced the grafting of amines onto CNC. The dialyzed final product contained amine functionalized CNC and aminated

polymers that were produced from side reactions. Further purification of the system was obtained through centrifugation. The sediment contained amine groups directly grafted on the surface of CNC through amide bonds. Potentiometric titration and elemental analysis confirmed the presence of high amine content in our modified CNC samples. TEM microscopy showed similar structural properties of the nanocrystals along with some minor aggregation. Zeta potential and relative viscosity measurements also proved the presence of amine groups. The positive zeta potential values at low pH for the amine CNC particles resulted in higher relative viscosity due to electrostatic interactions. At pH 4, CNC–NH₂(P), interacted with negatively charged SDS and settled down in a short time (~9 min). The rapid settling of CNC–NH₂(P) in the presence of negatively charged molecules can have potential applications in water treatment and personal care. Both CNC–NH₂(T) and CNC–NH₂(P) can be further modified and used in different applications.

Acknowledgments

References

1. de Souza Lima MM, Borsali R. *Macromol Rapid Commun* 2004;**25**:771–87.
2. Yu X, Tong S, Ge M, Wu L, Zuo J, Cao C, et al. *Carbohyd Polym* 2013;**92**:380–7.

3. Jasmani L, Eyley S, Wallbridge R, Thielemans W. *Nanoscale* 2013;**5**:10207—11.
4. Hemraz UD, Boluk Y, Sunasee R. *Can J Chem* 2013;**91**:974—81.
5. Yang S-J, Lin F-H, Tsai K-C, Wei M-F, Tsai H-M, Wong J-M, et al. *Bioconjugate Chem* 2010;**21**:679—89.
6. Cohen JL, Schubert S, Wich PR, Cui L, Cohen JA, Mynar JL, et al. *Bioconjugate Chem* 2011;**22**:1056—65.
7. Heinze T, Koschella A, Brackhagen M, Nachtkamp K. *Macromol Symp* 2006: 74—82.
8. Zarth CSP, Koschella A, Pfeifer A, Dorn S, Heinze T. *Cellulose* 2011;**18**:1315—25.
9. Heinze T, Genco T, Petzold-Welcke K, Wondraczek H. *Cellulose* 2012;**19**: 1305—13.
10. Dong S, Roman M. *J Am Chem Soc* 2007;**129**:13810—1.
11. Nielsen LJ, Eyley S, Thielemans W, Aylott JW. *Chem Commun (Camb)* 2010;**46**: 8929—31.
12. Pahimanolis N, Hippi U, Johansson L-S, Saarinen T, Houbenov N, Ruokolainen J, et al. *Cellulose* 2011;**18**:1201—12.
13. Akhlaghi SP, Berry RC, Tam KC. *Cellulose* 2013;**20**:1747—64.
14. Mahmoud KA, Mena JA, Male KB, Hrapovic S, Kamen A, Luong JHT. *ACS Appl Mater Inter* 2010;**2**:2924—32.
15. Zaman M, Xiao H, Chibante F, Ni Y. *Carbohydr Polym* 2012;**89**:163—70.
16. Ren J, Sun R, Liu C. *J Appl Polym Sci* 2007;**105**:3301—8.
17. Ren J-L, Peng F, Sun R-C, Kennedy JF. *Carbohyd Polym* 2009;**75**:338—42.
18. Liu Z, Ni Y, Fatehi P, Saeed A. *Biomass Bioenerg* 2011;**35**:1789—96.
19. Khalil MI, Beliakova MK, Aly AA. *Carbohyd Polym* 2001;**46**:217—26.
20. Brochu S, Ampleman G. *Macromolecules* 1996;**29**:5539—45.
21. Dragan S, Ghimici L. *Angew Makromol Chem* 1991;**192**:199—211.
22. Azzam F, Heux L, Putaux J-L, Jean B. *Biomacromolecules* 2010;**11**:3652—9.
23. Filpponen I, Argyropoulos DS. *Biomacromolecules* 2010;**11**:1060—6.
24. Filpponen I, Sadeghifar H, Argyropoulos DS. *Nanomater Nanotechnol* 2011;**1**: 34—43.

Appendix F Permissions to reprint and reuse

Copyright Clearance Center RightsLink®

Home | Account Info | Help | Live Chat
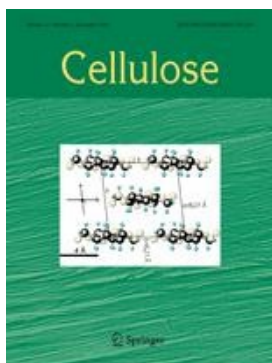
Title: About the structure of cellulose: debating the Lindman hypothesis

Author: Wolfgang G. Glasser

Publication: Cellulose

Publisher: Springer

Date: Jan 1, 2012

Copyright © 2012, Springer Science+Business Media B.V.

Logged in as:
César Brinatti
Account #:
3000946024

LOGOUT

Order Completed

Thank you for your order.

This Agreement between César Brinatti ("You") and Springer ("Springer") consists of your license details and the terms and conditions provided by Springer and Copyright Clearance Center.

Your confirmation email will contain your order number for future reference.

Get the printable license.

License Number	3957051250116
License date	Sep 27, 2016
Licensed Content Publisher	Springer
Licensed Content Publication	Cellulose
Licensed Content Title	About the structure of cellulose: debating the Lindman hypothesis
Licensed Content Author	Wolfgang G. Glasser
Licensed Content Date	Jan 1, 2012
Licensed Content Volume	19
Licensed Content Issue	3
Type of Use	Thesis/Dissertation
Portion	Figures/tables/illustrations
Number of figures/tables /illustrations	1
Author of this Springer article	No
Order reference number	92
Original figure numbers	Figure 1
Title of your thesis / dissertation	Calorimetric study on the interactions between ionic surfactants and pristine and modified cellulose nanocrystals (CNC)
Expected completion date	Sep 2016
Estimated size(pages)	150
Requestor Location	César Brinatti Rua Josué de Castro, S/N
	Campinas, São Paulo 13083-970 Brazil Attn: César Brinatti
Billing Type	Invoice
Billing address	César Brinatti Rua Josué de Castro, S/N
	Campinas, Brazil 13083-970

Attn: César Brinatti

Total   0.00 USD

ORDER MORE   **CLOSE WINDOW**

Copyright Clearance Center RightsLink®

Home | Account Info | Help | Live Chat

ACS Publications
Most Trusted. Most Cited. Most Read.

Title: Cellulose Nanocrystals: Chemistry, Self-Assembly, and Applications

Author: Youssef Habibi, Lucian A. Lucia, Orlando J. Rojas

Publication: Chemical Reviews

Publisher: American Chemical Society

Date: Jun 1, 2010

Copyright © 2010, American Chemical Society

Logged in as:
César Brinatti
Account #:
3000946024

LOGOUT

PERMISSION/LICENSE IS GRANTED FOR YOUR ORDER AT NO CHARGE

This type of permission/license, instead of the standard Terms & Conditions, is sent to you because no fee is being charged for your order. Please note the following:

- Permission is granted for your request in both print and electronic formats, and translations.
- If figures and/or tables were requested, they may be adapted or used in part.
- Please print this page for your records and send a copy of it to your publisher/graduate school.
- Appropriate credit for the requested material should be given as follows: "Reprinted (adapted) with permission from (COMPLETE REFERENCE CITATION). Copyright (YEAR) American Chemical Society." Insert appropriate information in place of the capitalized words.
- One-time permission is granted only for the use specified in your request. No additional uses are granted (such as derivative works or other editions). For any other uses, please submit a new request.

If credit is given to another source for the material you requested, permission must be obtained from that source.

BACK | CLOSE WINDOW

ROYAL SOCIETY OF CHEMISTRY LICENSE
TERMS AND CONDITIONS

Sep 27, 2016

This Agreement between César Brinatti ("You") and Royal Society of Chemistry ("Royal Society of Chemistry") consists of your license details and the terms and conditions provided by Royal Society of Chemistry and Copyright Clearance Center.

License Number	3957060277497
License date	Sep 27, 2016
Licensed Content Publisher	Royal Society of Chemistry
Licensed Content Publication	Nanoscale
Licensed Content Title	Preparation, properties and applications of polysaccharide nanocrystals in advanced functional nanomaterials: a review
Licensed Content Author	Ning Lin,Jin Huang,Alain Dufresne
Licensed Content Date	Mar 27, 2012
Licensed Content Volume Number	4
Licensed Content Issue Number	11
Type of Use	Thesis/Dissertation
Requestor type	academic/educational
Portion	figures/tables/images
Number of figures/tables /images	1
Format	print and electronic
Distribution quantity	100
Will you be translating?	no
Order reference number	
Title of the thesis/dissertation	Calorimetric study on the interactions between ionic surfactants and pristine and modified cellulose nanocrystals (CNC)
Expected completion date	Sep 2016
Estimated size	150
Requestor Location	César Brinatti Rua Josué de Castro, S/N Campinas, São Paulo 13083-970 Brazil Attn: César Brinatti
Billing Type	Invoice
Billing Address	César Brinatti Rua Josué de Castro, S/N Campinas, Brazil 13083-970 Attn: César Brinatti
Total	0.00 USD

Terms and Conditions

This License Agreement is between {Requestor Name} ("You") and The Royal Society of Chemistry ("RSC") provided by the Copyright Clearance Center ("CCC"). The license consists of your order details, the terms and conditions provided by the Royal Society of Chemistry, and the payment terms and conditions.

RSC / TERMS AND CONDITIONS

INTRODUCTION

The publisher for this copyrighted material is The Royal Society of Chemistry. By clicking "accept" in connection with completing this licensing transaction, you agree that the following terms and conditions apply to this transaction (along with the Billing and Payment terms and conditions established by CCC, at the time that you opened your RightsLink account and that are available at any time at .

LICENSE GRANTED

The RSC hereby grants you a non-exclusive license to use the aforementioned material anywhere in the world subject to the terms and conditions indicated herein. Reproduction of the material is confined to the purpose and/or media for which permission is hereby given.

RESERVATION OF RIGHTS

The RSC reserves all rights not specifically granted in the combination of (i) the license details provided by your and accepted in the course of this licensing transaction; (ii) these terms and conditions; and (iii) CCC's Billing and Payment terms and conditions.

REVOCATION

The RSC reserves the right to revoke this license for any reason, including, but not limited to, advertising and promotional uses of RSC content, third party usage, and incorrect source figure attribution.

THIRD-PARTY MATERIAL DISCLAIMER

If part of the material to be used (for example, a figure) has appeared in the RSC publication with credit to another source, permission must also be sought from that source. If the other source is another RSC publication these details should be included in your RightsLink request. If the other source is a third party, permission must be obtained from the third party. The RSC disclaims any responsibility for the reproduction you make of items owned by a third party.

PAYMENT OF FEE

If the permission fee for the requested material is waived in this instance, please be advised that any future requests for the reproduction of RSC materials may attract a fee.

ACKNOWLEDGEMENT

The reproduction of the licensed material must be accompanied by the following acknowledgement:

Reproduced ("Adapted" or "in part") from {Reference Citation} (or Ref XX) with permission of The Royal Society of Chemistry.

If the licensed material is being reproduced from New Journal of Chemistry (NJC), Photochemical & Photobiological Sciences (PPS) or Physical Chemistry Chemical Physics (PCCP) you must include one of the following acknowledgements:

For figures originally published in NJC:

Reproduced ("Adapted" or "in part") from {Reference Citation} (or Ref XX) with permission of The Royal Society of Chemistry (RSC) on behalf of the European Society for Photobiology, the European Photochemistry Association and the RSC.

For figures originally published in PPS:

Reproduced ("Adapted" or "in part") from {Reference Citation} (or Ref XX) with permission of The Royal Society of Chemistry (RSC) on behalf of the Centre National de la Recherche Scientifique (CNRS) and the RSC.

For figures originally published in PCCP:

Reproduced ("Adapted" or "in part") from {Reference Citation} (or Ref XX) with permission of the PCCP Owner Societies.

HYPERTEXT LINKS

With any material which is being reproduced in electronic form, you must include a hypertext link to the original RSC article on the RSC's website. The recommended form for the hyperlink is http://dx.doi.org/10.1039/DOI suffix, for example in the link http://dx.doi.org/10.1039/b110420a the DOI suffix is 'b110420a'. To find the relevant DOI suffix for the RSC article in question, go to the Journals section of the website and locate the article in the list of papers for the volume and issue of your specific journal. You will find the DOI suffix quoted there.

LICENSE CONTINGENT ON PAYMENT

While you may exercise the rights licensed immediately upon issuance of the license at the end of the licensing process for the transaction, provided that you have disclosed complete and accurate details of your proposed use, no license is finally effective unless and until full payment is received from you (by CCC) as provided in CCC's Billing and Payment terms and conditions. If full payment is not received on a timely basis, then any license preliminarily granted shall be deemed automatically revoked and shall be void as if never granted. Further, in the event that you breach any of these terms and conditions or any of CCC's Billing and Payment terms and conditions, the license is automatically revoked and shall be void as if never granted. Use of materials as described in a revoked license, as well as any use of the materials beyond the scope of an unrevoked license, may constitute copyright infringement and the RSC reserves the right to take any and all action to protect its copyright in the materials.

WARRANTIES

The RSC makes no representations or warranties with respect to the licensed material.

INDEMNITY

You hereby indemnify and agree to hold harmless the RSC and the CCC, and their respective officers, directors, trustees, employees and agents, from and against any and all claims arising out of your use of the licensed material other than as specifically authorized pursuant to this licence.

NO TRANSFER OF LICENSE

This license is personal to you or your publisher and may not be sublicensed, assigned, or transferred by you to any other person without the RSC's written permission.

NO AMENDMENT EXCEPT IN WRITING

This license may not be amended except in a writing signed by both parties (or, in the case of "Other Conditions, v1.2", by CCC on the RSC's behalf).

OBJECTION TO CONTRARY TERMS

You hereby acknowledge and agree that these terms and conditions, together with CCC's Billing and Payment terms and conditions (which are incorporated herein), comprise the entire agreement between you and the RSC (and CCC) concerning this licensing transaction, to the exclusion of all other terms and conditions, written or verbal, express or implied (including any terms contained in any purchase order, acknowledgment, check endorsement or other writing prepared by you). In the event of any conflict between your obligations established by these terms and conditions and those established by CCC's Billing and Payment terms and conditions, these terms and conditions shall control.

JURISDICTION

This license transaction shall be governed by and construed in accordance with the laws of the District of Columbia. You hereby agree to submit to the jurisdiction of the courts located in the District of Columbia for purposes of resolving any disputes that may arise in connection with this licensing transaction.

LIMITED LICENSE

The following terms and conditions apply to specific license types:

Translation

This permission is granted for non-exclusive world English rights only unless your license was granted for translation rights. If you licensed translation rights you may only translate

this content into the languages you requested. A professional translator must perform all translations and reproduce the content word for word preserving the integrity of the article.
Intranet
If the licensed material is being posted on an Intranet, the Intranet is to be password-protected and made available only to bona fide students or employees only. All content posted to the Intranet must maintain the copyright information line on the bottom of each image. You must also fully reference the material and include a hypertext link as specified above.
Copies of Whole Articles
All copies of whole articles must maintain, if available, the copyright information line on the bottom of each page.
Other Conditions
v1.2
Gratis licenses (referencing $0 in the Total field) are free. Please retain this printable license for your reference. No payment is required.
If you would like to pay for this license now, please remit this license along with yourpayment made payable to "COPYRIGHT CLEARANCE CENTER" otherwise you will be invoiced within 48 hours of the license date. Payment should be in the form of a check or money order referencing your account number and this invoice number {Invoice Number}.
Once you receive your invoice for this order, you may pay your invoice by credit card.
Please follow instructions provided at that time.
Make Payment To:
Copyright Clearance Center
Dept 001
P.O. Box 843006
Boston, MA 02284-3006
For suggestions or comments regarding this order, contact Rightslink Customer Support: customercare@copyright.com or +1-855-239-3415 (toll free in the US) or +1-978-646-2777.

Questions? customercare@copyright.com or +1-855-239-3415 (toll free in the US) or +1-978-646-2777.

Copyright Clearance Center | RightsLink®

Home | Account Info | Help | Live Chat

Title: Cellulose nanocrystal-poly(oligo(ethylene glycol) methacrylate) brushes with tunable LCSTs

Author: Nathan Grishkewich,Seyedeh Parinaz Akhlaghi,Yao Zhaoling,Richard Berry,Kam C. Tam

Publication: Carbohydrate Polymers

Publisher: Elsevier

Date: 25 June 2016

Copyright © 2016 Elsevier Ltd. All rights reserved.

Logged in as:
César Brinatti
Account #:
3000946024

LOGOUT

Order Completed

Thank you for your order.

This Agreement between César Brinatti ("You") and Elsevier ("Elsevier") consists of your license details and the terms and conditions provided by Elsevier and Copyright Clearance Center.

Your confirmation email will contain your order number for future reference.

Get the printable license.

License Number	3957060754621
License date	Sep 27, 2016
Licensed Content Publisher	Elsevier
Licensed Content Publication	Carbohydrate Polymers
Licensed Content Title	Cellulose nanocrystal-poly(oligo(ethylene glycol) methacrylate) brushes with tunable LCSTs
Licensed Content Author	Nathan Grishkewich,Seyedeh Parinaz Akhlaghi,Yao Zhaoling,Richard Berry,Kam C. Tam
Licensed Content Date	25 June 2016
Licensed Content Volume	144
Licensed Content Issue	n/a
Licensed Content Pages	8
Type of Use	reuse in a thesis/dissertation
Portion	figures/tables/illustrations
Number of figures/tables /illustrations	1
Format	both print and electronic
Are you the author of this Elsevier article?	No
Will you be translating?	No
Order reference number	
Original figure numbers	Figure 7
Title of your thesis/dissertation	Calorimetric study on the interactions between ionic surfactants and pristine and modified cellulose nanocrystals (CNC)
Expected completion date	Sep 2016
Estimated size (number of pages)	150
Elsevier VAT number	GB 494 6272 12
Requestor Location	César Brinatti Rua Josué de Castro, S/N

Campinas, São Paulo 13083-970
Brazil
Attn: César Brinatti

Rightslink® by Copyright Clearance Center

Total 0.00 USD

ORDER MORE   **CLOSE WINDOW**

M Gmail   **César Brinatti <entropeople@gmail.com>**

Permission Request Form: Cesar Brinatti

CONTRACTS-COPYRIGHT (shared) <Contracts-Copyright@rsc.org>   Tue, Sep 27, 2016 at 11:17 AM
To: "entropeople@gmail.com" <entropeople@gmail.com>

Dear Cesar,

The Royal Society of Chemistry (RSC) hereby grants permission for the use of your paper(s) specified below in the printed and microfilm version of your thesis. You may also make available the PDF version of your paper(s) that the RSC sent to the corresponding author(s) of your paper(s) upon publication of the paper(s) in the following ways: in your thesis via any website that your university may have for the deposition of theses, via your university's Intranet or via your own personal website. We are however unable to grant you permission to include the PDF version of the paper(s) on its own in your institutional repository. The Royal Society of Chemistry is a signatory to the STM Guidelines on Permissions (available on request).

Please note that if the material specified below or any part of it appears with credit or acknowledgement to a third party then you must also secure permission from that third party before reproducing that material.

Please ensure that the thesis states the following:

Reproduced by permission of The Royal Society of Chemistry

and include a link to the paper on the Royal Society of Chemistry's website.

Please ensure that your co-authors are aware that you are including the paper in your thesis.

Regards

Antonella Tesoro
Customer Sales Support
Royal Society of Chemistry
Thomas Graham House,
Science Park, Milton Road,
Cambridge-CB4 0WF
Tel. +44 (0) 1223 432 675
tesoroa@rsc.org

Main Reception Tel. +44 (0) 1223 42 0066
www.rsc.org

Winner of The Queen's Awards for Enterprise, International Trade 2013

Copyright Clearance Center

RightsLink®

Home Account Info Help Live Chat

Title:	Cost-effective and Scalable Chemical Synthesis of Conductive Cellulose Nanocrystals for High-performance Supercapacitors
Author:	Xinyun Wu,Victor Luc Chabot,Brian Kihun Kim,Aiping Yu,Richard M. Berry,Kam C. Tam
Publication:	Electrochimica Acta
Publisher:	Elsevier
Date:	20 August 2014

Copyright © 2014 Elsevier Ltd. All rights reserved.

Logged in as:
César Brinatti
Account #:
3000946024

LOGOUT

Order Completed

Thank you for your order.

This Agreement between César Brinatti ("You") and Elsevier ("Elsevier") consists of your license details and the terms and conditions provided by Elsevier and Copyright Clearance Center.

Your confirmation email will contain your order number for future reference.

Get the printable license.

License Number	3957070345152
License date	Sep 27, 2016
Licensed Content Publisher	Elsevier
Licensed Content Publication	Electrochimica Acta
Licensed Content Title	Cost-effective and Scalable Chemical Synthesis of Conductive Cellulose Nanocrystals for High-performance Supercapacitors
Licensed Content Author	Xinyun Wu,Victor Luc Chabot,Brian Kihun Kim,Aiping Yu,Richard M. Berry,Kam C. Tam
Licensed Content Date	20 August 2014
Licensed Content Volume	138
Licensed Content Issue	n/a
Licensed Content Pages	9
Type of Use	reuse in a thesis/dissertation
Portion	figures/tables/illustrations
Number of figures/tables /illustrations	1
Format	both print and electronic
Are you the author of this Elsevier article?	No
Will you be translating?	No
Order reference number	
Original figure numbers	Figure 5b
Title of your thesis/dissertation	Calorimetric study on the interactions between ionic surfactants and pristine and modified cellulose nanocrystals (CNC)
Expected completion date	Sep 2016
Estimated size (number of pages)	150
Elsevier VAT number	GB 494 6272 12
Requestor Location	César Brinatti Rua Josué de Castro, S/N

Campinas, São Paulo 13083-970

Brazil
Attn: César Brinatti

Total   0.00 USD

ORDER MORE   **CLOSE WINDOW**

Brazil
Attn: César Brinatti

Copyright Clearance Center

RightsLink®

Home | Create Account | Help | Live Chat

ACS Publications Most Trusted. Most Cited. Most Read.

Title: Structural and Energetic Studies on the Interaction of Cationic Surfactants and Cellulose Nanocrystals

Author: César Brinatti, John Huang, Richard M. Berry, et al

Publication: Langmuir

Publisher: American Chemical Society

Date: Jan 1, 2016

Copyright © 2016, American Chemical Society

PERMISSION/LICENSE IS GRANTED FOR YOUR ORDER AT NO CHARGE

This type of permission/license, instead of the standard Terms & Conditions, is sent to you because no fee is being charged for your order. Please note the following:

- Permission is granted for your request in both print and electronic formats, and translations.
- If figures and/or tables were requested, they may be adapted or used in part.
- Please print this page for your records and send a copy of it to your publisher/graduate school.
- Appropriate credit for the requested material should be given as follows: "Reprinted (adapted) with permission from (COMPLETE REFERENCE CITATION). Copyright (YEAR) American Chemical Society." Insert appropriate information in place of the capitalized words.
- One-time permission is granted only for the use specified in your request. No additional uses are granted (such as derivative works or other editions). For any other uses, please submit a new request.

BACK | CLOSE WINDOW

Rightslink® by Copyright Clearance Center

Copyright Clearance Center   RightsLink®   Home   Account Info   Help   Live Chat

Title:	Use of isothermal titration calorimetry to study surfactant aggregation in colloidal systems
Author:	Watson Loh,César Brinatti,Kam Chiu Tam
Publication:	Biochimica et Biophysica Acta (BBA) - General Subjects
Publisher:	Elsevier
Date:	May 2016

Copyright © 2015 Elsevier B.V. All rights reserved.

Logged in as:
César Brinatti
Account #:
3000946024

LOGOUT

Order Completed

Thank you for your order.

This Agreement between César Brinatti ("You") and Elsevier ("Elsevier") consists of your license details and the terms and conditions provided by Elsevier and Copyright Clearance Center.

Your confirmation email will contain your order number for future reference.

Get the printable license.

License Number	3956811440339
License date	Sep 26, 2016
Licensed Content Publisher	Elsevier
Licensed Content Publication	Biochimica et Biophysica Acta (BBA) - General Subjects
Licensed Content Title	Use of isothermal titration calorimetry to study surfactant aggregation in colloidal systems
Licensed Content Author	Watson Loh,César Brinatti,Kam Chiu Tam
Licensed Content Date	May 2016
Licensed Content Volume	1860
Licensed Content Issue	5
Licensed Content Pages	18
Type of Use	reuse in a thesis/dissertation
Portion	full article
Format	both print and electronic
Are you the author of this Elsevier article?	Yes
Will you be translating?	No
Order reference number	
Title of your thesis/dissertation	Calorimetric study on the interactions between ionic surfactants and pristine and modified cellulose nanocrystals (CNC)
Expected completion date	Sep 2016
Estimated size (number of pages)	150
Elsevier VAT number	GB 494 6272 12
Requestor Location	César Brinatti Rua Josué de Castro, S/N Campinas, São Paulo 13083-970 Brazil Attn: César Brinatti
Total	0.00 USD

ORDER MORE   CLOSE WINDOW

Copyright
Clearance
Center

RightsLink®

Home | Account Info | Help | Live Chat

Title: Synthesis of amine functionalized cellulose nanocrystals: optimization and characterization

Author: Seyedeh Parinaz Akhlaghi,Masuduz Zaman,Nishil Mohammed,César Brinatti,Rasim Batmaz,Richard Berry,Watson Loh,Kam Chiu Tam

Publication: Carbohydrate Research

Publisher: Elsevier

Date: 29 May 2015

Logged in as:
César Brinatti
Account #:
3000946024

LOGOUT

Order Completed

Thank you for your order.

This Agreement between César Brinatti ("You") and Elsevier ("Elsevier") consists of your license details and the terms and conditions provided by Elsevier and Copyright Clearance Center.

Your confirmation email will contain your order number for future reference.

Get the printable license.

License Number	3956820030058
License date	Sep 26, 2016
Licensed Content Publisher	Elsevier
Licensed Content Publication	Carbohydrate Research
Licensed Content Title	Synthesis of amine functionalized cellulose nanocrystals: optimization and characterization
Licensed Content Author	Seyedeh Parinaz Akhlaghi,Masuduz Zaman,Nishil Mohammed,César Brinatti,Rasim Batmaz,Richard Berry,Watson Loh,Kam Chiu Tam
Licensed Content Date	29 May 2015
Licensed Content Volume	409
Licensed Content Issue	n/a
Licensed Content Pages	8
Type of Use	reuse in a thesis/dissertation
Portion	full article
Format	both print and electronic
Are you the author of this Elsevier article?	Yes
Will you be translating?	No
Order reference number	
Title of your thesis/dissertation	Calorimetric study on the interactions between ionic surfactants and pristine and modified cellulose nanocrystals (CNC)
Expected completion date	Sep 2016
Estimated size (number of pages)	150
Elsevier VAT number	GB 494 6272 12
Requestor Location	César Brinatti Rua Josué de Castro, S/N Campinas, São Paulo 13083-970 Brazil Attn: César Brinatti
Total	0.00 USD

ORDER MORE   **CLOSE WINDOW**

Appendix G Alternative format permission

Se a Tese ou Dissertação for reproduzida em formato alternativo (com artigos anexados), este documento, preenchido e assinado, deve ser inserido no trabalho como Anexo.
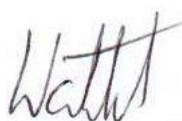
DECLARAÇÃO

As cópias dos documentos de minha autoria ou de minha coautoria, já publicados ou submetidos para publicação em revistas científicas ou anais de congressos sujeitos a arbitragem, que constam da minha Tese de Doutorado, intitulada "Calorimetric study on the interactions between ionic surfactants and pristine and modified cellulose nanocrystals (CNC)" não infringem os dispositivos da Lei nº 9.610/98, nem o direito autoral de qualquer editora.

Local e data

Campinas, 23 de setembro de 2016

Autor R.G. nº 29741249-8 SSP/SP

Orientador RG nº 4007973219 SSP/RS